Development and Performance Evaluation of Carbon-Polymer Composite Bipolar Plate for Proton Exchange Membrane Fuel Cell

Submitted in partial fulfilment of the requirements for the degree of

Doctor of Philosophy

by

BIRAJ KUMAR KAKATI

DEPARTMENT OF CHEMICAL ENGINEERING

INDIAN INSTITUTE OF TECHNOLOGY GUWAHATI

Guwahati – 781 039

March, 2011

Development and Performance Evaluation of Carbon-Polymer Composite Bipolar Plate for Proton Exchange Membrane Fuel Cell

Submitted by

Biraj Kumar Kakati

Department of Chemical Engineering

Indian Institute of Technology Guwahati

Guwahati – 781 039

March, 2011

Dedicated to my parents...

Department of Chemical Engineering
Indian Institute of Technology Guwahati
Guwahati – 781 039
Assam, India

STATEMENT

I do hereby declare that the matter embedded in this thesis is the result of investigations carried out by me in the Department of Chemical Engineering, Indian Institute of Technology Guwahati, Guwahati, Assam, India, under the supervision of Dr. Anil Verma, Department of Chemical Engineering, Indian Institute of Technology Guwahati, Guwahati, Assam, India.

In keeping with the general practice of reporting scientific observations, due acknowledgement has been made wherever the work described is based on the findings of other investigators.

_ _ _ _ _ _ _ _ _ _ _ _ _ _ _ _ _ _ _ _

Dated: 22nd March, 2011
IIT Guwahati

Biraj Kumar Kakati
Department of Chemical Engineering
Indian Institute of Technology Guwahati
Guwahati – 781 039

Department of Chemical Engineering
Indian Institute of Technology Guwahati
Guwahati – 781 039
Assam, India

CERTIFICATE

It is certified that the work contained in the thesis entitled "Development and Performance Evaluation of Carbon-Polymer Composite Bipolar Plate for Proton Exchange Membrane Fuel Cell", by Mr. Biraj Kumar Kakati, for the award of degree of Doctor of Philosophy, has been carried out under my supervision and that this work has not been submitted elsewhere for a degree.

Dated: 22nd March, 2011
IIT Guwahati

_ _ _ _ _ _ _ _ _ _ _ _ _ _ _ _ _ _ _ _

Dr. Anil Verma
Assistant professor
Department of Chemical Engineering
Indian Institute of Technology Guwahati
Guwahati – 781 039

Preface

The title of this thesis, and the experimental investigations embedded in it, reflect a blend of science and engineering in the study of development, characterization, and performance evaluation of composite bipolar plate for fuel cell application. The thesis gives a detailed overview on the development of a highly conductive composite bipolar plate for proton exchange membrane fuel cells (PEMFCs), which fulfills all the stringent requirements given by US-DOE and other front runner organizations in the field of fuel cell.

The historical background of fuel cell, types of fuel cell, and different parts of PEMFC are covered within the 1st chapter. However, emphasis is given on the bipolar plates, materials, properties, and its importance. The importance of carbon-polymer composite bipolar plate for PEMFC is also discussed at the end of the 1st chapter.

A literature review on the development of composite bipolar plates has been included in the 2nd chapter. The literature review includes a brief discussion on the important scientific findings reported in the available literature from 1978 to till date. The outcomes of the most significant literatures are summarized at the end of the chapter and the objective of the thesis was formulated based on the literature review.

The 3rd chapter covers the materials and methodology to develop and evaluate the performance of the bipolar plate. A brief description about the materials used, and also the synthesis of graphene have been described in the first half of this chapter. The rest of the chapter includes development and characterization of composite bipolar plates. Moreover, methodologies for fuel cell testing using the developed bipolar plates are also discussed at the end of the chapter.

Chapter 4 describes the electrical conductivity modeling of the composite bipolar plates for multi-component system. The electrical conductivity of composite bipolar plate was modeled by applying modified GEM equation.

The results and discussion of the research is included in the 5th chapter. This chapter includes the characterization of procured raw materials and synthesized graphene followed by the characterization of developed carbon composite bipolar plates. The effects of NG, CB, CF, and graphene on the properties of composite bipolar plate are discussed in this chapter. Moreover, the performance of the developed composite bipolar plates was discussed at the end of the 5th chapter.

The results of the modeling is included in the in the 4th chapter. The results predicted by the model are compared and verified with the experimental results.

An overall conclusion of the research work is included in the 7th chapter. Moreover, it also includes the future scope of research on the development, characterization and evaluation of carbon composite bipolar plate for fuel cell application. The chapter will help the future researchers in formulating their objective to develop composite bipolar plates to improve fuel cell performance. I have attempted to cover and cite all the available significant literatures relevant to the current research. However, the off topic scientific reports are avoided carefully throughout the thesis. I have tried to organize thesis in such a manner so that it may depict a clear picture to the reader on the development and characterization of graphene followed by the development, characterization, and evaluation of carbon-polymer composite bipolar plates for PEMFC.

_ _ _ _ _ _ _ _ _ _ _ _ _ _ _ _ _ _ _

Biraj Kumar Kakati

22nd March, 2011

Guwahati – 39

Acknowledgement

It is my pleasure to thank those who made this thesis possible. I recollect numerous occasions and moments which make me proud to be a part of this world class Centre of Excellence. It is my privilege to be amidst some intellectual genius, who guided in my pursuit of knowledge. I owe my deepest gratitude to all of them.

The first and foremost appreciation goes to my supervisor Dr. Anil Verma for his valuable guidance throughout the research work. I thank him for his encouragement, guidance and support from the initial to the final level, which enabled me to develop a better understanding of the subject and leads to a successful completion. I would like to acknowledge my sincere gratitude to my doctoral committee members, Dr. Tamal Banerjee, Dr. G. Pugazhenthi and Dr. U.K. Saha, for their insightful advices and suggestions throughout the research. I also acknowledge the kind advice and suggestion of Dr. Manabendra Sarma and Dr. Bulu Pradhan during my research work.

My sincere thanks go to the Head of the Department of Chemical Engineering and also to the faculty members for their constant inspiration and valuable suggestions. The kind and constant help of the staff member of the department is also duly acknowledged. I am also thankful to the Indian Institute of Technology Guwahati for providing me with the infrastructure and facilities for advanced research. I would also like to convey my sincere thanks to the Head of Central Instruments Facility (CIF), IIT Guwahati, for providing me the analytical facilities such as SEM, FESEM, TEM, and DSC. My sincere thanks go to Chandan Borgohain, Kula Kamal Senapati, and Madhurjya Borah for their help in using the analytical facilities of CIF.

I extend my sincerest thanks to Ramesh K. Guptha, V.P. Appaji, V.K. Yamsani, Shivdeep Gaagat, and Rajroshan Dhruw for extending helping hands in various part of the research work. Moreover, my special thanks go to Leela, Avijit and Lepakshi-ba for their constant encouragement and help during the course of the research. I would also

like to acknowledge the nice company of Rupesh, Dhiraj, and Deepak during my research in the fuel cell laboratory. I am also thankful to my colleague and friends Somen, Ashok, Ujwala, Kabita-ba, Pankaj-da, Gunin, and Buljit-da, for their constant help, motivation, and enthusiastic company and all the wonderful time we spent in various events.

I gratefully acknowledge the financial support of the Board of Research in Nuclear Sciences (BRNS), Department of Atomic Energy, Government of India, for the above project (No. 2007/36/19-BRNS/1000). I also acknowledge Indian Institute of Technology Guwahati for providing senior research fellowship for the research work.

At last but not least, I am highly indebted to my parents their endless love and inspiration. Finally, my Ph. D. endeavor could not be completed without the endless love, unending support, and blessings from my elder brothers and sisters. My sincere apology goes to them whom I forget to mention but helped me at any part of the research work.

_ _ _ _ _ _ _ _ _ _ _ _ _ _ _ _ _ _ _

Biraj Kumar Kakati

22nd March, 2011

Guwahati – 39

Abstract

Bipolar plate is a key component of low temperature fuel cells, which may contribute up to 80% of the total weight of the proton exchange membrane fuel cell (PEMFC) stack. Different type of materials like metal, coated metal, graphite, composites etc. are under investigation to develop bipolar plates with high electrical and thermal conductivity, mechanical strength, flexibility, corrosion resistance, and low hydrogen permeability. Moreover, the bipolar plates must be thermally stable in the fuel cell operating temperature. Pure graphite bipolar plate is a good candidate for fuel cell application, owing to its high electrical conductivity and good corrosion resistance. However, low formability, high gas permeability, low mechanical strength, low flexibility, and cumbersome machining of complex flow-field limit the application of pure graphite bipolar plates. Similarly, corrosion of metal and uneven expansion of coated metal limit the applicability of metal based bipolar plate. Therefore, scientists and researchers are giving attention towards the development of carbon-polymer composite bipolar plate due to its low density, good corrosion resistance, light weight, good flexibility, and ease in machining or in-situ molding of flow fields during processing. The aim of this research is to develop a carbon-polymer composite bipolar plate with low density, high electrical and thermal conductivity, high flexural strength, high hardness, less hydrogen permeability and good corrosion resistance.

Monolayer graphene was developed by thermochemical reduction of NG. The synthesized graphene was characterized by SEM, EDX, XRD, HRTEM, ED, AFM, FTIR and BET. The absence of graphite 002 and 004 peaks in the diffractogram shows that monolayer graphite formed. The yield of monolayer graphene was also confirmed by SEM, HRTEM, ED, and XRD analyses. The AFM analysis of the graphene showed that the thickness was around 1 Å. The developed graphene was used as reinforcement along with natural graphite (NG), carbon black (CB), and carbon fiber (CF) to develop carbon-polymer composite bipolar plate. Similarly, three types of thermoset polymer, viz.,

resol-phenol formaldehyde (resol-PF), novolac-phenol formaldehyde (novolac-PF), and vinyl ester resin (VER), were used for compression molding of the composite bipolar plates. The NG/resin composite bipolar plates were developed and characterized to find out the optimum molding temperature. Similarly, the effects of NG, CB, and CF content on the properties of the composite bipolar plates were also studied. The developed bipolar plates were characterized thoroughly for electrical conductivity, thermal conductivity, flexural strength, shore hardness, corrosion resistance, hydrogen permeability, and morphological analysis. The in-plane electrical conductivities of the NG/CB/CF/resin composite bipolar plates, for the optimum compositions, were recorded as 415.05, 285.54, and 355.05 $S \cdot cm^{-1}$, respectively for resol-PF, novolac-PF, and VER. Similarly, the through-plane electrical conductivities of those composite bipolar plates were 99.70, 91.79, and 95.95 $S \cdot cm^{-1}$, respectively. Therefore, the through-plane electrical conductivities of the bipolar plates were edge behind the target value of 100 $S \cdot cm^{-1}$. The flexural strengths of the NG/CB/CF/resin composite bipolar plates, at the optimum compositions, were 54.23, 55.28, and 53.50 MPa, respectively. The thermal conductivity of those composites were 145.3, 128.26, and 132.4 $W \cdot m^{-1} \cdot K^{-1}$, respectively. The corrosion analysis of the bipolar plates was carried out in simulated rigorous PEMFC and AFC environment. The corrosion current density of the NG/CB/CF/resin composite bipolar plates, at the optimum compositions were well below the target of 1 $\mu A \cdot cm^{-2}$. Similarly, the hydrogen permeabilities of the bipolar plates were in the order of 10^{-9} $cm^3 \cdot cm^{-1} \cdot s^{-1}$ at 50°C. The optimum compositions of the NG/CB/CF/resin bipolar plates were further reinforced with 1% graphene, at the expense of NG, to improve the electrical conductivities. The in-plane electrical conductivities of the graphene reinforced composites were recorded as 435.31, 311.33, and 376.03 $S \cdot cm^{-1}$, respectively for resol-PF, novolac-PF, and VER resins. The through-plane electrical conductivities of those composites were 130.17, 123.5, and 129.79 $S \cdot cm^{-1}$, respectively. The reinforcement with 1% graphene also improved the mechanical strength of the composite marginally. The

corrosion current density of the composite in simulated rigorous PEMFC environment was still in the order of 1 $\mu A \cdot cm^{-2}$. Similarly, the hydrogen permeability of the composite was also in the order of 10^{-9} $cm^3 \cdot cm^{-1} \cdot s^{-1}$ at 50°C. The overall properties of the graphene reinforced composites were well above the target values of the bipolar plates for PEMFC.

A PEMFC set-up was developed to study the performance of the developed bipolar plates in real fuel cell. The use of graphene in the composite bipolar plates also showed around 10% improvement in the power density of the PEMFC. The peak power density of the PEMFC with the optimum composition of the NG/CB/CF/resol-PF composite bipolar plates was 397 $mW \cdot cm^{-2}$ at a current density of 752 $mA \cdot cm^{-2}$. The reinforcement with 1% graphene to the above composite bipolar plates increased the peak power density of the PEMFC to 437 $mW \cdot cm^{-2}$ at a current density of 827 $mA \cdot cm^{-2}$.

Keywords: Bipolar plate; Composite; Electrical conductivity; Fuel cell; Graphene; Reinforcement

Contents

List of tables

List of figures

List of symbols

A	area (cm^2)
b	breadth (cm)
d	thickness (cm)
D	maximum deflection at the center (mm)
E	electrode potential (V)
F	load (N)
I	current (A)
i	current density ($A \cdot cm^{-2}$)
K	gas permeability constant ($cm^3 \cdot cm^{-1} \cdot s^{-1}$)
l	length (cm)
L	support span distance (mm)
P	pressure (MPa)
q	heat flux ($W \cdot m^{-2}$)
R	rate of cross-head speed ($mm \cdot min^{-1}$)
t	time (s)
T	temperature (K)
V	voltage (V)
w	weight (g)
x	distance between two points (cm)
Z	rate of strain ($mm \cdot mm^{-1} \cdot min^{-1}$)
E_{corr}	corrosion potential (V)
$E_{\circ}$	equilibrium potential (V)
b_a	anodic Tafel constant ($V \cdot decade^{-1}$)
b_c	cathodic Tafel constant ($V \cdot decade^{-1}$)

i_{corr}	corrosion current density ($A \cdot cm^{-2}$)
$i_{\circ}$	exchange current density ($A \cdot cm^{-2}$)
σ	electrical conductivity ($S \cdot cm^{-1}$)
ϕ	volume fraction (%)
ϕ_c	percolation threshold (%)
ξ	effective demagnetization factor
φ	amount of hydrogen (cm^3)
χ_f	flexural strength (MPa)
κ	thermal conductivity ($W \cdot m^{-2} \cdot K^{-1}$)

Subscripts:

l	low conductivity medium
h	high conductivity medium
m	composite
δ	dimensionless parameter

List of abbreviations

AFC	**alkaline fuel cell**
AFM	**atomic force microscope**
BMC	**bulk molding compound**
CB	**carbon black**
CF	**carbon fiber**
CNT	**carbon nanotube**
DMFC	**direct methanol fuel cell**
ED	**electron diffraction**
EG	**expanded graphite**
FTIR	**Fourier transform infra-red**
GDL	**gas diffusion layer**
GN	**graphene**
GO	**graphite oxide**
HMTA	**hexamethylene tetramine**
MCFC	**molten carbonate fuel cell**
MEA	**membrane electrode assembly**
MPL	**microporous layer**
MWNT	**multi-walled nanotube**
NG	**natural graphite**
PAFC	**phosphoric acid fuel cell**
PEM	**proton exchange membrane**
PEMFC	**proton exchange membrane fuel cell**
PET	**polyethylene terephthalate**
PF	**phenol formaldehyde**
POBDS	**poly-oxy-benzene-disulfide**

PP	**polypropylene**
PPS	**polyphenylene sulfide**
PVDF	**polyvinylidene fluoride**
SAED	**selected area electron diffraction**
SEM	**scanning electron microscope**
SOFC	**solid oxide fuel cell**
TEM	**tunneling electron microscope**
US-DOE	**United States Department of Energy**
VER	**vinyl ester resin**
XRD	**X-ray diffractometer**

Chapter 1

Introduction

Introduction

1.1 Background

The global primary energy demand is increasing day by day and it is expected to increase around 50% by 2035 and during that time the demand for the electricity will be more than double. It has been predicted that 70% of this increase will come from developing nations, led by China and India [Gruenspecht, 2010]. The International Energy Outlook in 2010 predicted that world petroleum demand will increase from the current 86.1 million barrels per day to 110.6 million barrels per day in 2035. In the meantime, there would be a two-fold increase in the world oil prices. Moreover, the oil reserves have declined substantially, as compared to the discovery of new oilfields, in the recent past. Thus the present world energy scenario reveals that within the next few decades conventional fuel resources (e.g. oil, gas, etc.) would face severe shortage. Moreover, huge consumption of fossil fuels causes environmental concerns, such as global warming, which in turn enforce the need to reduce emission of carbon dioxide (CO_2), nitrogen oxides (NO_x), sulfur oxides (SO_x), volatile organic chemicals (VOCs), and particulates. Therefore, due to the probable shortage of conventional fossil fuels in the next few decades as well as the pollution associated with their use, scientists and technologists are in the search of nonconventional and efficient energy sources [Martinot and Sawin, 2009]. There are different kinds of nonconventional energy resources and technologies on which a large number of studies are being carried out worldwide. In this aspect, fuel cell is found to be one of the most stringent and promising power sources for automotive and domestic applications in future [Li and Sabir, 2005]. Fuel cell is an electrochemical device that converts the chemical energy in a fuel directly into the electrical energy. Fuel cells are not limited by thermodynamic limitations of heat engines, such as the Carnot efficiency, as the intermediate steps of producing heat and mechanical work are avoided and thus they

may generate the electrical power with high efficiency without noise [Chen, 2003; Li, 2007]. In addition, generation of power by the fuel cell is a clean process when the fuel (generally hydrogen) is produced by the electrolysis of water using solar energy. Unlike batteries the fuel cells can generate power continuously as long as the fuel and oxidant are supplied. Due to these attractive features researchers, governments, as well as industrialists are showing great interest in developing fuel cell for power generation.

1.2 Brief history of fuel cell

Fuel cells have been known to science for more than 170 years. Though, generally considered a curiosity in the 18th century, but the fuel cells became the subject of intense research and development during the 19th century. In 1800, British scientists William Nicholson and Anthony Carlisle had described the process of using electricity to decompose water into hydrogen and oxygen [Kahlbaum and Darbishire, 1899]. In 1838, Welsh lawyer turned scientist William Robert Grove, took the idea of electrolysis of water one step further in the reverse order [Grove, 1839]. The main objective of his research work was to combine hydrogen and oxygen to generate electricity. To conduct that experiment, Grove connected 30 electrochemical cells together in series. He used two platinum electrodes in each cell, where one end of each electrode was immersed in a container of sulfuric acid. The other ends of the electrodes were sealed separately and hermetically in containers of oxygen and hydrogen. The projecting ends of the electrodes were connected together through a delicate galvanometer. It was observed that a constant current was flowing between the anode and the cathode. After 24 hours, Grove noticed that the water level rose in both the sealed tubes. By combining thirty sets of these electrodes in a series, he created what he called a "gas battery" and later known as the fuel cell.

In 1889, Ludwig Mond and Carl Langer developed a hydrogen-oxygen fuel cell, with thin perforated platinum electrode, that produced a current of around 6.45 $mA \cdot cm^{-2}$ at 0.73 volts [Hoogers, 2003]. They were the first to demonstrate the practical hardware to sustain the fuel cell reaction. In 1893, Friedrich Wilhelm Ostwald experimentally determined the interrelated roles of the electrodes, electrolyte, oxidizing and reducing agents, anions, and cations in the fuel cells [Andujar and Segura, 2009]. Moreover, he provided much of the theoretical understanding of how fuel cells operate. Ostwald explained the correlation of physical properties and chemical reactions at the point of contact among electrode, gas, and electrolyte. His exploration of the underlying chemistry of fuel cells laid the foundation for later fuel cell researchers. Francis Thomas Bacon began work on alkaline fuel cells in the late 1930s, and by 1939 he built a cell using nickel electrodes operating under pressure as high as 3000 psi [Bacon, 1969; Demirbas, 2009]. During World War II, Bacon worked on developing a fuel cell that could be used in Royal Navy submarines, and in 1958 demonstrated an alkaline fuel cell using a stack of 10-inch diameter electrodes. Later, the Pratt & Whitney licensed Bacon's work for the Apollo spacecraft fuel cells [Bacon, 1985]. Contemporarily, Emil Baur of Switzerland conducted extensive research into the area of high temperature fuel cell, which used molten silver as the electrolyte [Baur and Preis, 1937; 1938]. He, along with students at Braunschweig and Zurich, also developed another unit that used a solid electrolyte of clay and metal oxides. The concept of using a sulfonated polystyrene ion-exchange membrane as the electrolyte in a hydrogen–oxygen fuel cell was first introduced by W.T. Grubb in 1955 and patented in 1959. Later, General Electric (GE) announced an initial success in mid-1960 when W.L. Grubb and L.W. Niedrach developed a small fuel cell for a program with the U.S. Navy's Bureau of Ships (Electronics Division) and the U.S. Army Signal Corps [Grubb and Niedrach, 1960]. Later, sulfonated polystyrene membranes were

replaced in 1966 by Nafion ionomer, which proved to be superior in performance and durability to sulfonated polystyrene. At this early stage of development, the membranes showed lifetimes of up to 3,000 h at low current densities and temperatures of 50 °C [Zaidi, 2009].

After Gemini program NASA decided to operate the next space programme with Alkaline Fuel Cell (AFC) systems [Stone and Morrison, 2002]. However, GE continued working on its proton exchange membrane fuel cell (PEMFC) units and by the mid 1970s water electrolysis technology using PEM was developed for U.S. Navy Oxygen Generating Plant [Appleby, 1996]. In the 1980s, the British Navy adopted PEM electrolyzer for its submarine fleet and other companies also started to look at PEMFC systems for the commercial development and end-use applications.

In 1990, Jet Propulsion Laboratory in Pasadena, California, in collaboration with the University of Southern California, developed the Direct Methanol Fuel Cell (DMFC) as a variant of PEMFC [Surampudi et al., 1994]. It was designed to supply electricity for field troops in the Armed Forces and for applications in NASA. However, the slow reaction kinetics of methanol and crossover through the membrane reduces the applicability of DMFC [Yang et al., 2001].

The PEMFC technology has evolved a lot since the first commercial development of the PEMFC unit in the 1960s. The general consensus amongst electronics manufacturers is that they will have commercially viable portable products soon. Though the DMFC remains the technology of choice for the majority of electronics developers, but the PEMFC units are considered to be the most prevalent alternative for automotive and stationary applications [Hogarth and Ralph, 2002]. The level of interest in PEMFC is

likely to grow from strength to strength in future as more high profile companies would come forward with the advancement of hydrogen storage solutions.

1.3 Basic principle of fuel cell

Fuel cells are basically galvanic cells in which conversion of fuel takes place electrochemically at ambient or elevated temperature and chemical energy of the fuel is directly converted into electrical energy. The schematic of a PEMFC is shown in fig.1.1. A single fuel cell consists of a catalyst coated cathode, an electrolyte, a catalyst coated anode, and two bipolar plates. Moreover, a complete fuel cell does have end plates, fittings, and necessary connectors. The anode provides an interface between the fuel and the electrolyte, catalyzes the fuel reaction as shown in eq.1.1, and provides a pathway through which free electrons are conducted to a load via an external circuit. The cathode provides an interface between the oxygen and the electrolyte, catalyzes the oxygen reduction reaction (eq.1.2), and provides a path through which free electrons are conducted from the load to the oxygen electrode via the external circuit. The electrolyte acts as the separator between hydrogen and oxygen to prevent mixing and, therefore, prevents direct combustion. It completes the electrical circuit by transporting protons from the anode side to the cathode side. The transmitted protons react with the oxygen and electrons to produce water on the cathode side as shown in eq.1.2. The overall reaction in which the hydrogen and the oxygen combine to produce water is shown in eq.1.3. The Gibbs free energy of the overall reaction is around $-237.13\ kJ{\cdot}mol^{-1}$. At a pressure of 1 bar and a temperature of 25°C, the corresponding open circuit potential corresponding to the Gibbs free energy of the overall reaction is 1.229 V.

The reaction mechanism of PEMFC is shown below.

Anode reaction: $H_2 \rightarrow 2H^+ + 2e^-$ (1.1)

Cathode reaction: $\frac{1}{2}O_2 + 2H^+ + 2e^- \rightarrow H_2O$ (1.2)

Overall reaction: $H_2 + \frac{1}{2}O_2 \rightarrow H_2O + heat$ (1.3)

Fuel cell is similar to a battery as it has anode, cathode, and electrolyte. But it is different from a battery as it does not contain any fuel in it; instead the energy in the fuel, which is fed from the outside, is used to generate electricity.

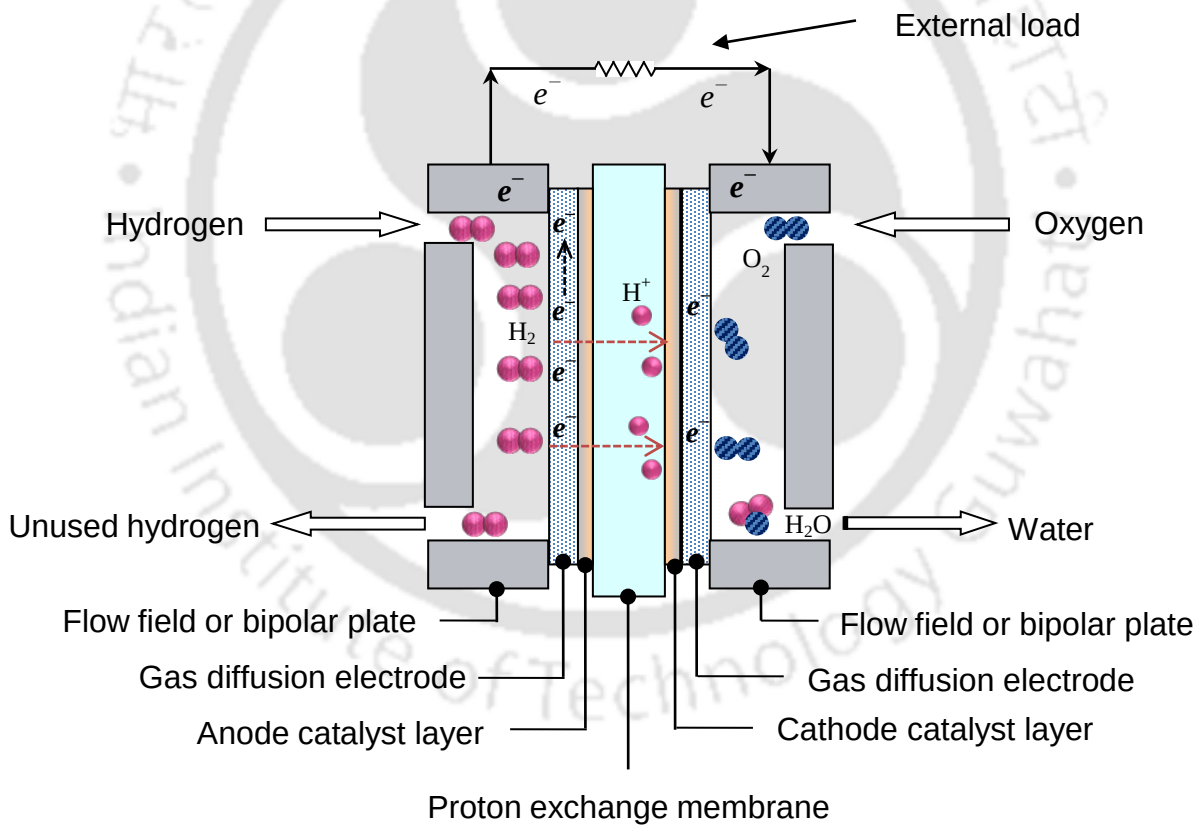

Figure 1.1: Schematic of a PEMFC

Table 1.1: Detailed classification of fuel cells

	Low temperature fuel cell				High temperature fuel cell	
	PEMFC	DMFC	AFC	PAFC	MCFC	SOFC
Electrolyte	Proton exchange membrane	Proton exchange membrane	Aqueous KOH	Conc. H_3PO_4	Molten carbonate	Pervoskites (Ceramic)
Electrodes	Carbon paper	Carbon paper	Transition metals	Carbon	Nickel and nickel oxide	Pervoskite, pervoskite-metal cermet
Catalyst	Pt	Pt and/or Pt-Ru	Pt	Pt	Electrode material	Electrode material
Interconnect	Carbon or metal	Carbon or metal	Metal	Graphite	Stainless steel or Nickel	Nickel, ceramic, steel
Operating temperature (°C)	25 – 80	< 100	50 − 200	≈ 220	≈ 650	800 – 1000
Fuel	Hydrogen	Methanol	Hydrogen	Hydrogen	Natural gas, coal	Natural gas, coal
Mobile ion	H^+	H^+	OH^-	H^+	CO_3^{--}	O^{--}
Prime cell components	Carbon based	Carbon based	Carbon based	Graphite based	SS based	Ceramic
Power range	Watts / kilowatts	Watts	Watts / kilowatts	Kilowatts	kilowatts / megawatts	Megawatts
Areas of application	Automotive, domestic, distributed power	Vehicles, small appliances	Space	Distributed power generators	Power plants, combined heat and power	

1.4 Types of fuel cell

Fuel cells are generally categorized either by their electrolyte or by the operating temperature. The characteristics of the electrolyte material determine the kind of chemical reactions that take place in the cell, the optimal operating temperature in which the cell operates, the fuel required, and other factors. These characteristics, in turn, affect the applications for which these cells are most suitable. There are several types of fuel cell currently under development, each with its own advantages, limitations, and potential applications. Table 1.1 summarizes the detailed classification of fuel cells.

1.5 Different components of PEMFC

As mentioned in section 1.2, the basic components of a PEMFC are (i) a catalyst coated anode, (ii) a catalyst coated cathode, (iii) a solid polymer electrolyte, and (iv) two flow field plates. Usually, carbon papers are used as the electrode material for PEMFC system. The membrane sides of the electrodes are usually coated with a microporous layer of fine grade carbon particles. The MPL or the gas diffusion layer (GDL) regulates the uniform distribution of fuel and oxidant over the catalyst layer [Wang et al., 2006]. The hydrogen and oxygen gases are supplied to the anode and the cathode with the help of the flow field plates. The most widely implemented electrolyte in PEMFC is Nafion, manufactured by DuPont. Nafion and related polymers are comprised of perfluorinated back-bones, which provide chemical stability, and of sulfonated side-groups which aggregate and facilitate hydration. The hydrated acidic regions allow facile transport of protons through the membrane [Ma et al., 2003]. The electrons generated at the anode side (eq.1.1) are drawn with the help of the conductive flow field plate. The fig.1.2 shows the individual components of a PEMFC stack with three unit cells. In a fuel cell stack, these flow field plates are designed such that one side of the plate is used for hydrogen gas flow and the

other side is used for oxygen gas flow. Thus, in such configuration the flow field plates are known as bipolar plates. The roles of bipolar plates are elaborated in the next section.

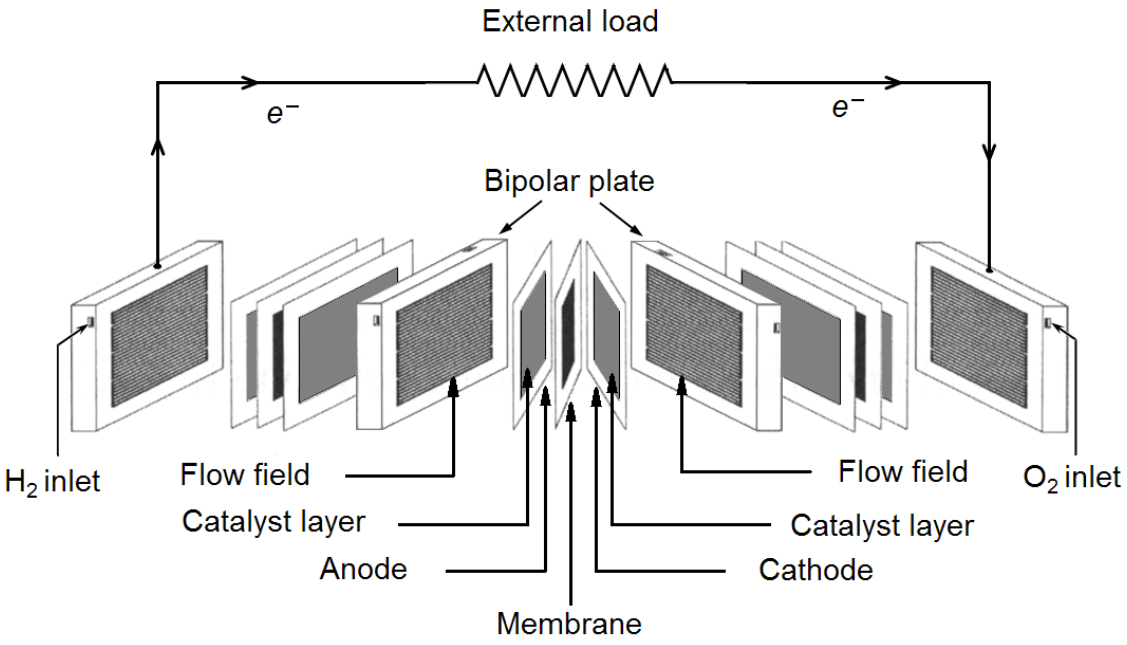

Figure 1.2: Schematic of a PEMFC stack with three unit cells

1.6 Bipolar plate

It is needless to mention that the fuel cell is a high current and low voltage electrochemical power source. In ideal condition, the open circuit potential of the cell is 1.229 V and it further reduces when current is drawn from the cell. Therefore, several cells have to be connected in series to generate a useful voltage and equivalent power output. Such a collection of fuel cells in series with repetitive units is known as fuel cell stack. A marginal increase in the ohmic resistance, due to the interconnections of the individual cell, costs to a high power loss. Therefore, to reduce the unwanted ohmic loss, there is a need of an interconnector which connects the entire anode surface of a cell directly to the cathode of the adjacent cell and vice versa. The electrically conductive interconnector between two adjacent unit cells is termed as the bipolar plate [Larminie

and Dicks, 2000]. Figure 1.2 shows a PEMFC stack with two such bipolar plates. Bipolar plate serves as an anode face to one cell and cathode face to another cell. However, the plates at the ends of a stack have the monopolar/unipolar configuration with either the anode flow field or the cathode flow field. Bipolar plate is one of the vital components of low temperature fuel cells, which may contribute up to 80% of the total weight of the PEMFC stack [Hermann et al., 2005]. Recent cost analysis shows that 38% of the total cost of the PEMFC stack is incurred by the bipolar plate followed by the cost of electrodes, membrane, and catalysts as 32, 12 and 11%, respectively as shown in fig.1.3 [Kamarudin et al., 2006].

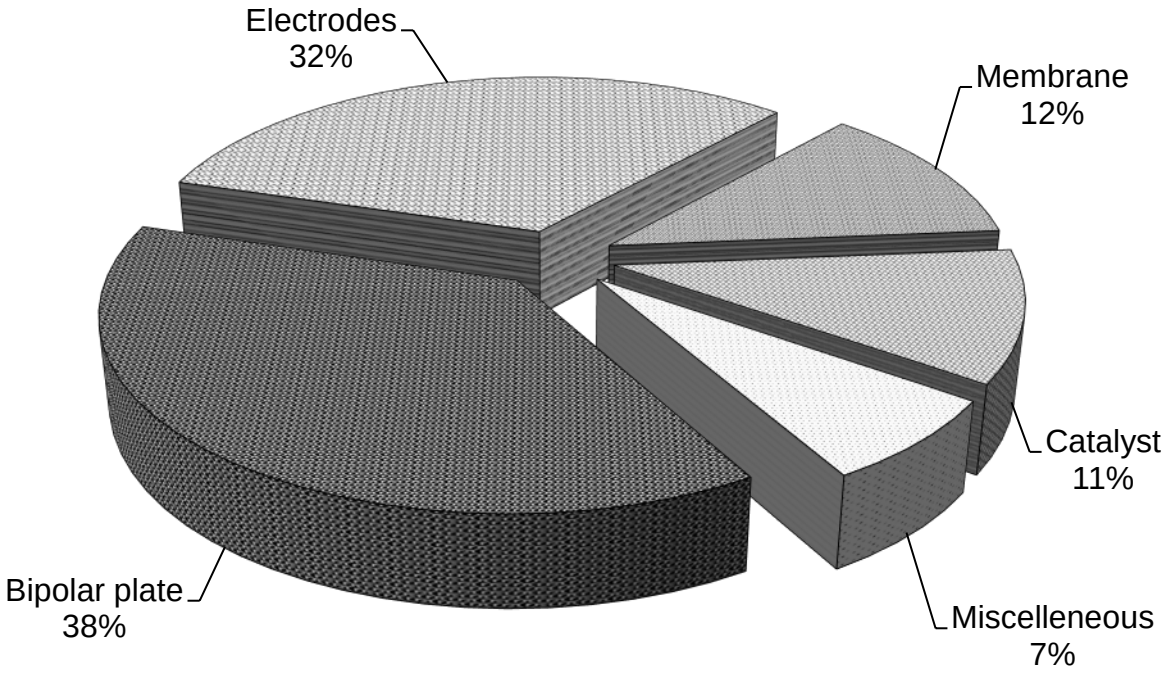

Figure 1.3: Component cost of PEMFC stack

The main functions of the bipolar plates in a PEMFC stack are [Larminie and Dicks, 2000], to

(i) support the membrane electrode assembly (MEA) robustly,

(ii) distribute reactant gases uniformly over the active areas,

(iii) conduct current between adjacent cells,

(iv) remove heat from adjacent cells, and

(v) prevent leakage of reactant gases and coolant.

Moreover, the bipolar plate also plays an important role in humidification and water management within the cells. Therefore, to facilitate the above mentioned functions, the bipolar plates must have [Middleman et al., 2003],

(i) less porosity with high mechanical strength,

(ii) high bulk electronic conductivity with low contact resistance,

(iii) high thermal conductivity,

(iv) integrated and uniformly distributed channels,

(v) high corrosion resistance to the fuel cell environment, and

(vi) easy processability for designing flow fields.

The development of materials suitable for use as bipolar plates is technically exigent for not only to maintain multifunctional characteristics but also to reduce the cost and weight of the bipolar plate. The U.S. Department of Energy's (US-DOE) 'Fuel Cells in Transportation Program' has set a bipolar plate cost target of $ 10/kW, which roughly deciphers into a cost range of $1–2 per plate (500 cm^2 area) [US-DOE weblink]. The US-DOE suggested various properties for a suitable bipolar plate for PEMFC application.

Table 1.2 shows the latest benchmark required for the bipolar plate [US-DOE weblink; Liao et al., 2008].

Table 1.2: Various benchmark for bipolar plates in PEM fuel cell application

Required properties	**Target values**
Low density	$< 2\ g{\cdot}cm^{-3}$
Low gas permeability	$< 2\times10^{-6}\ cm^{3}{\cdot}cm^{-2}{\cdot}s^{-1}$ at 80°C and 3atm
High electrical conductivity	$> 100\ S{\cdot}cm^{-1}$
High thermal conductivity	$> 10\ W\ (m\ K)^{-1}$
High flexural strength	> 50 MPa*
Highly flexible	3–5 % deflection at mid-span
High shore hardness	> 40*
High corrosion resistance	$< 1\ \mu A{\cdot}cm^{-2}$

* Plug power's target

The above properties may be achieved by choosing the suitable material for the bipolar development. The next section discusses different types of bipolar plate based on the material used.

1.7 Types of bipolar plate

Different type of materials like metal sheet, coated metal sheet, graphite, flexible graphite, carbon composites etc. are under investigation for the development of suitable bipolar plates. Each material possesses the ability to meet one or more of the recommended target (table 1.2). However, finding a suitable bipolar plate having all the required properties along with low cost is still in progress. Different types of materials that have been widely used for the development of bipolar plates for PEMFC application are discussed below.

1.7.1 *Metal bipolar plates*

Hermann et al., 2005, reviewed and discussed different types of materials for the bipolar plate in PEMFC. They have suggested that the metal or coated metal might be a good

choice keeping in mind the reduction in thickness and easy processibility (flow field design) of the bipolar plate. Moreover, metal bipolar plates have high mechanical strength, high durability to shocks and vibrations, very high electrical and thermal conductivities, and no gas permeability [Yuan et al., 2005, Tawfik et al., 2007]. However, the main drawback of the metallic bipolar plate is the low corrosion resistance to the harsh acidic, humid, and redox environment of PEMFC. The dissolution of metal ions due to the corrosion may also contaminate the membrane and poison the catalyst. As a result, the lifetime as well as performance of the fuel cell decreases [Davies et al., 2000]. Several metals and their alloys though exhibit considerable corrosion resistance to the PEMFC environment by forming a passive surface layers on it, but increases the surface resistivity of the plate and eventually reduces the performance of the cell [Wind et al., 2002]. Therefore, considerable attempts are being made using noble metals, stainless steel, and various coated materials with nitride and carbide based alloys to improve the corrosion resistance of the metals used, without sacrificing surface contact resistance [Antunes et al., 2010; Lee and Lim, 2010; Wu et al., 2009; Fu et al., 2008; Wang et al., 2004; Davies et al., 2000]. However, still the corrosion of the metal plate and uneven expansion of coated metal at the fuel cell temperature are the limitations.

1.7.2 *Graphite bipolar plates*

In the early PEMFC designs, and still in the laboratory use, bipolar plates were made of pure graphite into which flow channels were machined [Rinn and Bornbaum, 2005]. Graphite was already known for its extensive application as a bipolar plate in phosphoric acid fuel cell (PAFC) [Ghouse et al., 1998, 2000; Steele and Heinzel, 2001]. The nature of graphite makes it an excellent choice for bipolar plate fabrication as far as material requirements are concerned. It offers the advantages of low density, high corrosion resistance to fuel cell environment, high thermal conductivity, high electrical

conductivity, and very low contact resistance. However, the graphite bipolar plates are prone to hydrogen gas permeability and brittle in nature. Therefore, machining the flow field over the pure graphite plate is complicated, time consuming, and labor intensive process. Before machining, the raw graphite material has to be cut into slabs of the required thickness followed by vacuum-impregnating with some resin material for gas-tightness [Washington et al., 1994, Wang et al., 2005], grinding and polishing to the desired surface finish. The channels and ribs of the graphite bipolar plate made in this way are of several millimeters. Therefore, scientists and researchers are searching for an alternative bipolar plate material due to the low formability, high gas permeability, low mechanical strength, and low flexibility of graphite.

1.7.3 *Carbon based composite bipolar plates*

In order to overcome the issues relating to graphite and metal based bipolar plates, the efforts are being made in recent years to develop polymer composite bipolar plates [Dhakate et al., 2007; Lee, 2009]. Several researchers and developers studied the metal-based polymer composite bipolar plates and its possible use in fuel cell [Hermann et al., 2005; Kuo and Chen, 2006; Yokoyama et al., 2008; Lee et al., 2009; Hsiao et al., 2010]. However, the preferential removal of metal ions in the PEMFC environment reduces the applicability of metal based polymer composite bipolar plate. In this regard, composite made of carbon based materials, and polymer as binder, is a promising alternative to both metal and pure graphite bipolar plates, and has the advantages of low-cost, ease in machining or in situ molding of complex flow fields during processing, good corrosion resistance, and light weight [Adrianowycz et al., 2009; Chang et al., 2002; Chervinko et al., 2003; Cho et al., 2004; Du et al., 2010; Huang et al., 2005; Kuan et al., 2004; Lee et al., 2007; Rio et al., 2000; Ruge and Buchi, 2001; Wolf and Porada, 2006; Yin et al., 2008]. Therefore, carbon based composite bipolar plates have got significant attention in

the recent past. However, it is to be noted that the development of a carbon composite bipolar plate with high electrical conductivity and high mechanical strength is really challenging. Carbon based composite bipolar plates have been made using thermoplastic (poly-propylene, polyethylene, polyvinylidene fluoride, etc.) or other thermosetting resins (phenolics, epoxies, vinyl ester, etc.). In the early years of development of graphite-polymer composite bipolar plate, thermoplastics were preferred as the binder material. However, in the late eighties, the preference changed to thermosetting resin matrix precursor due to its short processing time, low melt flow viscosity, and the large fill factor [Mehta et al., 2003; Cunningham and Baird, 2007]. Moreover, thermoset resins provide heat and corrosion resistance without shrink or excessive stress.

In this study, attention has been given towards the development of composite bipolar plate with thermosetting resins and carbon based materials, in order to fulfill all the benchmarks provided in table 1.2 for fuel cell application. An extensive literature survey on the carbon composite bipolar plate has been carried out and reported in the next chapter.

Chapter 2

Literature Review

Literature Review

The importance of bipolar plates and its importance in the development of a PEMFC system have been discussed in the previous chapter. Extensive research and development efforts are being given worldwide to develop bipolar plates in order to improve the performance of PEMFC stack. It was discussed in the previous chapter that the carbon based composite could be a potential candidate for the bipolar plate. This chapter provides an extensive literature survey emphasizing recent advancement in the research and development of composite bipolar plate for PEMFC.

2.1 Recent advances in composite bipolar plate

The fuel cell technology and the innovations related to it were reviewed by Appleby (1992). He quoted that the weight of the bipolar plate may be several times that of the other active stack components. Moreover, the weight of the total stack may be about two to three times the weight of the cell components, including bipolar plate. He also estimated the cost incurred by the graphite bipolar plates and its substrate component which was around \$90 kW^{-1} [Appleby, 1994]. It was the highest cost incurred by any component in a PAFC system. Therefore, to find significant applications of fuel cell in 21^{st} century, he emphasized on the innovative approaches in material and engineering design of cell components, particularly the bipolar plate. He suggested the use of light weight material such as those used in certain aerospace engineering. Prater (1994) also mentioned the use of composite bipolar plate for stationary applications of PEMFC. It is found that carbon composite is a promising alternative to both metal and pure graphite bipolar plates, and has the advantages of low-cost, ease in machining or in-situ molding of complex flow fields during processing, good corrosion resistance, and light weight [Hermann et al., 2005; Mathur et al., 2008]. Mehta and Cooper (2005) have done

extensive studies on PEMFC design and development and reported the state of art of development of bipolar plate by various processes. The common resins used to develop bipolar plates were polyvinylidene fluoride (PVDF), polypropylene (PP), polyethylene terephthalate (PET) and phenol formaldehyde (PF), vinyl ester resin (VER), polyphenylene sulfide (PPS), and epoxy resins [Mehta and Cooper, 2005; Cunningham and Baird, 2006]. However, the properties of the bipolar plate developed by different processes were not reported. An extensive effort has been given worldwide to develop carbon composite bipolar plate with high electrical conductivity, mechanical strength, corrosion resistance, thermal conductivity, and low permeability to hydrogen. Moreover, the composite bipolar plate must be flexible enough to withstand the compaction pressure in stacking. Due to high compression pressure during stacking, the rigid bipolar plates imprint on the MEA and prone to damage the GDL. Plate with adequate flexibility reduces the deformation of GDL.

Colling et al. (1978) in Ashland Chemical Co., Columbus, Ohio, worked for U.S. Army Mobility Equipment Research and Development Command to evaluate the possibility of using a composite bipolar plate in hydrogen fuel cells. Their aim of that program was to screen, select, prepare, and evaluate various graphite/resin composites that could be molded as bipolar plates for the hydrogen fuel cell. They used novolac type phenol formaldehyde resin as a binder along with graphite and carbon black. The prepared bipolar plates were characterized for electrical conductivity, flexural strength, hydrogen imperviousness, and thermal stability. They attempted to optimize the composition of the bipolar plate. They suggested that 25wt% of resin should be mixed with 6wt% of hexamethylene tetramine catalyst and the recommended resin to filler composition was 3:1 by weight. Moreover, the authors also blended different grades of graphite material to fabricate composite bipolar plate with high electrical conductivity. The highest electrical

conductivity of the composite for the optimum composition was below 100 $S \cdot cm^{-1}$ and flexural strength of the same composite was around 27 MPa. Radio tracer technique was used to quantify the amount of extractable materials leached from the bipolar plates under prolonged H_3PO_4 treatment at 180°C. Leaching of organic C-14 from the resin material was reported using that process. The hydrogen gas permeability of the sample was satisfactory upto 2.72 atm pressure. However, the author did not study the other important properties of the composite bipolar plate and they worried about the long term performance degradation of the fuel cell due to leaching of organic C-14. They also reported that cracks were visible in some of the test samples after 20 hours of post curing at 200°C. They suggested that increase in the molding time might help to overcome this problem. Nevertheless, this may be the first reported literature on possibilities of using composite bipolar plate in PEMFC. Later, the method of preparation and composition of phenolic resin-graphite composite was optimized by Yin et al. (2007). The authors studied the effect of PF content, molding temperature, and molding time on the electrical and mechanical properties of the composite. It was reported that the electrical conductivity of the composite decreased but the mechanical strength of the composite increased with the increase in PF content. On the other hand, the electrical conductivity of the composite showed decreasing trend initially upto 220°C and 45 min molding time. With further increase in the molding temperature and time the electrical conductivity reached its maximum value for molding temperature of 240°C and molding time of 1 h. The electrical conductivity again showed decreasing trend with increase in temperature as well as molding time. The mechanical strength of the composite was found to be maximum at the same condition. The best electrical conductivity and three-point bending strength of the composite were 142 $S \cdot cm^{-1}$ and 61.6 MPa, respectively, when the PF content was 15% and molded at 240°C for 1 h. However, the composition needs to be

tested for other properties of the bipolar plate too. They have also used carbon nanotube (CNT) to enhance the electrical conductivity and mechanical strength of the composite [Yin et al., 2008]. The authors did not achieve significant improvement in the electrical conductivity and flexural strength of the composite. They reported that reinforcement with 3% of Fenton/UV treated CNT improved the electrical conductivity from 142 to 145.2 $S \cdot cm^{-1}$. Similarly, the improvement on the mechanical strength of the composite was also around 10% only. Therefore, CNT is not a cost effective reinforcement for the development of composite bipolar plate.

The surface modification of NG-PF composite with expanded graphite (EG) was carried out by Li et al. (2008). The green NG-PF composite was sandwiched between two thin layers of EG to improve the surface conductivity of the composite bipolar plate. The original contact resistance of the composite was around 3.86 $m\Omega \cdot cm^2$ and it was reported to be reduced by around 37% using that process. However, the additional thin films of EG increased the bulk resistance of the composite and it increased linearly with the thickness of the EG layers. This effect might be due to the inclusion of the contact resistance between the original NG-PF composite and EG layers. Moreover, the individual resistance of the two EG layers also came into picture. The bulk resistance of the composite, with lowest contact resistance, was reported as 26.46 $m\Omega \cdot cm$ which was beyond the benchmark shown in table 1.2. Similarly, the surface modification of the NG-PF composite also increased the corrosion current density of the bipolar plate from 0.20 to 0.63 $\mu A \cdot cm^{-2}$. Though these values were well below 1.0 $\mu A \cdot cm^{-2}$, the upper limit of corrosion current density set by US-DOE for composite bipolar plate, but the simulated PEMFC environment was not rigorous [Ma et al., 2000; Wang et al., 2004; Fu et al., 2008; Choi et al., 2009]. From this study, it can be understood that the method of surface modification with EG may be a viable solution to decrease the contact resistance of such

plate which have high bulk electrical conductivity (through-plane conductivity). In such cases, a reduction in the contact resistance may be possible by compromising certain amount of bulk conductivity of the composite.

Kang et al. (2010) studied the effect of graphite particle size and its content on the properties of composite bipolar plate made up of resole type PF resin and NG. However, the through-plane electrical conductivity of the composite was significantly low at the optimum composition. The air permeability of the composite, for the optimum composition, was around 1.7×10^{-5} $cm^3 \cdot cm^{-2} \cdot s^{-1}$, which was quite high in comparison to the targeted benchmark for hydrogen permeability (table 1.2). Therefore, further improvements were required to address the above mentioned drawbacks of the NG-PF composite bipolar plate.

In the beginning of 1980s, Lawrence developed low cost composite bipolar plate in GE motors using electrically conductive graphite and thermoplastic fluoropolymer. The bipolar plates were compression molded using a mixture of graphite and fluoropolymer in a weight ratio of 5:2 to 16:1. They claimed that the bipolar plates showed excellent corrosion resistance to various corrosive environments. However, the bulk electrical conductivity of the composite was below 0.4 $S \cdot cm^{-1}$, that was extremely low in comparison to the required value as shown in table 1.2. The process for molding corrosion resistant composite bipolar plate was also patented by Hoggins and Watts (1982) of Ashland Chemical Co., Columbus, Ohio. The authors basically optimized the bipolar plate fabrication process invented by their predecessor Colling and his colleagues. They used furfural (OC_4H_3CHO) as a wetting agent to the resin-graphite system. The authors followed the idea of mixing different grades of graphite to achieve the desired properties of the bipolar plate. They prepared the graphite filler by mixing 100 grams

Asbury graphite 7101, 80 grams Asbury graphite 4015, and 20 grams Asbury 250-micro graphite. Later, 75 grams of graphite mixture was mixed thoroughly in an Osterizer blender with 25 grams of phenol formaldehyde resin containing 6% hexamethylene tetramine (HMTA). The amount of furfural added to the resin-graphite mixture was kept 1.5%. The whole mixture was then compression molded in a nickel coated steel mold at 100°C and cured at 185°C; under 22 MPa pressure. The authors carried out the corrosion testing of the bipolar plate in simulated fuel cell environment. They simulated the fuel cell environment by treating the bipolar plate for 450 hours in 85.6% H_3PO_4 at 190°C and recorded weight loss upto 7.1%. Hence, there was a chance of membrane and catalyst contamination by the dissolution of the bipolar plate material. Later, Tomantschger et al., (1986) developed low cost AFC using composite bipolar plate. They also claimed that the iR contribution from the bipolar plate to each unit cell was minimized by the use of composite material. Spurrier (1986) developed an apparatus which was a specially designed liquid electrolyte fuel cell that used several graphite-resin composite bipolar plates. At the end of the same year, Spurrier and his colleagues used compression molded graphite-resin composite bipolar plate to design and improve flow channel configuration. They claimed to achieve better performance in fuel cell by improving the flow field design and maintaining more uniform pressure drop across the plates. Similarly, Granata Jr. and Woodle (1989) also used composite bipolar plate to design skewed reactant and oxidant flow field channels for uniform distribution of stack compression load. Takahashi et al. (1990) used graphitic molding technique to develop composite bipolar plate by a mixture of graphite powder and mesophase pitch. They used mesophase pitch as a binder in spite of conventional polymeric resin. However, the electrical conductivity of the developed bipolar plate was around 20 $S \cdot cm^{-1}$ which was quite low in comparison to the

benchmark. The flexural strength of the developed bipolar plates was also quite below the target values.

Abens (1995) worked in a joint venture of Energy Research Corporation and Texas A&M University to develop lightweight composite bipolar plate for PEMFC. In the project, they focused on the selection and evaluation of conductive plastic material for bipolar plates. They also worked on the optimization of structures of electrode and MEA, followed by the evaluation of cell performance with different active areas. However, the main objective of the project was found to be limited to testing and evaluation of different type of conductive plastic composites from three different sources (LNP Engineering Plastics Inc., RTP Co., DuPont, and Bekaert). The conductive plastic samples were actually a conductive filler reinforced thermoplastic polymer. The conductive samples were further treated to improve the bulk electrical conductivity. The treatments were categorized as (i) hot pressing of carbon cloth to the plastic surface, (ii) introducing some carbon particles within the conductive plastic, (iii) sanding the surface, and (iv) application of silver epoxy to the conductive plastics. The samples with electrical conductivity higher than 1 $S \cdot cm^{-1}$ were used to fabricate the bipolar plates for evaluation of performance in single cell tests. Though the power density was an order of magnitude below the criterion proposed by the U.S. DOE, but the author believed that the gravimetric power density could be achieved by the use of lightweight bipolar plates.

Busick and Wilson (1998), used VER as a binder and graphite as an electrically conductive filler to develop composite bipolar plates for PEMFC. The composition and method of preparation of the bipolar plate was later patented by them [Wilson and Busick, 2001]. The molding compound was prepared by gradually and thoroughly mixing the graphite powder to the resin. The resin was premixed with the required amount of

catalyst and promoter in a hand mixer. The thick paste was then compression molded at 100°C under 140 kg·cm^{-2} pressure for 15 min. The developed bipolar plates were post-cured in an oven at around 80°C for 2 h. It was reported that 65–70 wt% graphite was required to achieve electrical conductivities higher than or equal to 100 S·cm^{-1}. Therefore, 68 wt% of the graphite powder was selected as the baseline composition to develop composite bipolar plate for fuel cell testing. The highest electrical conductivity was reported as 120 S·cm^{-1} with flexural strength of around 31 MPa. Moreover, the hydrogen permeability of the composite was reported as untraceable. The performance of the fuel cell with these bipolar plates was comparable to that with the SS bipolar plates. According to the authors, other additives may further improve the performance and/or processability of the composite bipolar plate. They suggested that certain microfiber can be added to improve the flexural as well as tensile strength of the composite. Similarly, changes in the catalyst/promoter system might give rapid cure and also extend the shelf life of the precursor compound. However, they did not discuss about thermal conductivity, corrosion resistance, and thermal stability. It was also not specified whether the electrical conductivity was measured for in-plane or through-plane. Scholta et al. (1999) used proprietary graphite composite bipolar plate (SGL 001) for testing and evaluation of performance of a PEMFC. They showed that the performance of the PEMFC, using their bipolar plates, was edge over the performance of the cell with SS bipolar plates.

Sammes and Boersma (2000), and Chalk et al. (2000) investigated technical requirements and challenges of fuel cell in residential and transportation applications, respectively. Sammes and Boersma (2000) and Chang et al. (2000) emphasized on the use of graphite-resin composite bipolar plate, over machined graphite plate, for high volume manufacturing process. Similarly, Chalk et al. (2000) reported that the compression

molded carbon composite bipolar plates, developed in The Institute of Gas Technology, USA, showed performance similar to the machined graphite bipolar plates. They also expected the goal of $10/kW could be achieved at a production level of 500,000 units per year. However, detailed compositions of the bipolar plates were not reported.

Besmann et al. (2000) developed carbon-carbon composite bipolar plates for PEMFCs by slurry molding a chopped fiber preform followed by sealing with chemically vapor-infiltrated carbon. They prepared the slurry by dispersing 400μm long PAN based carbon fiber (CF) in water based phenolic resin. The fiber to phenolic resin mass ratio was 4:3 and the slurry was vacuum molded at 150°C to produce isotropic preform material with 18 vol% fiber. The machined bipolar plates were later treated by chemical vapor infiltration technique at around 1500°C. The bipolar plate was coated with a conductive carbon layer during chemical vapor infiltration. Moreover, the open porosity of the bipolar plate was also reduced by this process. The reported bulk electrical conductivity of the composite was around 200–300 $S \cdot cm^{-1}$. They also reported the biaxial flexural strength (not three-point flexural strength) of the composite bipolar plate as around 175 MPa. However, a few of the important parameters of the bipolar plates such as gas permeability, corrosion resistance, and flexibility were not tested. It was comprehended that costs should not be a barrier to use their plates in PEMFC applications.

The study so far showed that the composite bipolar plate, using inorganic material, was in a very preliminary and conceptual stage of development till the late 2000. However, in recent years, the composite bipolar plate got immense attraction being one of the vital components of the PEMFC. Davis (2002) developed composite bipolar plate for electrochemical cells using core layer of a metal with the expectation that the cladding layers would protect the metal from corrosion in the fuel cell environment. However,

corrosion testing of the composite bipolar plate was not studied and there may be a possibility of development of micro-cracks due to uneven expansion of the plate in fuel cell environment. It was also expected to have high electrical and thermal conductivity of the cladded composite bipolar plate. However, the through-plane electrical conductivity and thermal conductivity were also not reported. Del Rio et al. (2002) developed composite bipolar plate by compression molding PVDF-CB preform. They mixed PVDF with powdered CB in a Haake torque rheometer type internal mixer at 200°C for 15min. The preform mixture was then compression molded with the help of a hydraulic press to fabricate bipolar plate of 3mm thickness. The dynamic mechanical analysis and electrical conductivity of the composite was measured. However, the electrical conductivity of the composite bipolar plates was not up to the mark. The maximum electrical conductivity of the composite was reported as 2.36 $S \cdot cm^{-1}$ for 40 wt% CB content at 30°C. The electrical conductivity of the same composite decreased further with increase in temperature and reached 1.94 $S \cdot cm^{-1}$ at 90°C. The developed bipolar plate showed poor performance in fuel cell testing as compared to graphite bipolar plate, when tested in fuel cell. The maximum output power with the graphite bipolar plate was around 100 $mW \cdot cm^{-2}$ at 200 $mA \cdot cm^{-2}$ while, with the developed bipolar plate, it was around 65 $mW \cdot cm^{-2}$ at 150 $mA \cdot cm^{-2}$. Chen and Kuo (2006), used Nylon 6 as binder to develop CB filled composite bipolar plate using injection molding technique. However, the highest reported electrical conductivity was only 11.67 $S \cdot cm^{-1}$ for 35% CB loading. Subsequently, the fuel cell performance was inferior due to the high resistance of their bipolar plate showed inferior performance in fuel cell testing. The authors also concluded that their injection molded composite bipolar plates were not suitable for high temperature PEMFC application and it could contribute to the high internal resistance of the PEMFC stack. Therefore, further investigations were required to enhance the electrical conductivity of the composite.

Loutfy and Hecht (2003) developed and patented a composite bipolar plate by embedding a plurality of electrically conducting elements within the channels of a plastic sheet. The conducting elements were made of aligned CF-polymer composite cylinder. The plastic sheet was having serpentine flow field pattern, where conductive elements were embedded perpendicular to the plate in a regular pattern. The conducting elements were embedded in such a way that one end of each element being in electrical contact with the anode of a fuel cell and the other end of the element being in electrical contact with the cathode of the adjacent cell, or vice versa. In unipolar configuration the other end of the element being in electrical contact with an electrical conductor for collecting electrons produced across the electrodes. The inventors claimed to decrease the cost of the bipolar plate as the plastic content of the plate was more than 70%. However, the authors did not report any property of the bipolar plate and its performance in fuel cell. The technique of Loutfy and Hecht (2003) was replicated by Chen et al. (2005) to develop a heterogeneous composite bipolar plate for PEMFC application. They used toothbrush technique to replace the rib with bunch of CFs. By this method, they changed the nature of the contact between the bipolar plate and the electrode, from a hard flat surface to the soft tips of millions of flexible fibers against the carbon electrode. Therefore, reported contact resistance was half of that of a pure graphite bipolar plate. The cell equipped with the plate showed better performance compared to the one with the conventional graphite plate. However, the authors emphasized that a further investigation was required for best material selection, as well as long term studies.

Iqbal et al. (2003) developed electrically conductive nanocomposite bipolar plate with molded channels for use in a PEMFC. The developed bipolar plate was made up of a resin and a plurality of multiwall CNTs along with another reinforcing agent in order to serve to provide added mechanical strength. The suggested reinforcing agents were any of

chopped glass fiber, chopped CF, and/or mats of CF. The reinforcing agent was kept at about 10–25 wt% and the CNTs were kept at about 10–60 wt%. The resin, nanotube, and the reinforcing agents were mixed in a commercial blender and made into pellets. The pellets were then either compression molded or injection molded to develop the final bipolar plates. The bipolar plates were claimed to achieve a mechanical strength of around 52 MPa with a deflection of 9.14 mm at yield. Moreover, it was claimed that the performance of the fuel cell using the nanocomposite bipolar plates was comparable to that of a cell having a commercially available resin densified pure graphite bipolar plate. However, the electrical conductivity, hydrogen permeability, and other important properties of the bipolar plates were not reported. Du et al., 2004, developed poly(arylene disulfide) based graphite nanocomposites by in-situ ring opening polymerization. The electrical conductivity of the developed nanocomposite was 10^{-3} S·cm^{-1} for 5 wt% graphite content. They reported the possibility of using their nanocomposite as a bipolar plate material for PEMFC. However, the electrical conductivity of the nanocomposite was far below the benchmark for electrical conductivity of bipolar plate (table 1.2). Chen et al. (2004), used selective laser sintering technique to develop phenolic resin bonded graphite composite bipolar plate. Novolac type phenolic resin powder was mixed with 31 μm size natural graphite powder in a roller mixer and subsequently loaded into a selective laser sintering machine to develop green bipolar plates. The bipolar plates were later impregnated with carbon black and carbonized in a vacuum furnace. The flexural strength of the composite was reported as around 12 MPa which was far below the target value. Similarly, the electrical conductivity of the composite was recorded as 80 S·cm^{-1} and it was also below the target electrical conductivity. Cho et al. (2004) also developed graphite-polymer composite bipolar plate by compression molding technique. The lowest bulk electrical resistivity of the composite was reported as 131.1 Ω·cm, while it was

measured as 16.85 Ω·cm for graphite by the same method. However, the contact resistance of the composite was found comparable to that of the graphite. The flexural strength of the composite was reported as 20.5 and 38.6 MPa for in-situ channeled bipolar plate and plain bipolar plate. The authors reported that the bipolar plate showed no leakage under 5 bar pressure. However, they did not explain the measurement technique and also did not mention the type of gas used in the experiment.

Table 2.1: The BMC formulation used by Kuan et al. (2004)

Component	Composition	BMC composition
VER (wt%)	75	20–40
Low profile agent (wt%)	8	
Styrene monomer (wt%)	17	
tert-Butyl peroxybenzoate (phr)*	1.8	
Zinc stearate (phr)	3.5	
MgO (phr)	1.8	
Graphite powder (wt%)		60–80
Total (wt%)		100

*phr: parts per hundred parts of resin

A novel composite bipolar plate for PEMFC was developed by bulk molding compound (BMC) technique and characterized for electrical, physical, mechanical, and thermal properties by Kuan et al. (2004). They studied the effect of graphite content and size of the graphite powder on the properties of a composite bipolar plate. The BMC was prepared by mixing VER, low profile agent (PS/SM series), styrene monomer, thickening agent (MgO), releasing agent (ZnSt), tert-Butyl peroxybenzoate, and graphite in a kneader for 30 min. The BMC formulation used by Kuan et al. (2004) has been shown in table 2.1. The BMC was thickened for 48 hours, in room temperature, before compression molding at 140 for 5 min. The graphite content was varied from 60–80 wt% while the resin (blended resin) content was varied from 20–40 wt%. They used various sizes

(1000−177, 177−125, 125−74, 74−53, and less than 53 μm) graphite particle to study the effect of its size on the properties of the bipolar plate. The electrical conductivity of the composite increased from 5×10^{-5} to 172.41 $S\cdot cm^{-1}$ as the graphite content was increased from 60 to 80 wt%. Similarly, the electrical conductivity of the composite decreased from 153.8 to 39.68 $S\cdot cm^{-1}$ as the graphite size was decreased from 1000 to 53 μm or less. Porosity and oxygen permeability were tested and reported as 0.06% and 5.82×10^{-8} $cm^3\cdot cm^{-2}\cdot s^{-1}$, respectively, when the graphite content was 75 wt%. The flexural strength and flexibility of the composite decreased with the increase in graphite content. The flexural strength of the composite for optimum graphite content (75wt%) was reported as around 32 MPa. They found the thermal decomposition temperature for 5% weight loss of the composite bipolar plate was observed at around 250°C. The corrosion current density of the composite for the same composition was recorded as $3.6\times10^{-7}A\cdot cm^{-2}$. However, they did not mention the detailed method and electrochemical environment for studying corrosion of the composite. The single cell and 6 cells stack performance evaluations were carried out by the developed bipolar plate. The author reported that the bipolar plate showed promising aspect in PEMFC application. The BMC technique was also used by Liao and his group to develop the CNT reinforced NG-VER composite bipolar plate [Liao et al., 2008(a,b); Hsiao et al., 2010; Liao et al., 2010 (a)]. However, the authors used 70% NG as the optimum filler content and 0−2% acid treated multiwall CNT to the BMC to improve the properties of composite bipolar plate. The acid treated CNTs were dispersed ultrasonically in poly(oxyalkylene)amines with molecular weight of 400 and 2000 $g\cdot mol^{-1}$ (denoted as POP400 and POP2000). The dispersed CNTs were again dried in a vacuum oven at 60°C to obtain MWNTs/POP-diamines. These samples along with the raw CNTs and acid treated CNTs were used as reinforcements with the BMC composition to develop composite bipolar plate. The in-plane electrical conductivity of

the composite for optimum CNT content was recorded as 496, 529, 633, and 744 $S \cdot cm^{-1}$ for raw CNT, acid-treated CNT, MWNT/POP400, and MWNT/POP2000, respectively. However, the through-plane electrical conductivity of the composites was not studied. There was a nominal change in the three-point flexural strength of the composite upon reinforcement with treated CNTs. The flexural strengths of the same composites were reported as 37.51, 37.96, 39.22, and 41.55 MPa, respectively. Similarly, the effect of CNTs on the porosity of the composite was not very significant. The lowest porosity of the composite was recorded as around 0.17% for MWNTs/POP2000 reinforced composite. Without CNTs, the porosity of the same composite was 0.27%. The fuel cell showed best *i–V* performance using the MWNTs/POP2000 reinforced composite bipolar plate. This improvement may be due to the higher electrical conductivity and less porosity of the composite in comparison to the other bipolar plates considered in the study. The detailed mechanism of increasing mechanical strength with the addition of MWNTs/POP2000 was reported by the author later [Liao et al., 2010(a)]. However, the hydrogen permeability, through-plane electrical conductivity, thermal conductivity, and corrosion resistance of the composite were not studied.

Hsiao et al. (2010, a) studied the effect of NG particle size on the flowability of BMC and formability of composite bipolar plate. It is worthy to mention that the BMC composition of the bipolar plate reported by Liao et al. (2008, a), was used in this study. The author reported that the BMC material with graphite particle size of 125–177μm showed better flowability in comparison to that with the smaller graphite particles. However, flowability of the BMC material decreased on addition of the MWCNT. Therefore, the amount of nanomaterial content was suggested to be kept as nominal as possible. Hsiao et al. (2010,b) further extended the work by sandwiching a metal mesh in between two layers of the BMC material. The mechanical strength of the composite increased as expected.

However, the use of aluminum mesh decreased the through-plane electrical conductivity of the composite from 37.8 to 22.9 $S \cdot cm^{-1}$ due to the high ohmic resistance of the passivation layer on the aluminum surface. The effect of decrease in through-plane electrical conductivity of the composite was observed in the *i–V* performance analysis of single cell. The inclusion of aluminum mesh affected negatively on the performance of the fuel cell. Moreover, the uneven expansion of metal and composite in the fuel cell temperature (usually around 80°C) might develop some micro-cracks in the bipolar plates. Similarly, accidental exposure of the metal mesh to the fuel cell environment will increase the corrosion remarkably, and it may contaminate the membrane as well as the catalyst inside the cell. Therefore, it is wise to avoid the use of such type of metal mesh for the development of bipolar plate.

Heinzel et al. (2004) used injection molding technique to develop thermoplastic based carbon composite bipolar plate. However, the authors did not reveal the ingredient and its composition. Basically, they focused on the possibilities of injection molding technique for mass production of bipolar plates. Moreover, they optimized the key production steps and preparations were made for small and medium series production. Various electrical properties of the composite and performance of fuel cell using it were reported by the author. The through-plane bulk electrical conductivity of the composite was recorded as around 175 $S \cdot cm^{-1}$, while the volume electrical conductivity (including contact resistance with the GDL) was reported as around 28 $S \cdot cm^{-1}$ only. The comparison of resistances with that of pure graphite bipolar plate revealed that the resistance of the injection molded bipolar plate was largely affected by the contacting pressure. In low contact pressure, the injection molded bipolar plate exhibited very high volume resistance in comparison to that of the pure graphite plate. The in-situ performance of the bipolar plate in a single or fuel cell stack was neither studied nor compared with the commercial bipolar plate.

However, the performance of a 20 cell stack using the developed bipolar plate was reported. On the other hand, they assessed the economic and commercial perspective of injection molded bipolar plates. They claimed that the cost of the injection molded bipolar plate could be reduced substantially for large volume production. It is to be noted was that the bulk electrical conductivity of those bipolar plates were around 50 $S \cdot cm^{-1}$ only. Moreover, the other important properties of the bipolar plates were not reported. Muller et al. (2006) also used injection molding technique to develop carbon composite bipolar plate. The composition of the bipolar plate was not disclosed in the literature. The flexural strength of the composite was reported in the range of 40−50 MPa and it was well above the US-DOE target value. However, the in-plane and through-plane electrical conductivities were only around 55 and 20 $S \cdot cm^{-1}$, respectively. Similarly, the flexural strength of the composite was around 40 MPa. Corrosion testing was carried out by leachate analysis of bipolar plates in dilute sulfuric acid (pH 4.5) at 85 °C for 2000 h. An amount of 50g of the composite material was stored in 250ml of the acid in PP bottles in a heat chamber. The elemental analysis of the leachate products was carried out and they reported that 75 ppm of Na and around 70 ppm TOC was leached out. Therefore, there was a possibility of membrane and catalyst contamination by the dissolution of the bipolar plate material.

Mighri et al. (2004) developed electrically conductive thermoplastic blends (PP and PPS) for injection and compression molding of bipolar plates using carbon as filler. They studied the properties of the bipolar plate upto 60 wt% loading of the NG, CB, and CF. The bipolar plates showed good flexural strength of around 50 MPa for PP samples and 84 MPa for PPS samples. However, the electrical conductivity of the composite was below 1 $S \cdot cm^{-1}$. The authors suggested that high electrical conductivity may be achieved by decreasing the percolation threshold. They expected that the blending of polymers and

preferentially locating the CB in one of the polymer phases can enhance the electrical conductivity of the composite bipolar plate. The purpose may be fulfilled by preferentially locating the CB particles at the polymer-blend interface in a co-continuous polymer blends. Later, Wu and Shaw (2005) used the technique to develop CNT filled PET-PVDF composite bipolar plate. The authors further extended their work to PET/nylon 6,6, PET/PP, and PET/high-density polyethylene blends also [Wu and Shaw, 2006]. The authors applied the concept of triple-continuous structure to several polymer-polymer blends loaded with CNTs, with the aim to obtain polymer-based composites with high enough electrical conductivities and sufficient mechanical properties for the bipolar plate of PEMFC. However, the highest in-plane and through-plane electrical conductivities, for CNT filled PET/PVDF composite, were reported as 0.0590 and 0.0114 $S \cdot cm^{-1}$. The authors also observed the presence of micro-cracks in some of the composites and they believed that the low electrical conductivity might be a result of it. They also revealed that all their reported work was limited to low carbon concentration system with the electrical conductivity of 10^{-2} $S \cdot cm^{-1}$ or lower. Therefore, due to the low electrical conductivity of the bipolar plate, their work can be considered as more conceptual rather than expecting it for end uses. The concept of polymer-polymer blending and triple continuous structure was further utilized by Du and Jana (2007) to develop composite bipolar plate for PEMFCs. They blended an aromatic resin (diglycidyl ether of bisphenol A; Epon® 826) with an aliphatic epoxy resin (polypropylene glycol glycidyl ether; Araldite® DY3601) to prepare the resin matrix. A particular amount of curing agent was added to both the resin individually before mixing them. The blended resin was diluted with acetone and a required amount of expanded graphite (EG) and CB was added to the solution. The preform mixture was then dried by keeping in a vacuum oven for 24 h at 60°C, and then 2 h at 110°C to get preform powder. The preform powder

was then compression molded at curing temperature of 180°C for 4-6 h, followed by post curing in vacuum oven at 200°C for 6 h. The in-plane electrical conductivity of the bipolar plate was 500 $S \cdot cm^{-1}$ with 40 wt% EG and 5 wt% CB. However, the through-plane electrical conductivity of the said composition was only 79 $S \cdot cm^{-1}$. Similarly, the area specific resistance of the composite was around 12 $m\Omega \cdot cm^{-2}$, which was below the US-DOE benchmark. The flexural strength of the composite was around 44 MPa with a flexural modulus of around 15 GPa. The hydrogen permeability, thermal conductivity, and corrosion resistance of the composite were not reported. Moreover, the *i–V* performance of fuel cell using the bipolar plates was also not reported. The authors further studied and reported the hygrothermal effects on the properties of the same composite bipolar plate [Du and Jana, 2008].

Radhakrishnan et al. (2007) studied the effect of processing conditions on the electrical properties of the bipolar plates. They used PPS and polyether sulfone (PES) as binder with NG powder to prepare the composite by compression molding process. In the process, they used both solution blending and powder mixing process. They reported that heat treatment of the samples at 100°C for few hours led to a significant change in electrical conductivity of the samples. However, the reported electrical conductivity of the composite was in the order of 10 $S \cdot cm^{-1}$. Thus they have suggested that a third additional conducting component may provide high electrical conductivity of the composite. The effect of resin content and the processing conditions on the properties of PPS bonded NG composite bipolar plates were later carried out by Xia et al. (2008). The author optimized the resin content, processing temperature, and processing time for the said composite. The optimum molding temperature for the composite was around 380°C for 30 min. The flexural strength and the in-plane electrical conductivity of the composite were 52.4 MPa and 118.9 $S \cdot cm^{-1}$, respectively. However, the other properties of the PPS-

NG composite were not reported and the molding temperature was relatively higher in comparison to the convention resin bonded composite bipolar plate [Xia et al., 2008]. Another study was carried out by Dweiri and Sahari (2007), to develop PP based composite bipolar plate for PEMFC applications. They investigated the electrical properties of carbon-based PP composite bipolar plates and got the highest electrical conductivity as 7 $S \cdot cm^{-1}$ at 80% graphite content for the PP/SG samples. Later, they studied the effect of CB for constant PP content and could get a bipolar plate with electrical conductivity of 36 $S \cdot cm^{-1}$. However, the electrical conductivity of the composite was yet not sufficient to reach the US-DOE benchmark (table 1.2). The work similar to that done by Dweiri and Sahari, 2007, was also carried out by Liao and his group [Liao et al., 2008(b); 2010(b)] by replacing CB with multiwall CNTs. The highest in-plane electrical conductivity of the composite was recorded as 548 $S \cdot cm^{-1}$ for low crystalline PP based composite with 4% CNT content. The flexural strength of the composite for the same composition was reported as 32.5 MPa only. Therefore, the bipolar plate showed inferior performance in comparison to graphite bipolar plate in fuel cell testing. This effect may be due to the high contact resistance of the PP based composite with GDL. Moreover, the thermal stability of the PP based composite was relatively less.

Huang et al. (2005) used wet lay sheet forming technology followed by compression molding to develop bipolar plate. The wet-lay sheet was developed by graphite particles, thermoplastic fibers, and CFs by slurry making process using a paper making machine. The thermoplastic fibers of PET or PPS were mixed with water, and the suspension was agitated in a pulper for 10 min. The CFs, along with the graphite particles, were added to the above slurry and mixed thoroughly for 3–6 min. The final slurry was then fed to the paper making machine under controlled rate. The sheet material formed in the paper

making machine was then conveyed through an oven set at the melting point of the thermoplastic fibers, to evaporate the water and partially melt the thermoplastic fibers. The sheet was then cut into pieces and molded to bipolar plate in a compression molding machine. The flexural strength of the composite bipolar plate was reported as 53 and 96 MPa for the PET and PPS based composite bipolar plate, respectively. The in-plane electrical conductivity of the PPS based composite plate was reported in the range of 200−300 $S \cdot cm^{-1}$. However, the through-plane electrical conductivities of the PPS and PET based composites were 20 and 50 $S \cdot cm^{-1}$, respectively. Similarly, the half cell resistance of the bipolar plate indicated that the through-plane conductivity of the material required some improvement.

The above method for the development of bipolar plates from graphite filled wet-lay thermoplastic materials was further studied by Cunningham et al. (2007) followed by Cunningham and Baird (2007). The in-plane and through-plane electrical conductivities for the optimum composition was 271 and 19 $S \cdot cm^{-1}$ for 70wt% Timcal graphite, 6 wt% Conoco CF, and 24 wt% PPS content. The flexural strength of the composite was around 95.8 MPa. The in-plane and through-plane electrical conductivities, as well as the mechanical strength, decreased further for PVDF based composite bipolar plate. The low wettability of PVDF may be the sole reason for the decrease in mechanical strength. The half-cell resistance measurement showed higher resistance for PVDF based composite. The authors suggested that reduction in the channel depth may help in lowering the half-cell resistance of the bipolar plate. However, it will eventually decrease the flow rate of hydrogen and oxygen as well as it may increase the possible leakage of hydrogen gas through the plate. The hydrogen gas permeability of the composite was not reported by the authors. Moreover, the slurry making process to develop the wet-lay laminate may increase the processing cost of the bipolar plate.

The laminate skin layer method for the development of composite bipolar plate was also used by Maheswari et al. (2007). However, the method of preform laminate skin layer preparation was slightly different. In this method, they developed carbon paper by impregnation and carbonization of raw carbon papers. The porosity of the developed carbon papers was 75-80%. Several such carbon papers were impregnated and sandwiched by slurry of PF resin-NG-CB mixture which was later compression molded to develop the bipolar. The maximum flexural strength of the composite was around 80MPa with the in-plane electrical conductivity of around 230 $S \cdot cm^{-1}$. Though the flexural strength and in-plane electrical conductivity of the composite was good, but the interfacial contact resistance of the plate was quite high (0.1 $\Omega \cdot cm^{-2}$ under a pressure of 4 $kg \cdot cm^{-2}$). Moreover, the porosity of the composite was more than 1.1% and the effect of hydrogen gas permeability was also revealed in the fuel cell performance analysis. The bipolar plates were later immersed in 5% H_2SO_4 solution for 5 h at 50°C and no significant corrosion was reported. However, the method of corrosion testing was not identical to the harsh electrochemical environment of PEMFC and there was a risk of substantial corrosion under the influence of electric field over a prolonged time. Above all, the method of development of bipolar plate was time consuming and expensive. Kim et al. (2010) used the above method with further modification in which they used commercially available plain weave carbon fabrics to develop laminate skin layered composite bipolar plate. The in-plane electrical conductivity of the composite for a single layer of carbon fabric and a total filler content of 75 vol% was reported as around 200 $S \cdot cm^{-1}$. This value decreased to around 180 $S \cdot cm^{-1}$ for five layers of carbon fabrics. However, the through-plane electrical conductivity of the composite for one and five layers of carbon fabrics were only 33 and 22 $S \cdot cm^{-1}$, respectively. Therefore, the bipolar plate did not show enough through-plane electrical conductivity for PEMFC application.

The author also developed composite bipolar plate using CF-epoxy prepreg. However, the anisotropy in the electrical conductivity of the composite was more predominant in this case. The in-plane and through-plane electrical conductivities of the composite, for CF-epoxy prepreg, were around 370 and 5 $S \cdot cm^{-1}$, respectively. The flexural strength of the composite was reported as 42 and 100 MPa for one and five layers of carbon fabric, respectively. The mechanical strength of the composite was increased with the increase in number of carbon fabrics. Therefore, the authors suggested that a plain weave carbon fabric, inserted into graphite-epoxy composite, might improve the mechanical strength of the composite.

Wolf and Porada (2006) used liquid crystal polymer (LCP) as a binder to develop CF reinforced composite bipolar plate for PEMFC application. Two different types of CF, with length around 180 and 360 μm, were used for the development of the composite. The composite was further reinforced with Vulcan-XC 72R grade CB to enhance the electrical conductivity of the composite. The authors claimed that the composite had sufficient mechanical strength and low hydrogen permeability to use as the bipolar plate. However, the maximum electrical conductivity reported for the LCP-CF-CB composite was only 5.6 $S \cdot cm^{-1}$. Moreover, the through-plane electrical conductivity, corrosion resistance, thermal conductivity, flexural strength, and flexibility of the composite were not reported. Similar kind of research was also carried out by Hwang et al. (2008), where epoxy resin bound CFs was used to develop composite bipolar plate for fuel cell applications. However, the author used the commercially avaiable high modulus pitch-based unidirectional CF-epoxy prepreg to develop the composite bipolar plate. The in-plane electrical and thermal conductivity of the composite were well above the DOE target values. However, the through-plane thermal conductivity of the composite was only 5 $W \cdot m^{-1} \cdot K^{-1}$ and it was far below the DOE benchmark for fuel cell's bipolar plate. The

unidirectional and anisotropic property of the CF is solely responsible for low through-plane conductivities. The air permeability of the composite was reported as 1.4×10^{-6} $cm^3 \cdot cm^{-2} \cdot s^{-1}$ which seems to be less than the target permeability of the composite bipolar plate. However, it is worthy to mention that the target permeability was set for hydrogen at 80°C under 3atm pressure and it must be higher than that of air. Therefore, the through-plane properties of the developed bipolar plates were not adequate to meet the DOE benchmark and further studies were required to meet the target for overall properties of the bipolar plate.

Dhakate et al. (2007), followed by Mathur et al. (2008), used the concept of multiple fillers to develop compression molded thermoset resin based composite bipolar plates. They used CB and CF along with NG to develop phenolic resin bonded composite bipolar plate. The authors successfully achieved the in-plane electrical conductivity target of bipolar plate for PEMFC applications. However, the maximum value of through-plane electrical conductivity was within 60–70 $S \cdot cm^{-1}$. The flexural strength and shore hardness of the composite were more than 60 MPa and 50. Therefore, the bipolar plates were having adequate mechanical strength to fulfill the criteria set by US-DOE for PEMFC application. The author reported a systematic and comparative study on the effect of different fillers on electrical conductivity and mechanical strength of the phenolic resin bonded graphite composite bipolar plate. However, the thermal conductivity, corrosion resistance, and hydrogen permeability of the composite were not studied thoroughly. Composite bipolar plate of graphite particles and epoxy resin was also studied by Lee et al. (2007). They have reported highest electrical conductivity of 10 $S \cdot cm^{-1}$ for 90% graphite. To achieve the mechanical properties, one or two layers of woven CFs were used with the original graphite-resin composite. They reported a highest tensile strength of 56.89 MPa for two layers of CF with 90% graphite. However, the electrical

conductivity of the fiber mixed composites was not mentioned. The effect of fillers on the properties of polymer composite bipolar plate was studied by Lee et al. (2009). The epoxy modified phenolic novolac resin was used as binder along with SG, CB, and CNT. The authors reported that the highest in-plane electrical conductivity 254.7 $S \cdot cm^{-1}$ was achieved for 73 vol% SG and 2 vol% CNT. The mechanical strength of the composite for the above composition was reported as around 48 MPa. The author suggested that the multiwall CNT could improve both the electrical as well as mechanical properties of the composite. However, the through-plane electrical conductivity, corrosion resistance, thermal conductivity, and hydrogen permeability of the composite were not investigated. The vapor grown CF was used by Seo and Park (2009) to improve the electrical, thermal, and mechanical properties of the poly(methyl methacrylate) polymer for possible bipolar plate application. However, the electrical resistivity of the composite was around 10^3 ohm·cm, even for 15wt% CF content, and therefore not suitable candidate for bipolar plate.

Several researchers have used EG, by replacing NG fully or partially, as an electrically conductive filler to develop composite bipolar plate for fuel cell application [Blunk et al., 2006(a,b); Xio et al., 2006; Yan et al., 2006; Du and Jana, 2007, 2008; Dhakate et al., 2008 (a,b); Dhakate et al., 2009]. Blunk et al. (2006, a) used EG with PVDF by dry mixing and with epoxy resin by wet mixing to develop compression molded composite bipolar plate. They studied the effect of EG content on the through-plane resistance and contact resistance of the composite in a set-up similar to fuel cell. They reported that EG content of more than 20 vol% with epoxy resin would decrease the through-plane resistance to 13.2 $m\Omega \cdot cm^2$. However, for PVDF based composite the same through-plane resistance was achieved with more than 80 vol% EG content. The contact resistance of the epoxy based composite was reported to be in the range 20–60 $m\Omega \cdot cm^2$ under 20

$kg \cdot cm^{-2}$ pressure. The flexural strength of the epoxy based composite was 34.1 MPa and the hydrogen permeability was reported as 1.2×10^{-6} $cm^3 \cdot cm^{-2} \cdot s^{-1}$ at around 1.7 atm pressure, for 20 vol% EG content. The detailed methodology of hydrogen permeability measurement was not reported. However, later, they explained the detail methodology for hydrogen permeability measurement and the reported values were quite high in comparison to the required limit as shown in table 1.2 [Blunk et al., 2006(b)].

Heo et al (2006) optimized the processing condition and composition of novolac type phenolic resin bonded EG-NG composite bipolar plate. Phenol powder, EG, and NG were mixed at an initial ratio of 25:7.5:67.5 wt% and shaken for approximately 30min to obtain a uniform mixture, which was then poured into an aluminum mold. The mold was then transferred to a compression molding machine and pre-cured at 100°C for upto 20 min under various pressures. The preformed plate was then transferred to a steel mold with inbuilt flow pattern and pressed at 150°C for 30 s under 10 MPa pressure. The in-plane electrical conductivity and flexural strength of the composite for optimum composition were reported as around 250 $S \cdot cm^{-1}$ and 50 MPa, respectively. It was expected that the two-step manufacturing process, consisting of pre- and main-curing, had the potential to produce composite bipolar plates rapidly. However, the through-plane electrical conductivity, hydrogen permeability, and corrosion resistance of the composite bipolar plates were required to study in future. The study of compression molded resin impregnated EG bipolar plates in PEMFC stack was carried out by Yan et al. (2006). The contact resistance of the EG-resin composite bipolar plate was relatively higher than that of the pure graphite bipolar plate. The performance of the fuel cell with the EG-resin composite bipolar plate was edge behind when it was compared with pure graphite bipolar plate. Graphite nanosheets (highly expanded form of EG termed as NanoG) and EG were used individually with poly (arylene disulfide) or poly-oxy-benzene-disulfide

(POBDS) to develop composite bipolar plates for fuel cell applications [Xiao et al., 2006]. The electrical conductivity for a composite with 50 and 60 vol% NanoG content was reported as 162 and 188 $S \cdot cm^{-1}$, respectively. The electrical conductivity of the composite for the same EG content was around 128 and 133 $S \cdot cm^{-1}$, respectively. However, the contact resistance of the composite, under high pressure, was almost similar for both EG and NanoG fillers. The corrosion testing of both the bipolar plates were carried out in 0.01M HCl + 0.01M Na_2SO_4 in room temperature and the corrosion current density of POBDS-NanoG (40:60) composite and POBDS-EG (40:60) composite was reported as 4.2×10^{-8} and 1.7×10^{-6} $A \cdot cm^{-2}$, respectively. However, it is to be noted that the simulated PEMFC environment was quite mild [Ma et al., 2000; Wang et al., 2004; Fu et al., 2008; Choi et al., 2009]. Moreover, the scanning range during the corrosion study was between −0.5 and $+0.5V_{SCE}$ which was narrow in comparison to the PEMFC half cell voltages. The polarization current of the bipolar plate in 600 mV_{SCE} under oxygen condition was 6.5 $\mu A \cdot cm^{-2}$, while it was recorded to $-2.6\mu A \cdot cm^{-2}$ in 240 mV_{SCE} under hydrogen condition. Therefore, the overall corrosion current density of the composite in the simulated PEMFC environment was around 9.1 $\mu A \cdot cm^{-2}$ and it was very high with respect to the US-DOE benchmark (table 1.2). Moreover, the through-plane electrical conductivity, thermal conductivity, and hydrogen permeability of the composite were not reported. Dhakate et al. (2008, 2009) also did a series of studies on the properties of EG-PF composite bipolar plate. The in-plane electrical conductivity of the composite for 50 wt% EG was around 150 $S \cdot cm^{-1}$. By the addition of 5wt% CB along with 50wt% EG, they successfully improved the electrical conductivity of the composite to 285 $S \cdot cm^{-1}$ [Dhakate et al., 2008 (b)]. The flexural strength and shore hardness of the composite for both the compositions were almost similar and it were around 50 MPa and 50, respectively. It was reported that the air permeability (qualitative only) of the plate

was almost nil upto 0.78MPa. However, hydrogen permeability of the bipolar plate was not reported which is more important than air permeability. Moreover, the corrosion resistance, through-plane electrical conductivity, and thermal conductivity of the composite were also not reported. Bhlapibul and Pruksathorn (2008) developed composite bipolar plate using polyester resin and PF resin individually with graphite-CF mixture to study the effect of additives, such as TiO_2 and ZnSt. However, the electrical conductivity of the composite was 20 $S{\cdot}cm^{-1}$. Similarly, the maximum mechanical strength achieved by any of the developed composite did not exceed 20 MPa. It was shown that the fuel cell had inferior performance using the developed bipolar plate in comparison to the commercial bipolar plate. Moreover, the corrosion study was not reported to assess the effect of metallic elements present in the additives under harsh electrochemical environment.

In order to find the electrochemical corrosion of carbon polymer composite the literature survey has been done. It has been found that the carbon-polymer composite bipolar plates generally show good corrosion resistance in the PEMFC environment [Heinzel et al., 2004]. However, at high electronegative potentials, carbon is thermodynamically feasible to be reduced to methane because carbon has a narrow window of stability in potential-pH diagram [Bakkar et al., 2009]. Hihara et al. (1995) reported that in the absence of electric potential, carbon materials such as NG, CB, and CF have high chemical stability when exposed to aqueous electrolyte. They have also reported that neither methane nor visual fiber degradation was detected when pitch-based graphite fibers were cathodically polarized. Graphite is practically inert in alkaline and neutral solution. However, in acidic solution the corrosion of graphite was observed with CO_2 evolution [Kinoshita and Bett, 1973; Guenbour et al., 2006; Li and Xing, 2008]. Kinoshita and Bett (1973) studied the electrochemical oxidation of CB in phosphoric acid environment and evaluated the CO_2

evolution rate. They have reported that the corrosion of CB occurred in two steps, (i) the formation of a surface oxide and (ii) the evolution of CO_2. Similarly, Guenbour et al. (2006) studied the corrosion of graphite in phosphoric acid and suggested same kind of mechanism. Recently, Li and Xing (2008) reported the electrochemical oxidation of carbon, in a general form, in two steps. In the first step, carbon oxidizes (eq.2.1),

$$C_x \rightarrow C_x^+ + e^- \qquad 2.1$$

where C_x denotes the form of carbon.

Thereafter, the product C_x^+ further hydrolyzes to its oxide (eq.2.2),

$$C_x^+ + yH_2O \rightarrow C_xO_y + 2yH^+ \qquad 2.2$$

There is hardly any literature, which reported on the electrochemical corrosion of composite bipolar plate in rigorous PEMFC. Some of the researcher carried out corrosion testing either in the absence of an electric field [Maheswari et al., 2007; Dhakate et al., 2008] or in a simulated mild PEMFC environment [Xiao et al., 2006; Yen et al., 2008; Li et al., 2008]. The electrochemical corrosion testing of the composite bipolar plate should be studied in rigorous PEMFC environment to find the accelerated results due to aging of the composite.

A summary of the comprehensive literature review on the research and development of composite bipolar plate has been discussed in the following section.

2.2 Summary of literature review

From the literature review so far, it is quite evident that some crucial properties of the composite bipolar plate have not been studied thoroughly. The through-plane electrical conductivity, hydrogen permeability, corrosion resistance, and thermal conductivity are the main properties among them. The through-plane electrical conductivityof a bipolar

Table 2.2: Summary of the achievement on the properties of composite bipolar plate reported in selected literatures of recent past

References	Composition	Electrical conductivity ($S \cdot cm^{-1}$)		Flexural strength (MPa)	Deflection at mid-span (%)	H_2 permeability $\times 10^{-6}$ ($cm^3 \cdot cm^{-2} \cdot s^{-1}$)	Thermal conductivity ($W \cdot m^{-1} \cdot K^{-1}$)	Corrosion current density ($\mu A \cdot cm^{-2}$)
		in-plane	through-plane					
US-DOE benchmark (2009)	**Composite**	**100***		**50**	**3–5**	**< 1**	**20**	**1**
Besmann et al. (2000)	CF/PF=4/3 wt%	200–300	×	175 (*biaxial*)	×	2	×	6
Wilson and Busick (2001)	VER:32 wt.%; NG:68 wt.%	120	×	31	×	×	×	×
Del Rio et al. (2002)	PVDF:60wt.%; CB:wt.40%	2.36	×	×	×	×	×	×
Mighri et al. (2004)	PPS:43.7%; CB:8.5%; CF:4%	10	×	84	×	×	×	×
Huang et al. (2005)	PPS:24%; NG:70%; CF:6%	271	19	95.8	×	×	×	×
Yen et al. (2006)	BMC:25%; NG:75%	260	×	50.1	×	×	×	0.1 at 0.01 M HCl + 0.01M Na_2SO_4
Heo et al. (2006)	EG:7.5%; NG:67.5%; PF:25%	250	×	50	×	×	×	×
Xiao et al. (2006)	poly(arylenedisulfide) :50%; nano-graphite:50%	138.7	×	32.05	×	×	×	1.7 (methodology unknown)
Yin et al. (2007)	PF:15%; NG:85%	142	×	61.6	×	×	×	×
Lee et al. (2007)	SG:90%; Epoxy resin: 10%; CF fabric	10	×	56.89	×	×	×	×

References	Composition	Electrical conductivity ($S \cdot cm^{-1}$)		Flexural strength (MPa)	Deflection at mid-span (%)	H_2 permeability $\times 10^{-6}$ ($cm^3 \cdot cm^{-2} \cdot s^{-1}$)	Thermal conductivity ($W \cdot m^{-1} \cdot K^{-1}$)	Corrosion current density ($\mu A \cdot cm^{-2}$)
		in-plane	through-plane					
Dhakate et al. (2007)	PF:35%; NG:50%; CB10%; CF:5%	150	60	60	×	×	×	×
Dweiri and Sahari (2007)	PP:20%; CB:25%; NG:55%	36	×	×	×	×	×	×
Du and Jana (2007)	EG:35%; CB:5%; Epoxy resin:60%	200	×	72	×	×	×	×
Liao et al. (2008)	BMC:25%; NG:73%; acid treated CNT:2%	744	×	41.55	×	0.17% (*porosity*)	×	×
Yin et al. (2008)	PF:15%; NG:82%; CNT:3%	145.2	×	68.6	×	×	×	×
Xia et al. (2008)	PPS:25%; NG:75%	118.9	×	52.4	×	×	×	×
Hwang et al. (2008)	Epoxy resin bonded unidirectional CF	300	×	180	×	1.4 (*air*)	85 (‖) 5 (⊥)	×
Lee et al. (2009)	PF:25%; SG:73%; CNT:2%	254.7	×	48	×	×	×	×
Hsiao et al. (2010)	BMC:27%; CNT:2%; NG:75% + Al mesh	~ 600	22.9	×	×	35.5	×	×
Kang et al. (2010)	PF:20%; NG:80%	324.7	31.1	41.9	×	7.6 (*air*)	×	×

NG: natural graphite
SG: synthetic graphite
EG: expanded graphite
CB: carbon black
CF: carbon fiber
CNT: carbon nanotube

PF: phenol formaldehyde
VER: vinyl ester resin
PPS: polyphenylene sulfide
PVDF: polyvinylidene fluoride
PP: polypropylene
BMC: bulk molding compound

× Not available
‖ Parallel to the plane
⊥ Perpendicular to the plane
* Not mentioned whether for in-plane or through-plane

plate, in a fuel cell stack, is more important than the in-plane electrical conductivity, as electrons are collected by the plate at the anode side and migrate through the plate to the cathode side of the cell. At the same time, electrochemical corrosion poses one of the big challenges in selecting the bipolar plate materials. The thermal conductivity of the bipolar plate also plays crucial role in the stack operation. It is observed that the vital properties of the bipolar plate are studied by the researchers but the available literatures lack to show that a particular bipolar plate has all the required properties. The different properties of the carbon-polymer composite bipolar plate reported in selected scientific and technical literatures have been enlisted in the table 2.2 based on the discussion in the literature review (section 2.1). It is conclusive from table 2.2 that the through-plane electrical conductivity of the bipolar plate is hardly discussed. It has seen that the US-DOE or other literatures have not specified whether the target is for in-plane or through-plane electrical conductivity. The literature survey shows that the in-plane electrical conductivity of the composite bipolar plate has been merely achieved. However, the targets for in-plane and through-plane electrical conductivities have not been achieved simultaneously by any of the cited literatures. Therefore, there is a scope of improvement in the electrical conductivity of the composite bipolar plate. It is quite cleared that graphite particles should be the base filler in resin bonded composite bipolar plate. However, the graphite alone can not offer the sufficient properties as filler to the bipolar plate, that is suitable for PEMFC application. Mighri et al. (2004) suggested that the blending of polymers and preferentially locating the conductive filler in one of the polymer phases can enhance the electrical conductivity of the composite bipolar plate. The concept of polymer-polymer blending was later used by Wu and Shaw (2005, 2006). However, the electrical conductivity of the composite bipolar plate was very poor. It is also observed from the table that the electrical conductivities of the thermoset resin bonded composite bipolar

plates are relatively higher than that of the thermoplastic based composites. It is also observed that the use of multiple fillers, instead of single filler, enhances the electrical conductivity of the composite significantly [Dhakate et al., 2007; Yin et al., 2008; Lee et al., 2009; Hsiao et al., 2010(a)]. Moreover, reinforcement with a nominal amount of nanomaterial along with the graphite can increase the electrical conductivity of the composite significantly [Radhakrishnan et al., 2007; Yin et al., 2008; Hsiao et al., 2010]. It is expected that the inclusion of nanomaterial will also improve the through-plane electrical conductivity and decrease the anisotropy of the graphite based composite bipolar plates. The mechanical properties of the composite bipolar plates may also be improved by the addition of any fibrous material [Mighri et al., 2004; Huang et al., 2005; Lee et al., 2007; Hwang et al., 2008]. The flexibility (deflection at mid-span), H_2 permeability, thermal conductivity, and corrosion behavior of the composite bipolar plates need to be studied thoroughly to develop composite bipolar plate suitable for fuel cell. The objective of the current research is set as per the above literature survey and discussed in the next section.

2.3 Aim and objectives

There are vigorous efforts to develop polymer composite bipolar plates to replace the electro-graphite bipolar plates in PEMFC. However, it is observed from the detailed literature review that all the required target properties of the composite bipolar plate have not been studied thoroughly. A detailed study is required for the development of a composite bipolar plate which can fulfil the benchmark given in table 1.2.

The major objective of this thesis is to develop a carbon composite bipolar plate for PEMFC, which can satisfy all the requirements specified in table 1.2. To achieve the objective, the following investigations were carried out.

- Selection and characterization of raw materials suitable for composite bipolar plates,
- Synthesis of monolayer graphene from NG,
- Characterization of the developed graphene using,
    a. SEM analysis,
    b. XRD analysis,
    c. HRTEM and SAED analysis,
    d. FTIR analysis,
    e. AFM analysis,
    f. Raman spectroscopy analysis,
    g. Thermogravimetric analysis, and
    h. BET surface area analysis.
- Development of composite bipolar plates by compression moulding technique.
- Optimization of processing conditions of molding for fabrication of the composite bipolar plate.
- Characterization of the developed bipolar plates for
    a. density,
    b. hydrogen gas permeability,
    c. through-plane and in-plane electrical conductivities,
    d. thermal conductivity,
    e. flexural strength and flexibility,
    f. shore hardness,
    g. corrosion resistance,
    h. thermogravimetric analysis, and
    i. morphological analysis.

- Model development for electrical conductivity and its validation with the experimental results.
- Designing of mold for fabrication of bipolar plate with inbuilt flow channels.
- Evaluation of the composite bipolar plate in PEMFC,
    a. development of MEA and fuel cell hardware,
    b. development of PEMFC test rig, and
    c. performance evaluation of the fuel cell.

Chapter 3

Experimental

Experimental

A brief introduction of the materials used and the synthesis of graphene are discussed in the first part of the chapter. The experimental methodologies for characterization of the raw materials, graphene and developed composite bipolar plates are discussed in the later part of the chapter.

3.1 Materials

It has been discussed in the previous chapter that thermosetting resin is a good choice for the binder matrix for the development of a composite bipolar plate. Therefore, three different types of thermosetting resins; viz. novolac-PF resin, resol-PF resin, and VER; were selected as the polymer matrix for this study. Similarly, graphite being the choice for conductive filler due to its high electrical conductivity and excellent corrosion resistance in fuel cell environment. Vulcan XC72 grade CB, and PAN based CF were chosen as the other conductive fillers. Moreover, single layer graphene was produced thermochemically from NG and used to reinforce the composite. The detailed properties of the materials have been discussed in the next section.

3.1.1 *Phenolic resin*

Phenolic resins were among the first resins composed by deliberate synthesis and are therefore among the earliest synthetic binders of any kind [Stoye, 1996]. Phenolic resins are oligomers synthesized by repeatedly linking phenolic (hydroxy-aromatic) monomers with aldehyde. Phenolic resin manufacturers polymerize phenol (C_6H_5OH) by substituting formaldehyde (HCHO) on the phenol's aromatic ring via a condensation reaction. The general chemistry of the polymerization of phenol with formaldehyde and are discussed herewith.

The raw materials in the preparation of phenolic resins are phenol or its homologues, and aldehyde, especially formaldehyde and equivalents thereof. In aqueous solution, formaldehyde exists in equilibrium with methylene glycol. Depending on the pH of the catalyst, two general PF resin types, novolac and resol, can be formed.

3.1.1.1 *Novolac-PF resin*

An acidic catalyst and a molar excess of phenol to formaldehyde are conditions used to make novolac resins. The following simplified chemistry illustrates the wide range of polymers possible. The initial reaction is between methylene glycol and phenol as shown in eq.3.1.

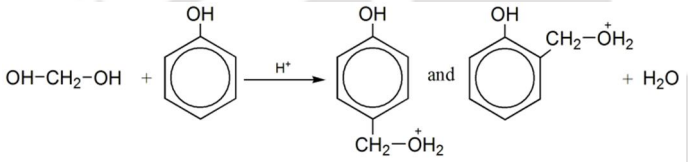

3.1

According to Zhang et al. (1997), the novolac molecule itself is a molecule with certain numbers of phenols connected by ortho-ortho, para-para, and ortho-para methylene linkage as shown in eq.3.2.

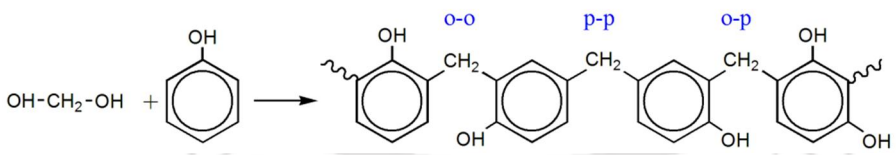

3.2

The final novolac PF is solid in room temperature and unable to react further without the addition of a cross-linking agent. Because an additional agent is required to complete the resin's cure, the industry commonly refers to novolac resins as “two-stage” or “two-step” products. The most common PF resin cross-linking agent is hexamethylenetetramine, also known as hexa, hexamine, or HMTA. HMTA cures the resin by further linking and polymerizing the molecules to an infusible state (eq.3.3) [Kurachenkov and Igonin, 1971; Zhang and Solomon, 1994; Zhang et al., 1997].

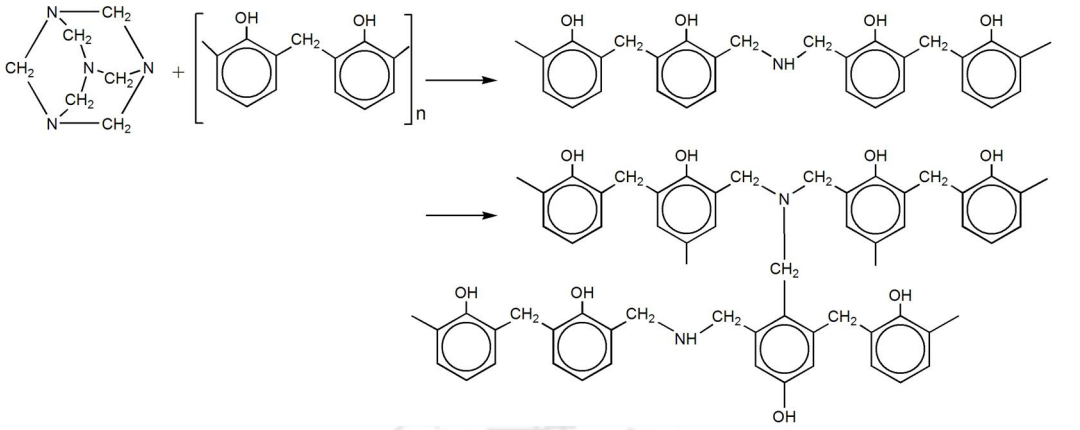

3.3

Tipcolite® grade advanced novolac type PF resin, in the form of free flowing powder, was supplied by Tipco Industries Ltd., Gujarat, India. It was a cream colored powder containing straight PF resin with 9% of HMTA content. The resin was stored in an airtight container to prevent unwanted cross linking before use. The thermogravimetric analysis of the as supplied resin was carried out to measure the solid content and ash content. Similarly, the DSC analysis of the resin was also carried out to study the curing behavior of the resin. The detailed properties of the novolac PF resin used in the study is listed in table 3.1.

Table 3.1: Typical properties of novolac type PF resin

Typical property	Typical value
Appearance	Cream colored free flowing powder
Melting point	96°C
Norton flow @ 125 °C	43 mm
Gel time @ 160 °C	36 s
HMTA content	9 %
Sieve analysis (+150#)	×
Sieve analysis (+200#)	1%
Sieve analysis (+300#)	×
Sieve analysis (+325#)	5%
Shelf life @ 25 °C	6 months

3.1.1.2 *Resol-PF resin*

A basic (alkaline) catalyst and, usually but not necessarily, a molar excess of formaldehyde is used to make resol type PF resins [Maciel et al., 1984; Lenghaus et al., 2000; Lenghaus et al., 2001]. The following two stages (eq.3.4) describe a simplified view of the reaction: First, phenol reacts with methylene glycol to form methylol phenol.

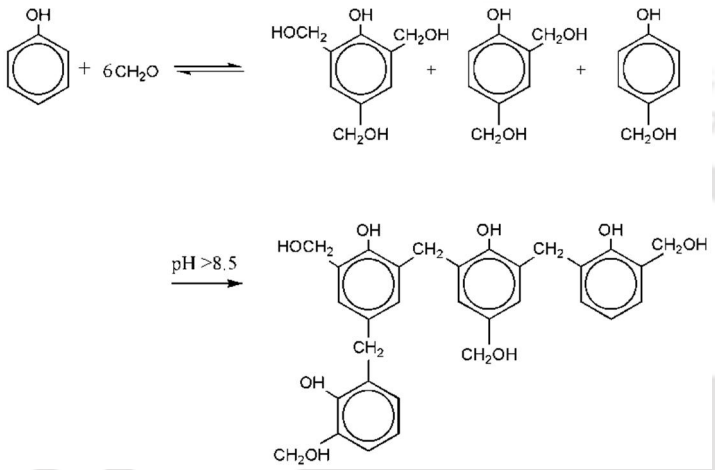

3.4

In an alkaline condition, at a pH of 8.5 or more, this reaction gives the highest degree of methylolation, and therefore preferentially gives methylol phenol virtually without condensation reaction. In fact, the commercial resols are a mixture of polycyclic molecule lined to one another via methylene bridge as shown in the second step of eq.3.4 [Chanda and Roy, 2006; Lenghaus et al., 2000]. The resol type PF resins do not require any curing agent and hence known as "single-stage" or "one-step" type products [Maciel et al., 1984; Lenghaus et al., 2001]. The simplified curing mechanism of resol resin under thermal excitation is shown in eq.3.5.

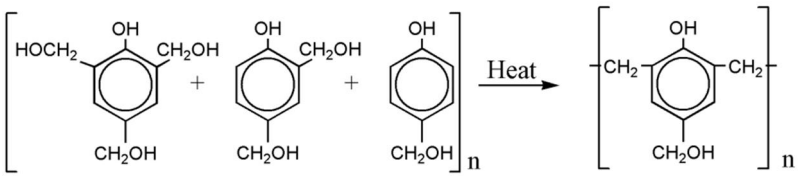

3.5

Tipcolite® grade advanced resol type liquid PF resin was supplied by Tipco Industries Ltd., Gujarat, India. It was a reddish-brown colored thick liquid with 58–62% solid content. The resol-PF resin was stored in an airtight container to prevent unwanted crosslinking. The resin was subjected to TGA and DSC analysis to study the curing behavior of it. The detailed properties of the resol PF resin used in the study is listed in table 3.2.

Table 3.2: Typical properties of resol-PF resin

Typical property	Typical value
Appearance	Reddish brown viscous liquid
Viscosity @ 25°C	230 cps
Solid Content @ 135°C	58–62%
Gel time @ 150°C	90–130 s
Specific gravity @ 25°C	1.16 $g \cdot cm^{-3}$
Water solubility	Nil
Solvent solubility	Alcohols, Ketones
Shelf life @ 25°C	2 months

3.1.2 *Vinyl ester resin*

Vinyl ester resin (VER) is a variant of polyester resins where the reactive sites (˙C═C˙) are positioned at the ends of the molecular chain [Casit and Talbot, 1998; Rosu et al., 2006; Yang et al., 2008]. A basic VER preparation using diglycidyl ether of bisphenol-A epoxy resin and methacrylic acid can be represented as in the eq.3.6 [Rao et al., 1986].

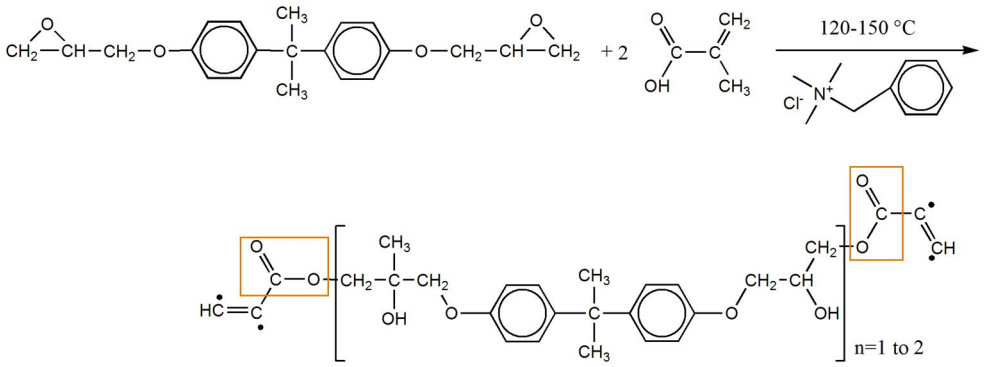

3.6

The reaction occurs at 120–150 °C in presence of benzyl trimethyl ammonium chloride catalyst. The VERs are yellowish brown colored viscous liquid. The curing of VER requires promoter, accelerator, and catalyst. The cured VER takes the following reticulated structure (eq.3.7) [Scott et al., 2002].

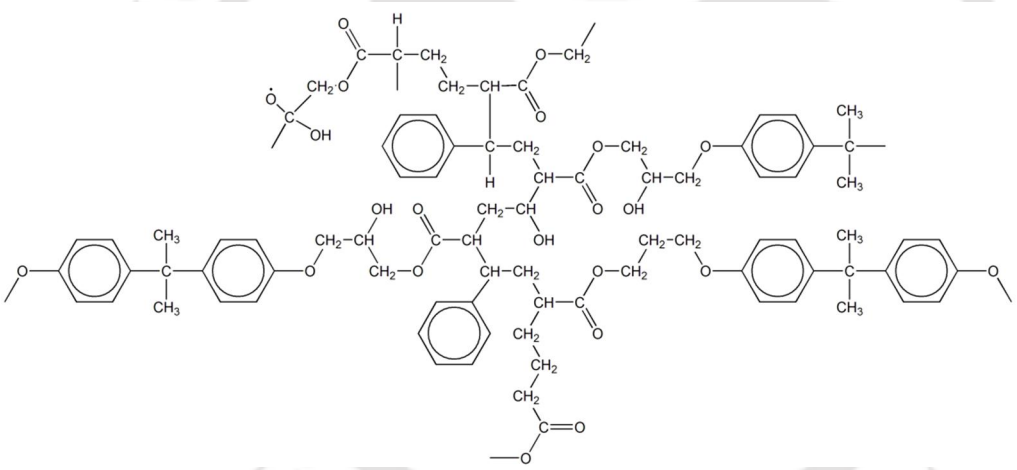

3.7

The general purpose industrial grade VER (MECHSTER 5310) supplied by Mechemco Industries, Mumbai, India. The promoter, accelerator, and catalyst were also supplied along with the resin. The resin was subjected to TGA and DSC analysis to study the curing behavior. The detailed properties of the VER used in the study are listed in table 3.3.

Table 3.3: Typical properties of VER

Typical property	Typical values
Appearance	Yellowish brown liquid
Viscosity @ 25°C	450±50 cps
Specific gravity @ 25°C	1.16 $g \cdot cm^{-3}$
Peak exotherm temperature	140–145 °C
Solid Content @ 140°C	64–66 %
*Gel time @ 25°C	15–20 min
Solvent solubility	Alcohols, Ketones
Shelf life @ 25°C	6 months

* with 1.5% promoter, 1.5% accelerator, and 1.5% catalyst

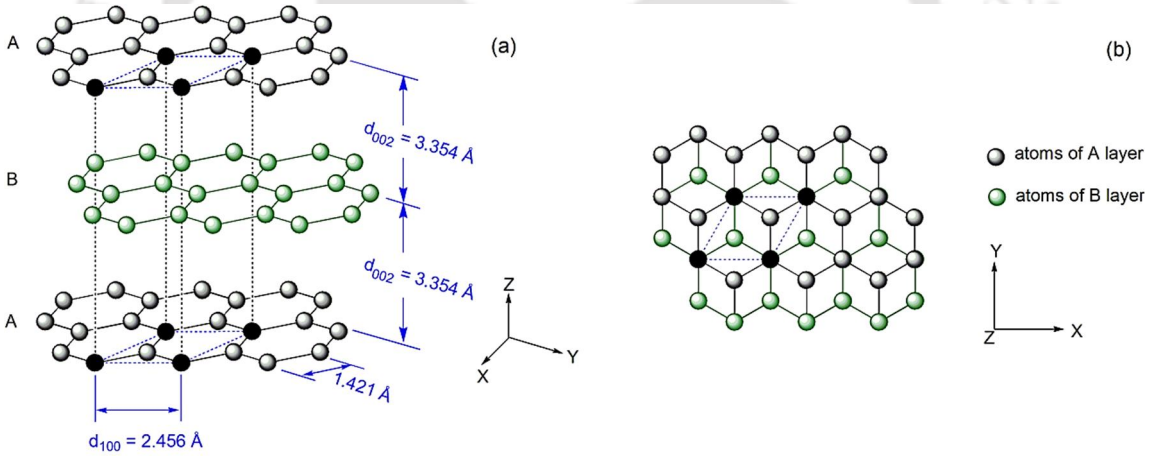

Figure 3.1: Crystal structure of graphite showing ABAB… stacking; (a) perspective view, and (b) top view

3.1.3 *Natural graphite*

The NG is an inexpensive additive that is multifunctional when utilized in paints, coatings, and a myriad of other applications. It also provides chemical inertness, refractoriness, electrical conductivity, thermal conductivity, lubricity, UV inertness, and fire retardant properties. The NG is one of the most widely used reinforcements for

composite bipolar plate mainly due to its chemical inertness and high electrical conductivities.

Graphite in different forms is used to develop various electrically conductive polymer composite. Graphite is the most stable form of conductive solid carbon ever discovered [Bundy et al., 1996; Burchell, McEnaney, 1999]. The most common crystal form of graphite is hexagonal and consists of a stack of layers separated by 3.354 Å in the stacking sequence ABABAB…. The unit layer of graphite is known as graphene (or carbon layer plane). The graphene is an extended honeycomb array of carbon atoms where each sp^2 hybridized carbon atom is bonded to three surrounding carbon atoms with σ-bonding (bond length 1.421 Å). The fourth valence electron does not take part in covalent bonding and it takes part in weak van der Waal bonding (π-bonding) with another layer of graphene sheet at a distance of 6.708 Å (fig.3.1). The unit crystal is shown by dotted lines in fig.3.1(a) [Pierson, 1993]. The fourth electron may be easily displaced from the electron shell by an electric field and hence graphite has very high electrical and thermal conductivities. However, the graphite crystal shows highly anisotropic behavior. The electrical and the thermal conductivities along the plane are quite different than the through-plane conductivities [Powel, 1972; Liu et al., 2008].

Table 3.4: Typical properties of as supplied Timrex® NG powder

Typical property	Typical value
Appearance	Fine black powder
Bulk density (electron density)	2.26 g·cm^{-3}
Particle size (average)	54.60 µm
Purity	≥ 95%
Ash content	2.3–5%
Moisture content	0.2–0.5%

Timrex® grade NG powder with purity of 95% and average size of 54.60 µm were supplied by Nickunj Eximp. Entp. Pvt. Ltd., Mumbai, India. The properties of the raw NG powder are listed in table 3.4. The NG powder was characterized with SEM, BET, XRD, TGA, and laser particle analyzer and the results discussed are in the chapter 5.

3.1.4 *Carbon black*

Carbon black (CB) is the accepted generic name for a family of small particle size carbon pigments which are formed in the gas phase by thermal decomposition of hydrocarbons [Pierson, 1993]. In general, the generic name "carbon black" now refers to a group of industrial products consisting of furnace blacks, channel blacks, thermal blacks, and lamp blacks. They are materials composed of elemental carbon in the form of near-spherical particles of colloidal size, coalesced mainly into particle aggregates obtained by partial combustion or thermal decomposition of hydrocarbons. Carbon blacks are currently sold in the form of hundreds of commercial grades which vary in particle size, aggregate size and shape, porosity, and surface chemistry. Their most important properties for inks, coatings, and plastics are related to the final product appearance (e.g., blackness, tone, and tint), UV protection, and electrical conductivity [Sanchez-Gonzalez et al., 2005]. The electrical conductivity is also an important property for other applications of carbon blacks, such as their use in electronic components, cables, electrodes, electrode additives, and so on [Uchida et al., 1995; Frysz et al., 1996; Lu and Chung, 2002]. The electrical applications of carbon materials have been reviewed recently by Chung, 2004. The high electrical conductivity, as well as the chemical resistance, makes the CB a potential candidate for composite bipolar plate. Various types of CB have been studied by the scientists and researchers as reinforcement to resin matrix to enhance the electrical conductivity of the composite bipolar plate [Mighri et al., 2004; Wu and Shaw, 2005; Chen and Kuo, 2006; Dhakate et al., 2007].

Table 3.5: Typical properties of as received Vulcan XC72 carbon black

Typical property	Typical values
Physical appearance	Black pearl
Bulk density (electron density)	1.2 $g \cdot cm^{-3}$
Average particle size	3 µm
Purity	≥ 95 %
Volatile content	≤ 2.0 %
Moisture content	< 1.0 %
Ash content	≤ 0.1 %

In this investigation, Vulcan XC72 CB has been used to enhance the electrical property of the composite bipolar plates. Vulcan XC72 grade CB was received from CABOT India Ltd., Mumbai, India. The typical properties of the Vulcan XC72 grade CB is listed in the table 3.5. The CB was characterized by particle size analyzer, BET, TGA, XRD, and SEM. The results of these characterizations are discussed in the chapter 5.

3.1.5 *Carbon fiber*

Carbon fibers (CFs) are commonly used to enhance the mechanical properties of the composite. The types of CF used may vary from application to application. Currently, these fibers are produced from three types of materials, viz. (i) polyacrylonitrile (PAN), (ii) rayon, and (iii) petroleum pitch. PAN is recognized as the most important and promising precursor for the development of carbon fibers.

PAN based CFs are thermally stable, have highly oriented molecular structure, and possess excellent mechanical strength. PAN based CF, in chopped form (about 2mm in length), was used in the current study to achieve the target mechanical properties of the composite bipolar plate. T-300 grade PAN based CF was supplied by Torayca, Japan. The typical properties of the T-300 grade CF is listed in the table 3.6.

Table 3.6: Typical properties of as received T-300 grade carbon fiber

Typical property	Typical values
Physical appearance	fine thread
Bulk density (electron density)	1.76 g·cm^{-3}
Fiber diameter	6 μm
Purity	99.9 %

3.1.6 *Graphene*

Graphene is a one-atom-thick planar sheet of sp^2-bonded carbon atoms (bond length 1.421 Å) that are densely packed in a honeycomb crystal lattice. The term graphene was coined as a combination of graphite and the suffix -ene by Boehm et al., 1994. Graphene is often referred as the mother of all graphitic materials [Srinivasan, 2007; Geim and Novoselov, 2007; Falko and Geim, 2010]. Many graphene sheets stacked together to form the crystalline or "flake" form of graphite.

The salient properties of a single layer graphene are –

(i) It has highest thermal conductivity known till date (up to ~ 5,300 W·m^{-1}·K^{-1}), and about 10 times higher than metals such as copper and aluminum [Stankovich et al., 2006].

(ii) Graphene has highest electrical conductivity ever known. It is in the order of 10^6 S·cm^{-1} which is around 10 times higher than that of graphite [Stankovich et al., 2006].

(iii) It is 100–200 times stronger than steel. It has ultra-high Young's modulus (approximately 1,000 GPa) and highest intrinsic strength (~ 130 GPa estimated) [Stankovich et al., 2006].

(iv) Have high specific surface area (up to ~ 2,675 $m^2 \cdot g^{-1}$) twice that of CNTs [Novoselov et al., 2004].

(v) Graphene sheets in solid form has a density of 1–2.2 $g \cdot cm^{-3}$ and has minimal viscosity impact [Jang et al., 2007].

The concept of graphene was well known to the scientific community for many decades, however the isolation of graphene was quite elusive, resisting any attempt on its experimental work until 2004 [Novoselov et al., 2004]. The graphene can be developed by various methods. These methods can be broadly categorized as (i) mechanical method [Novosalov et al., 2004; Geim and McDonald, 2007], (ii) epitaxial growth method [Berger et al., 2004], (iii) direct chemical reduction method [Stankovich et al., 2007], (iv) electrochemical method [Valles et al., 2008; Liu et al., 2008], and (v) thermochemical method [Schniepp et al., 2006; McAllister et al., 2007; Chandra et al., 2010]. The thermochemical production of graphene from graphite is one of the most suitable processes to develop graphene and graphene oxide in large volume.

Therefore, graphene was produced thermochemically from graphite to use as reinforcement to the composite bipolar plate. The detail methodology of the production of graphene is described in the next section.

3.1.6.1 *Synthesis of graphene from NG*

The synthesis of graphene from NG by thermochemical method involves three basic key steps, (i) oxidation of NG to synthesize graphite oxide or intercalated graphite, (ii) thermal exfoliation of graphite oxide to prepare expanded graphite, and (iii) reduction of expanded graphite to produce graphene. The different steps involved in the production of graphene are shown in fig.3.2 and detailed methodology is explained below.

3.1.6.1.1 Synthesis of graphite oxide

Graphite oxide was first prepared by Oxford chemist Benjamin C. Brodie in 1859, by treating graphite with a mixture of potassium chlorate ($KClO_3$) and fuming nitric acid (HNO_3) [Brodie, 1959]. However, $KClO_3$ is highly explosive in the above condition and it is not easy to handle. In 1957 Hummers and Offeman developed a safer, quicker, and more efficient process, using a mixture of sulfuric acid (H_2SO_4), sodium nitrate ($NaNO_3$), and potassium permanganate ($KMnO_4$) [Hummers and Offeman, 1958]. Therefore, this method was adapted to produce the graphite oxide. First, a certain amount of dry NG and $NaNO_3$ was mixed with concentrated H_2SO_4 in a conical flask. The above mixture was thoroughly stirred with the help of a mechanical stirrer for few minutes. Then KM_nO_4 was added to the above mixture and the suspended solution was again rigorously stirred for some time. Later, water was added slowly to the above mixture and kept for some time. The mixture was then treated and diluted with 2% H_2O_2. The H_2O_2 was added to the above solution to reduce the residual permanganate to soluble manganese ion. During the above process the temperature of the mixture was maintained below subzero temperature. The final mixture was then filtered and washed thoroughly with running millipore water. The extracted mixture was then dried in a vacuum oven at 135 °C for 24 h to obtain the graphite oxide.

3.1.6.1.2 Thermal exfoliation of graphite oxide

The above dry mixture of graphite oxide was then transferred to a clean silica crucible. The crucible along with the mixture was subjected to thermal shock in an inert environment at about 1050°C. A semi-automatic and programmable furnace was used for the above purpose. The graphite oxide has been thermally reduced and expanded extensively to produce graphene. The material was then kept for further treatments.

3.1.6.1.3 Purification of synthesized graphene

The thermal exfoliation of graphite oxide usually produces oxidized graphene and it may also have trace amount of K and Mn. It was further treated with H_2O_2 and dispersed with the help of ultrasonication for some time. The treated mixture was again centrifuged and washed thoroughly with sufficient amount of millipore water. The sample was then kept in a vacuum oven at 60°C for 12 h. Finally, the graphene was produced and it was stored in an air tight vacuum desiccator for further characterization and use.

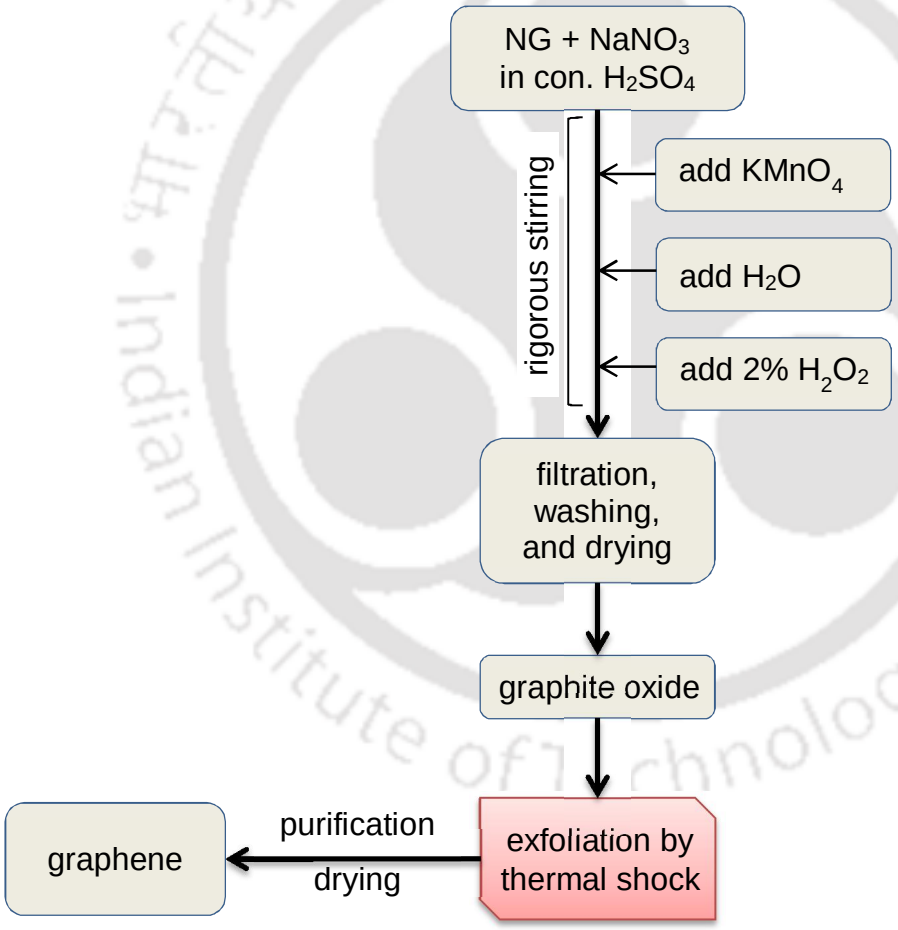

Figure 3.2: Different stages of thermochemical reduction of NG to synthesize monolayer graphene

3.2 Development of composite bipolar plate

The carbon composite bipolar plates were developed by solution blending of reinforcement(s) with resin followed by the compression molding of the dry mixture. An appropriate amount of resin volume fraction was dissolved in acetone and mixed thoroughly with the reinforcements (NG and/or CB and/or CF and/or graphene). For VER based composite, the catalyst, the promoter, and the accelerator were also added to the resin. Mixing of the reinforcements in the resin solution was done with the help of a mechanical stirrer for around 30 min. The homogeneous mixture was then allowed to dry at a temperature of 25°C. The mixture was stirred with a glass rod in regular interval to avoid formation of lumps. If necessary, the completely dried mixture was again ground to powder form. The dry and powdered mixture of the resin and reinforcement was then transferred to the cavity of a specially designed mold for compression molding.

The powdered mixture, transferred in to the mold, was then pressed at around 86°C and cured at 220°C for PF based composites. The VER based composites were compression molded at 180°C. The curing temperatures for resol-PF, novolac-PF, and VER were found out by characterizing several composite bipolar plates compression molded at different temperatures. The curing time was 1 h for both the resins and the samples were removed after proper cooling. The bipolar plates were then either cut into several sizes for different characterizations or these were used for testing in PEMFC. Figure 3.3 shows the schematic and a sample photograph of the developed bipolar plate with inbuilt flow channels.

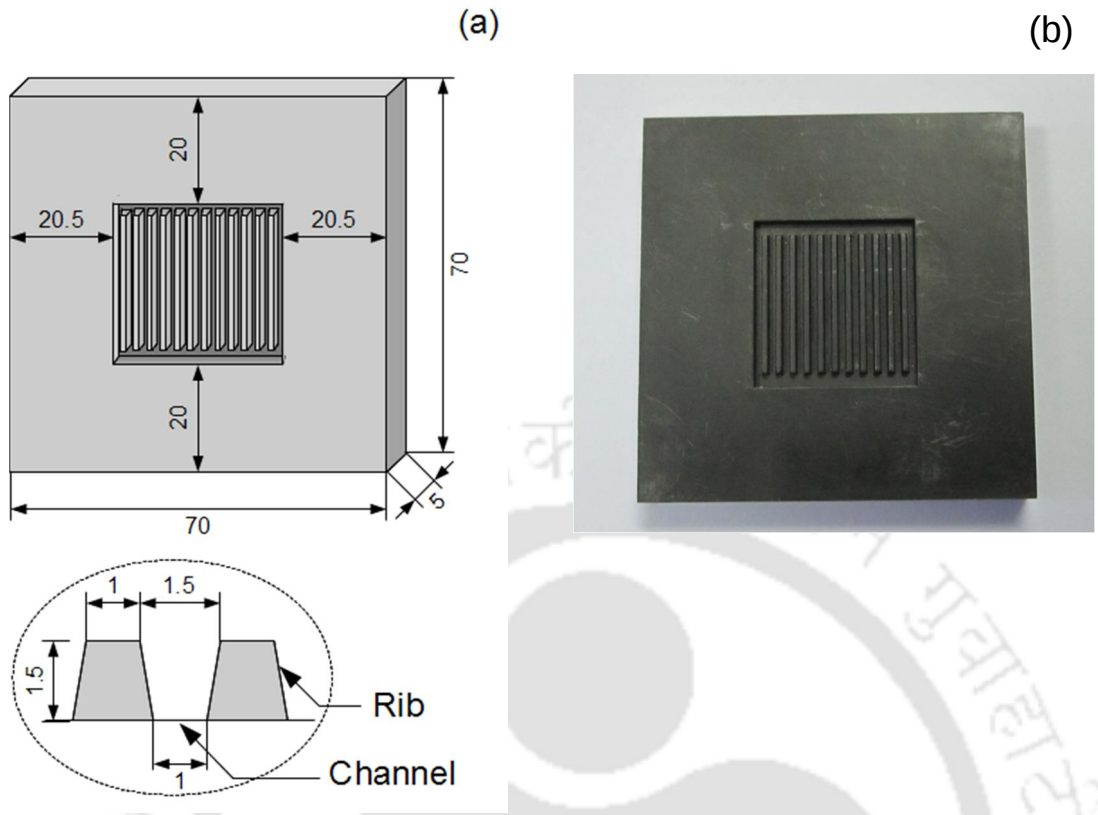

Figure 3.3: (a) schematic of the bipolar plate with magnified view of the channels and ribs (all the dimensions are in mm), and (b) photograph of a developed bipolar plate

The mold was designed and fabricated using H-13 steel material. The flow field design (parallel pattern) was kept simple as our aim was not on the flow field design part of the bipolar plate. The schematic of the fabricated bipolar plate is shown in fig.3.3 along with the dimensions.

3.3 Characterization

The raw materials used for the development of the composite bipolar plates were studied for morphological analysis, thermogravimetric analysis, particle size analysis, BET surface area analysis. The developed bipolar plates were characterized for density, hydrogen permeability, electrical conductivity, thermal conductivity, flexural strength, shore hardness, corrosion resistance, and thermal stability. Moreover, the developed bipolar plates were also studied for morphological analysis using SEM.

3.3.1 *Characterization of procured raw materials*

The DSC analysis of the procured resin and the thermogravimetric analysis of the all raw materials were carried out. The morphological analysis of NG, CB and CF were carried out using SEM, XRD, particle size analyzer, and BET surface area analyzer. However, characterization of graphene is shown separately in section 3.3.2.

3.3.1.1 *DSC analysis of the resins*

The curing behavior of different resins was analyzed by heat flux DSC analyzer (make: NETZSCH; model: STA 449F3). Approximately 5 mg of the resin was encapsulated in an aluminum crucible and punctured on the top side of the capsule. The sample was placed in the slotted region of the furnace and it was heated along with a known reference material with a heating rate of 5°C·min^{-1} to obtain the energy change with the temperature. The samples were tested from 25–900°C.

3.3.1.2 *Thermogravimetric analysis of resins*

The thermal behavior of the procured raw materials was studied using thermogravimetric analyzer (make: Mettler Toledo; model: SDTA 851e). Approximately 5 mg of the raw material was taken in a 70µL alumina crucible and analyzed in the range of 25–900°C; at a heating rate of 5°C·min^{-1} under nitrogen atmosphere condition.

3.3.1.3 *SEM analysis*

The surface morphology of NG, CB, and CF was studied using scanning electron microscope (make: LEO; model: 1430vp). The powder samples were dispersed in isopropanol with the help of an ultrasonic bath. The thoroughly dispersed solution was spread over a conductive aluminum sheet and kept in the oven to remove the volatile content. The dried powder samples and the bipolar plates were conductive. Therefore, the

samples were directly mounted on the stub and subjected to SEM analysis without any conductive coating.

3.3.1.4 *XRD analysis*

The XRD analysis of the NG, CB, and CF were carried out in an advanced diffractometer (make: Brucker; model: D8 Advanced X-ray diffractometer). The samples were dried and kept over a slide which was later fixed in the XRD analyzer. The X-ray gun in the XRD analyzer uses a monochromatized Cu-K_α radiation. The wavelength of the Cu-K_α X-ray is approximately 1.5406 Å at 40 kV and 40 mA operating voltage and current, respectively. The XRD gun was swept from 5–80° with a step size of 0.05° and scan rate of 0.5 s.

3.3.1.5 *Particle size analysis*

Particle size analysis of the NG and CB was carried out in a laser particle size analyzer (make: Malvern Instruments; model: MASTERSIZER 2000) by dispersing the sample in water. The instrument was corrected for background correction prior to particle size analysis.

3.3.1.6 *BET surface area analysis*

The surface area of the NG and CB was measured in BET surface area analyzer (make: Beckman-Coulter; model: SA 3100) using nitrogen adsorption isotherm at 77 K. The relative pressure used to obtain the BET area is in the range 0.05–0.2. Prior to nitrogen purging, all the samples were thoroughly outgassed for 3 h at 300°C to remove the moisture or volatile content.

3.3.2 *Characterization of developed graphene*

The developed graphene was characterized using SEM, XRD, TGA, and BET surface area analyzer as discussed in the previous section. The composition of the developed graphene was analyzed quantitatively by Energy Dispersive X-Ray (EDX) (make: Oxford

Instruments; model: INCA X-sight). Moreover, graphene was also characterized using High Resolution Transmission Electron Microscope (HRTEM), Electron Diffraction (ED), Atomic Force Microscopy (AFM), and Fourier Transform Infrared (FTIR) analyses. The methodologies for these characterizations are given below.

3.3.2.1 *HRTEM and ED analysis*

The developed graphene was studied in HRTEM (make: JEOL; model: JEM 2100). The HRTEM is an imaging mode of the TEM that allows the imaging of the crystallographic structure of a sample at atomic scale. The nanoscale crystallographic properties (upto 0.8 Å) of a sample can be carried out due to the high resolution of HRTEM. The samples were dispersed ultrasonically in isopropanol for 1 h. The homogeneously dispersed sample was then spread over a 300 mesh size copper grid. The grid along with the sample was then transferred to a petridish and dried in a vacuum oven to remove the volatile content. The TEM grid along with the sample was mounted on a single axis tilt sample holder and inserted into the TEM goniometer. The sample was optically aligned and subjected to further analysis. The selected area electron diffraction (SAED) was also studied over a limited area to study the detailed information about the crystalline nature of the graphene film. The lattice points on the diffraction pattern were identified and used to study the single layer graphene properties [Alford et al., 2007; Avinash et al., 2010; Zhang et al., 2010].

3.3.2.2 *AFM analysis*

The atomic force microscopy (AFM) of the graphene sample was carried out to study the nano-level morphology. Graphene sample was mixed with isopropanol and dispersed thoroughly by ultrasonication. The homogeneously dispersed sample was then spread over an ultra-flat mica substrate and kept in a vacuum oven to remove the volatile

content. The slide was then used to carry out the AFM analysis. The 3D image was taken to study the surface morphology of the graphene whilst the thickness of the sample was measured by the height profile at the edge of a graphene sheet [Shen et al., 2009; Chen and Yan, 2010; Chandra et al., 2010; Soldano et al., 2010;].

3.3.2.3 *FTIR analysis of graphene*

The graphene samples were analyzed with a Fourier Transform Infrared (FTIR) spectrometer (make: Perkin–Elmer; model: Spectrum One spectrometer) to identify the presence of functional groups. The dry and purified graphene samples were finely ground with KBr pallet in a marble mortar and pestle. This powder mixture was then pressed in a mechanical press to form a translucent thin pellet. The pallet was scanned in the range of 500–4000 cm^{-1}. The FTIR spectrograms were compared with standard spectrogram to identify the presence of functional groups.

3.3.3 *Ex-situ characterization of the bipolar plate*

The developed bipolar plates were tested for density, hydrogen permeability, flexural strength, shore hardness, electrical conductivity, thermal conductivity, corrosion resistance, morphology, and thermal stability. Moreover, developed bipolar plates were also tested in a PEMFC as described in the section 3.3.4. The TGA and SEM analyses of the developed composite bipolar plate have been carried out as per the procedure described in the sections 3.3.1.2 and 3.3.1.3. The TGA analysis of the composite bipolar plates was carried out in the temperature range 25–500°C at a heating rate of $5°C \cdot min^{-1}$.

3.3.3.1 *Density*

The bulk density of the developed composite bipolar plates was measured as per the ASTM C559 standard method. This test method covers the determination of the bulk density of manufactured items of carbon and graphite. The bipolar plate was cut into

rectangular parallelopiped shape and all the sides were polished with the help of a fine emery paper. The dimensions of the sample were measured with the help of a vernier caliper. The least count of the vernier caliper was 0.002 cm (make: Aerospace instruments). The weight (w) of the sample (in g) was measured using a high precision electronic balance (make: Denver Instrument, model: SI-234) that has a least count of 0.1 mg. The length (l), breadth (b), and thickness (d) of the sample (in cm) were measured at least three times and the average of these values was considered to calculate density. The density of the bipolar plate was calculated as per the eq. 3.8.

$$\rho = \frac{w}{lbd}\ g\cdot cm^{-3} \qquad 3.8$$

3.3.3.2 *Hydrogen permeability*

An experimental setup has been designed and fabricated to measure the hydrogen permeability of the composite under pressurized condition and at different temperature. A schematic of the experimental setup is shown in fig.3.4. All the parts of the experimental setup were made of stainless steel. The bipolar plate samples were cut into the size of 30mm×30mm and all the sides were polished with fine grade emery paper. The sample was fixed in a sample holder made up of two circular stainless steel flanges. A silicone gasket was used on both the sides of the sample to prevent leakage of the gas. The top flange was connected to a hydrogen gas supply line. A bypass valve was provided to release pressure, particularly at the end of the experiment. The pressure of hydrogen gas over the bipolar plate was controlled with the help of a regulator attached to the hydrogen gas cylinder. A ceramic band heater was used to heat the sample holder along with the sample and temperature was maintained with the help of a digital temperature controller. The hydrogen permeates through the composite was collected in a cylinder connected on the other side of the sample holder.

The hydrogen gas permeability was checked at a pressure difference of 2 bar across the bipolar plate at different temperature. The gas was sampled from the downstream side and analyzed using a hydrogen leak detector. The bipolar plate was kept up to 12 hours under pressure to measure the hydrogen permeability at different temperatures.

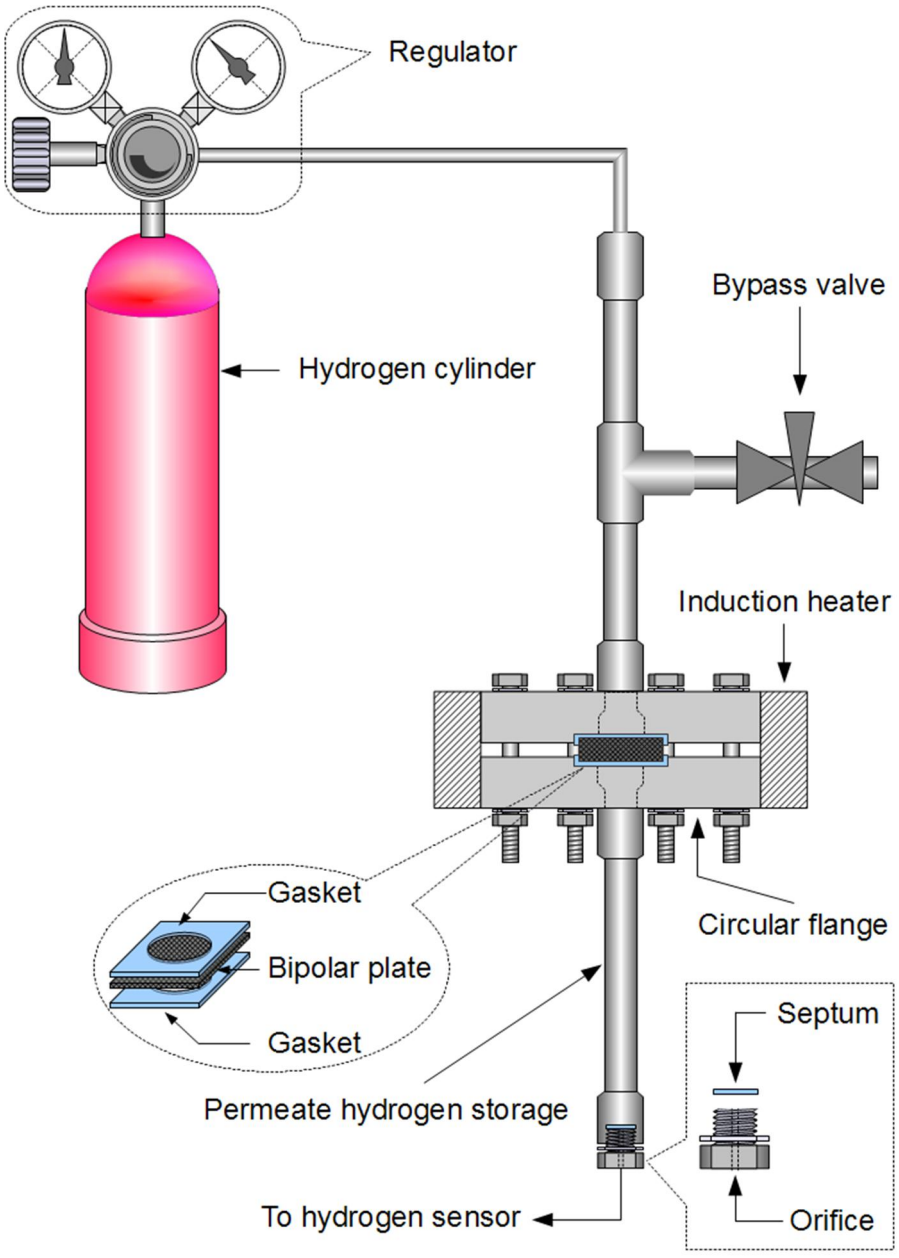

Figure 3.4: Schematic of hydrogen permeability measurement unit

The hydrogen permeability (K) of the composite bipolar plate, at a pressure (P), was calculated as per the following equation [Yasuda, 1975].

$$K = \frac{\varphi}{A} \times \frac{d}{t} \ cm^3 \cdot cm^{-1} \cdot s^{-1} \qquad 3.9$$

where, d be the thickness of the plate (0.5 cm), and φ is the amount of hydrogen (cm^3) passed through an area $A\,(4.91\,cm^2)$ of the bipolar plate over a time t (s).

3.3.3.3 *Flexural strength and flexibility*

The flexural strength and the flexibility of the composite bipolar plates are important properties as the bipolar plates may undergo high bending force during clamping within the fuel cell hardware. The three-point flexural strength of the bipolar plate was evaluated using a universal testing machine (make: Dipak Polyplast Pvt. Ltd., model: UTM DUTT-101) as per the ASTM D790.

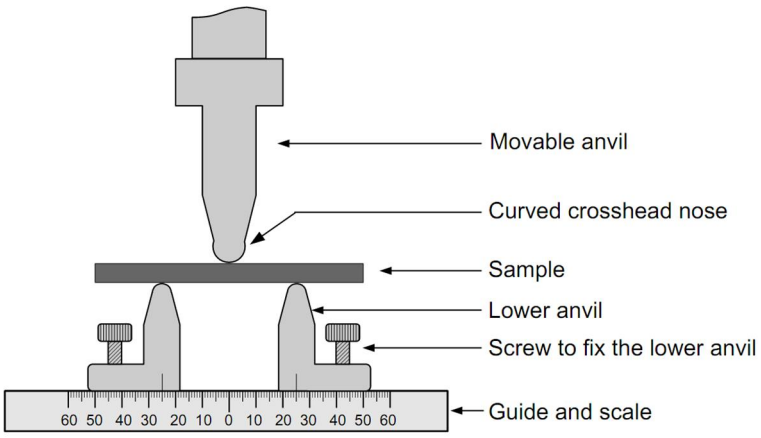

Figure 3.5: Schematic of a three point flexural strength measurement fixtures

The test specimens were prepared by cutting a rectangular piece of the bipolar plates. The length (l), breadth (b), and depth (d) of the test samples were measured with the help of a vernier caliper. The thickness of the samples was around 5 mm and the breadth was

kept around 12.5 mm. The sample was then polished with the help of a fine grade emery paper. The span length was kept 16 times to that of thickness of the sample as per the ASTM D790. The sample was mounted over the lower anvil as shown in the fig.3.5. The crosshead speed of the loading point was maintained at 0.5mm·min^{-1}. The rate of cross head speed could be calculated from the following equation.

$$R = \frac{ZL^2}{6d} \text{ mm·min}^{-1} \qquad 3.10$$

where, R = rate of cross-head speed in mm·min^{-1}, L = span distance in mm, and Z = rate of strain at the outer side of the sample, mm·mm^{-1}·min^{-1}. Z shall be equal to 0.01 as per the standard.

The movable anvil started applying load to the specimen at the specified cross-head rate, and the simultaneous load-deflection data was monitored with the help of a computer. The break load and the maximum deflection were recorded accordingly. The flexural strength of the composite bipolar plate was calculated using eq.3.11.

$$\chi_f = \frac{3FL}{2bd^2} \qquad 3.11$$

where F = load at a given point on the load deflection curve in N,

L = support span distance in mm,

b = width of the test sample in mm,

d = depth of the test sample in mm.

Similarly, the percentage of deflection at mid-span (D_{mid}) of the bipolar plate samples were also calculated using eq.3.12 [Sessions, 1976; Marianowsky, 2001].

$$D_{mid} = \frac{D}{L/2} \times 100\% \qquad 3.12$$

where, D = maximum deflection at the center of the beam in mm.

The reported values of the flexural strength and percentage of deflection at mid-span of the bipolar plate is an average of four test samples.

3.3.3.4 *Shore hardness*

Shore hardness was measured with the help of a scleroscopic hardness tester (Imai Testing Machine Manufacturing Company Limited, model: Hardscope) as per the ASTM C886. It is a dynamic indentation type hardness test in which a diamond tipped hammer is allowed to fall vertically from a fixed height over the test specimen. The height of the rebound of the diamond tipped hammer was noted down and it was equal to the shore hardness of the composite bipolar plate.

3.3.3.5 *Electrical conductivity*

Electrical conductivity of the bipolar plate was measured as per the ASTM C611 method using conventional four probe technique at a constant current supply. The schematic of the electrical conductivity measurement set-up is shown in fig.3.6. The bipolar plate samples were polished with fine grade silicone carbide emery paper to reduce the skinning effect. Later, the polished samples were cleaned with acetone. The surface treated samples were sandwiched between two carbon papers to ensure the good electrical contact between the sample and the metal. Keithley electrometer (model-6514) was used as the constant current source. The electrical conductivity (σ) of the bipolar plate was determined using eq. 3.13.

$$\sigma = \mathrm{K} \times \mathrm{K}' \times \frac{\mathrm{I}}{\mathrm{V}} \times \frac{\mathrm{x}}{\mathrm{bd}}\ \mathrm{S \cdot cm^{-1}} \qquad 3.13$$

where, b (cm) and d (cm) are the breadth and thickness of the sample, respectively. The constant current supplied through the sample is represented by I (A), and V (V) is the voltage drop between two points separated by a distance x (cm) along x-direction. The

constants K and K' are the correction factors for geometry and thickness of the sample [Barbir, 2005]. However, current is supplied through the sample and − 0.4. Therefore, the quantities K and K' are close to unity [Smits, 1958]. The same set-up was also used to measure the through-plane electrical conductivity by changing the orientation of the bipolar plate as shown in fig.3.6 [Kakati et al., 2010].

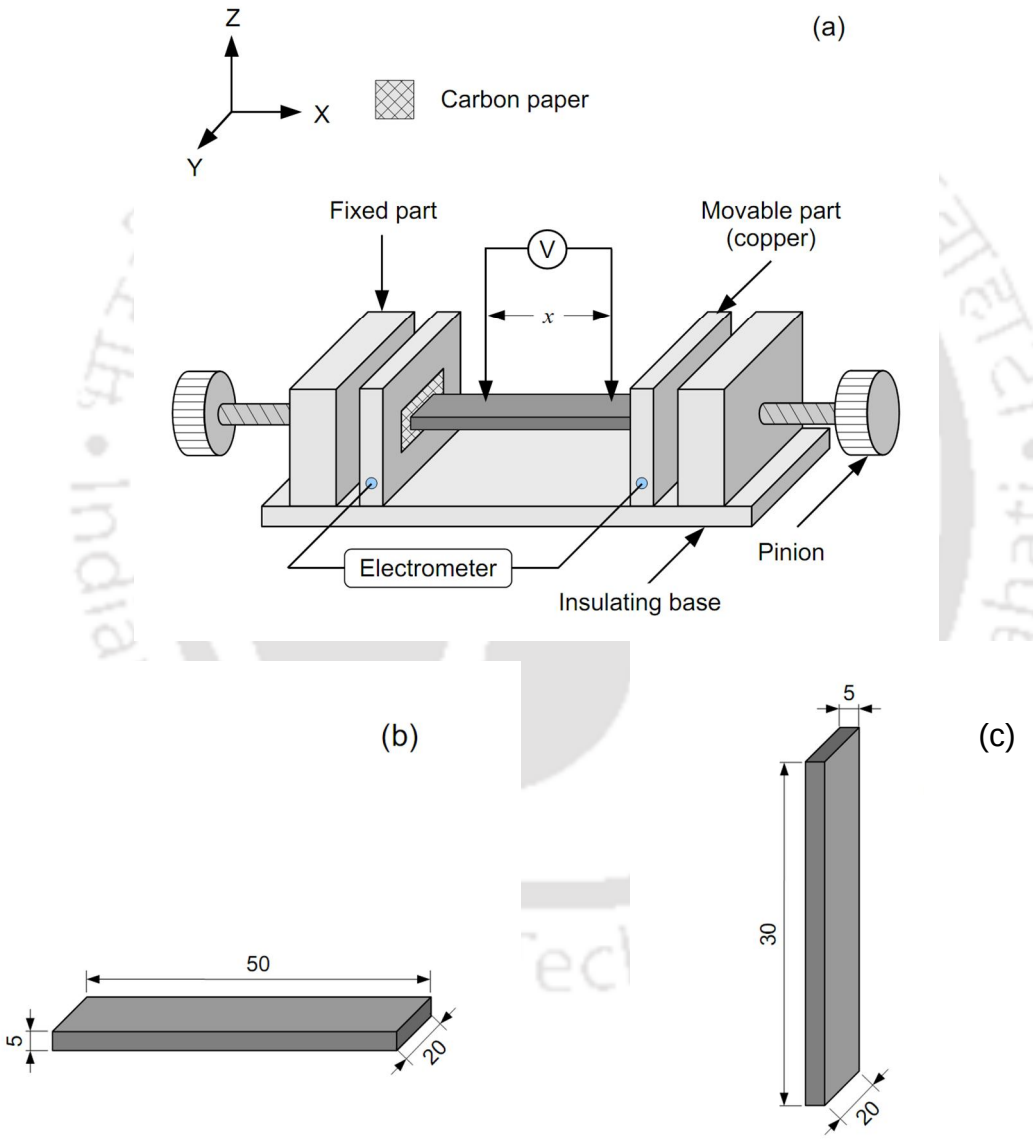

Figure 3.6: (a) Schematic of the electrical conductivity measurement set-up and orientation of the sample for (b) in-plane and (b) through-plane electrical conductivity measurement

3.3.3.6 *Thermal conductivity*

The thermal conductivity of the composite was measured with the help of Heat Conduction Unit (make: Gunt, model: WL 370). Figure 3.7(a) shows the basic linear thermal conductivity measurement unit. The control unit was used to supply power to the heater in the heating zone while water was passing through the cooling zone to achieve the steady heat conduction. The temperature at different points along the sample was measured with the help of the thermocouple attached at the respective points (points 1–8). The temperature at the points 1, 2 and 3 will record the temperature at the heating zone. Similarly, the temperature at 6, 7 and 8 will provide the temperature on the cooling zone. The temperature across the bipolar plate sample can be measured at the point 4 and 5. The thermal conductivity unit was calibrated with the help of a standard sample before conducting the experiment for the composite bipolar plate.

To conduct the experiment a sample bipolar plate was cut and fixed within a PTFE sample holder as shown in fig.3.7(b,c). The water flow rate to the cooling zone was maintained approximately at 1.0 $l \cdot h^{-1}$. The heating zone was heated by supplying a very nominal power of 1–3 W. The temperature at different points was successively recorded at regular interval to find out the steady state steady-state heat transfer. The temperature at the points 4 and 5 were recorded at steady-state condition for thermal conductivity measurement.

If x be the distance between the points 4 and 5, and the temperature recorded at these points are T_4 and T_5, respectively, then the heat flux (q) transferred from the heating zone to the cooling zone will be represented by eq.3.14.

$$q = \kappa \times \frac{T_4 - T_5}{x} \ W \cdot m^{-2} \qquad 3.14$$

where, κ = thermal conductivity of the composite bipolar plate in $W \cdot m^{-2} \cdot K^{-1}$.

The thermal conductivity unit was calibrated with the help of standard sample to avoid experimental error.

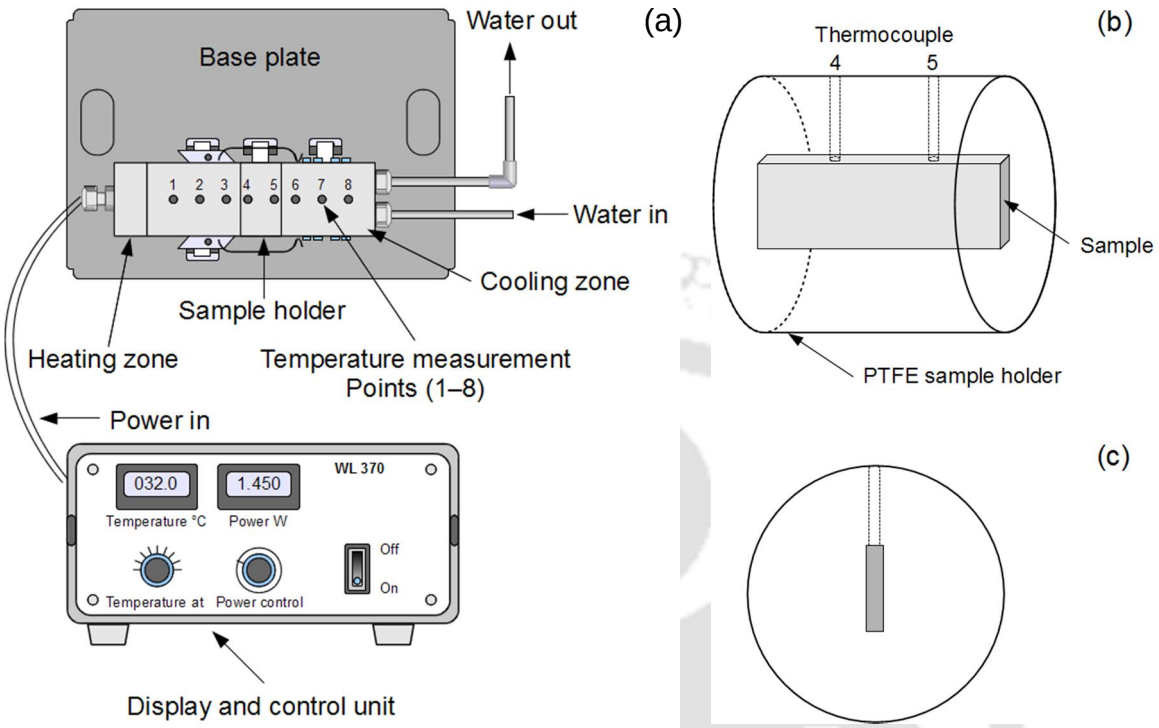

Figure 3.7: Schematic of the (a) thermal conductivity measurement unit, (b) isometric view, and (c) cross sectional view of the PTFE sample holder with bipolar plate

3.3.3.7 *Corrosion study*

The corrosion behavior of the bipolar plate was studied with the help of potentiodynamic polarization and cyclic voltammetry analysis using a potentiostat (make: CH Instruments; model: CHI-600B).

3.3.3.7.1 Potentiodynamic polarization

Corrosion study using linear sweep voltammetry was carried out in a three-electrode electrochemical cell. Bipolar plate with 6 cm^2 area was used as a working electrode, Ag/AgCl as a reference electrode and Pt wire was used as a counter electrode. The corrosion study of the bipolar plate was carried out in 0.1M, 1.0M H_2SO_4, and 1.0M

NaOH solution at 25°C in a voltage range from –1.0 to +1.0 V vs. Ag/AgCl electrode. Moreover, the bipolar plates were also tested in a rigorous simulated PEMFC environment prepared by 1.0M H_2SO_4 solution aerated at 80°C [Duo et al., 2003; Powell and Childs, 1972; Ma et al., 2000; Wang et al., 2004; Fu et al., 2008; Choi et al., 2009]. The corrosion study was also carried out in 1.0M NaOH solution aerated at 80°C, which is a simulated rigorous environment of an alkaline fuel cell (AFC) [Kakati et al., 2010].

Classical Tafel analysis was performed by extrapolating the linear portions of a log current density versus potential plot to obtain the corrosion current density and potential at their intersection (fig.3.8). It is assumed that the rate of the corrosion process is controlled by the kinetics of the electron transfer reaction at the working electrode as it is generally the case for corrosion reaction [Wang et al., 2004]. An electrochemical reaction under kinetic control follows the Tafel equation (eq.3.15),

$$i = i_o \exp\left(2.303 \frac{E - E_o}{b}\right) \qquad 3.15$$

where, i = current density ($A \cdot cm^{-2}$) resulting from the reaction, $i_\circ$ = a reaction dependent constant called the exchange current density ($A \cdot cm^{-2}$), E = electrode potential (V), $E_\circ$ = equilibrium potential (V), and b = Tafel constant (constant for a particular reaction).

The Tafel equations for both the anodic and cathodic reactions in a corrosion system can be combined to generate the Butler-Volmer equation (eq.3.16).

$$i = i_{corr} \left[\exp\left(2.303 \frac{E - E_{corr}}{b_a}\right) - \exp\left(-2.303 \frac{E - E_{corr}}{b_c}\right)\right] \qquad 3.16$$

Where, i_{corr} = corrosion current (A), E_{corr} = corrosion potential (V), b_a = anodic Tafel constant (V/decade), b_c = cathodic Tafel constant (V/decade). The voltage reported in the thesis is with respect to the standard hydrogen electrode.

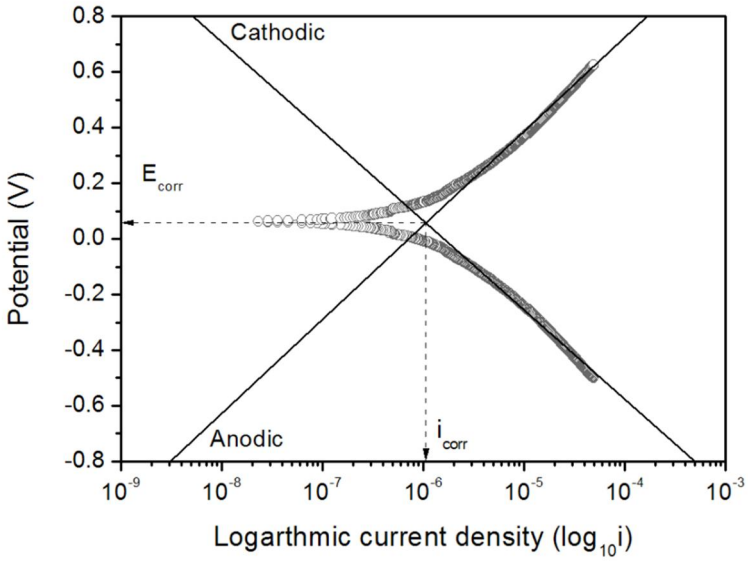

Figure 3.8: Tafel plot showing corrosion current density and corrosion potential

3.3.3.7.2. Cyclic voltammetry

Cyclic voltammetry of the bipolar plate was carried out in rigorous acidic (1.0M H_2SO_4) as well as alkaline (1.0M NaOH) environment at a scan rate of $1mV{\cdot}s^{-1}$. The electrochemical cell was aerated and heated at 80°C during the experiment [Kakati et al. 2010].

3.4 Fuel cell testing

A fuel cell was developed using the composite bipolar plates. The developed fuel cell was used to characterize the composite bipolar plate in the real environment of PEMFC. The fuel cell was developed and used to study the i–V performance in a sequential process discussed in the following subsection.

3.4.1 *Fabrication of PEMFC setup*

A PEMFC and the necessary setup were developed to study the performance of composite bipolar plate in the real environment of fuel cell. The end plates for the fuel cell were fabricated using a 6 mm thick copper plate. The schematic of the two end plates

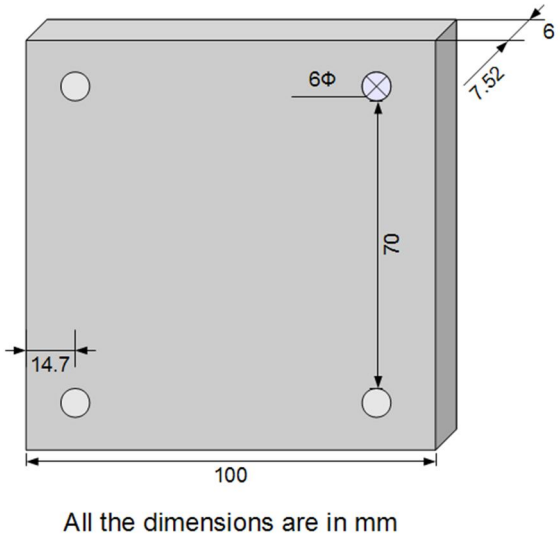

Figure 3.9: A schematic of the fabricated end plates for PEMFC

are shown in fig.3.9. The MEA was sandwiched between two bipolar plates of same composition, followed by the end plates and tightened with the help of the allen bolts.

An experimental setup for the fuel cell testing was designed and the schematic of the setup is shown the fig.3.10(a). The hydrogen was fed from the cylinder through a bubbler humidifier to the anode side, whereas oxygen was directly fed to the cathode side of the fuel cell. It is to be noted that much effort was not given on the humidification system. Therefore, the humidification was kept constant for all the studies in order to get the comparative results. The flow rate of hydrogen and oxygen was controlled with the help of two rotameters. The temperature of the fuel cell was controlled with the help two heating pads attached to each end plate. The current and voltage across the cell was monitored with the help of help of a precision multimeter (make: Sanwa, model: PC 5000). Figure 3.10(b) shows a photograph of the developed fuel cell testing set-up.

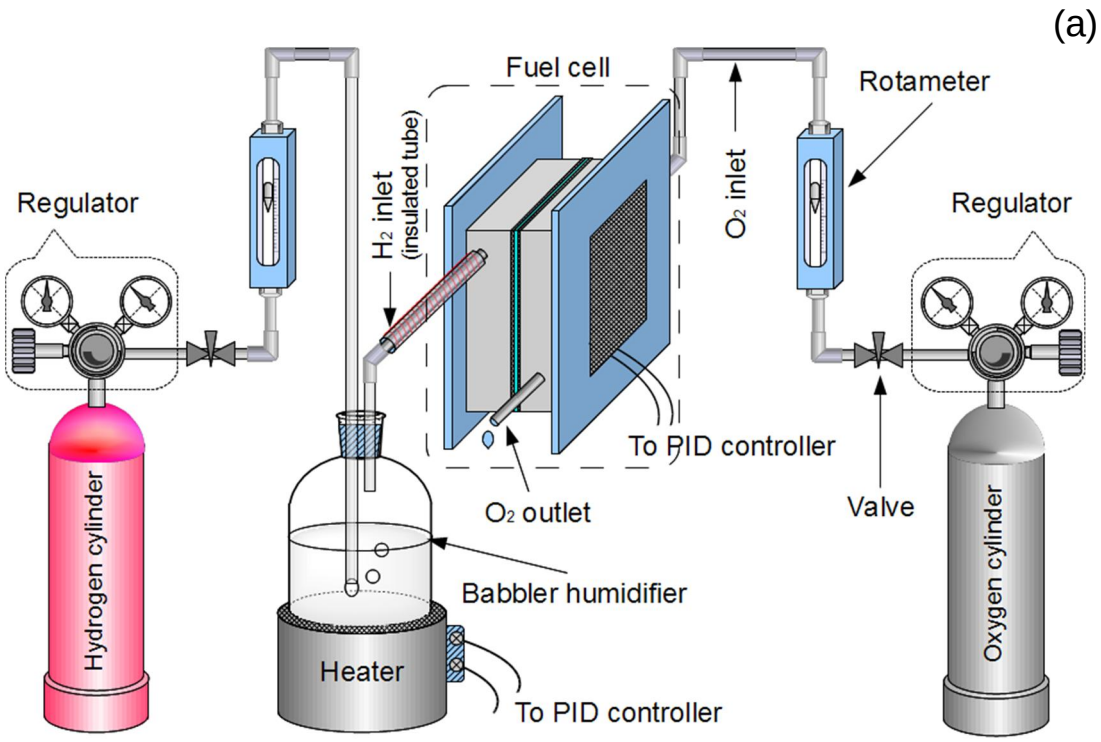

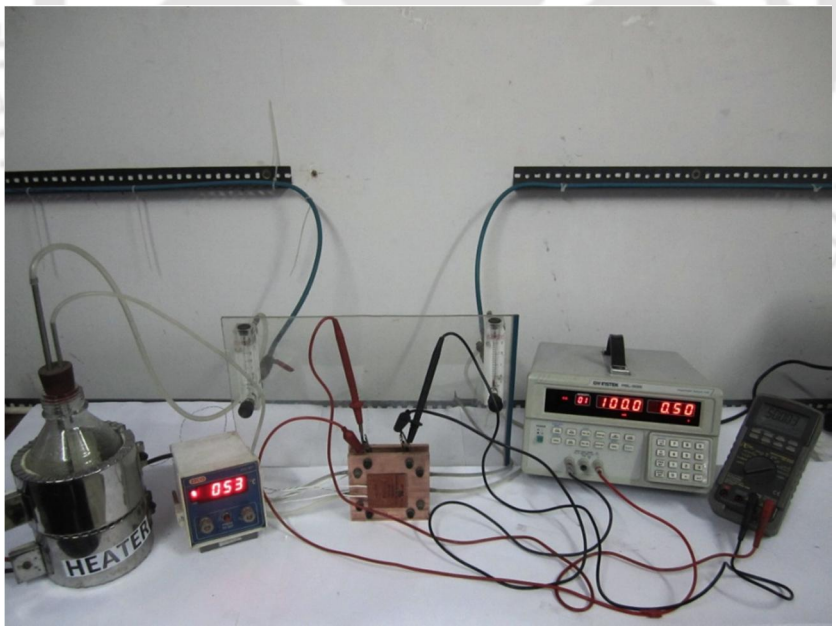

Figure 3.10: (a) A schematic of the PEMFC testing set-up and (b) snapshot of the PEMFC arrangement

3.4.2 *Fabrication of MEA*

Nafion 115 membrane was cut in square size for pretreatment. The membrane was first treated in 0.5M H_2SO_4 solution for 1.0 hour at 80°C. The acid treated membrane was then boiled and cleaned in hot water for 1.0 hour at the same temperature. The membrane was then treated in 0.5M H_2O_2 for 1.0 hour at same temperature followed by cleaning with water as mentioned earlier. Finally, the treated membrane was wiped with tissue paper to remove the surface water.

The carbon supported platinum catalyst (Pt:C=40:60) was used develop the catalyst layer over the GDL. The anode and cathode catalyst loading were kept as 0.5 and 1.0 $mg \cdot cm^{-2}$, respectively. The catalyst was then dispersed in 3ml isopropyl alcohol together with 2ml water by sonicating it for 20 min. The homogeneous dispersion of catalyst was then sprayed over the respective GDL with the help of a spray gun at 110°C. Before going for hot pressing, the naturally cooled GDL with the catalyst layer were heat treated in an air oven for about 12 h at 80°C. The catalyst coated GDLs were placed on the both sides of a previously treated nafion 115 membrane. The assembly of the membrane and catalyst coated electrodes were then compression molded at 100°C for 3 min under a $45kg \cdot cm^{-2}$ pressure. The MEA was then cooled to room temperature by setting a cooling time of 30 min. The final MEA was then tested in fuel cell using the developed bipolar plate. A picture of the developed MEA and its schematic, showing sequence different layers, are shown in fig.3.11.

3.4.3 *Fuel cell performance analysis*

The developed MEA was sandwiched between two similar bipolar plates and tested for $i-V$ performance of the fuel cell. The hydrogen and oxygen flow rates were maintained to be 0.5 and 1.0 lpm, respectively. The temperature of the fuel cell was controlled with

the help of a digital temperature controller. The output current and voltage was measure with the help of two digital multimeters. A rheostat was used as a variable load to control the output current of the fuel cell. The $i-V$ performance of the fuel cell was recorded at different operating temperatures.

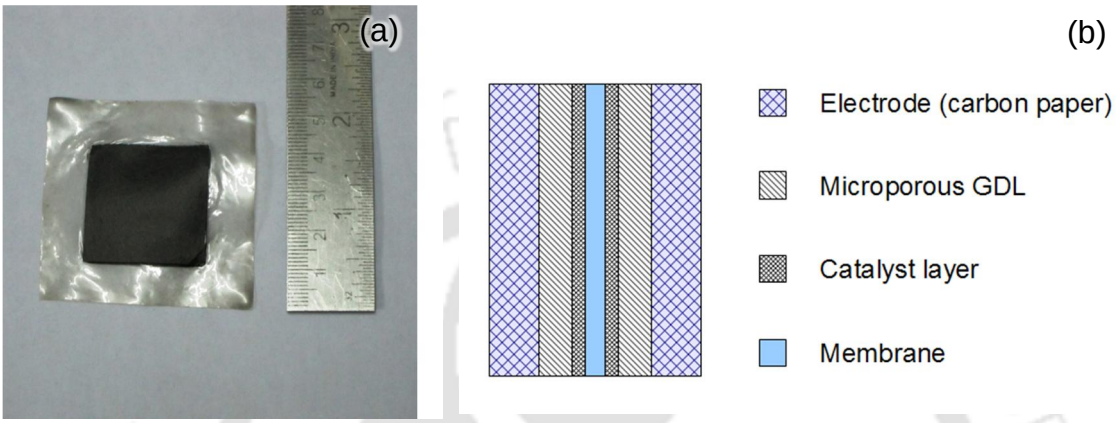

Figure 3.11: The snapshot of (a) the developed MEA, and (b) its schematic

Chapter 4

Electrical Conductivity Modeling

Electrical conductivity modeling

In this chapter a model for electrical conductivity has been developed for binary composition (NG and resin). Though the model predicts well the experimental data but it has limitations due to the image processing technique. Therefore, a different model discussed to predict the electrical conductivity of composite bipolar plate with multiple fillers (NG, CB, and CF).

4.1 Modeling for electrical conductivity of composite bipolar plate

As discussed in the chapter 2, the graphite is an excellent candidate for development of bipolar plate, but low mechanical strength, brittleness, and cumbersome flow field machining limit its practical use in large scale application [Dhathathreyan and Rajalakshmi, 2007]. Furthermore, the pure graphite bipolar plates are usually prone to leakage of hydrogen gas and hence require impregnation with a resin material for gas-tightness [Washington et al., 1994; Wang et al., 2005]. Eventually, the resin impregnation, polishing, and machining of flow field are added up to the high cost of the bipolar plate. Therefore, scientists and researchers are searching for an alternative material and it is found that the carbon composite material is one of the most promising candidates for bipolar plate applications. Graphite, being one of the best electrically conductive and non-corrosive materials, is used along with resin to form a composite bipolar plate [Cho et al., 2004; Yin et al., 2007; Pozio et al., 2008; Heras et al., 2009]. However, the properties of graphite-resin composite bipolar plate are not up to the benchmark as discussed in table 1.2. Therefore, different type of fillers such as NG, SG, CB, CF, CNT, etc. are also being reinforced to achieve the target properties of the composite bipolar plate for fuel cell applications. Typically, resin is an electrically insulating material with electrical conductivity in the order of 10^{-15} $S \cdot cm^{-1}$, whereas the electrical conductivities of graphene, NG, CB and CF are around 10^{6}, 10^{5}, 100 and 600

$S \cdot cm^{-1}$, respectively [Powell and Childs, 1972; Probst and Grivei, 2002; Barton et al., 2007].

The electrical properties of composites with binary mixtures of conducting and insulating materials have been studied and predicted for over many decades [Wang and Anderson, 1999]. The electrical conductivity of such composite is basically determined by the electrical conductivities of the individual components and the percolation thresholds [Srivastava and Mehra, 2009; Bhattacharya et al., 2009]. Gurland (1966) studied the compacted mixtures of silver balls and Bakelite powder, and observed a pronounced threshold when the volume fraction of the metal became 30%. The work of Malliaris and Turner (1971) has shown that the value of the threshold concentration may also vary with the preparation methods. Moreover, the shape of the fillers and their orientation within the matrix strongly influence the electrical properties of the composite. Two naturally occurring limiting cases, viz. symmetric and asymmetric, have been observed in such composites. Landauer (1978) traced the evolution of the theory for the conductivity of mixtures with conducting and insulating materials from Maxwell, through the Clausius-Mossotti approximation and the Bruggeman symmetric and asymmetric-effective-media theories to percolation theory. The effective-media theories attempt to predict the effective conductivity of the composite/mixtures with homogeneous filler distribution. A conductor-insulator transition is observed to occur over a wide range of volume fractions in the symmetric-media theory [Thongruang et al., 2002]. However, there is no such transition in asymmetric media theory.

Mamunya et al. (2002) proposed a model for electrical and thermal properties of Nickel-resin and Cu-resin composite systems, near percolation threshold. However, the proposed model was not suitable for the case of composite bipolar plate as the conductive filler

content is far more than the percolation threshold [Dweiri and Sahari, 2008; Du and Jana, 2008]. Carmona and Ravier (2002) reviewed the electrical conductivity of the CB filled polymers using percolation model. The percolation model could serve only as a first approximation for the prediction of the electrical conductivity of CB-polymer composites. Therefore, Balberg (2002) modified the existing percolation model and proposed the percolation-tunneling model to describe the electrical conductivity of such a composite.

Ondracek and Kravchenko (1999) have shown a model for electrical conductivity of iron and iron carbide composite. The electrical conductivity of the iron and iron carbide was 10^5 and 227 $S \cdot cm^{-1}$, respectively. They have considered the shape factor and orientation factor of the filler (iron) in the matrix (iron carbide) and found a good agreement between the model and experimental values of the electrical conductivities. However, the model was not applicable for the systems, where the two components of the mixture had wide difference in their electrical conductivities. It is worth mentioning that the electrical conductivities of resin and graphite in the composite bipolar plate are far apart in the order of 10^{20}–10^{22} $S \cdot cm^{-1}$. Moreover, Ondracek paper described only a qualitative method to find out the shape and orientation factors of the filler in the composite. Therefore, Ondracek model was modified to predict the electrical conductivity of NG–resin composite bipolar plate, for a wide range of filler volume fraction. Concept of digital image processing (DIP) was utilized to quantitatively find out the orientation and shape factors of the electrical filler (graphite) particles in the composite bipolar plate.

McLachlan (1987,a) introduced a more simplified general effective-media (GEM) equation for the conductivity of binary mixtures. The GEM equation reduces to Bruggeman's symmetric and asymmetric theories in certain limits and has the mathematical form of the percolation equation when the ratio of the conductivities of the

two-components is extremely large. Barton et al. (2007) developed a model based on GEM equation to predict the electrical conductivity of synthetic graphite-liquid crystal polymer composite bipolar plate. They worked with three fillers composite and found a good agreement between the model and experimental values of the electrical conductivities [Barton et al., 2008], as far as the electrical conductivity of the filler components are not quite far away. Therefore, the model was not accounted for the through-plane electrical conductivity of the composite bipolar plate. The literature shows that the present models are suitable for predicting the electrical conductivity of composite with either for two-, three-, or four-component systems. Thus a suitable model for electrical conductivity of composite with multi-component systems is required to study. Both the models are discussed in the following sections.

4.2 Model for electrical conductivity of bipolar plate with binary composition

Ondracek model (eq.4.1) was used as a basis to predict the electrical conductivity of the composite,

$$1-\phi_h = \left(\frac{\sigma_l}{\sigma_m}\right)^p \frac{\sigma_h-\sigma_m}{\sigma_h-\sigma_l}\left(\frac{\sigma_m+q\cdot\sigma_l}{\sigma_l-q\cdot\sigma_h}\right)^r \qquad 4.1$$

where, σ is the electrical conductivity, subscripts l, h, and m represent the low, high conductivity phases, and then composite; ϕ is the volume fraction. The constants p, q and r are the functions of shape factor (F_h) and orientation factor ($\cos\alpha_h$) as defined by eqs.4.2, 4.3, and 4.4,

$$p = \frac{F_h(1-2F_h)}{1-(1-F_h)\cos^2\alpha_h - 2F_h(1-\cos^2\alpha_h)} \qquad 4.2$$

$$q = \frac{1-(1-F_h)\cos^2\alpha_h - 2F_h(1-\cos^2\alpha_h)}{2F_h(1-\cos^2\alpha_h)+(1-F_h)\cos^2\alpha_h} \qquad 4.3$$

$$r = p + \frac{\left(1 - F_f\right) 2F_h}{2F_h\left(1 - \cos^2 \alpha_h\right) + \left(1 - F_h\right)\cos^2 \alpha_h} - 1 \qquad 4.4$$

Ondracek's model fails to predict the electrical conductivity of the composite system when the difference between the electrical conductivities of filler and insulating matrix is extremely high [Lux, 1993]. This is due to the negative value of the term $\left(\sigma_l - q\sigma_h\right)$ in eq.4.1. Thus the model needs modification to fit for electrical conductivity of composite bipolar plate for fuel cell application. A dimensionless factor was introduced to address the remedy and found out empirically. The proposed modified model is given by eq.4.5,

$$1 - \phi_h = \left(\frac{\sigma_l}{\sigma_m}\right)^{p'} \frac{\sigma_h - \sigma_m}{\sigma_h - \sigma_l} \left|\frac{\sigma_m + q \cdot \sigma_l}{\sigma_l - q \cdot \sigma_h}\right|^r \qquad 4.5$$

where, $p' = \delta p$ and δ is the dimensionless parameter. The other terms have their usual meaning.

Shape and orientations factors are assumed to be characteristic of an ellipsoid, which allow the calculation of conductivity of the binary mixtures. The orientation factor is represented by $\cos\alpha$, where α is the angle between the major axis of the ellipsoid (generated by the graphite particle or clusters) and the electric field as shown in the fig.4.1. The orientation factor of individual particle will be different from particle to particle in the real composite. Therefore, the average orientation factor of the graphite particles in the composite was considered as the weighted average of all the orientation factors as given by eq.4.6,

$$\text{Average orientation factor } (\cos\alpha) = \frac{\sum n_i \cos\alpha_i}{\sum n_i} \qquad 4.6$$

where, n_i is the number of particles having the same orientation factor.

The shape factor is defined as the ratio of minor to major axis of the ellipsoid. The

weighted average of the shape factor of individual particle or cluster was used to predict the electrical conductivity of the NG/resin composite using eq.4.5 [Kakati et al., 2009]. Though the model predicts the experimental data well but the model is still not suitable to predict the electrical conductivity of composite bipolar plate with multiple conductive filler. Therefore, another model was adapted to model the electrical conductivity of the composite bipolar plate with two-, three-, and four-component systems.

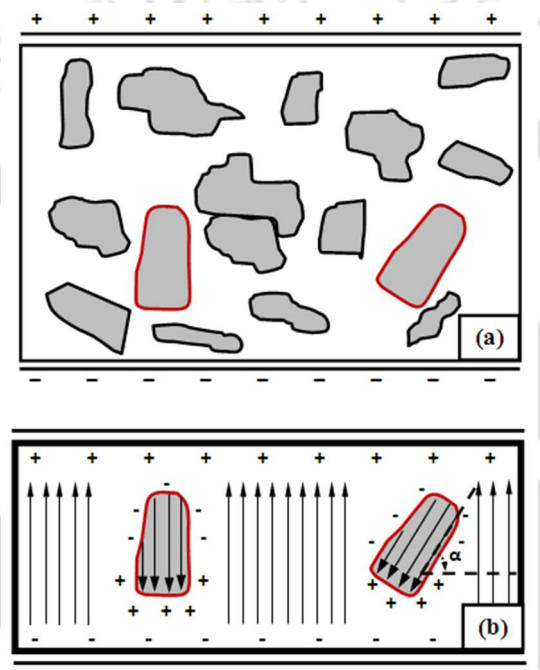

Figure 4.1: Modeling of real binary composite showing (a) particles and clusters within the polymer matrix and (b) electric field induced due to the orientation of the particles

4.3 Model for electrical conductivity of the bipolar plate with multiple filler content

The Bruggeman's effective media equations can be applied to predict the electrical conductivity of percolating, heterogeneous systems [McLachlan, 1986, 1987(a,b), 1988, 1989, 1990]. However, these equations have the limitations in predicting the electrical conductivity of the systems over the entire range of filler compositions. McLachlan

developed the GEM equation, which becomes Bruggeman's symmetric-media equation when the filler volume fraction (ϕ) is negligible in comparison to that of the matrix [McLachlan, 1987(a)]. On the other hand, the GEM equation reduces to Bruggmen's asymmetric-media equation as the polymer matrix being completely filled with the conductive filler, corresponding to the limit as $\phi \to 1$. This is the case when there is very less resin or insulating matrix. The GEM equation for two-components is written as following [McLachlan, 1987(a)].

$$\frac{\phi_l\left(\sigma_l^{1/t}-\sigma_m^{1/t}\right)}{\sigma_l^{1/t}+A\sigma_m^{1/t}}+\frac{\phi_h\left(\sigma_h^{1/t}-\sigma_m^{1/t}\right)}{\sigma_h^{1/t}+A\sigma_m^{1/t}}=0 \qquad 4.7$$

where, σ is the electrical conductivity, subscripts l, h, and m represent the low, high conductivity phases, and then composite; ϕ is the volume fraction; $A=\frac{1-\phi_c}{\phi_c}$; where ϕ_c is the percolation threshold of the high conductivity phase; the orientation of the conductive particles are defined by t, where $t=\frac{1-\phi_c}{1-\xi}$ for oriented ellipsoids, and $t=n\phi_c$ for randomly oriented ellipsoids, ξ is the effective demagnetization co-efficient of the ellipsoids within the matrix, and n is a constant.

It is found in the published literature that GEM equation fairly predicts the electrical conductivity of a composite when the conductive fillers are regular in shape [King et al., 2001; Heiser et al, 2004; Keith et al., 2006; Barton, 2007, 2008]. The GEM equation is effective in predicting the electrical conductivity of the composite when its value is between the electrical conductivity of the components, and if the electrical conductivities of the matrix and filler is far apart [Barton et al., 2008]. Barton et al. (2007) considered the electrical conductivity of SG and CF as 10^5 and 10^3 S·cm^{-1}, respectively. However, the electrical conductivities of SG and CF were considered as 50 and 598 S·cm^{-1} in the

subsequent publications [Barton et al., 2008]. It has been found that the model fits well when the electrical conductivities of the fillers are not differ by wide margin. But the ratio of the electrical conductivities of the fillers used to develop the bipolar plate is 10^4:59:10. The original GEM equation can predict the electrical conductivity of the composite bipolar plate effectively for such a complex composition only when it is modified suitably. There is a lack of published literature on electrical conductivity modeling of composite bipolar plate with four-components. Moreover, the GEM equation was not studied for both in-plane and through-plane electrical conductivities of the bipolar plate. Therefore, in this manuscript, GEM equation is extended to model the in-plane and through-plane electrical conductivities of the composite bipolar plate with multi-component systems. At this point, it should also be known that the US-DOE benchmark does not provide any information about the through-plane electrical conductivity for the composite bipolar plate.

It can be seen from the eq.4.7, that the factor t has a significant effect on electrical conductivity of the composite. Let us consider the in-plane and through-plane electrical conductivities of a binary mixture of NG and PF resin with 60:40 compositions. The effect of t on the predicted electrical conductivity is shown in fig.4.2. The critical concentration (ϕ_c) of graphite for the particular resin-graphite system is considered as 3.5% [Tchmutin et al., 2003; Zhang, 2008]. Figure 4.2 shows that the electrical conductivity of the composite changes exponentially with the change in the values of t. There may be a change in the geometric environments with the change in number of fillers and its volume fraction. Furthermore, unlike synthetic graphite and CB, the NG has different in-plane and through-plane electrical properties. Therefore, it is required to define GEM equation in such a way that it can predict both the in-plane and through-plane

electrical conductivity of the composite bipolar plate for different compositions and different fillers. The parameter t for such a system may be defined by the expression

$$t = ae^{b\phi_i} \qquad 4.7$$

where, a and b are the constants for different composite systems.

The modified GEM equation is given by the following equation,

$$\sum_i \frac{\phi_i\left(\sigma_i^{1/t} - \sigma_m^{1/t}\right)}{\sigma_i^{1/t} + A\sigma_m^{1/t}} = 0 \qquad 4.8$$

where, t is defined by eq.4.7 [Kakati et al., 2011].

The electrical conductivities of the developed carbon composite bipolar plates were modeled using the above equation for two-, three-, and four-component systems.

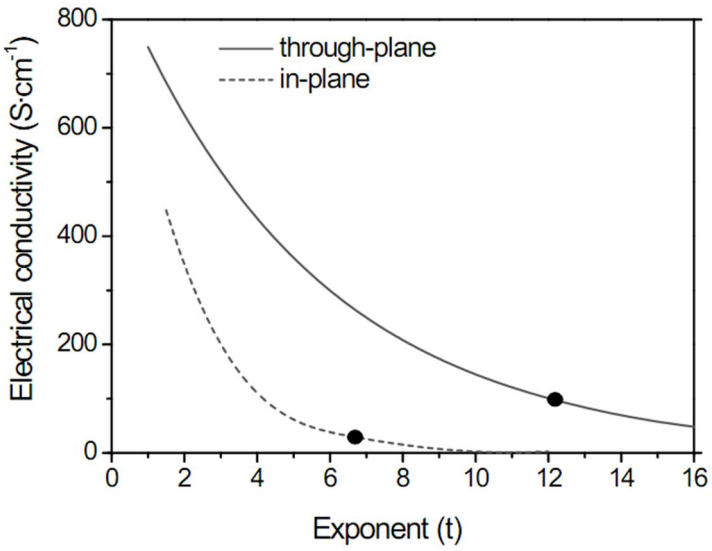

Figure 4.2: Dependence of the modeled electrical conductivity on the value of t

Chapter 5

Results and Discussion

Results and Discussion

The composite bipolar plates for PEMFC have been developed by compression molding technique. The novolac-PF, resol-PF, and VER were used as the resin matrix, and NG, CB, CF, and graphene were used as the conductive reinforcements. The procured resins were characterized by DSC and TGA to study the thermochemical and curing behavior. The conductive reinforcements were characterized by TGA, SEM, XRD, particle size analyzer, and BET analyzer as described in the section 3.3.1. The monoloyer graphene monolayer was synthesized by thermochemical exfoliation of NG. The development of the graphene was confirmed by HRTEM, ED, AFM, and FTIR. The composite bipolar plates were developed with different composition of resin to filler volume fractions. The ex-situ and in-situ characterizations of the developed bipolar plates were carried out as per the discussion in the sections 3.3.3 and 3.4.3, respectively. The morphological analysis of the composite was carried out as per the discussion in the section 3.3.1.3. The different characterizations and the performance evaluation of the fuel cell are discussed in the following sections.

5.1 Characterization of procured raw materials

5.1.1 *DSC and TGA analyses of resins*

The DSC analysis of the resin was carried out to study the curing behavior of the resin at different temperatures. Moreover, the melting point, glass transition temperature, curing temperature, and degradation temperature were also found out using the DSC analysis. The DSC thermogram of the novolac-PF is shown in fig.5.1. The first endothermic peak at 85°C is attributed lowest viscosity of the novolac-PF resin. At the temperature range 45–120°C, the resin has the minimum viscosity and it is attributed due to the transition of the resin from soluble liquid to the gelled stage [Chow, 1983; Kenny et al., 1997; Kim et

al, 2003]. The second stage from 120–170°C, with an endothermic peak at 150°C, is attributed due to the continuous formation of an incompletely cross-linked network.

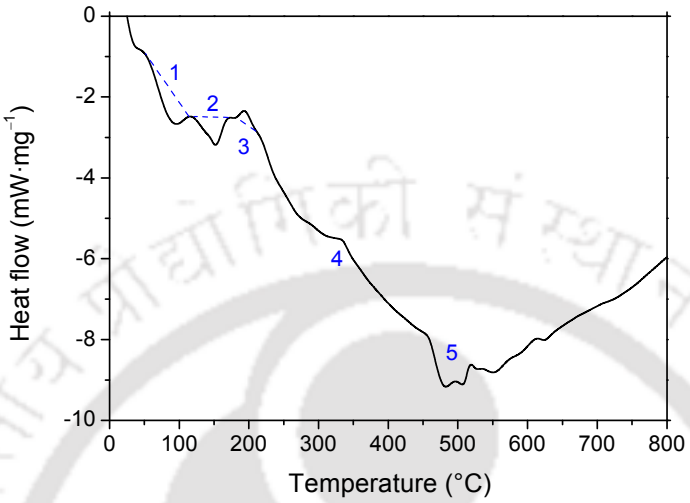

Figure 5.1: DSC thermogram of the novolac-PF resin showing various zones

The exothermic peak from 175–215°C occurs due to the curing of the resin in presence of HMTA. Actually, the third peak is a resultant of two simultaneous exothermic peaks. The first minor peak appears at the onset temperature of the resultant peak and it is associated with the accelerator HMTA. Polyreaction is the major reaction, and dehydrated condensation of hydroxymethyl occurs in this stage, which express long-chain molecules in the macroscopic view as shown in eq.3.4. The incompletely cross-linked resin in the previous stage undergoes further curing and ends with the fully cured infusible solid stage thermoset at around 215°C. In this stage, in the presence of a large excess of phenol, all the fomaldehyde bonded in the HMTA is incorporated in the form of methylene bridges. During this process ammonia is released to form methylene bridges [Kurachenkov and Igonin, 1971; Zhang and Solomon, 1994; Zhang et al., 1997, Yin et al., 2007]. Therefore, the novolac-PF based composite was cured at 220°C for complete curing of the resin matrix. The fourth peak at 330°C appears due to the exothermic reaction during

dissociation of the methylene bridge; as a result methane is released. The cured resin completely yields char at the fifth peak.

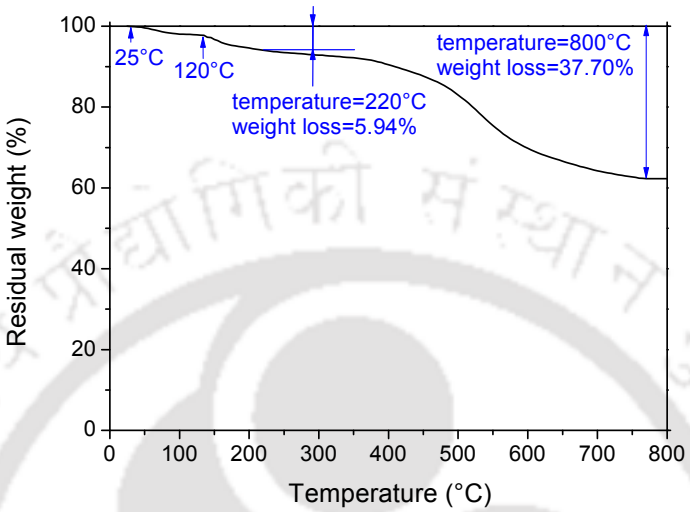

Figure 5.2: TGA theromogram of novolac-PF showing different weight loss zones

The thermogravimetric analysis of the resin was also carried out and the resultant thermogram is shown in the fig.5.2. The region for the first endothermic peak in DSC thermogram of the resin corresponds to the weight loss up to 120°C in the TGA. Similarly, the cross-linking and curing of the gelled resin to the infusible solid stage completes within 220°C with a weight loss of 5.94%. The major weight loss appears just after this stage and it was about 31.76% out of the total weight loss 37.70% up to 800°C. In this zone, from 400–800°C, the methylene bridge breaks down followed by the subsequent breaking of C−H and C−C bonds [Trick and Saliba, 1995].

The TGA analysis of the resol-PF was also carried out in the same condition. Figure 5.3 shows the TGA thermogram and major weight loss regions of the resol-PF resin. As described in the section 3.1.1.2, resol-PF resin is a "one-step" resin and hence the second weight loss zone of fig.5.2 is not visible in this thermogram (fig.5.3). In the temperature

range 80–220°C, distinct weight change was observed owing to the volatilization of water, solvent and other low molecular weight components. The curing of the resin occurs in the region 130–220°C. After completion of curing reaction, the resin starts degrading and it is prominent in the temperature range 350–750°C [Era and Mattila, 1976]. The degradation of the resol resin can be subdivided into two zones. In the first degradation zone, 350–550°C, the major evolved species are water and a mixture of cresols and phenols. In the second region, the products evolved are hydrogen, methane, carbon monoxide, water, and small amounts of carbon dioxide and ethane [Trick and Saliba, 1995]. Therefore, by observing the residual weight versus temperature thermogram, the resol-PF based composites were cured up to 220°C during compression molding.

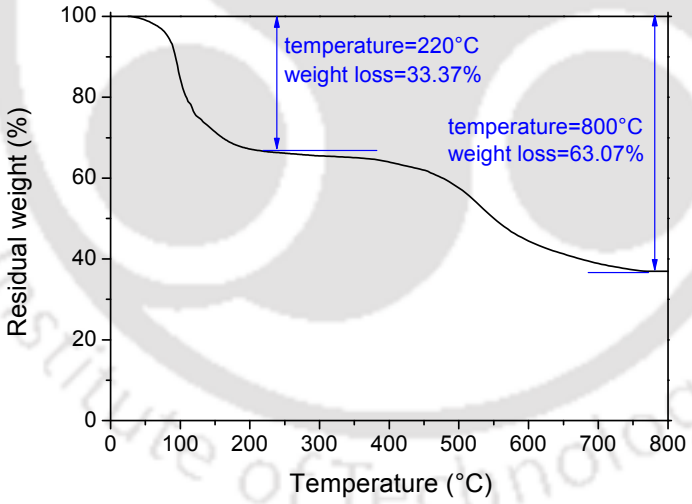

Figure 5.3: TGA theromogram of resol-PF showing different weight loss zones

The DSC thermogram of the VER is shown in fig.5.4. As observed in the DSC thermogram, there are basically four zones those are attributed to four different reactions. The first endothermic peak is attributed to a liquid stage of VER where the viscosity of

the resin is lowest. The second endothermic peak, from 122.45–165.27, is attributed due to the continuous formation of an incompletely cross-linked network. It can be referred as the transition of the gelled resin to the infusible stage [Gaur and Rain, 1992]. The third peak is the exothermic one and it occurs due to the curing of the VER. The fourth peak shows the degradation of the cured vinyl ester resin. The other peaks which appear after 400°C onwards are usually attributed due to the evolution of various gases upon thermal decomposition.

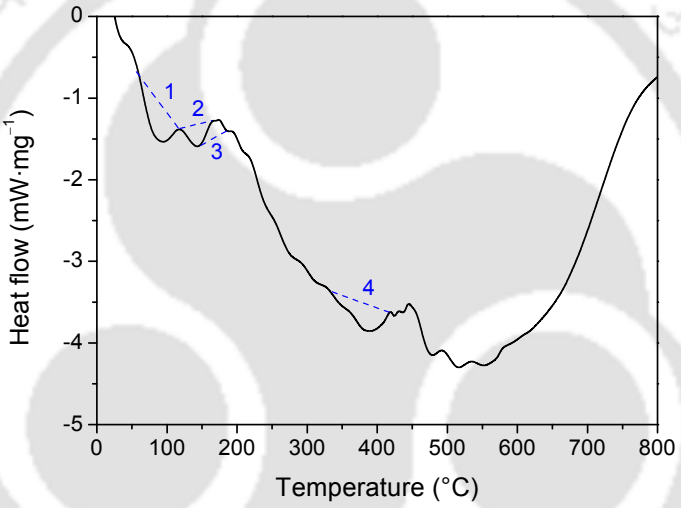

Figure 5.4: DSC thermogram of VER showing various zones

The TGA thermogram of the VER is shown in fig.5.4. It is observed that the thermal degradation of VER occurs mainly in two steps. The VER underwent firstly the natural evaporation of solvent and styrene at temperatures below 84°C and then the heat-induced-evaporation of styrene within temperatures of 84°C and 180°C [Guo et al., 2007]. During this time, the resin transformed from A to C stage, via B stage, and cross-linking within the resin completed. The weight loss up to 180°C was around 24.43% and the cured resin was almost stable up to 350°C. Therefore, the VER based composite was compression molded at 180°C. The maximum degradation occurs in the region from 350 to 550°C and

indicates the decomposition of the cured resin. The total weight loss at 600°C was around 85.29%.

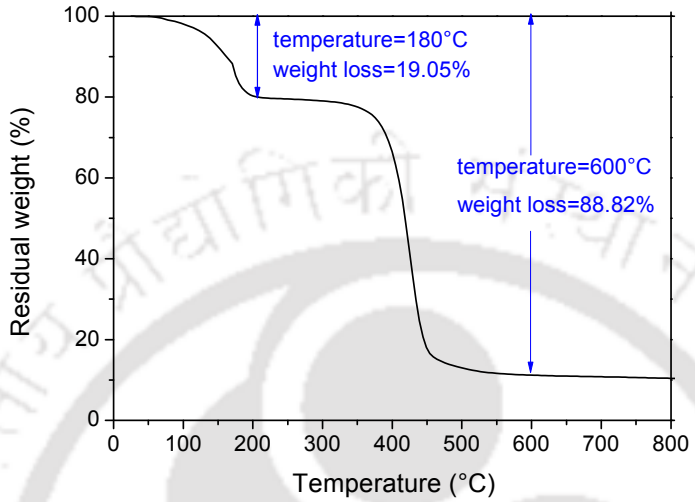

Figure 5.5: TGA thermogram of VER showing different weight loss zones

5.1.2 *Morphological analysis of NG, CB, and CF*

Figure 5.6 shows the SEM image of NG particles that were used to reinforce the composite bipolar plate. The morphological analysis shows the flaky nature of the NG particles. The layer by layer stacking texture is visible in the micrographs of the NG particles. The flakes were found to be irregular in shape and size. However, most of the particles, in the SEM analysis, were found to be in the range of 30–50μm size.

The SEM image of the CB particles is shown in the fig. 5.7. It is observed in the micrograph that the CB particles are almost spherical in nature. Though the CB particles are in agglomerated form but the diameter of most of the CB particles are around 100 nm. The size of the CB particles was further analyzed with the help of particle size analyzer which also showed similar results.

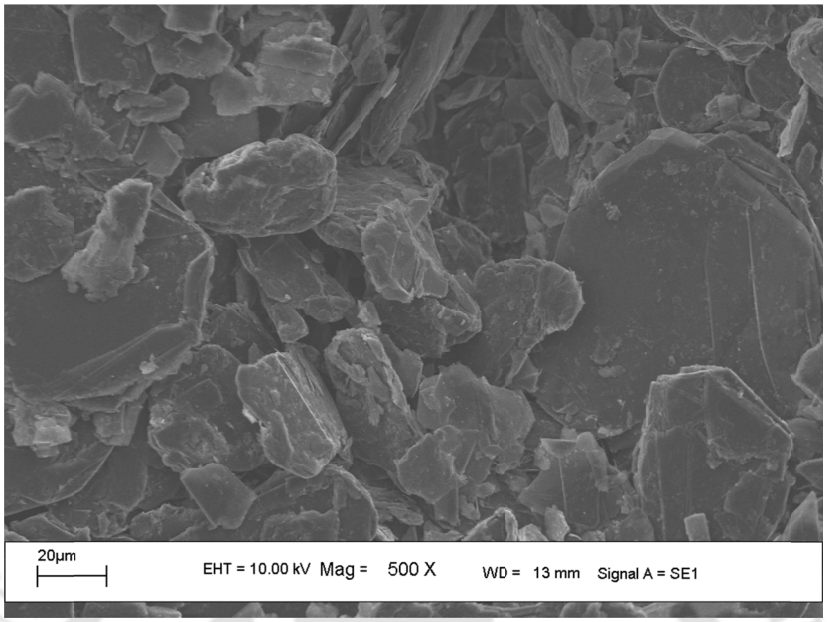

Figure 5.6: SEM image of NG particles

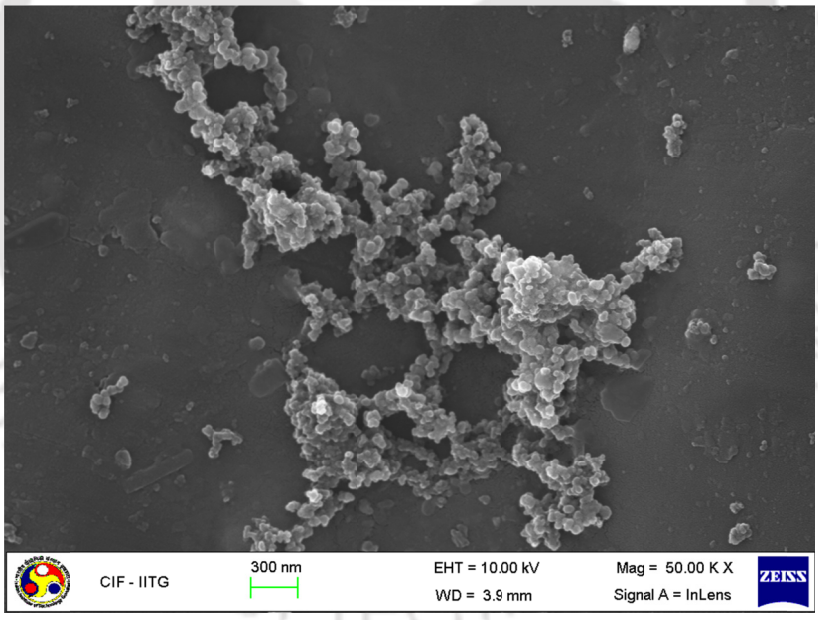

Figure 5.7: FESEM image of CB particles

The SEM image of the carbon fibers is shown in fig. 5.8. The diameter of a carbon fiber at higher magnification is shown in the inset of the figure. The diameter of the fiber was found to be around 6.5µm. It is obvious from the micrograph that the diameter of the fibers are almost uniform and it is within the range of 6–7µm. The micrograph shows that

the surface of the fibers was not perfectly smooth. The longitudinal grooves on the periphery of the fiber may be due to the manufacturing defects.

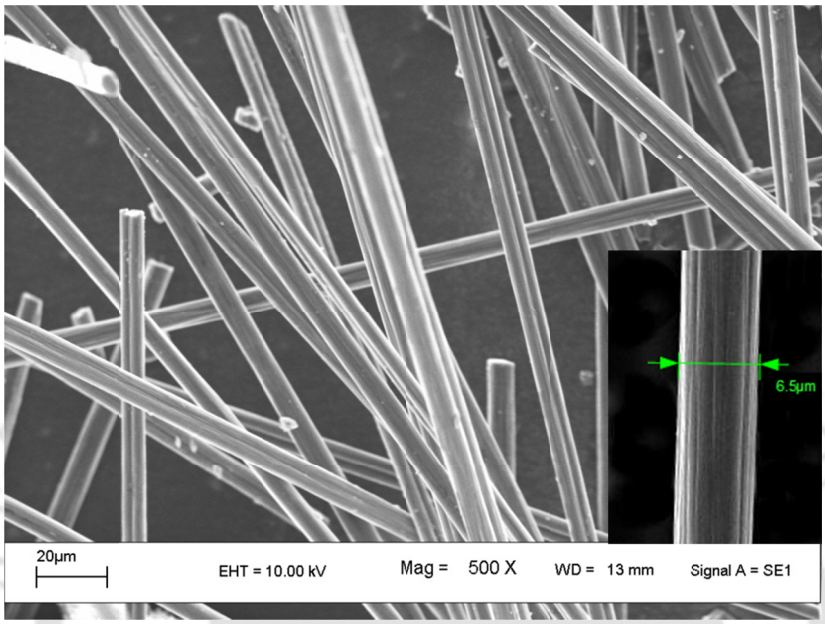

Figure 5.8: SEM image of CF

5.1.3 *XRD analysis of NG, CB, and CF*

The powder XRD analysis of the NG particles was carried out and the diffractogram is shown in fig. 5.9. The 002 graphite peak is visible at around 26.54°, which corresponds to the C-spacing (fig. 3.1) of the graphite crystal [Kinoshita, 1988]. The length of the C-axis of the graphite crystal was calculated from the XRD analysis of NG, and it was found to be 6.712Å. The detailed analysis of the XRD pattern shows that the lengths of the other two axes were 2.456Å. The graphite 101 and 004 peaks were also visible in the fig. 5.9 at 44.71° and 54.70°, respectively.

The XRD pattern of the Vulcan XC72 grade CB particles is shown in fig. 5.10. The broad diffraction peak for the CB was found at around 23.8°, which corresponds to the 002 reflection and shifted downwards as compared to the graphite (fig. 5.9). The shift of the 002 reflection to the lower values led to the larger d_{002} suggesting amorphous nature of

the CB particles. Furthermore, for turbostratic two-dimensional ordering, the 100 and 101 peaks merged into a broad 10X peak at around 43.8°. The location and width of these two diffraction peaks indicate that the CB has a coke-like structure with disordered carbonaceous interlayers [Carmo et al., 2008].

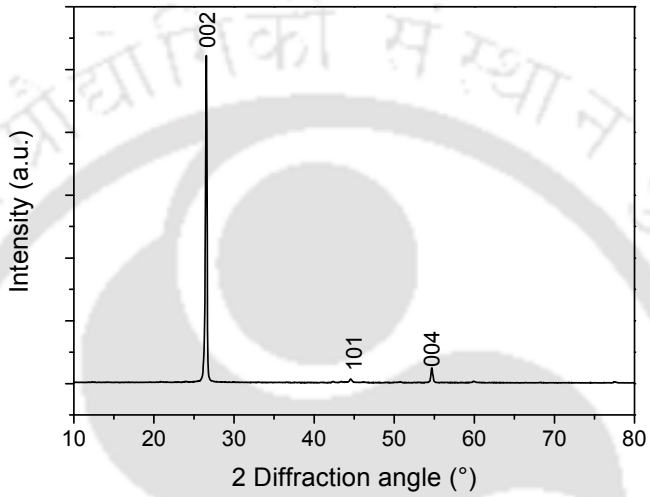

Figure 5.9: Powder XRD pattern of NG particles

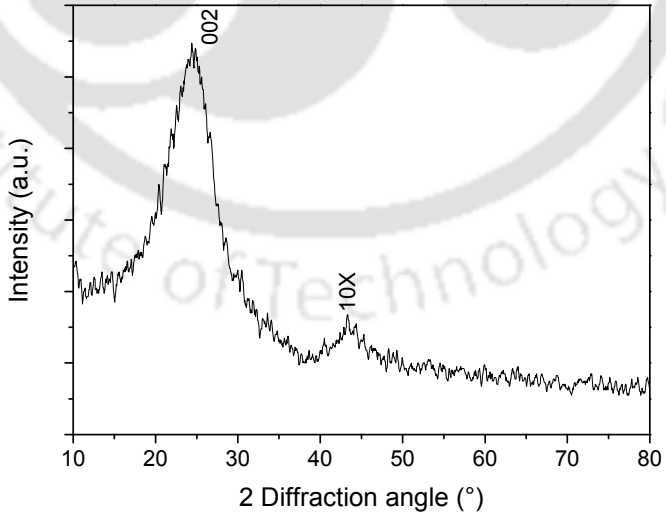

Figure 5.10: Powder XRD pattern of Vulcan XC72 grade CB particles

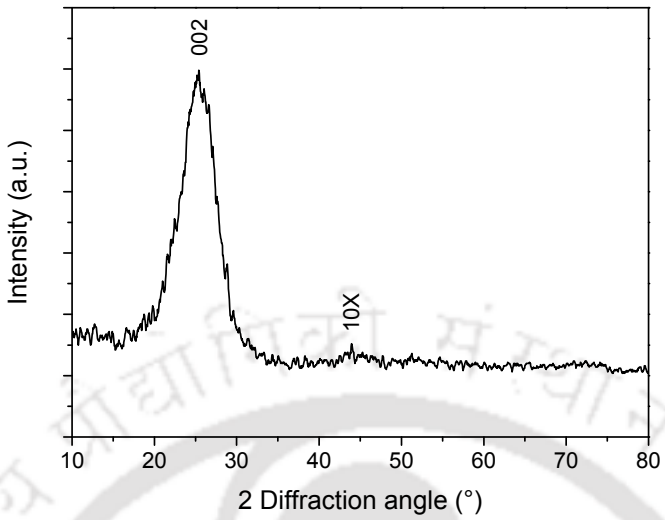

Figure 5.11: XRD pattern of T-300 grade graphitized CF

The XRD pattern of T300 grade graphitized CF is shown in fig. 5.11. The diffraction pattern of the CF shows a broad diffraction peak at around 25.11°. This diffraction peak corresponds to the disordered graphitic 002 plane [Wang et al, 2006]. The interlayer spacing d_{002} of the CF was found to be 3.543Å, which was more than the typical d_{002} spacing of graphite. Thus it can be concluded that the CF is not completely graphitized. Moreover, the other broad peak, appeared at around 44°, is because of merging of 100 and 101 peaks.

It may be noted that the NG, CB, and CF are the allotropes of carbon and thus the diffractograms signifies the same pattern. However, the crystallinity of the NG is higher than that of the CF and CB.

5.1.4 *Particle size analysis of NG and CB*

The particle size analyses of the NG and CB particles were carried as per the methodology described in section 3.3.1.5. Figure 5.12 shows the particle size distribution of NG and CB. From fig. 5.12(a), it is clearly visible that around 60 vol.% of the NG

particles are having diameter 30–80µm and a maximum of 8.37% NG particles have diameter equal to 52.48µm. Similarly, the particle size distribution of CB particle shows that the particles are widely distributed in the nano to micron range. It was found from the analysis that 56.13 vol.% of the CB particles were having diameter below 100nm, while 43.86 vol.% particles were having diameter in the range 100–1000nm. The relatively larger particles in the distribution might appear due to the agglomeration of CB particles. It was also confirmed by the FESEM analysis of the Vulcan XC72, as shown in fig. 5.7.

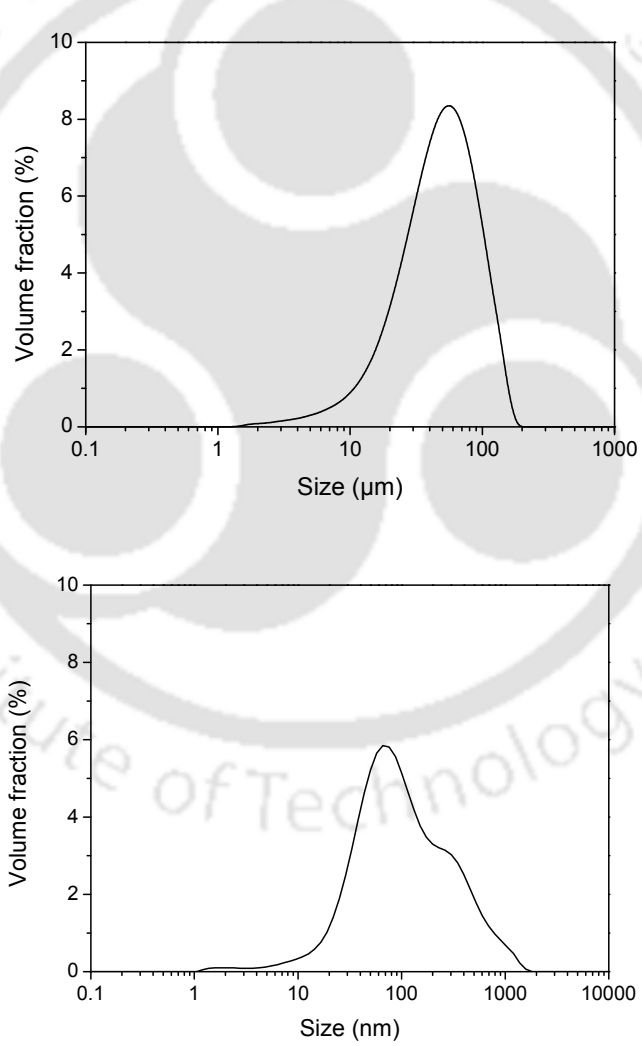

Figure 5.12: Laser particle size distribution of (a) NG and (b) Vulcan XC72 grade CB particles

5.1.5 *BET surface area analysis of NG and CB*

The BET surface area analyses of the NG and CB particles were carried out as per the procedure described in section 3.3.1.6. The nitrogen adsorption-desorption isotherms of NG and CB particles are shown in fig. 5.13(a) and 5.13(b). It is cleared from the isotherms that the NG and CB particles have hardly any porosity. The surface areas of the NG and CB particles were found to be around 21.98 and 249.64 $m^2 \cdot g^{-1}$.

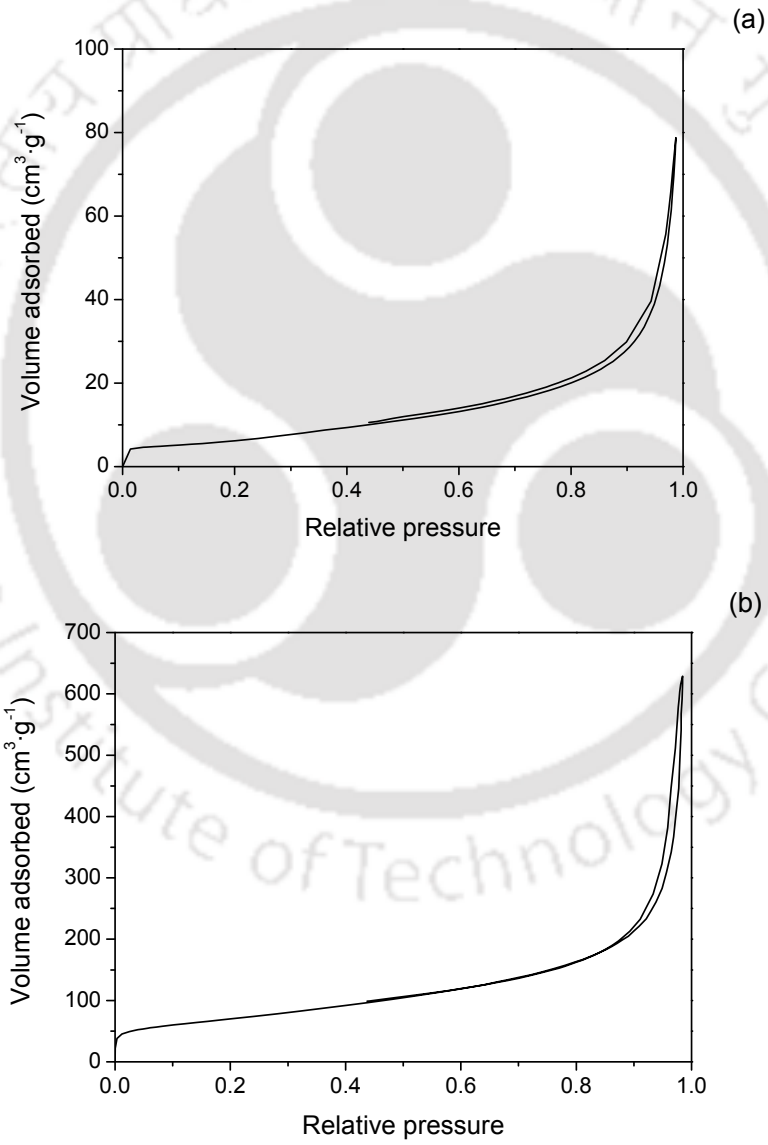

Figure 5.13: Nitrogen adsorption-desorption isotherm of (a) NG and (b) CB particles

5.2 Characterization of developed graphene

The developed graphene was thoroughly characterized by SEM, FESEM, EDX, AFM, XRD, HRTEM, ED, TGA, FTIR, and BET surface area analysis. The detail procedure for the above mentioned characterizations have been discussed in the section 3.3.

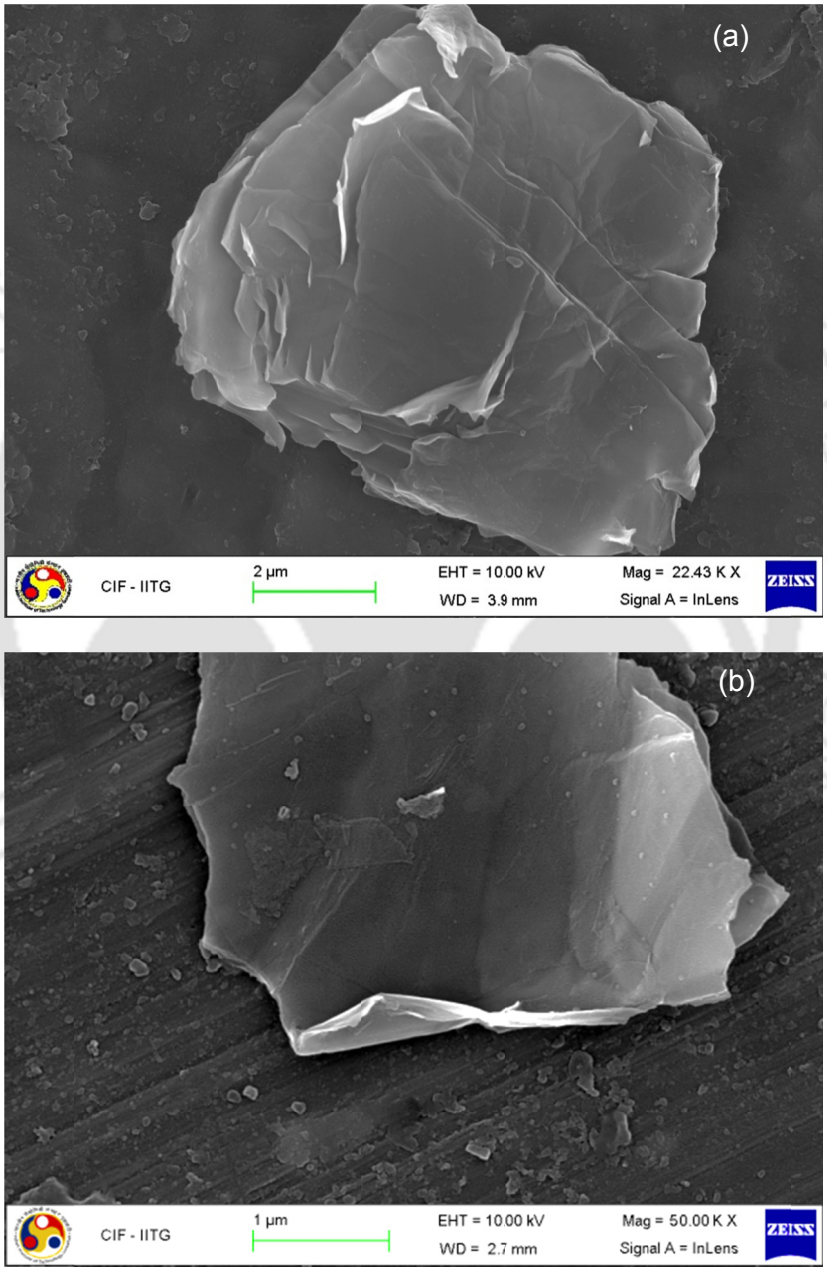

Figure 5.14: SEM image of (a) EG and (b) graphene

5.2.1 *SEM and EDX analyses of graphene*

The morphological analysis of the graphene was carried out using field emission SEM. The SEM image of EG is shown in fig. 5.14(a). It can be seen in the micrograph that the graphene layers are stacked one over the other in the EG. The fig. 5.14(b) shows the micrograph of a developed monolayer graphene. The atomically thin graphene monolayer is seen semitransparent in the micrograph. This is possible as the graphene monolayer has a thickness equal to the diameter of a sp^2 hybridized carbon atom [Novoselov et al., 2004]. The electron beam from the electron gun of the FESEM penetrates the graphene layer upon irradiation. Therefore, texture of the aluminum sample holder is also visible through the monolayer graphene.

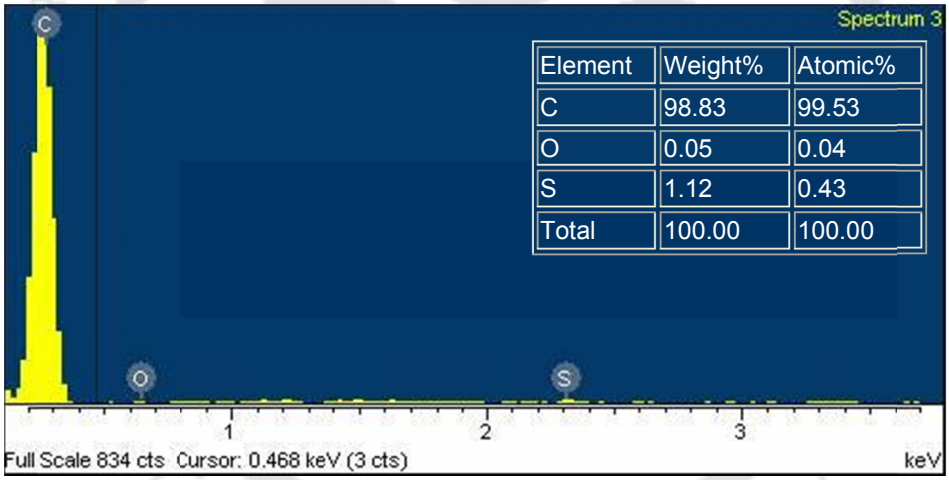

Figure 5.15: EDX analysis of the developed graphene

The elemental analysis was also carried out with the help of the EDX to detect the presence of extraneous materials. Figure 5.15 shows the EDX spectra along with the elemental analysis. The EDX analysis showed that the atomic proportion of carbon content in the graphene was 99.53%. The atomic percent of oxygen and sulfur content was 0.04 and 0.43%, respectively. The weight percent of the carbon content in the graphene was around 98.83%. It is to be noted that a harsh chemical environment of

involving $NaNO_3$, $KMnO_4$, and H_2SO_4 was used to synthesize the monolayer graphene. However, the absence of Na, K, and Mn in the EDX spectrum reveals that the metal ions were completely removed from the graphene during washing, cleaning, and purification procedures.

5.2.2 *XRD analysis of graphene*

Graphene was synthesized from the NG via the graphite oxide root. The graphite oxide was first using Hummers' method as discussed in section 3.1.6.1. The XRD diffractogram of graphene is compared with the diffractograms of graphite oxide and NG in fig. 5.16. During the production of graphite oxide the van der Waals bondings between two consecutive graphene layers may be broken and/or covalent bonding may be created through oxide ions as shown in fig. 5.17. Therefore, the 002 and the 004 diffraction peaks disappear in the diffractogram of graphite oxide. However, a new peak 001 appears at around 9.26° with d-spacing of 9.267Å. It shows that the interlayer distance between the two consecutive graphene layers was increased from 3.354 in NG to 9.267 Å in the graphite oxide. The graphite oxide was later reduced by thermal exfoliation and violently expanded to produce graphene layers. At this stage, all the graphene layers separate to form individual graphene sheets, without having any chemical bonding with another graphene sheet [Geng et al., 2009]. The 002 and 004 diffraction peaks in the diffractogram of NG completely vanishes in the case of graphene (fig. 5.17). The graphene is a 2D crystal with chicken wire structure of sp^2 hybridized carbon atoms and the graphene should align parallel to the substrate. Therefore, 004 and other low intensity peaks were also not visible in the diffractogram. The XRD does not give the information about the crystallinity of the graphene. Therefore, further analysis of the graphene was done to confirm the formation of graphene and to get the information about the crystallinity.

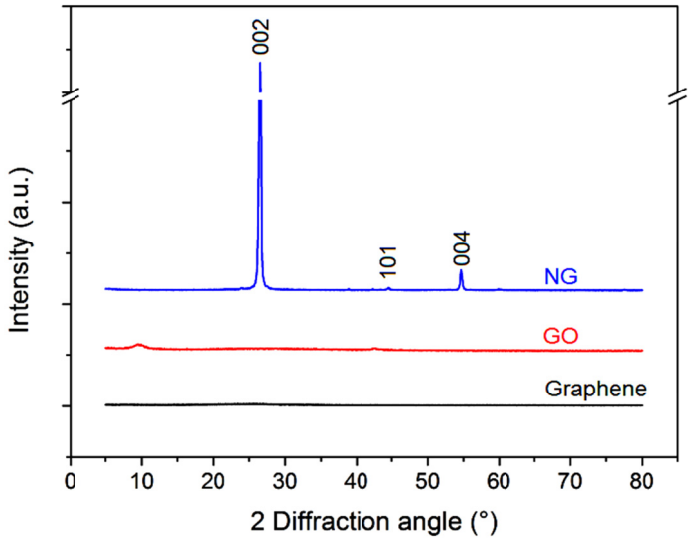

Figure 5.16: XRD diffractogram of synthesized graphene as compared with that of the graphite oxide (GO) and NG

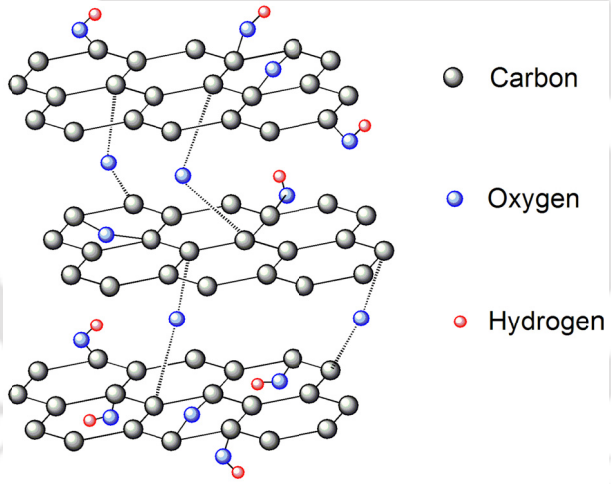

Figure 5.17: Schematic structural model of graphite oxide as reported by Schniepp et al. (2006)

5.2.3 *HRTEM and ED analyses of graphene*

The HRTEM image of the developed graphene is shown in fig. 5.18(a). Figure 5.18(a) shows that the developed graphene is nearly flat. Moreover, absence of Moiré fringes in the HRTEM image shows that a single layer graphene is developed [Park et al., 2010].

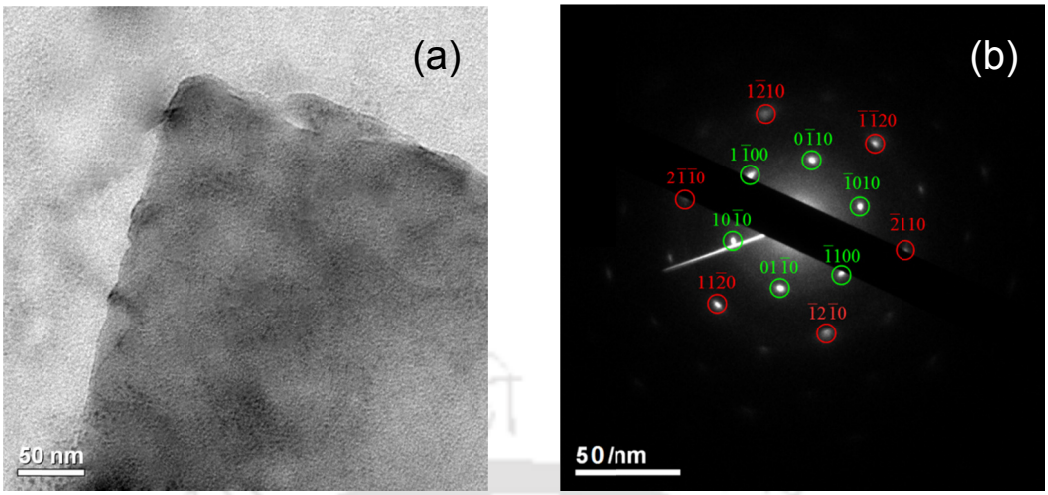

Figure 5.18: (a) HRTEM micrograph of developed graphene and (b) the SAED pattern of the graphene different lattice points in the reciprocal lattice

The presence of single layer of graphene on the irradiated sample was also confirmed with the SAED analysis. Figure 5.18(b) shows the ED pattern of the developed graphene. Strikingly, clear diffraction spots are observed in the ED pattern, which implies the crystalline nature of graphene. The ED shows a 6-fold pattern, which is consistent with a hexagonal lattice and the spots are labeled accordingly, using Miller-Bravais *hkil* notation in fig. 5.18(b). The simple hexagonal pattern of the sharp spots is similar to those obtained from monolayer graphene and leads immediately to several conclusions [Meyer et al., 2007; Valles et al., 2008; Park et al., 2010]. First, the sharp diffraction spots indicate that the graphene sheets are monocrystalline. Secondly, the diffraction spots show the long range orientational order of a hexagonal lattice pattern, similar to graphite. Thirdly, the absence of any diffraction spots other than those corresponding to the perfect graphite structure shows that the synthesized graphene was free from any functional groups; at least in the area under consideration. Meyer et al. (2007) proposed a methodology to use ED pattern to find out the number of graphene layers. It was observed that the relative intensities of the $\{0\bar{1}10\}$-type and $\{\bar{1}\bar{1}20\}$-type reflections are more than

or equal to 1.38. This indicates that the developed graphene has a monolayer structure [Meyer et al., 2007]. The thickness of the graphene layer was measured with the help of AFM analysis and discussed in the subsequent section.

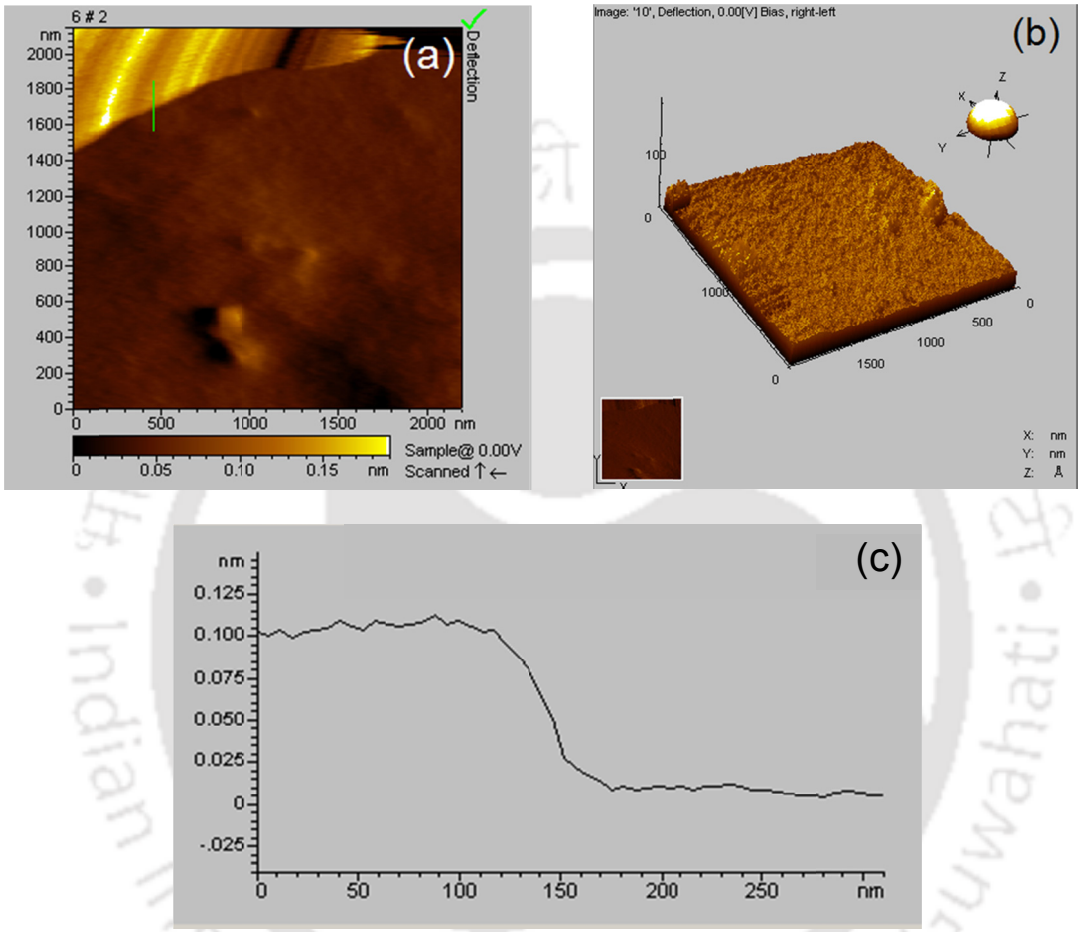

Figure 5.19: (a) AFM image showing surface morphology of a graphene sheet, (b) 3D profile of the graphene surface, and (c) height profile at the edge of the graphene layer at the position as shown by the green line in micrograph (a)

5.2.4 *AFM analysis of graphene*

The previous analyses showed that monolayer graphene was developed but the thickness of the graphene could not be determined so far. The specimen must be held perpendicular to the substrate to measure the thickness with the conventional SEM or HETEM. Owing

to this limitation, AFM analysis was conducted as per the procedure explained in section 3.3.2.2. Figure 5.19(a) shows the deflection profile of the AFM analysis of a graphene sheet. Figure 5.19(b) shows the 3D height profile of the area as shown in the image fig.5.19(a). However, the thickness of the graphene sheet was not cleared from the 3D profile. Therefore, the thickness of the graphene sheet was calculated by measuring the height profile at the edge of the sheet. The area of interest is shown in the deflection profile with a light green colored line. The height profile at the edge of the graphene sheet is shown in fig.5.19(c). It was found from the height profile that the thickness of the graphene sheet is around 1Å, which is quite near to the theoretical diameter of a sp^2 hybridized carbon atom [Schniepp et al., 2006; Stankovich et al., 2007; Ramanathan et al., 2008; Geng et al., 2009; Avinash et al., 2010].

5.2.5 *FTIR analysis of graphene*

The FTIR analysis of the graphene was carried out to investigate the presence of any functional group in the developed graphene. Figure 5.20 shows the FTIR spectrograph of the developed graphene. The IR-shift at 3440 cm^{-1} is attributed due to the moisture content on the graphene, whereas the IR-shift at 1006 cm^{-1} is attributed to the $C-OH$ stretching vibrations of secondary cyclic alcohols. Therefore, some $-OH$ radicals may be present in the form of cyclic alcohols at the periphery of the graphene sheets. Similalry, the peaks at 1426 and 1639 cm^{-1} are attributed to the $C-H$ bending vibrations and $C=C$ stretching vibrations, respectively. The broad peak at 2097 cm^{-1} was observed, which may be again attributed to the $C=C$ stretching vibrations with terminal $-H$ radical [Avinash et al., 2010]. Therefore, the developed graphene sheets may have a trace amount of $-OH$ or $-H$ radicals.

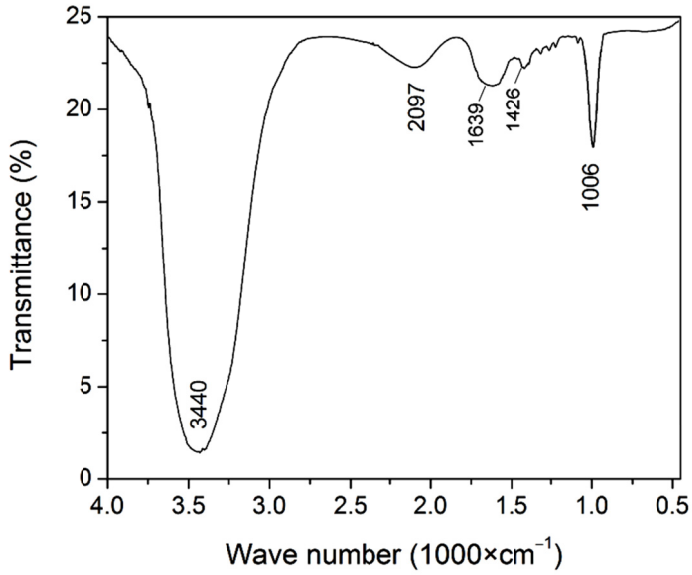

Figure 5.20: FTIR spectrograph of the graphene

5.2.6 *TGA analysis of graphene*

The thermal stability of the developed graphene was checked with the help of thermogravimetric analysis. The thermogram of graphene along with the NG is shown in fig.5.21 below. It can be observed in the thermogram that, up to 450°C, the weight loss of the graphene is almost identical to the weight loss of NG. However, the weight loss of graphene was slightly more than the NG. It suggests that the graphene has more moisture content than the graphite. It may be because of more specific area of the graphene than graphite. It can be seen in the fig.5.21 that the weight loss of graphene accelerates above 450°C. It may be a result of reduction of the functional groups present on the graphene. However, the total weight loss of the graphene up to 900°C was only around 10%.

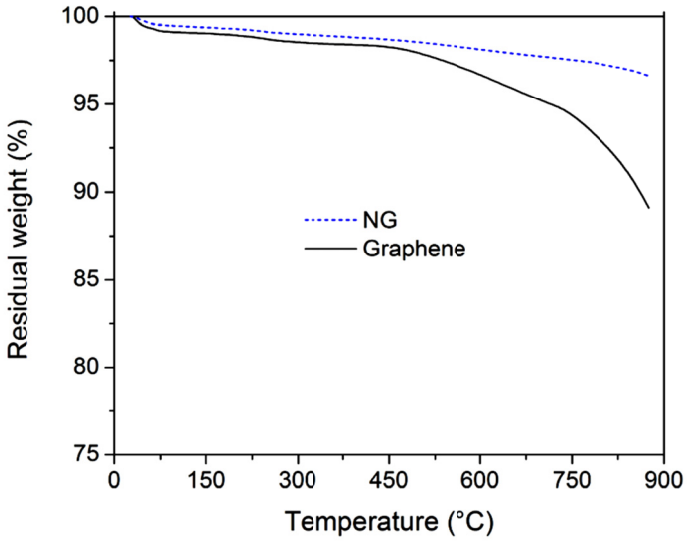

Figure 5.21: TGA thermograms of graphene and NG

5.2.7 *BET surface area analysis of graphene*

The BET surface area analysis of the developed graphene was carried out as per the procedure described in section 3.3.1.6. The BET surface measurements were obtained from nitrogen physisorption isotherms at 77 K and the isotherm is shown in fig.5.22. It is found from the isotherm that there is hardly any difference in the adsorption–desorption cycle, which confirms the non-porous graphene structure. The BET surface area of the developed graphene was calculated and found to be around 969.22 $m^2 \cdot g^{-1}$. However, it is found that the surface area of the developed graphene was less than the theoretical surface area of a single graphene sheet (2,675 $m^2 \cdot g^{-1}$) [Novoselov et al., 2004]. It is because in practical case the surface area of a particular mass of graphene sheets are used for the analysis. The graphene sheet may be stuck over another graphene sheet by physical means. Therefore, the resultant surface area of the graphene was less than the ideal surface area of an individual graphene sheet.

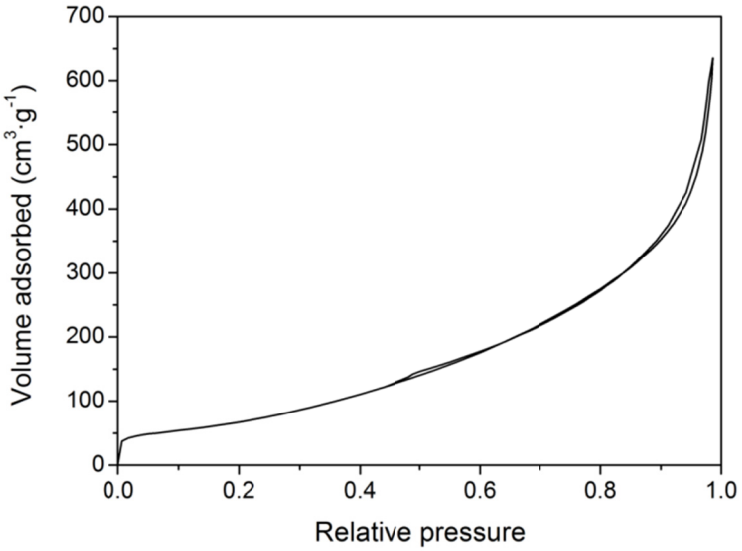

Figure 5.22: Nitrogen adsorption-desorption isotherm of graphene at 77 K

Till now, the resins, NG, CB, CF, and the developed graphene were thoroughly characterized. The novolac-PF, resol-PF, and VER were used as a binder along with the reinforcements (NG, CB, CF, and graphene) to develop the composite bipolar plate. Firstly, the molding temperatures for the three resins were optimized to the composite bipolar plates. Therefore, the resin/NG composite were initially developed at different temperature to find out the optimum molding temperature. The composites were later developed with different compositions of resins and NG to optimize the resin content. The optimum resin/NG composite was further reinforced step by step with CB, CF, and graphene, at the expense of NG, to develop efficient composite bipolar plate in order to achieve the target properties as described in the table 1.2. The ex-situ characterizations of the bipolar plates will be discussed in the next section, followed by the performance evaluation in the PEMFC.

5.3 Optimization of molding temperature

The composite bipolar plates were developed as per the procedure described in the section 3.2. The composite bipolar plates, for each resin matrix, were prepared by compression molding at different temperature, starting from 40°C below to 40°C above the curing temperatures[†]. The developed bipolar plates were characterized for mechanical strength and electrical conductivity. The optimum molding temperatures, for each resin based composite, were decided based on these basic properties of the bipolar plate.

5.3.1 *Effect of molding temperature on mechanical strength*

The effects of molding temperature on the flexural strength and modulus of the resol-PF, novolac-PF, and VER based composite bipolar plates are shown in fig.5.23. It was found that the flexural strength as well as the flexural modulus of the composite increases initially with the increase in the molding temperature. At the curing temperature, flexural strength and flexural modulus of the composite bipolar plates were highest for all the three resins. Thereafter, further increase in the molding temperature above curing temperature decreased the flexural strength and flexural modulus. The flexural strength and flexural modulus of the PF based composite were maximum at 220°C molding temperature. Similarly, for VER based composite the maximum flexural strength and modulus was observed at 180°C. It happens as the curing of PF and VER completes at 220 and 180°C and forms a completely infusible stage thermosets as described by the eqs. 3.4, 3.6, and 3.8. Yin et al. (2007) reported similar effect for novolac-PF/NG composite at molding temperature 240°C. The flexural strength and flexural modulus of the composite decreased due to the degradation of the PF resin at temperature above 220°C. The similar effect was also observed for VER based composite at molding temperature above 180°C.

[†] Curing temperatures for PF and VER were around 220 and 180°C, respectively (section 5.1.1).

The effect of molding temperature on the shore hardness of the composite was also studied.

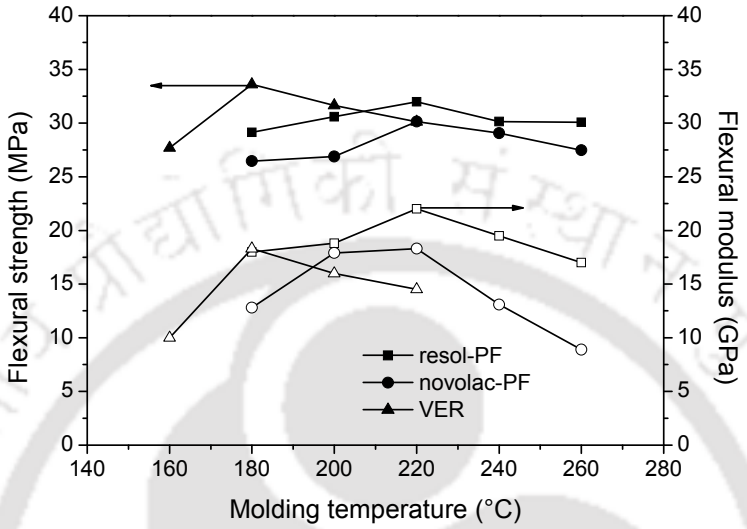

Figure 5.23: Effect of molding temperature on the flexural strength and flexural modulus of resin/NG composite bipolar plates

The scleroscopic shore hardness of the composite bipolar plates was measured as per the ASTM C886. The hardness is not a fundamental property and its value depends on the combination of yield strength, tensile strength, and modulus of elasticity of the composite. Therefore, the shore hardness of the composite bipolar plate is an important property to identify its suitability for the fuel cell application. The effect of molding temperature on the scleroscopic shore hardness of the composite bipolar plate is shown in fig.5.24. It can be observed in the fig.5.24 that the shore hardness of the composite bipolar plate follows a trend similar to the flexural strength and flexural modulus. Initially, the shore hardness of the composite increased with the increase of molding temperature, up to the curing temperature of the resins. Thus the maximum shore hardness of the composite was found at 180°C molding temperature for VER based

composite bipolar plate. Similarly, the maximum shore hardness of the PF based composites was found at 220°C molding temperature. It was observed in the DSC analysis that the resins undergo crosslinking and long-chain molecules formed at these temperatures. Therefore, shore hardness of the resin/NG composites was highest at these molding temperatures, which may be a result of better yield strength, tensile strength, and modulus of elasticity. Further increase in the molding temperature, above 220°C for PF- and 180°C for VER-based composite, degrades the cured resin macromolecular structure [Trick and Saliba, 1995]. Therefore, the shore hardness of the resin/NG composite bipolar plate was less when it was compression molded at above curing temperature.

The mechanical properties of the bipolar plates indicate that the optimum molding temperature of the composite should be the curing temperature. However, it needs to get confirmed for one of the most fundamental properties of the composite bipolar plate, i.e. electrical conductivity. Therefore, the electrical conductivity of the composite bipolar plates was studied to evaluate the optimum molding temperature.

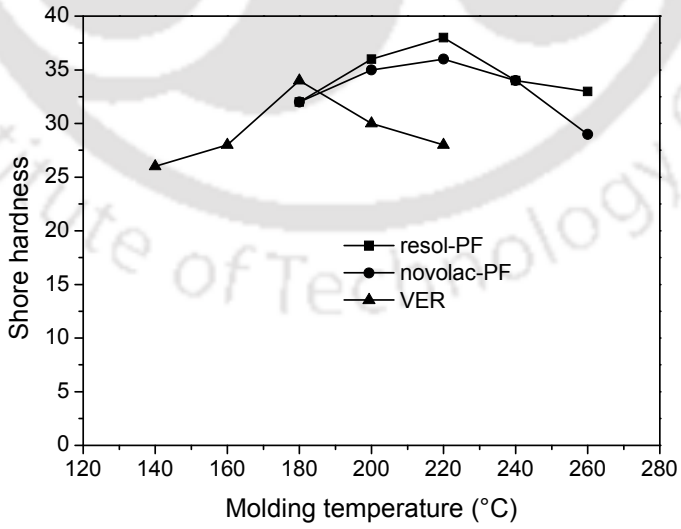

Figure 5.24: Effect of molding temperature on shore hardness of resin/NG composite bipolar plates

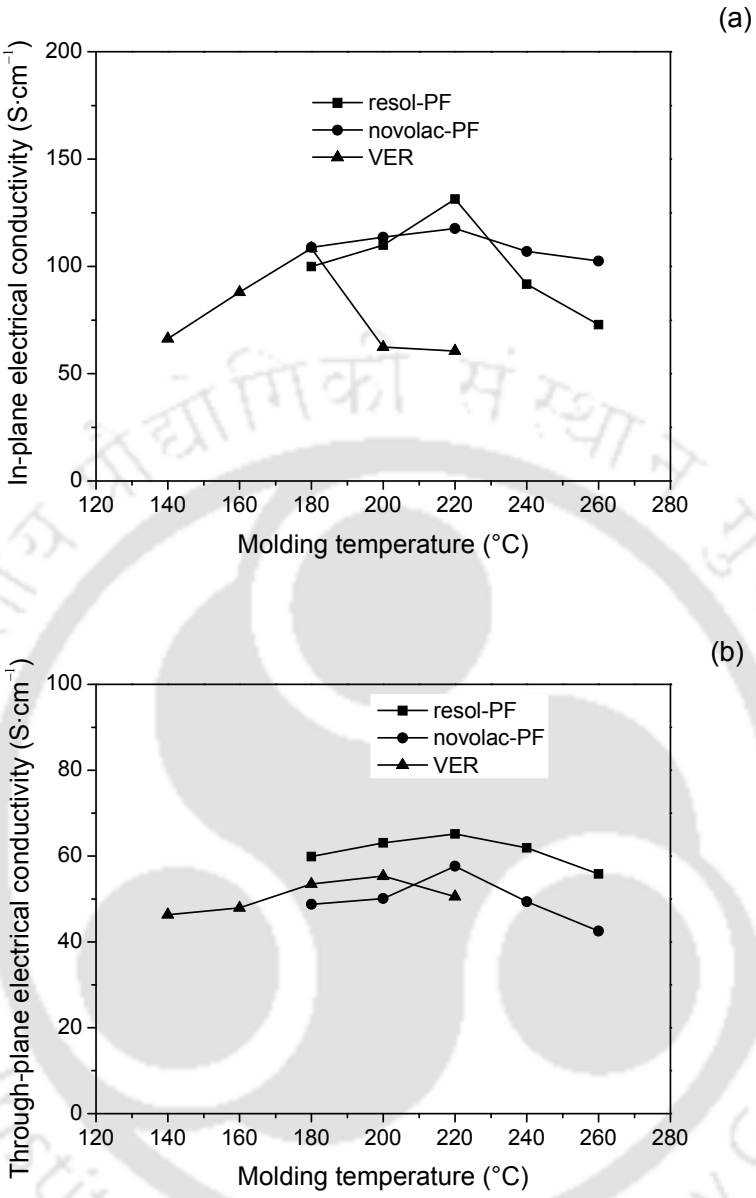

Figure 5.25: Effect of molding temperature on (a) in-plane and (b) through-plane electrical conductivities of the resin/NG composite bipolar plates

5.3.2 *Effect of molding temperature on electrical conductivity*

The effect of molding temperature on the electrical conductivities of the resol-PF/NG, novolac-PF/NG, and VER/NG composite bipolar plates were evaluated as per the procedure described in the section 3.3.3.5. The in-plane and through-plane electrical

conductivities of the composite for resol-PF, novolac-PF, and VER are shown in fig.5.25(a) and 5.25(b). The electrical conductivities of the composite followed the trend of mechanical strength.

It was observed from the DSC analysis that the PF resin can form a three-dimensional network skeleton structure by cross-linking till 215 °C. The curing and cross-linking of the PF completes within 220°C, in presence of HMTA. In case of VER, the curing completes at around 180°C. At this stage, the resin content in the composite is completely cured and formed a well connected network among the NG particles. Though resin is an insulating material, but electrons can pass through the barrier whenever the thickness of the insulating barrier is very thin. At higher molding temperature, the methylene bridge starts decomposing and therefore the three dimensional network structures. Moreover, release of methane gas at high temperature increases the porosity (confirmed and discussed later using hydrogen permeability) of the composite and reduces the electrical conductivity of the composite. Thus the electrical conductivity of the VER based composite too showed decreasing trend above 180°C.

It was observed from the above studies that the basic properties of the composite bipolar plate for PF/NG composite were optimum if compression molded at 220°C. Similarly, the optimum molding temperature for the VER/NG composite was found to be 180°C. The flexural strengths of the composite at optimum molding temperatures were recorded as 31.99, 30.15, and 33.59 MPa for novolac-PF, resol-PF, and VER respectively. Similarly, the highest in-plane electrical conductivities of the composite, at the optimum molding temperatures, were 131.33, 117.67, and 108.47 $S \cdot cm^{-1}$ for resol-PF, novolac-PF, and VER, respectively. The through-plane electrical conductivities of these composites were 60.17, 57.67, and 55.31 $S \cdot cm^{-1}$, respectively. Therefore, the optimum molding

temperatures for the PF and VER based composites were taken as 220 and 180°C, respectively, for further studies. The TGA analyses of the composites, for the three resin systems, were also carried out to study the thermal stability of the developed bipolar plate.

5.4 Effect of NG content on the properties of composite bipolar plate

The composite bipolar plates were developed with different volume fraction of resin and NG to find out the optimum resin content. All the composites were compression molded at the respective optimum molding temperatures of the resin/NG systems. The developed bipolar plates were characterized thoroughly for bulk density, hydrogen permeability, flexural strength, shore hardness, electrical conductivity, thermal conductivities, and corrosion current density. The developed bipolar plates were later tested in PEMFC to study the performance in real fuel cell.

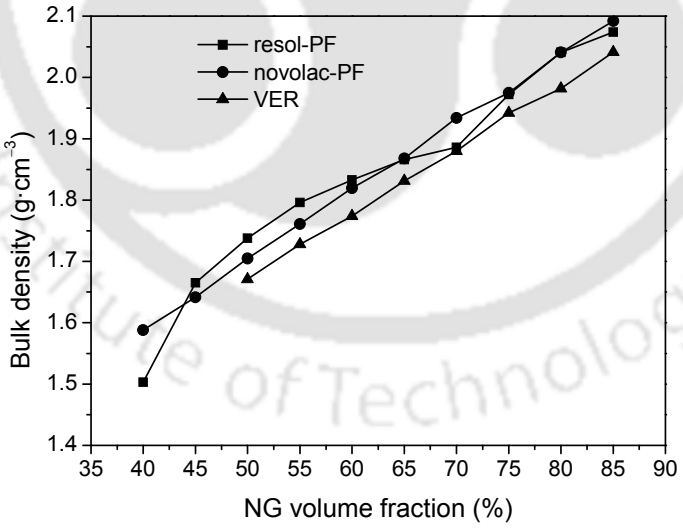

Figure 5.26: Effect of NG content on the density of the resol-PF, novolac-PF, and VER based composite bipolar plates

5.4.1 *Effect of NG content on the bulk density of composite bipolar plates*

The effect of NG content on the density of the composite bipolar plates for resol-PF, novolac-PF, and VER is shown in fig.5.26. It is observed from the figure that the density of the composite increases gradually with the increase in the NG volume fractions. The density of the NG is 2.26 $g \cdot cm^{-3}$, while the density of the resins are around 1.1 $g \cdot cm^{-3}$. Therefore, as per the mixing law, an increase in the resin content or decrease in the NG content will decrease the density of the composite. The figure shows that a NG volume fraction should be 75% or below to achieve the target (table 1.2) for density of the composite bipolar plate.

5.4.2 *Effect of NG content on hydrogen permeability of composite bipolar plate*

The hydrogen permeability of the composite bipolar plates was measured as per the method discussed in section 3.3.3.2. The effects of NG content on the hydrogen permeability of the resin/NG composite bipolar plates are shown in fig.5.27. It is observed from the figure that the hydrogen permeability of the composite increased with the increase in the NG volume fraction or decrease with the resin volume fraction. The resin matrix acts as a binder material in the composite bipolar plate. In order to achieve the target for electrical conductivity of the composite bipolar plate, the intrinsically insulating polymer resin must be filled with high loading of corrosion resistive conducting particles. But at higher NG loadings, the resin content is not enough to fill the interstices between NG particles. This phenomenon may lead to the development of microscopic pores during compression molding.

Figure 5.27(a) shows that the hydrogen permeability of the resol-PF/NG composite bipolar plate, at room temperature, increased more whenever the resin content surpassed 25%. Therefore, 25% resin content was considered as the optimum resin content for

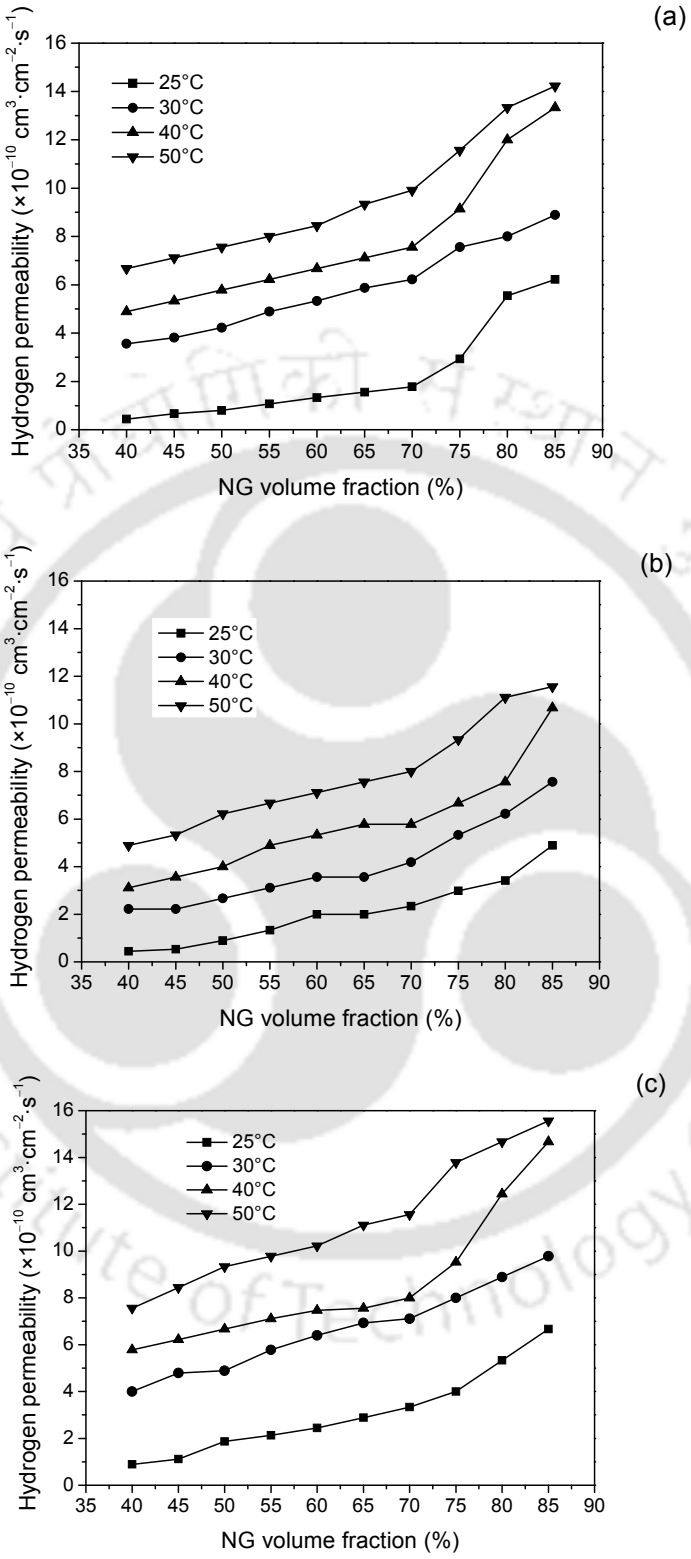

Figure 5.27: Effect of NG content on the hydrogen permeability of the (a) NG/resol-PF, (b) NG/novolac-PF, and (c) NG/VER composite bipolar plates under 2 bar pressure

resol-PF/NG. The optimum resin contents for the other two resins were 30 and 25% for novolac-PF and VER, respectively. At room temperature, the hydrogen permeability of the resol-PF, novolac-PF, and VER based composites were 2.93×10^{-10}, 2.54×10^{-10}, and 4.00×10^{-10} $cm^3\cdot cm^{-2}\cdot s^{-1}$, respectively. The increase in hydrogen permeability at higher graphite loading was also reported by Blunk et al. (2006). It was reported that the hydrogen permeability through the composite bipolar plate was diffusion driven for low graphite content. However, the hydrogen permeability through the plate was mostly governed by convection mechanism on higher filler loadings.

The effects of temperature on the hydrogen permeability of the NG/resin composites were also shown in the fig.5.27. The hydrogen permeability of the bipolar plates increased at elevated temperature. The polymer expands with increasing temperature and thereby creating more free volume due to segmental motions [Blunk et al., 2006]. Therefore, a gradual increase in the rate of hydrogen permeability was observed with increasing temperature.

5.4.3 *Effect of NG content on flexural strength and flexibility of composite bipolar plate*

Previous section showed that the hydrogen permeability of the composite bipolar plate for NG/resin composite was sufficiently less in comparison to the target values. Figure 5.28 shows the effects of NG content on the flexural strength and deflection at mid-span of the NG/resin composite bipolar plate. It can be observed from the figure that the flexural strength of the composite bipolar plate gradually decreases with the increase in the NG content. It happens as the cured resin has high flexural strength in comparison to the NG. The flexural strengths of cured resol-PF, novolac-PF, and VER are around 155, 225 and 120 MPa, respectively [Koizumi et al., 2010; Quireshi, 2001; VER datasheet]. However,

the NG is brittle in nature with very low flexural strength and modulus. Therefore, increase in NG content reduces the flexural strength of the composite. At lower NG content or at higher resin content, the cured resin mainly contributes to the high flexural strength of the composite, whereas increase in NG content reduces the flexural strength of the composite.

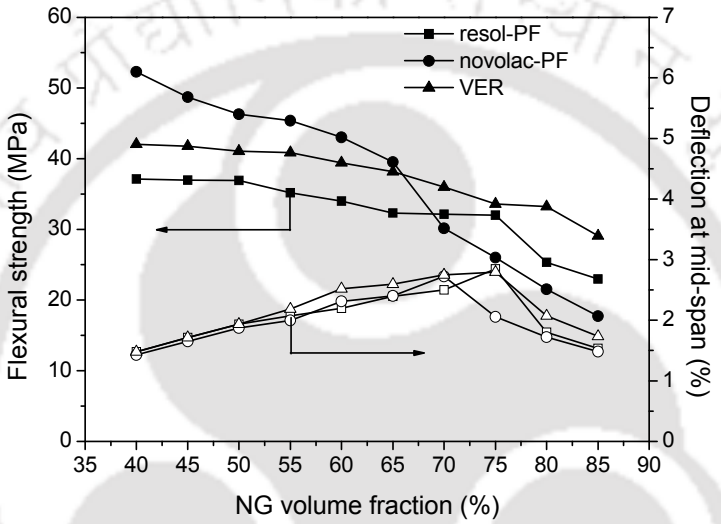

Figure 5.28: Effect of NG content on the flexural strength and deflection at mid-span of the resin/NG composite bipolar plate

The flexibility of the composite was determined by deflection at mid-span. The deflection at mid-span of the bipolar plate increases with the increase in NG content upto 75% for resol-PF and VER resin based composites. The maximum deflection at mid-span for the NG/novolac-PF composite bipolar plate was achieved at 70% NG content. Further increase in the NG content decreases the flexibility of the composite, for all the resins. At these resin contents, the flexural strengths of the NG/resol-PF, NG/novolac-PF, and NG/VER composites were around 31.99, 30.15, and 33.59 MPa, respectively. The deflections at mid-span for these composites were around 2.85, 2.73, and 2.79%,

respectively. The flexural strength and deflections at mid-span of these composites were below the target values.

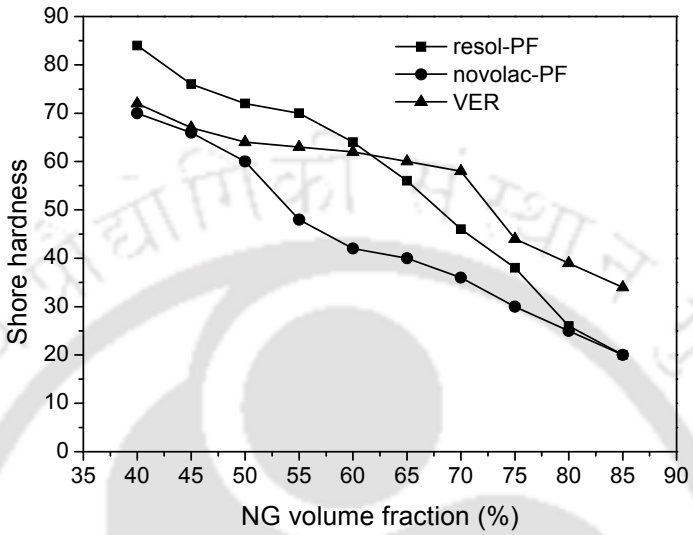

Figure 5.29: Effect of NG content on the shore hardness of the resin/NG composite bipolar plates

5.4.4 *Effect of NG content on shore hardness of composite bipolar plate*

The shore hardness of the composite bipolar plates was measured with the help of a scleroscopic hardness tester. Figure 5.29 shows the effect of NG content on the shore hardness of the NG/resin composite, which is similar to the effect on flexural strength. By definition, scleroscopic shore hardness is the rebound hardness of a material that is associated with the elasticity of the material. In the current study, the cured resins have higher elasticity in comparison to the NG. Therefore, the shore hardness of the NG/resin composites decreases with the increase in the NG content. It was found that the shore hardness of the resole-PF and VER based composites were higher than that of the novolac-PF based composite. At optimum resin content (based in the previous properties), the shore hardness of the NG/resol-PF, NG/novolac-PF, and NG/VER composite bipolar plates were 38, 36, and 44. Therefore, the shore hardness of the PF

based composites needs improvement so as to achieve the values. It was observed that the scleroscopic shore hardness of the VER based composite bipolar plate met the target value. However, the shore hardness of the composite bipolar plate was studied for all the compositions.

5.4.5 *Effect of NG content on electrical conductivity of composite bipolar plate*

The in-plane and through-plane electrical conductivities of the composite bipolar plates were measured using a four-probe setup as per the procedure described in the section 3.3.3.5. The effects of NG content on the in-plane and through-plane electrical conductivities of the NG/resin composite bipolar plates are shown in fig. 5.30(a) and 5.30(b). Figure 5.30(a) shows that the in-plane electrical conductivity of the composite increases with the increase in graphite content, for all the resin systems. It is because the electrical conductivity of the NG is in the order of 10^{6} S·cm^{-1} while it is 10^{-13} – 10^{-15} S·cm^{-1} [Powell et al., 1972; Quireshi, 2001] for the resins. The electrical conductivity of the composite depends on the distribution of the conducting NG particles within the polymer matrix [Kakati et al., 2009]. An increase in the NG content or decrease in the resin content decreases the insulating layer thickness between two neighboring NG particles and thus increases the bulk electrical conductivity of the bipolar plate. However, the hydrogen permeability of the composite increased with increase in NG content as it was seen in fig. 5.27. The fig. 5.30(a) shows that the in-plane electrical conductivities of the resol-PF, novolac-PF, and VER based composites were almost equal. However, resol-PF, and VER based composites were more conductive than that with the novolac-PF. Figure 5.30(b) shows that the through-plane electrical conductivities of the resol-PF, novolac-PF, and VER based composite bipolar plates. It is observed that the electrical conductivities of the composites bipolar plates are more isotropic at low NG content.

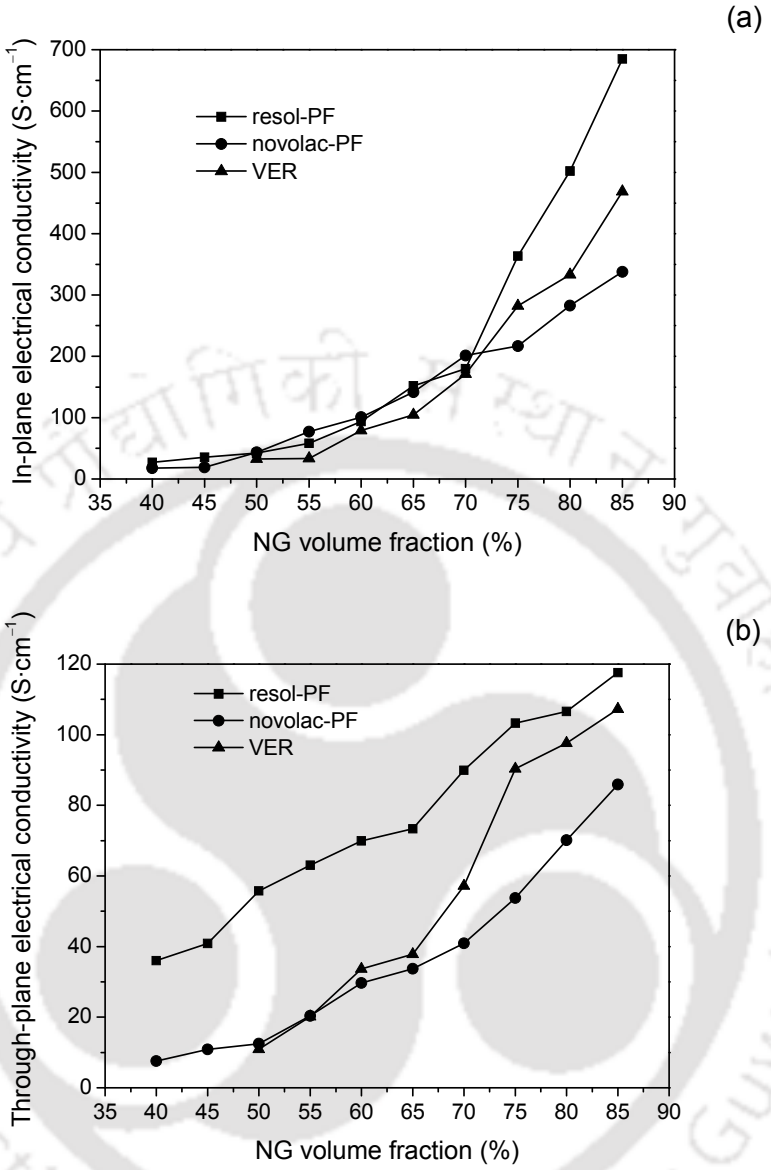

Figure 5.30: Effect of NG content on the (a) in-plane and (b) through-plane electrical conductivities of the NG/resin composite bipolar plates

However, anisotropic behavior becomes prevalent as the NG content increases. This is due to the flaky shape and anisotropic behavior of NG particles. At low NG content, the graphite flakes were isolated in the resin matrix and hence the anisotropy effect of the NG was not prevalent in the composite. But the insulating resin layer thins down with increase in the NG content and thus most of the NG flakes were in contact with each

other. The NG particles align themselves in the plane perpendicular to the compression force applied during the compression molding process. Therefore, the bipolar plates showed high in-plane electrical conductivity with higher NG content. Moreover, the resol-PF, novolac-PF, and VER based composites showed relatively high through-plane electrical conductivities. The in-plane electrical conductivities of the NG/resole-PF, NG/novolac-PF, and NG/VER based composites, at the optimum resin content, were 363.44, 201.26, and 282.30 $S \cdot cm^{-1}$, respectively. However, the thorough-plane electrical conductivities of the novolac-PF (NG:70%; novolac-PF:30%) and VER (NG:75%; VER:25%) based composite bipolar plates were below the target value. The through-plane electrical conductivities of these composites were 40.91 and 90.37 $S \cdot cm^{-1}$, respectively. The through-plane electrical conductivity of the resole-PF based composite (NG:75%; resol-PF:25%) was 103.30 $S \cdot cm^{-1}$ and it was just edge above the target value.

5.4.6 *Effect of NG content on thermal conductivity of composite bipolar plate*

The thermal conductivity of the composite bipolar plates was measured with the help of a thermal conductivity measurement unit following the procedure described in the section 3.3.3.6. The effects of different filler contents on the thermal conductivity of the composite bipolar plates are shown in fig. 5.31. It was observed in the fig. 5.31 that the thermal conductivities of the composite, for all the compositions, were well above the target values. The thermal conductivity of the composite bipolar plate increased with the increase in the NG content, irrespective of the resin type. However, the thermal conductivity of the CB and CF reinforced composite bipolar plates were also measured and reported hereby accordingly.

Kindly note that the thermal conductivities reported were for the in-plane conductivity of the composite. Like electrical conductivities, the in-plane thermal conductivities of the

composite bipolar plates are more. However, since the thickness of the composite bipolar plate was small and the in-plane thermal conductivity was high, the heat generated in the bipolar plate during operation may be efficiently transferred from the inside to outside of a stack through in-plane thermal conductive layers. Therefore, emphasis was given on the measurement of the in-plane thermal conductivity. The thermal conductivity of the NG/resin composite bipolar plates, for the optimum compositions, were 113.2, 105.3, and 110.2 $W \cdot m^{-1} \cdot K^{-1}$, respectively for resol-PF, novolac-PF, and VER. The thermal conductivity of the developed bipolar plates was well above the target value [Huang et al., 2004].

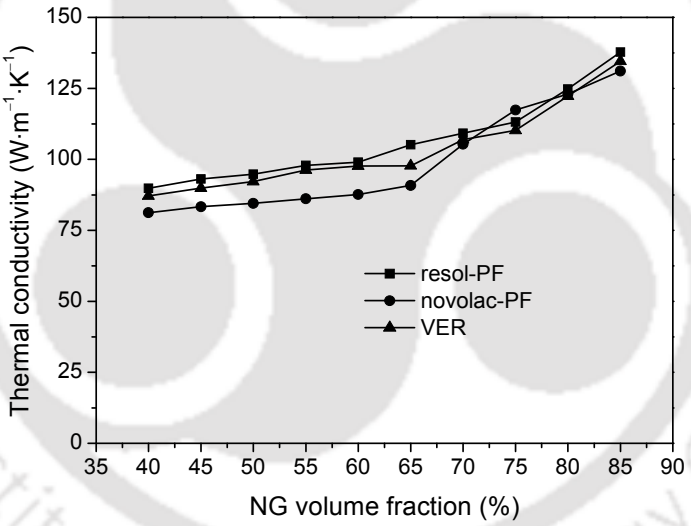

Figure 5.31: Effect of NG content on the thermal conductivity of the NG/resin composite bipolar plates

5.4.7 *Effect of NG content on corrosion of composite bipolar plate*

The corrosion studies of the composite bipolar plates were carried out with the help of potentiodynamic polarization and cyclic voltammetry. The detailed methodology of the corrosion studies has been explained in section 3.3.3.7.

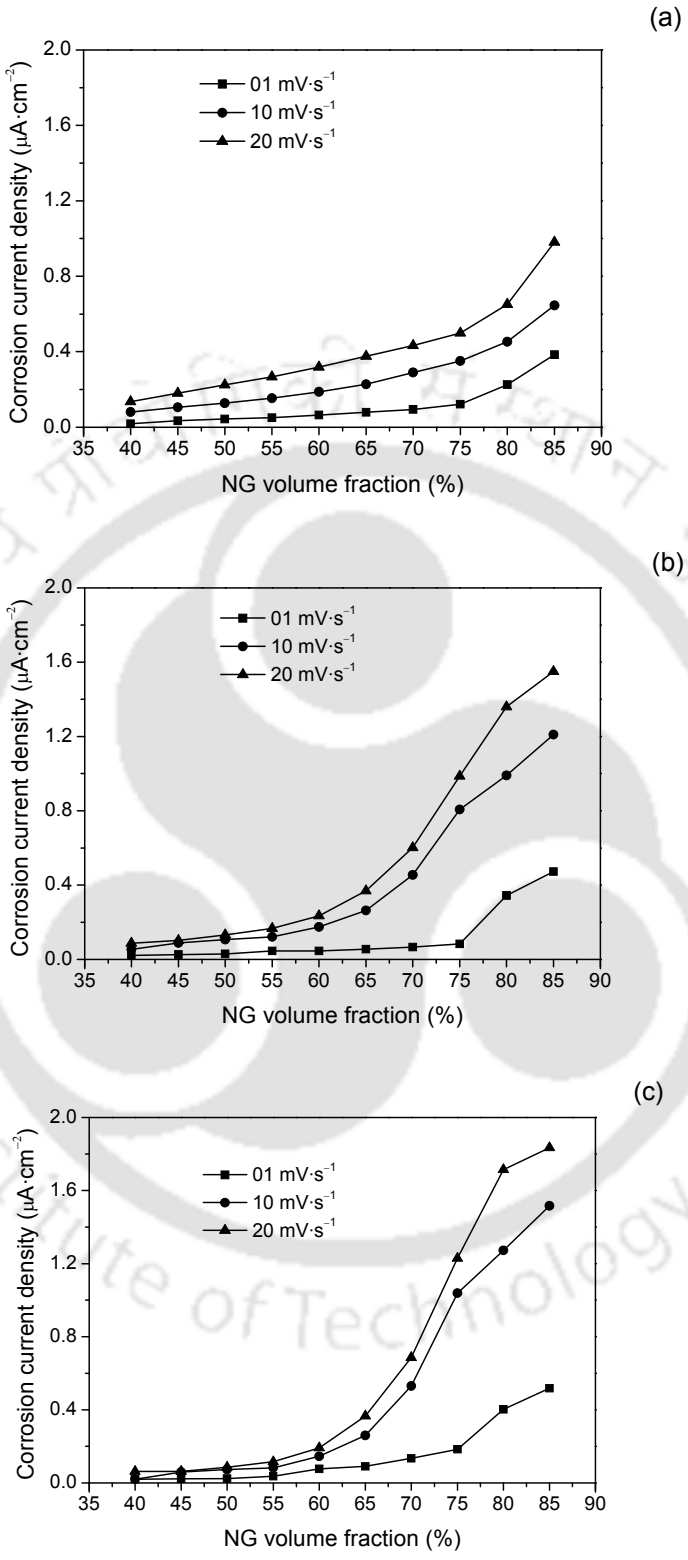

Figure 5.32: Effect of NG content on corrosion current density of (a) NG/resol-PF, (b) NG/novolac-PF, and (c) NG/VER composite bipolar plates tested in 0.1M H_2SO_4 at 25°C

5.4.7.1 *Potentiodynamic polarization*

The effects of NG content on the corrosion current density of the resol-PF/NG, novolac-PF/NG, and VER/NG composite bipolar plates, in 0.1M H_2SO_4 at 25°C, are shown in fig. 5.32(a), 5.32(b), and 5.32(c), respectively [Kakati et al., 2010]. The effects of scan rate on the corrosion current density of the composite bipolar plates are also shown in the respective figure. It can be seen from the figure that the corrosion current density of the composite increases with increase in the NG content. The corrosion current density increased as the insulating resin matrices were relatively more stable than the NG particles. Moreover, at low NG content, the NG particles were mostly covered by the insulating resin matrix due to the skinning effect. Therefore, the areas exposed to the electrochemical environment will be less. On the other hand, at high NG content, the area exposed to corrosion was high. Moreover, the hydrogen permeability of the composite at high NG content was relatively higher than the composite with low NG content. Therefore, the increased porosity of the composite will also accelerate the corrosion of the composite bipolar plate, at high NG loading. It was found that the corrosion current density of the VER based composite was highest among the three resin systems. This may be due to the contribution of the catalyst that was used for curing VER.

The potential scan rate may have significant effect on the amount of corrosion current produced. The scan rate is an important parameter as it simulates the system to the dynamic electrical load during operation of the fuel cell for an application such as in vehicles [Mulder et al., 2008]. Therefore, to evaluate the effect of the scan rate, the experiments were carried out with scan rate of 1, 10, and 20 $mV \cdot s^{-1}$. This would not disturb the double layer formed near the working electrode and remains fully charged so that the current-voltage relationship may reflect only the corrosion process at the potential range [Mulder et al., 2008]. Further increase in the scan rate over-predicts the data. Thus

for the prevailed experimental conditions, it was found that the scan rate should not be more than $20\,mV\cdot s^{-1}$. It can be seen in the fig. 5.32 that even at highest scan rate the corrosion current density was well below the undesired level. In fact, the voltage scan rate for any electrochemical experiment should be as low as possible. Henceforth, all the corrosion results will be reported for a voltage scan rate of $1\,mV\cdot s^{-1}$. The corrosion current densities of the NG/resol-PF, NG/novolac-PF and NG/VER composite bipolar plates, for optimum compositions, were 0.1052, 0.0658, and $0.1842\,\mu A\cdot cm^{-2}$, respectively.

The corrosion analyses of the NG/resin composite bipolar plates were also carried out in the rigorous simulated PEMFC and AFC environments. The corrosion current densities of the NG/resin composite bipolar plates at rigorous PEMFC and AFC environments are shown in fig. 5.33(a) and 5.33(b), respectively. The corrosion current densities of the composite bipolar plates were accelerated in the rigorous fuel cell environments. At the optimum resin content, the corrosion current densities of the resol-PF, novolac-PF and VER based composite bipolar plates, in rigorous PEMFC environment, were 0.1216, 0.1175, and 0.1900 $\mu A\cdot cm^{-2}$, respectively. Similarly, the corrosion current densities of those composites, in rigorous simulated AFC environments were 8.0900, 8.5409, and 9.3538$\mu A\cdot cm^{-2}$, respectively. It is visible from the fig. 5.33 that the corrosion current density of the composite increases rapidly when the NG volume fraction surpasses optimum composition.

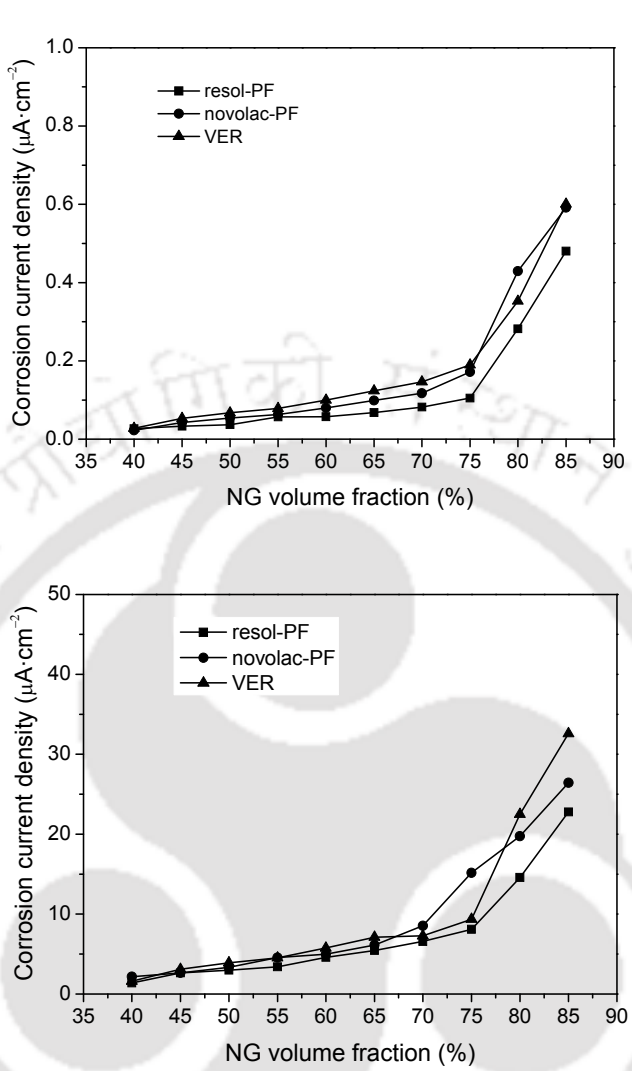

Figure 5.33: Effect of NG content on the corrosion current density of the NG/resin composite bipolar plate in rigorous simulated (a) PEMFC and (b) AFC environments; scan rate 1 $mV{\cdot}s^{-1}$

5.4.7.2 *Cyclic voltammetry*

The cyclic voltammetry was performed to study the electrochemical stability of the composite bipolar plates at different NG content in simulated rigorous PEMFC and AFC environments. The cyclic voltammograms of the NG/resin composite bipolar plates, at their optimum compositions, are shown in fig. 5.34. It can be seen from the fig. 5.34(a) that the bipolar plates were quite stable in the acidic environment. Figure 5.34(b) shows

the cyclic voltammetry in alkaline environment and a plateau can be seen in the region from 0.32–1.02V, which may be due to the passive layer formation during corrosion. However, the passive layer breaks down after 1.02V and the corrosion current density increases rapidly. It can also be seen that the voltammetric potential was shifted to more negative potential for NaOH than H_2SO_4 medium. Similar trends of cyclic voltammograms have also been reported for electrochemical electrodes made of glassy carbon and carbon fiber by Shuxuan et al. (2009) and Kelly et al. (1999), respectively.

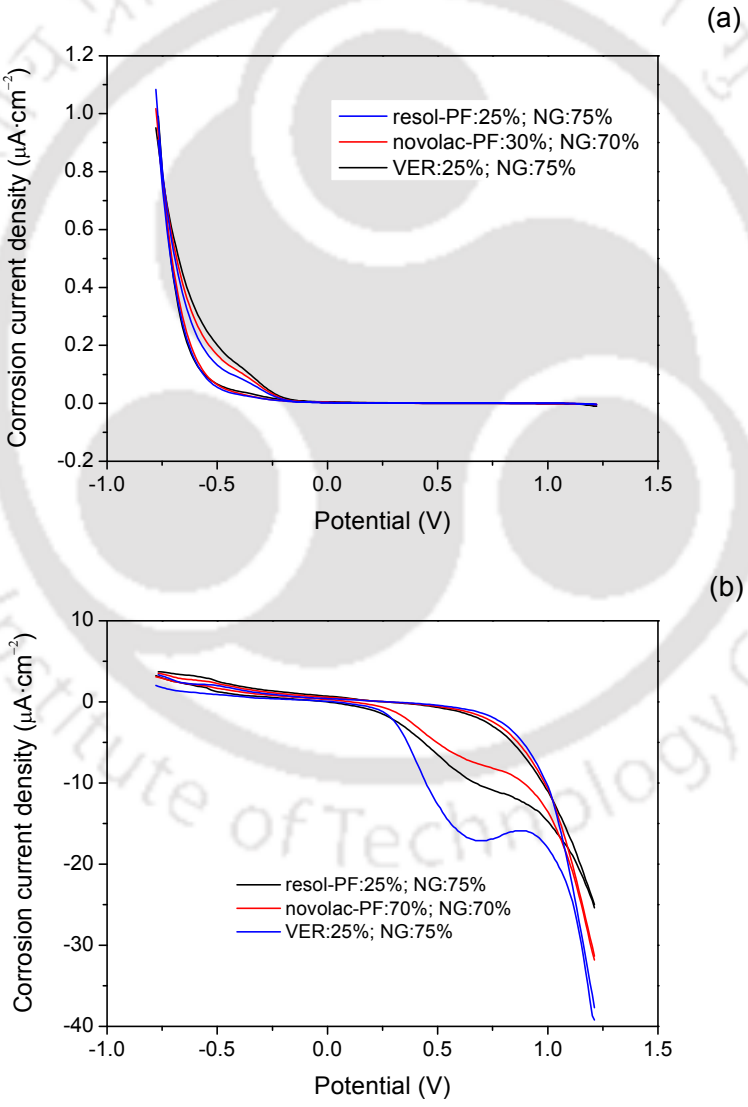

Figure 5.34: Cyclic voltammetry analyses of NG/resin composite bipolar plates in rigorous simulated (a) PEMFC and (b) AFC environments; scan rate 1 $mV \cdot s^{-1}$

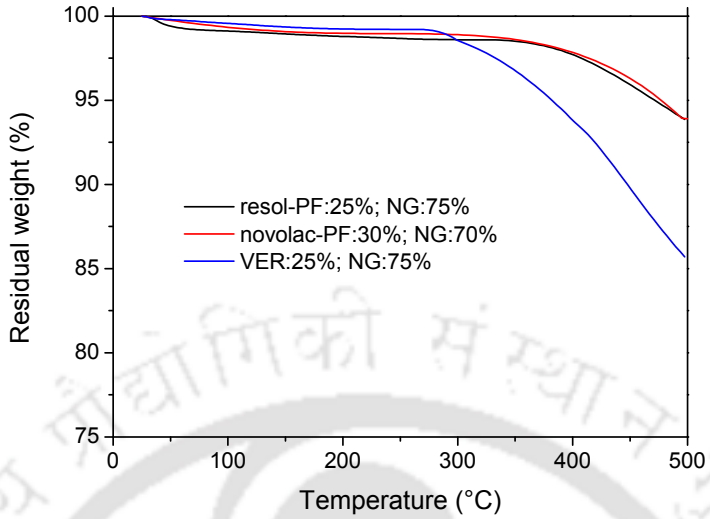

Figure 5.35: Thermal stability of the NG/resin composite bipolar plates at their optimum compositions

5.4.8 *Effect of NG content on the thermal stability of composite bipolar plate*

The thermal stability of the developed bipolar plates was studied, in the temperature range 25–500°C, as per the procedure described in section 3.3.1.2. The thermal stability of the composite bipolar plates, for the optimum compositions, is shown in fig.5.35. It can be observed from the thermograms shown in the fig.5.35 that the developed bipolar plates were thermally stable up to around 300°C. The residual weights of the composites bipolar plates at 300°C were 98.60, 98.90 and 98.58%, respectively. The high thermal stability of the composite bipolar plates was achieved as the resin content in the composite was fully cured.

5.4.9 *Morphological study of the resin/NG composite bipolar plates*

The morphological studies of the composite bipolar plates were carried out with the help of SEM analysis. The micrographs of the representative NG/resin composite bipolar plates are shown in fig. 5.36. Figure 5.36(a) shows the microstructure of the composite

bipolar plate with 25% resol-PF and 75% NG contents. From the figure, it is clearly visible that the NG flakes were aligned parallel to the surface of the composite bipolar plates. Therefore, the in-plane electrical conductivities of the composite bipolar plates were higher than the through-plane electrical conductivity. However, this effect might help in decreasing the hydrogen permeability of the composite bipolar plates. The similar orientation of the NG particles was also observed for the novolac-PF and VER based composite bipolar plates.

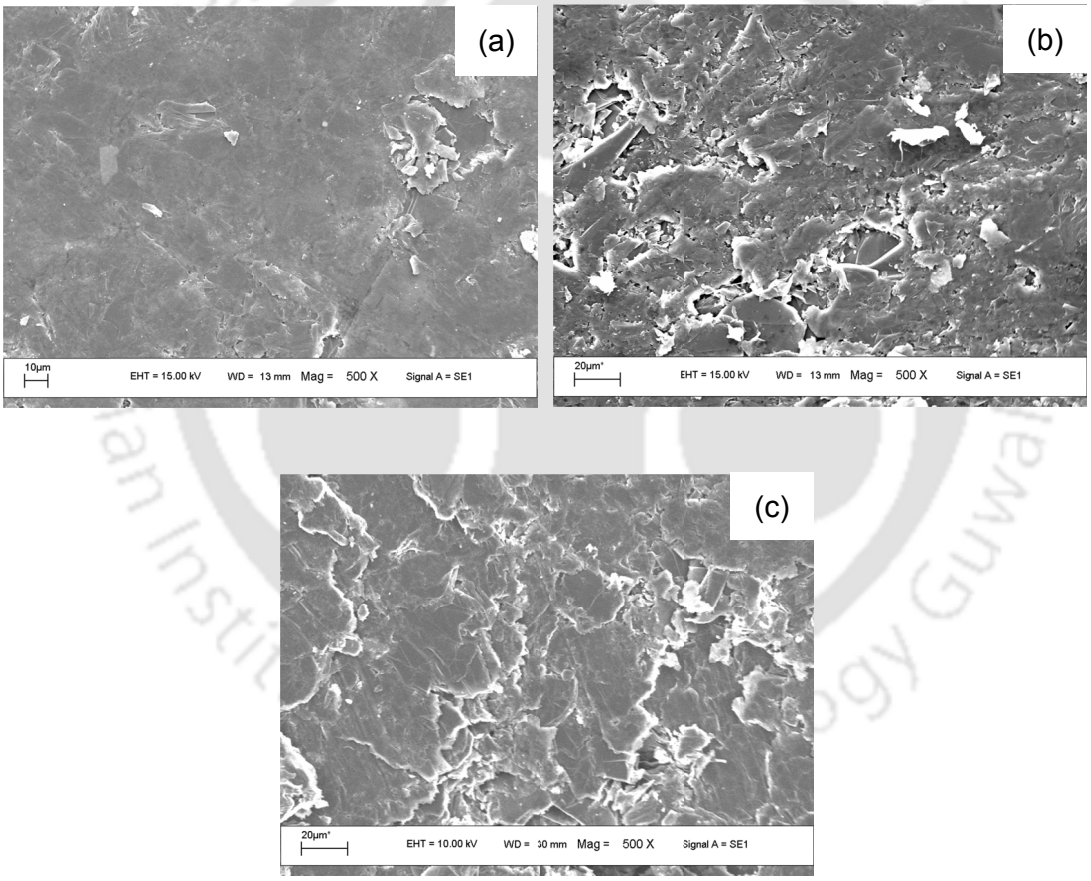

Figure 5.36: SEM images of representative NG/resin composite bipolar plates for (a) resol-PF:25%; NG:75%, (b) novolac-PF:30%; NG:70%, and (c) VER:25%; NG:75%

Table 5.1: Properties of NG/resin composite bipolar plates at the optimum compositions for different resin systems

Properties	**Target values**	**resol-PF:25%; NG:75%**		**novolac-PF:30%; NG:70%**		**VER:25%; NG:75%**	
Density ($g \cdot cm^{-3}$)	< 2.0	1.972		1.934		1.942	
H_2 permeability $\times 10^{-10}$ ($cm^3 \cdot cm^{-2} \cdot s^{-1}$)	10^4 (at 80°C and 3 bar)	2.93#	11.56*	2.33#	8.00*	4.00#	13.78*
Electrical conductivity ($S \cdot cm^{-1}$)	100	363.44 (∥)	103.30 (⊥)	201.26 (∥)	40.91 (⊥)	282.30 (∥)	90.37 (⊥)
Thermal conductivity ($W \cdot m^{-1} \cdot K^{-1}$)	10	113.20		105.30		110.20	
Flexural strength (MPa)	50	31.99		30.15		33.59	
Deflection at mid- span (%)	3–5	2.85		2.73		2.79	
Shore hardness	40	38		36		44	
Corrosion current density ($\mu A \cdot cm^{-2}$)	< 1	0.1052	0.1216†	0.0658	0.1175†	0.1842	0.1900†

∥ → in-plane ⊥ → through-plane

→ H2 permeability at 25°C under 2 bar pressure

* → H_2 permeability at 50°C under 2 bar pressure

† → in rigorous simulated PEMFC environment

resol-PF → resol type phenol formaldehyde

novolac-PF → novolac type phenol formaldehyde

VER → vinyl ester resin

NG → natural graphite

CB → carbon black

CF → carbon fiber

The effects of NG content on the properties of the NG/resin composite bipolar plates have been discussed on the previous section and the optimum resin content for the resol-PF, novolac-PF, and VER based composites were 25, 30, and 25%, respectively. The detailed properties of the NG/resin composite bipolar plates at their optimum composition are summarized in the table 5.1 and compared with the target values.

5.5 Effect of CB content on the properties of composite bipolar plate

It is observed from the table 5.1 that the density, hydrogen permeability, in-plane electrical conductivity, thermal conductivity, and the corrosion current density of the bipolar plates meet the target values. However, the through-plane electrical conductivities of the novolac-PF and VER based composite bipolar plates were below the target values of 100 $S{\cdot}cm^{-1}$.The shore hardness of the VER based composite was just edge over the target values. Similarly, the deflections at mid-span of all the three composites were below the target values. The shortfall in the required properties was thought to be achieved by replacing some of the NG with the other relevant reinforcement. For example, the high through-plane conductivity was thought to be achieved by introducing spherical conductive particles between the flaky graphite particles and the mechanical strengths by the fibrous conductive material. Therefore, CB and/or CF were used not only to increase the mechanical strength but also to increase the electrical conductivity of the composite.

The next section describes the effect of reinforcement of the CB at the expense of NG in the composite bipolar plate, keeping the resin fraction fixed at the above mentioned optimum values.

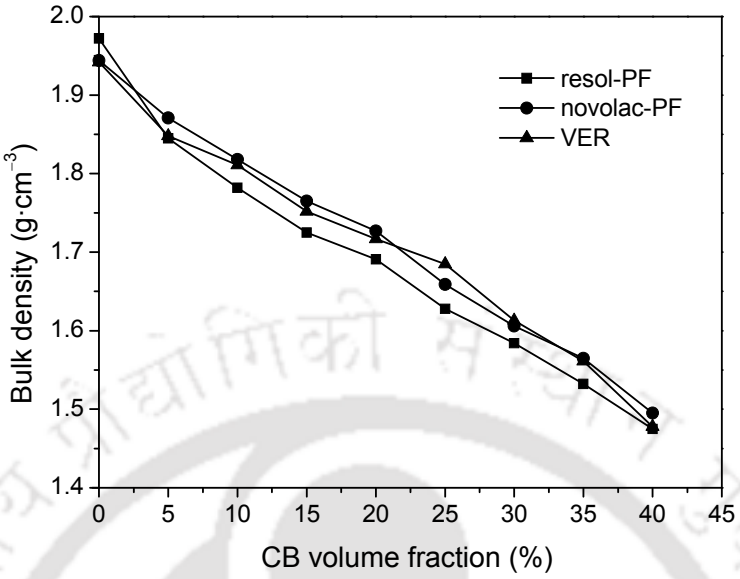

Figure 5.37: Effect of CB content on the density of the resol-PF, novolac-PF, and VER based composite bipolar plates

5.5.1 *Effect of CB content on the bulk density of composite bipolar plates*

The effects of CB content on the bulk density of the NG/CB/resin composite bipolar plates are shown in fig.5.37. It can be seen that the density of the composite decreases almost linearly with the increase in the CB content. The decreasing trend in the density of the composite was attributed due to the less density of CB ($1.2\,g\cdot cm^{-3}$) in comparison to NG ($2.26\,g\cdot cm^{-3}$). Moreover, it was found that the density of the composite followed the mixing law.

5.5.2 *Effect of CB content on the hydrogen permeability of the composite bipolar plates*

The effect of CB content on the hydrogen permeability of the composite bipolar plate is shown in fig.5.38. The reinforcement with CB reduces the hydrogen permeabilities initially upto 5% CB loading. The minimum hydrogen permeabilities of the NG/CB/resin

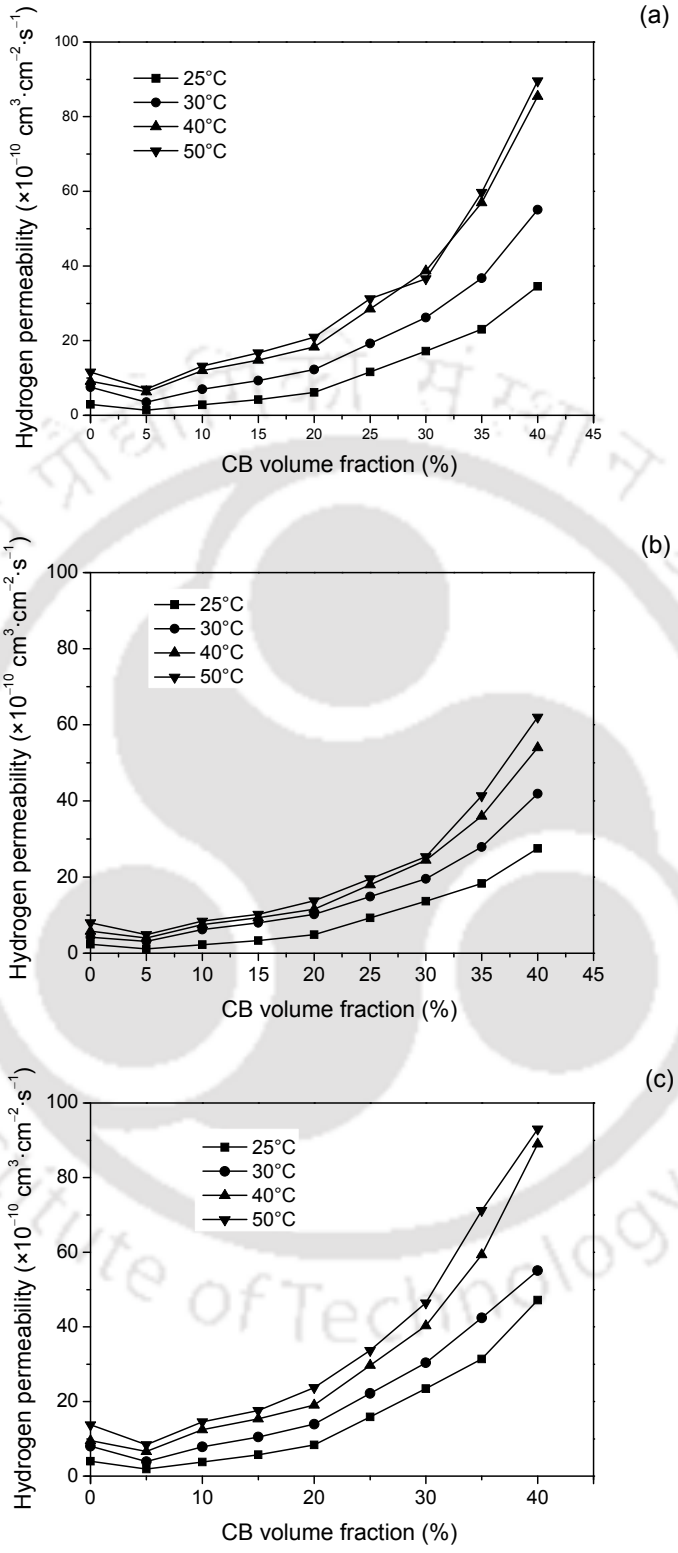

Figure 5.38: Effect of CB content on the hydrogen permeabilities of the (a) resol-PF/NG/CB, (b) novolac-PF/NG/CB, and (c) VER/NG/CB composite bipolar plates

composite bipolar plates were recorded as 1.79×10^{-10}, 1.78×10^{-10}, and 1.91×10^{-10} $cm^3 \cdot cm^{-2} \cdot s^{-1}$, respectively. However, the hydrogen permeability of the composite increases for CB loading above 5% and the rate of increase was significantly high for very high CB loading. This can be explained with the help of BET surface area analysis of the NG and CB. The surface area of the CB particles was 249.64 $m^2 \cdot g^{-1}$, while it was only 21.98$m^2 \cdot g^{-1}$for the NG particles. Therefore, at higher CB loading, the resin content was not sufficient to bind all the filler content. This affects the hydrogen permeability of the composite negatively. Moreover, the hydrogen permeability increases with the increase in temperature due to high diffusivity of the hydrogen gas. The same kind of negative effect was also observed in the case of electrical conductivity, mechanical strength, and thermal conductivity of the composite. The effect of CB on these properties will be discussed later in the respective sessions.

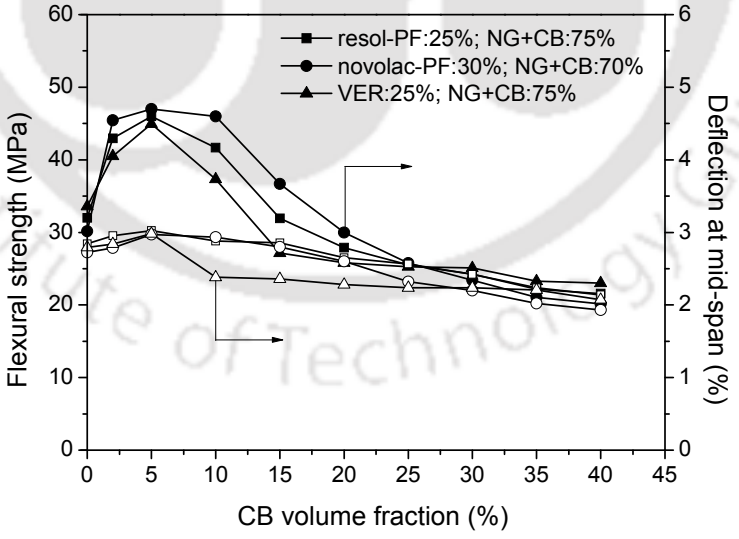

Figure 5.39: Effect of CB content on the flexural strength and deflection at mid-span of the NG/CB/resin composite bipolar plate

5.5.3 *Effect of CB content on flexural strength and flexibility of composite bipolar plates*

The effects of CB content on the flexural strength and deflection at mid-span of NG/CB/resin composite bipolar plates are shown in fig. 5.39. Figure 5.39 shows that the flexural strength of the composite bipolar plate increases with the addition of CB upto 5%, as the CB acts as an interconnector to the NG particles. Though the addition of CB upto 5%, increases the flexural strength but the deflection increases only slightly. It is probably due to the shape of the CB and its high requirement of resin to coat the CB surface, as explained earlier. The flexural strengths of the resol-PF, novolac-PF, and VER based composite bipolar plates, for 5% CB content, were 45.97, 47.00, and 44.95 MPa, respectively. The deflections at mid-span for these composites were 3.03, 2.97, and 2.98%, respectively. The deflections at mid-span for the novolac-PF and VER based composite, at the optimum composition, were edge below the target value. However, the deflection at mid-span for the NG/resol-PF was just above the lower target value.

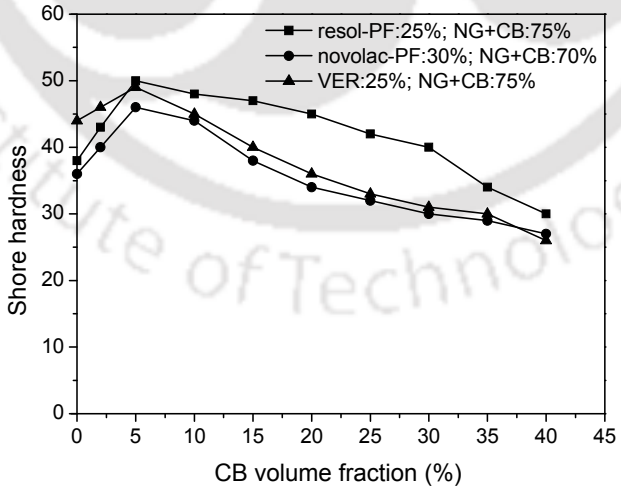

Figure 5.40: Effect of CB content on the shore hardness of the NG/CB/resin composite bipolar plates

5.5.4 *Effect of CB content on the shore hardness of composite bipolar plates*

The effects of CB on the shore hardness of the composite bipolar plates are shown in fig. 5.40. The effect of CB on the shore hardness of the NG/CB/resin composite was similar to the effect on flexural strength of the composite. The hardness of the composite bipolar plate increased initially up to 5%CB content. However, the shore hardness of the composite started decreasing after that. At low CB content, the tiny CB particles were more uniformly distributed among the entire resin matrix. Moreover, few CB particles occupied the interstices between two adjacent NG particles. Therefore, the strength as well as hardness of the composite increased in low CB content. However, as the CB content was further increased, the resin content was not enough to coat all the filler content as well as agglomeration of CB within the resin matrix started in the microscopic level. This left the material more porous and weak as seen in the case of hydrogen permeability and flexural strength of the composite.

5.5.5 *Effect of CB content on the electrical conductivity of composite bipolar plates*

The effects of CB particles on the in-plane and through-plane electrical conductivities of the NG/CB/resin composite bipolar plates are shown in fig. 5.41(a) and 5.41(b). At lower CB content, the particles fill the interstices between two neighboring graphite flakes. These CB particles act like electrical bridge between the NG flakes and increase the electrical conductivity [Du and Jana, 2007]. Increase in CB content beyond 5% reduces the conductivity of the bipolar plate because the electrical conductivity of the CB is around 100 $S \cdot cm^{-1}$, while it is around 10^6 $S \cdot cm^{-1}$ for NG. Therefore, the non-uniform distribution of CB particles and the low electrical conductivity of the CB in comparison with NG, decrease the electrical conductivity of the composite at high CB content. The electrical conductivity of the bipolar plate with 5% CB shows the highest in-plane and

through-plane electrical conductivities. The highest in-plane electrical conductivities of the NG/CB/resol-PF, NG/CB/novolac-PF, and NG/CB/VER composites were 424.96, 269.55 and 419.60S·cm^{-1}, respectively. Similarly, the highest through-plane electrical conductivities for these compositions were 115.71, 82.77, and 109.35S·cm^{-1}, respectively.

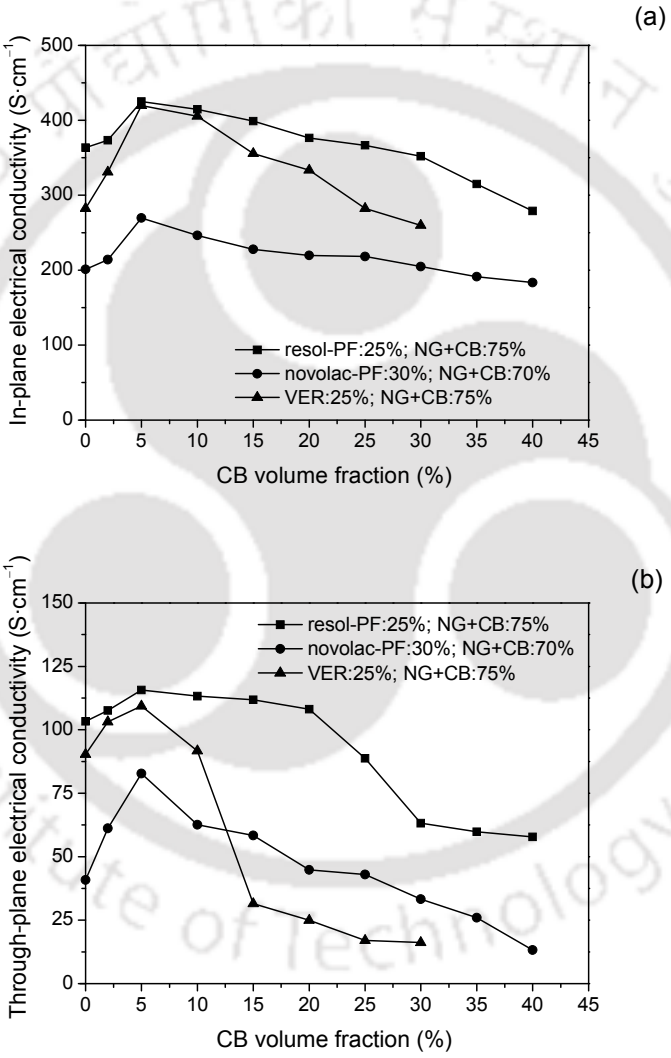

Figure 5.41: Effect of CB content on the (a) in-plane and (b) through-plane electrical conductivities of the NG/CB/resin composite bipolar plates

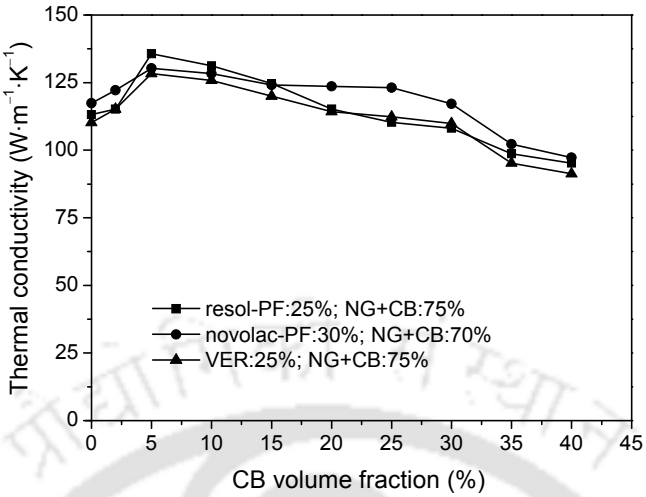

Figure 5.42: Effect of CB content on the thermal conductivities of the NG/CB/resin composite bipolar plates

5.5.6 *Effect of CB content on thermal conductivity of composite bipolar plates*

The effects of CB on the thermal conductivities of the NG/CB/resin composite bipolar plates were following the trend of electrical conductivity. The Vulcan XC72 grade CB is thermally conductive, though it is less conductive than NG. Therefore, the thermal conductivity of the composite bipolar plates for 5% CB content was little higher than those without CB. The thermal conductivities of the resol-PF, novolac-PF, and VER based composites, for 5%CB contents, were 135.71, 130.30, and 128.38 $W \cdot m^{-1} \cdot K^{-1}$, respectively.

5.5.7 *Effect of CB content on corrosion of the composite bipolar plates*

The potentiodynamic polarization and cyclic voltammetry analysis of the NG/CB/resin composite bipolar plates were carried out as per the methodology described in section 3.3.3.7.

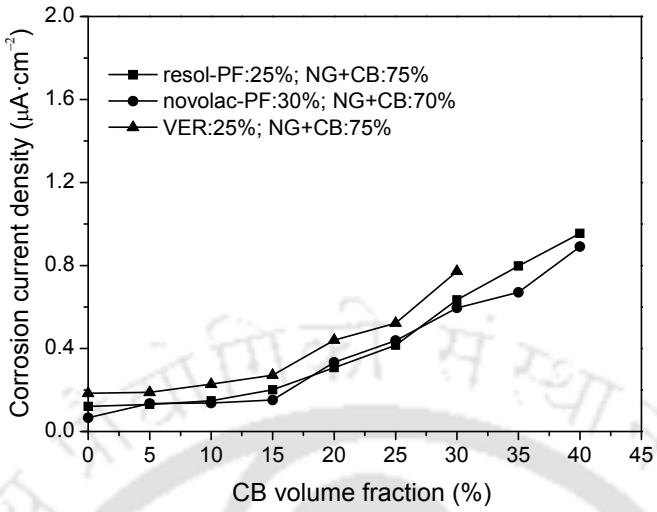

Figure 5.43: Effect of CB content on the corrosion current density of the composite bipolar plates tested in 0.1M H_2SO_4 at 25°C; scan rate 1mV·s^{-1}

5.5.7.1 *Potentiodynamic polarization*

The effects of CB content on the corrosion current densities of the composite bipolar plates were shown in fig. 5.43. It can be seen in the figure that the corrosion of the composite bipolar plates for resol-PF, novolac-PF, and VER based composites increases with the increase in the CB content. The corrosion current densities of the bipolar plates were almost identical for resol-PF and novolac-PF based composites. However, the VER based composites were relatively more corrosive due to the use of metal catalyst for VER curing reaction. The corrosion current densities of the resol-PF, novolac-PF and VER based composite bipolar plates, for 5% CB content, were 0.1305, 0.1350, and 0.1884 $\mu A \cdot cm^{-2}$, respectively.

The corrosion current densities of the NG/CB/resin composite bipolar plates were also measured in rigorous simulated PEMFC and AFC environments. The effects of CB on the corrosion current densities of the composite bipolar plates in rigorous simulated PEMFC

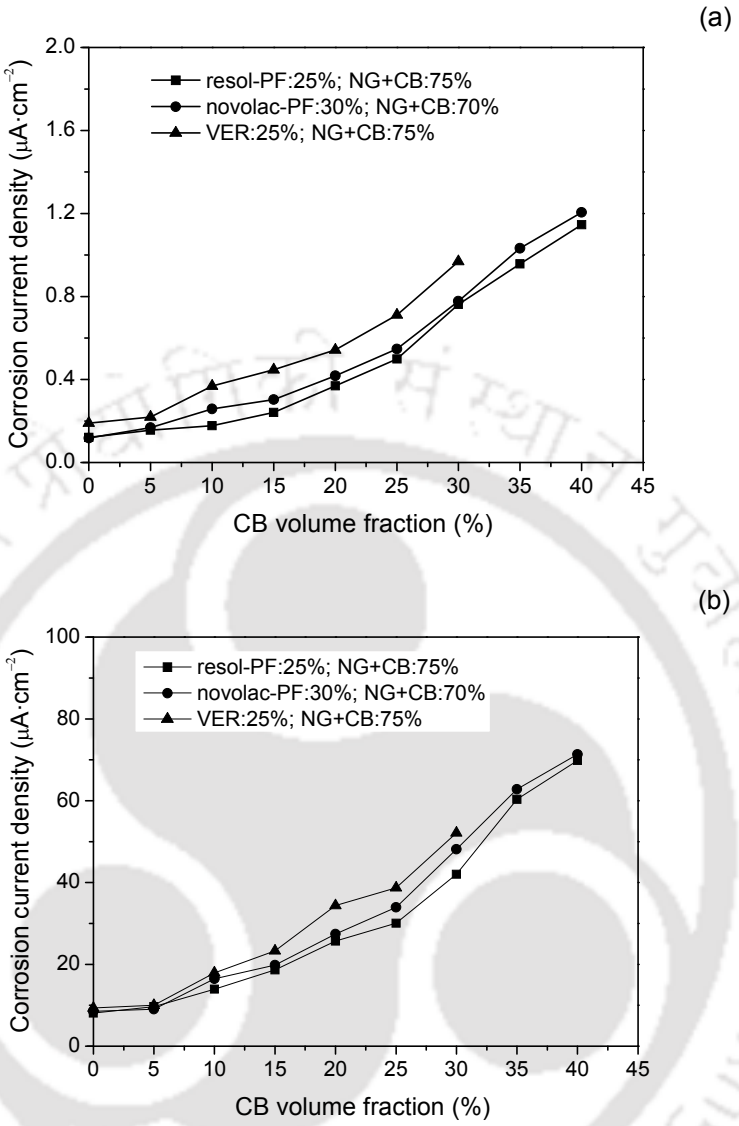

Figure 5.44: Effect of CB content on the corrosion current density of the composite bipolar plates tested in rigorous simulated (a) PEMFC and (b) AFC environments; scan rate 1mV·s^{-1}

and AFC environments are shown in fig. 5.44(a) and 5.44(b), respectively. The corrosion current densities of the composite increase rapidly above 5% CB content. The high surface to volume ratio of the CB increases the hydrogen permeability (fig. 5.38) in turn porosity as well as the active area of the bipolar plate. Moreover, the CB is more corrosive in aqueous environment than the NG [Siroma et al., 2007]. It can be seen in the

fig. 5.44(b) that the corrosion current density of the composite bipolar plates was more in the AFC environments. This happens as the alkaline medium is more corrosive to the bipolar plate than the acid medium. Moreover, the exposure of the CB particles to the aggressive AFC environment may lead to the preferential removal of the surface carbon atoms from the composite and hence corrosion current density increases with increase in CB content. In rigorous simulated PEMFC environment, the corrosion current densities of the resol-PF, novolac-PF, and VER based composite bipolar plates at their optimum compositions and 65% NG and 5% CB contents were 0.1566, 0.1688, and 0.2194 $\mu A \cdot cm^{-2}$, respectively. Similarly, corrosion current densities of these bipolar plates in rigorous simulated AFC environments were 9.651, 9.055, and 10.027$\mu A \cdot cm^{-2}$, respectively.

5.5.7.2 *Cyclic voltammetry*

The cyclic voltammetry analyses of the NG/CB/resin composite bipolar plates were carried out in the rigorous simulated PEMFC and AFC environments. The voltammograms of the optimum compositions of the composite bipolar plates in PEMFC and AFC environments are shown in fig. 5.45(a) and 5.45(b), respectively.

Figure 5.45(a) shows that the electrochemical stabilities of the NG/CB/resol-PF and NG/CB/novolac-PF composite bipolar plates are almost similar. However, the NG/CB/VER composite bipolar plates are electrochemically less stable than the PF based composite. Moreover, the electrochemical stability of the CB reinforced composites were also less than the NG/resin composite bipolar plates. The cyclic voltammograms in fig. 5.45(b) reveals that the electrochemical durability of the composite bipolar plates in the rigorous AFC environment is less than that in the rigorous AFC environment. However, the plateau appears in the voltammograms of NG/CB/resin composite similar to the

voltammograms of NG/resin composite bipolar plates as shown in fig. 5.34(b). The plateau in the voltammogram was ascribed to the formation of passive layer on the bipolar plate. Moreover, VER based composite showed less stability than the PF based composite bipolar plates. This may be attributed due to the higher porosity of the VER based composite bipolar plates.

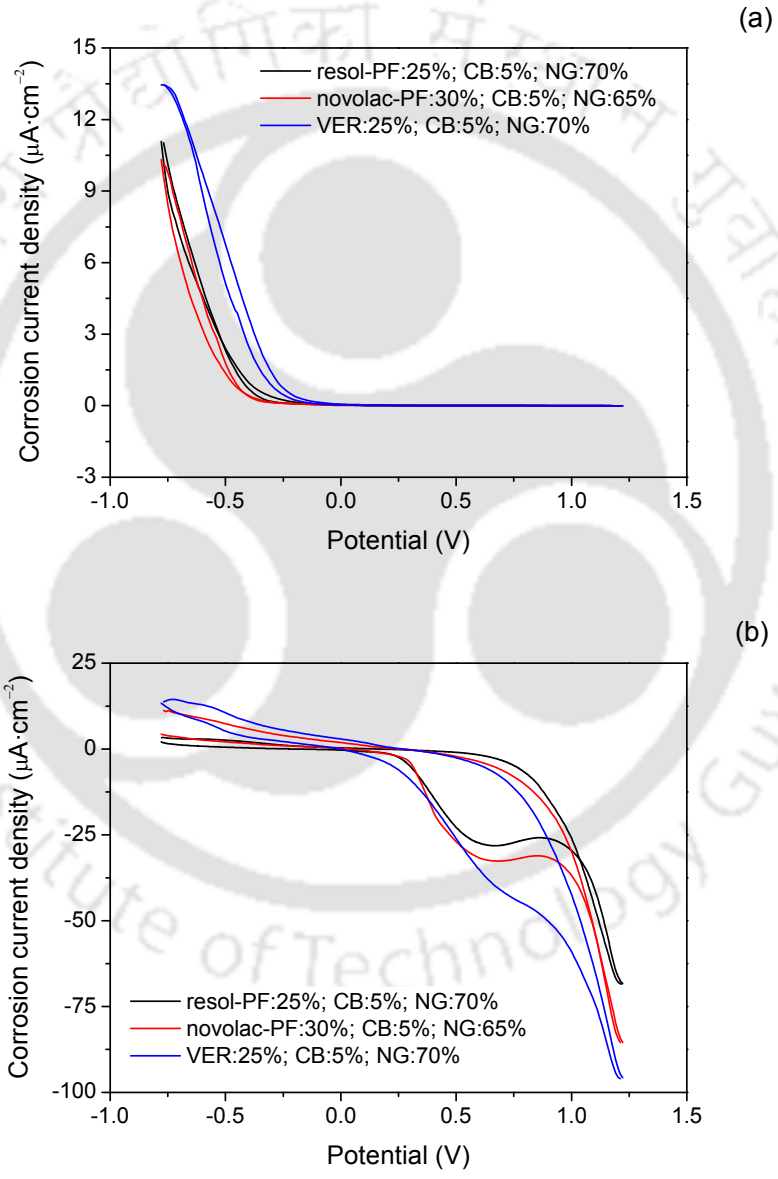

Figure 5.45: Cyclic voltammetry analyses of NG/CB/resin composite bipolar plates in rigorous simulated (a) PEMFC and (b) AFC environments; scan rate 1 $mV \cdot s^{-1}$

5.5.8 *Thermal stability of the NG/CB/resin composite bipolar plates*

The thermal stability of the CB reinforced composite bipolar plates were carried out, in the temperature range 25–500°C, as per the procedure described in section 3.3.1.2. Figure 5.46 shows the thermal stabilities of the NG/CB/resin composite bipolar plates at their optimum compositions. There was a minor decrease in the thermal stability of the composite bipolar plate upon CB reinforcements. It can be concluded from the voltammograms, that the bipolar plates wee thermally stable up to around 300°C. The residual weights of the NG/CB/resin composite bipolar plates, at their optimum compositions, were 98.54, 97.29, and 97.93%, respectively for resol-PF, novolac-PF, and VER. However, thermal stability of the NG/CB/VER composite bipolar plate, at above 300°C, was less than that of the NG/CB/PF composite bipolar plates. The TGA thermogram of VER in fig. 5.5 shows that the thermal stability of VER is inferior to the thermal stability of PF.

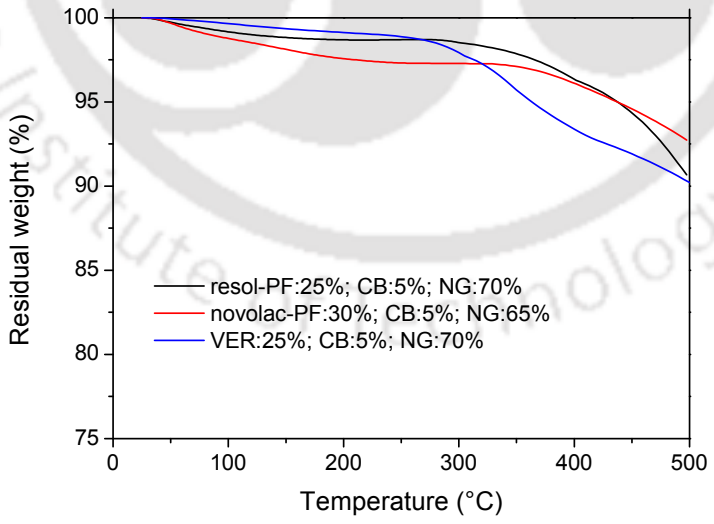

Figure 5.46: Thermal stability of the NG/CB/resin composite bipolar plates at their optimum composition

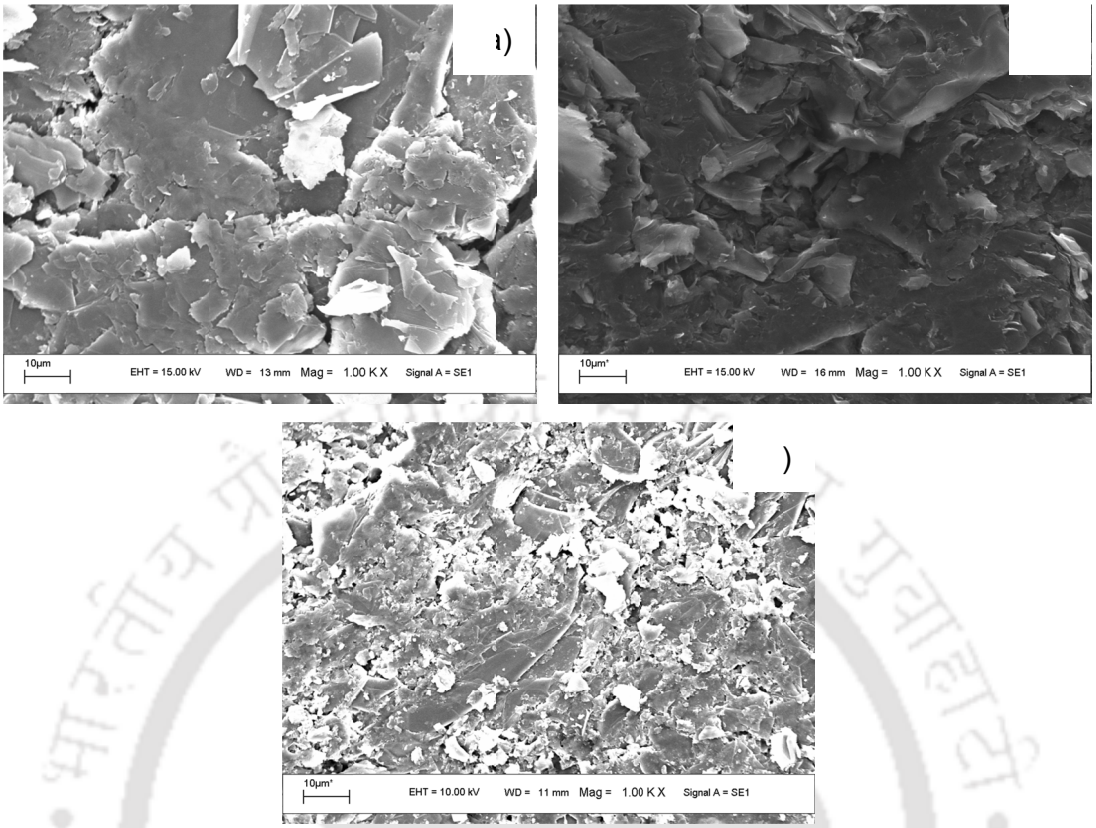

Figure 5.47: SEM images of representative NG/CB/resin composite bipolar plates for (a) resol-PF:25%; CB:5%; NG:70%, (b) novolac-PF:30%; CB:5%; NG:65%, and (c) VER:25%; CB:5%; NG:70%

5.5.9 *Morphological study of the NG/CB/resin composite bipolar plates*

The representative micrographs of the NG/CB/resin composite bipolar plates are shown in fig. 5.49. The figure shows that the NG particles are aligned parallel to the surface of the composite bipolar plates and the tiny CB particles are spread over them. The CB particles are visible as bright white discs in the micrographs. Moreover, the CB particles also occupy the interstices between two neighboring NG particles. This helped in increasing the electrical conductivity of the composite bipolar plates as explained in the fig. 5.47. In this particular case, the electrical conductivity of the NG/CB/resin composite can be explained following the path 1 and 2 in the fig. 5.53. It was also observed in the SEM images (fig.5.7) that few CB particles were in the nano-range. These particles may

also fill the nano-pores within the composite. As a result, the hydrogen permeability of the composite was lowest at 5% CB loading. The CB particles connecting different NG flakes are clearly visible in the fig. 5.47(a) and 5.47(c). However, in case of novolac-PF/NG/CB composites the population of CB particles could not be seen on the surface as most of the NG flakes covered the surface (fig. 5.47b).

The effects of CB content on the properties of the NG/CB/resin composite bipolar plates have been discussed on the section 5.5. The optimum CB content for the resol-PF, novolac-PF, and VER based composites were found to be 5% at the expense of NG. The detailed properties of the NG/CB/resin composite bipolar plates at their optimum compositions are summarized in table 5.2 and compared with the target values.

5.6 Effect of CF content on the properties of the composite bipolar plate

The effects of CB content on the properties of the NG/CB/resin composite bipolar plates have been discussed on the section 5.5. The optimum CB content for the resol-PF, novolac-PF, and VER based composites were found to be 5%. The detailed properties of the NG/CB/resin composite bipolar plates at their optimum compositions are summarized in table 5.2 and compared with the target values. It is observed that the density, hydrogen permeability, shore hardness, in-plane electrical conductivity, thermal conductivity, and corrosion current density of the bipolar plates, at their optimum compositions, fulfill the target values. However, the flexural strength and through-plane electrical conductivity of the novolac-PF based composite bipolar plates was below the target values of 50MPa and 100 $S{\cdot}cm^{-1}$, respectively. Similarly, the deflections at mid-span of all the three composites were below the target values. Therefore, CF was used at the expense of NG to improve the flexibility of the composite bipolar plate. However, the effects of CF on the other properties of the composite bipolar plates were also studied and reported herewith.

Table 5.2: Properties of NG/CB/resin composite bipolar plates at the optimum compositions for different resin systems

Properties	**Target values**	**resol-PF:25%; CB:5%; NG:70%**		**novolac-PF:30%; CB:5%; NG:65%**		**VER:25%; CB:5%; NG:70%**	
Density ($g \cdot cm^{-3}$)	< 2.0	1.845		1.871		1.848	
H_2 permeability $\times 10^{-10}$ ($cm^3 \cdot cm^{-2} \cdot s^{-1}$)	10^4 (at 80°C and 3 bar)	1.39#	7.06*	1.78#	4.89*	1.91#	8.42*
Electrical conductivity ($S \cdot cm^{-1}$)	100	424.96 (∥)	115.71 (⊥)	269.55 (∥)	82.77 (⊥)	419.60 (∥)	109.35 (⊥)
Thermal conductivity ($W \cdot m^{-1} \cdot K^{-1}$)	10	135.71		130.30		128.38	
Flexural strength (MPa)	50	45.97		47.00		44.95	
Deflection at mid- span (%)	3–5	3.03		2.97		2.98	
Shore hardness	40	50		46		49	
Corrosion current density ($\mu A \cdot cm^{-2}$)	< 1	0.1305	0.1566†	0.1350	0.1688†	0.1884	0.2194†

∥ → in-plane ⊥ → through-plane

\# → H2 permeability at 25°C under 2 bar pressure

* → H_2 permeability at 50°C under 2 bar pressure

† → in rigorous simulated PEMFC environment

resol-PF → resol type phenol formaldehyde

novolac-PF → novolac type phenol formaldehyde

VER → vinyl ester resin

NG → natural graphite

CB → carbon black

CF → carbon fiber

5.6.1 *Effect of CF content on the density of the NG/CB/CF/resin composite bipolar plates*

The effects of CF content on the density of the NG/CB/CF/resin composite bipolar plates are shown in fig. 5.48. The effect of CF content on the density of the composite bipolar plate was similar to the effect of CB. The density of the composite decreases with the increase in CF content as the density of CF is 1.76 g·cm^{-3}, while the density of NG is 2.26 g·cm^{-3}. It is seen in the fig. 5.48 that the densities of the NG/CB/CF/resin composite bipolar plates followed the mixing laws. The densities of the resol-PF, novolac-PF, and VER resin based composites at 5% CF content were 1.810, 1.845, and 1.825 g·cm^{-3}, respectively.

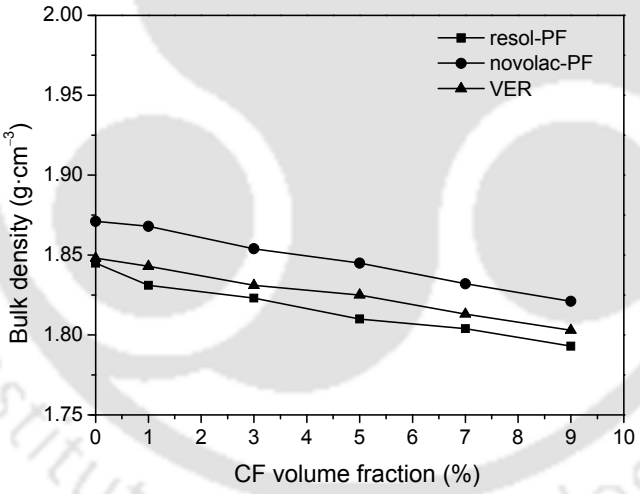

Figure 5.48: Effect of CF content on the density of the resol-PF, novolac-PF, and VER based composite bipolar plates

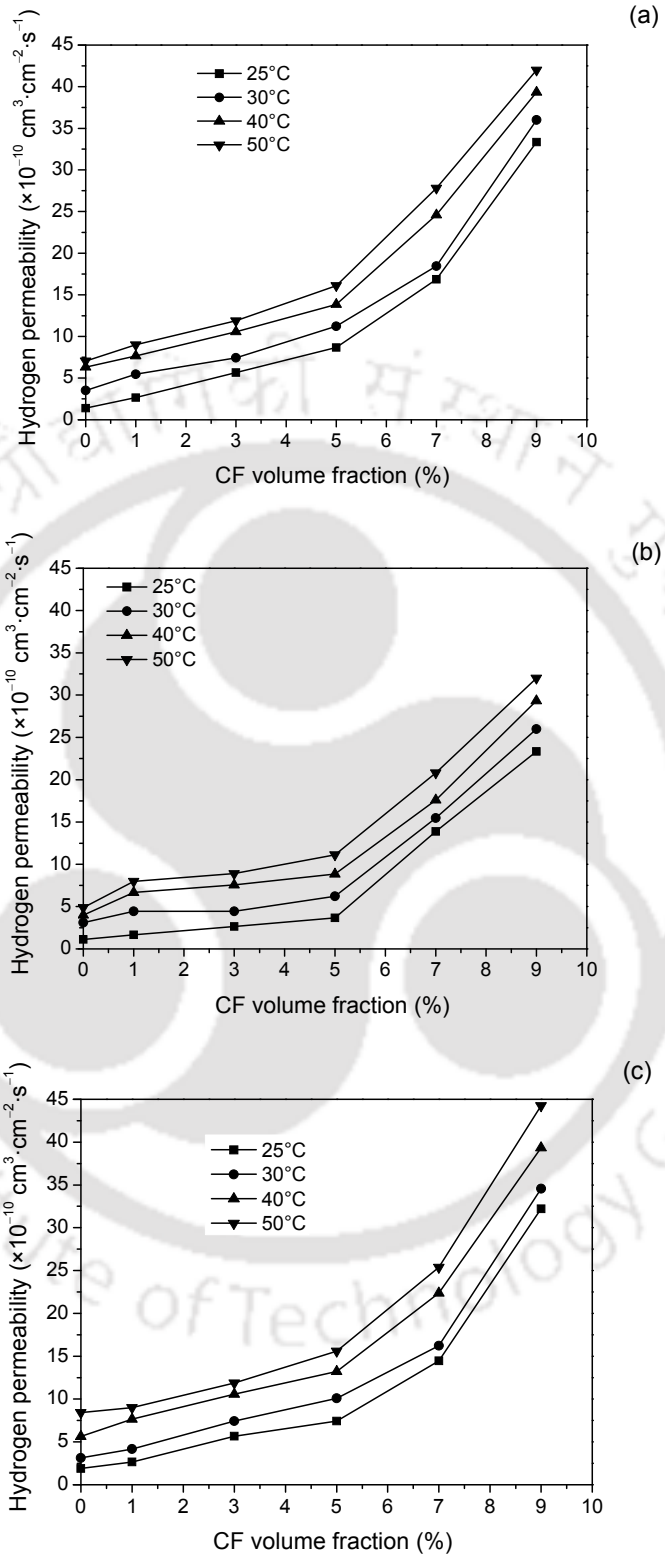

Figure 5.49: Effect of CF content on the hydrogen permeabilities of the resol-PF, novolac-PF, and VER based composite bipolar plates

5.6.2 *Effect of CF content on the hydrogen permeability of the NG/CB/CF/resin composite bipolar plates*

The effect of CF content on the hydrogen permeabilities of the NG/CB/CF/resin composite bipolar plates are shown in fig. 5.49. The hydrogen permeability of the composite increased gradually up to 5% CF content and then increases rapidly thereafter. The hydrogen permeabilities of the NG/CB/CF/resin composite bipolar plates at 5% CF content were recorded as 5.67×10^{-10}, 6.22×10^{-10}, and 7.42×10^{-10} $cm^3\cdot cm^{-2}\cdot s^{-1}$ for resol-PF, novolac-PF and VER, respectively. The hydrogen permeabilities of the composite bipolar plates for all the three resin systems increase with the increase in the temperature. However, the main objective to reinforce the composite with CF was to improve the mechanical strength of the bipolar plate keeping the hydrogen permeability within the required level. The haphazard orientation of the CF within the composites, at higher CF content, led to high hydrogen permeabilities. However, the hydrogen permeability was well within the required level at any combination of the plate under study. The effects of CF loading on the other properties of the composite bipolar plates are discussed in the next sections.

5.6.3 *Effect of CF content on flexural strength and flexibility of the NG/CB/CF/resin composite bipolar plates*

It was found that the deflections at mid-span of the NG/CB/resin composite bipolar plates were nearby lower target value. The flexural strength of CF is in the range of 1,870 MPa (datasheet, Torayca). Therefore, the CF was chosen at the expense of NG to reinforce the optimum composition (from section 5.5) of the above three resin based composites. Figure 5.50 shows the effect of CF on flexural strength and flexibility (deflection at mid-span) of the bipolar plate. It can be seen that the increase in the CF content increases the flexural strength as well as flexibility of the bipolar plate. It seems that a large amount of

NG should be replaced by CF to achieve the high flexural strength. However, the increase in the flexural strength should not have any adverse effect on atleast electrical conductivity as fuel cells are low voltage device and thus the source of voltage loss must be minimized. Therefore, considering the electrical conductivity (section 5.6.5), the optimum flexural strength was 55.28 MPa for 5% CF along with other constituents (novolac-PF:30%; NG: 60% and CB:5%). It is to be noted that the deflection at mid-span of the composite bipolar plate at this combination (novolac-PF:30%; NG:60%; CB:5% and CF:5%) is 5.2%, which fulfills our target values. Similarly, at 5% CF loading, the flexural strengths of the resol-PF and VER resin based composite were around 54.23 and 53.50 MPa, respectively. The deflections at mid-span of these two composites were 5.474 and 5.372%, respectively. Hence, the resol-PF and VER resin based composites were slightly more flexible than the novolac-PF based bipolar plate. Therefore, at NG substitution by 5% CF on the optimum compositions for three resin systems, the flexural strengths and deflections at mid-span of the composites were above the target values.

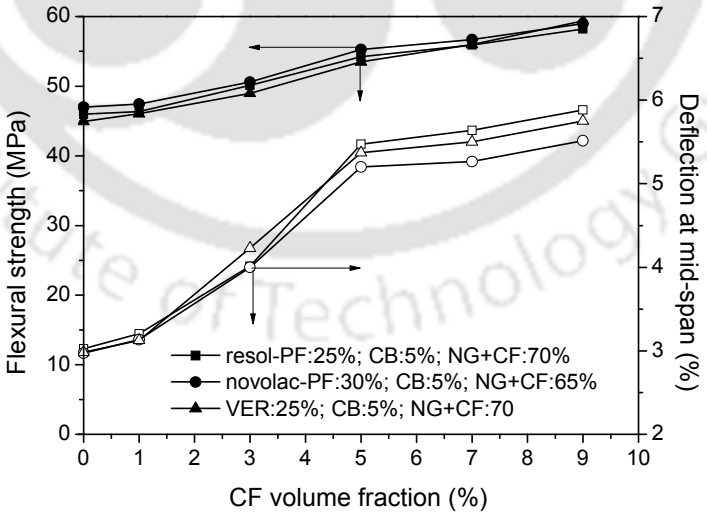

Figure 5.50: Effect of CF content on the flexural strengths and deflections at mid-span of the NG/CB/CF/resin composite bipolar plates

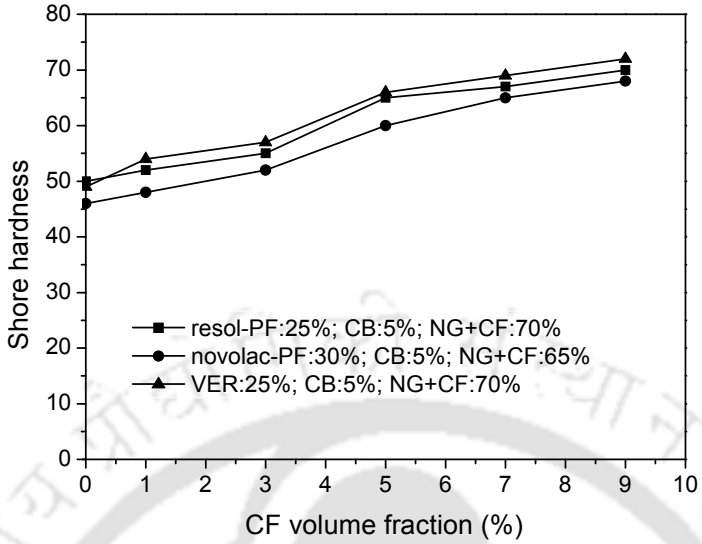

Figure 5.51: Effect of CF content on the shore hardness of the NG/CB/CF/resin composite bipolar plates

5.6.4 *Effect of CF content on shore hardness of the NG/CB/CF/resin composite bipolar plates*

The effects of CF on the shore hardness of the NG/CB/CF/resin composite bipolar plates are shown in fig. 5.51. It is seen in the figure that the shore hardness of the composite increased with increasing CF content. The increasing trend of shore hardness is due to the cushioning effect provided by the CF. The shore hardness of the composite bipolar plate at the optimum compositions were 65, 60, and 66 for resol-PF, novolac-PF, and VER based composites. Therefore, the values of shore hardness of these composites were well above the required values of the bipolar plate.

5.6.5 *Effect of CF content on electrical conductivity of the NG/CB/CF/resin composite bipolar plates*

The effect of CF content on the in-plane and through-plane electrical conductivities of the NG/CB/CF/resin composite bipolar plates are shown in fig.5.52(a) and 5.52(b),

respectively. In low CF content, the fibers tend to align parallel to surface of the plate. In the process, some CF connects two neighboring NG-NG and/or NG-CB particles and thus increases the electrical conductivity of the bipolar plate. In such a situation, the electronic conductivity mechanism within the composite may be by four means, as shown in fig.5.53. The electron can migrate from one end of the bipolar plate to the other end via any of the four paths, viz., (i) NG-NG, (ii) NG-CB-NG, (iii) NG-CF-NG, and (iv) NG-CF-CB-NG. Therefore, the electrical conductivities of the multi-filler (with different aspect ratios) composites are higher than the electrical conductivity of the single filler composites. However, at high CF loading, the orientation of the CF becomes non-uniform due to agglomeration and decreases the electrical conductivity of the bipolar plate. It is due to the fact that the electrical conductivity of CF is higher along the axis of the fiber as compared to the radial direction. Moreover, the high CF loading also increases the hydrogen permeability of the composite significantly. Therefore, the in-plane as well as the through-plane electrical conductivities of the composites decreased again. The maximum in-plane electrical conductivities of the composite bipolar plates were 425.43, 285.54, and 421.96 $S \cdot cm^{-1}$, respectively. Similarly, the highest through-plane electrical conductivities at the optimum composition of the composite bipolar plates were 117.15, 91.79 and 116.47$S \cdot cm^{-1}$, respectively. The in-plane as well as through-plane electrical conductivities of the developed bipolar plates were higher than the most of the commercially available composite bipolar plate. The electrical conductivity of the commercially available composite bipolar plate by Schunk Group is 111.11 and 52.63 $S \cdot cm^{-1}$ for in-plane and through-plane, respectively [datasheet, Schunk bipolar plate].

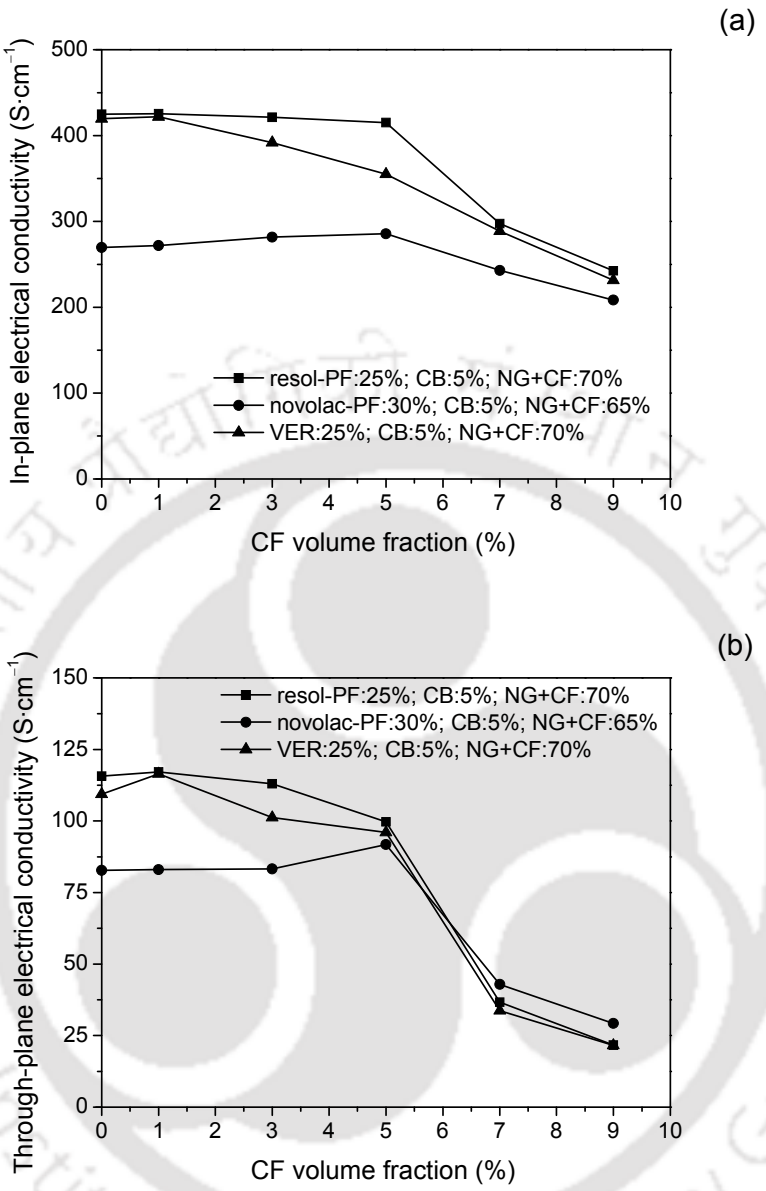

Figure 5.52: Effect of CF content on the (a) in-plane and (b) through-plane electrical conductivities of the NG/CB/CF/resin composite bipolar plates

It has been found that the in-plane electrical conductivities of the composite bipolar plates for all the resin systems were well above the target values. However, the through-plane electrical conductivity of the novolac-PF based composite bipolar plate was still lagging the target value.

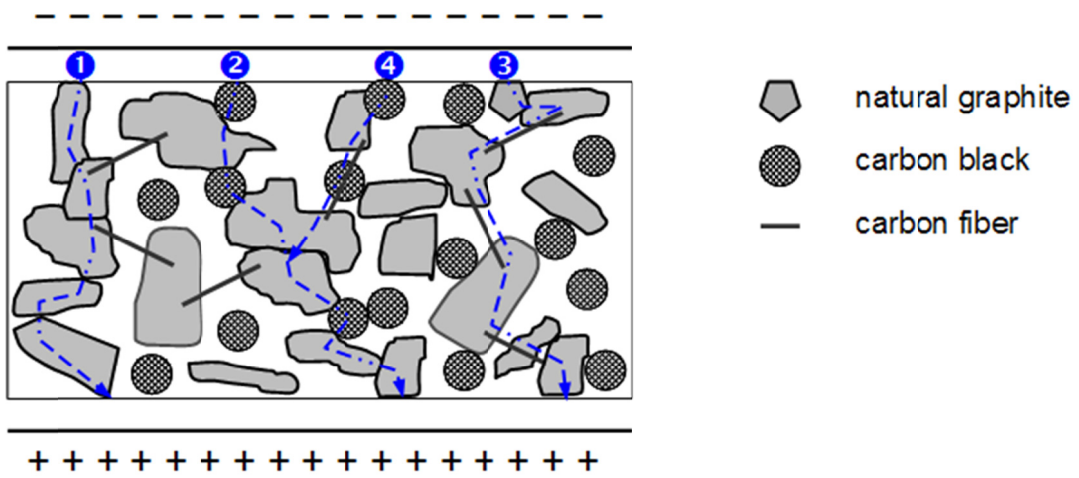

Figure 5.53: The proposed conductivity mechanism in a NG/CB/CF/resin composite bipolar plate

5.6.6 *Effect of CF content on thermal conductivity of the NG/CB/CF/resin composite bipolar plates*

The effect of CF on the thermal conductivity of the composite bipolar plates is shown in fig. 5.54. It was found that the reinforcement with CF enhances the thermal conductivity of the composite up to 5% CF loading. However, the thermal conductivity of the composite decreases for higher CF loadings due to the increase in porosity (confirmed by hydrogen permeability). The thermal conductivity of the CF, along the length, is 10.46 $W \cdot m^{-1} \cdot K^{-1}$, while it is 140–500 $W \cdot m^{-1} \cdot K^{-1}$ for NG along the basal plane [datasheet, Torayca]. At low CF content, the fibers tend to align parallel to the surface of the bipolar plate. Therefore, there was a marginal improvement in the thermal conductivity of the composite bipolar plate. At high CF loading, the fibers get agglomerated and thus are in a haphazard manner in the composite. Therefore, the thermal conductivity decreases with the increase in the CF content above 5% in the bipolar plate.

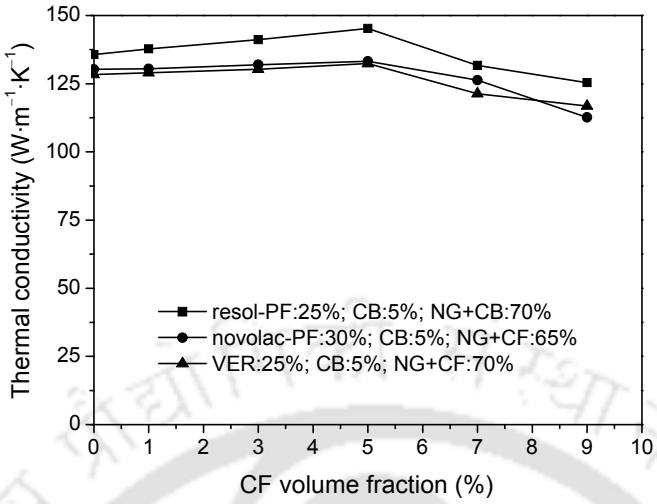

Figure 5.54: Effect of CF content on the thermal conductivity of the NG/CB/CF/resin composite bipolar plates

5.6.7 *Effect of CF content on corrosion of the NG/CB/CF/resin composite bipolar plates*

The corrosion studies of the NG/CB/CF/resin composite bipolar plates were carried out with the help of potentiodynamic polarization and cyclic voltammetry. The detailed methodology of the corrosion studies has been explained in section 3.3.3.7.

5.6.7.1 *Potentiodynamic polarization*

The corrosion current densities of the NG/CB/CF/resin composite bipolar plates are shown in fig. 5.55. From the figure, it is clearly visible that the corrosion current density of the composite bipolar plate increases with the increase in the CF content. Moreover, the corrosion current density increases rapidly after 5% CF loading. The rapid increased in the corrosion current density may be due to the increased porosity (confirmed by the hydrogen permeabilities) of the composites, as shown in fig.5.49. Moreover, the corrosion is higher when the CB and/or CF are reinforced in the NG/resin based bipolar plate. This was due to the more corrosive behavior of CB and CF as compared to NG. In fact, NG is

one of the most corrosion resistive materials. The Galvanic series indicate that the graphite is highly noble among many metal and alloys including platinum with respect to corrosion [Jones, 1996; Roberge, 2000; Hoeckelman, 2001].

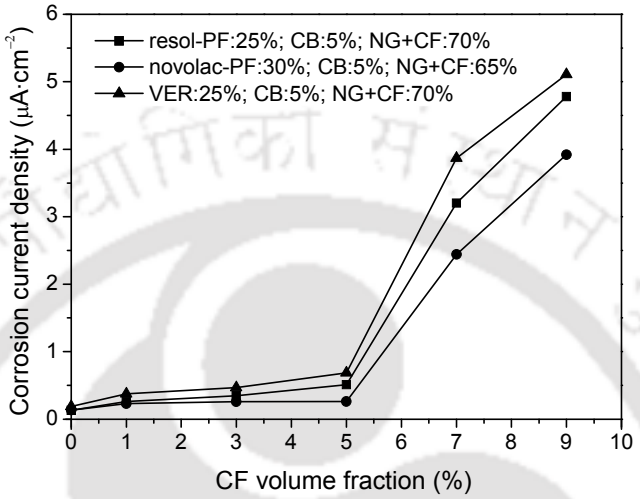

Figure 5.55: Effect of CF content on the corrosion current density of the composite bipolar plates tested in 0.1M H_2SO_4 at 25°C; scan rate 1mV·s^{-1}

The corrosion analyses of the bipolar plates were also carried out in rigorous conditions of the simulated fuel cell environment aerated at 1.0M electrolyte at 80°C. Figure 5.56(a) and 5.56(b) shows the effect of CF content on the corrosion current density of three sets of representative bipolar plates, from the three resin systems, in 1.0M H_2SO_4 and NaOH, respectively. From fig. 5.56, it can be seen that the corrosion current density increases with the increase in the CF content. The fig. 5.56(a) shows that the corrosion of the composite increases significantly for the rigorous PEMFC environment as compared to the normal PEMFC environment (fig.5.44). The corrosion current density of the rigorous AFC environment is also shown in the fig. 5.57(b). The corrosion of the composite bipolar plate in simulated rigorous AFC environment was much higher than the corrosion in the PEMFC environment. At 5% CF content, the corrosion current densities of the resol-PF, novolac-PF, and VER based composite bipolar plates in the PEMFC

environment were 1.00, 0.99 and 1.215 $\mu A \cdot cm^{-2}$, respectively. The corrosion current densities of these composites in simulated rigorous AFC environments were 18.79, 17.62, and 19.47 $\mu A \cdot cm^{-2}$, respectively. At this point it should be noted that the US-DOE has not defined the corrosion environment for the fuel cell. Therefore, the experiments were done in the normal as well as aggressive or rigorous fuel cell environment with respect to PEMFC and AFC.

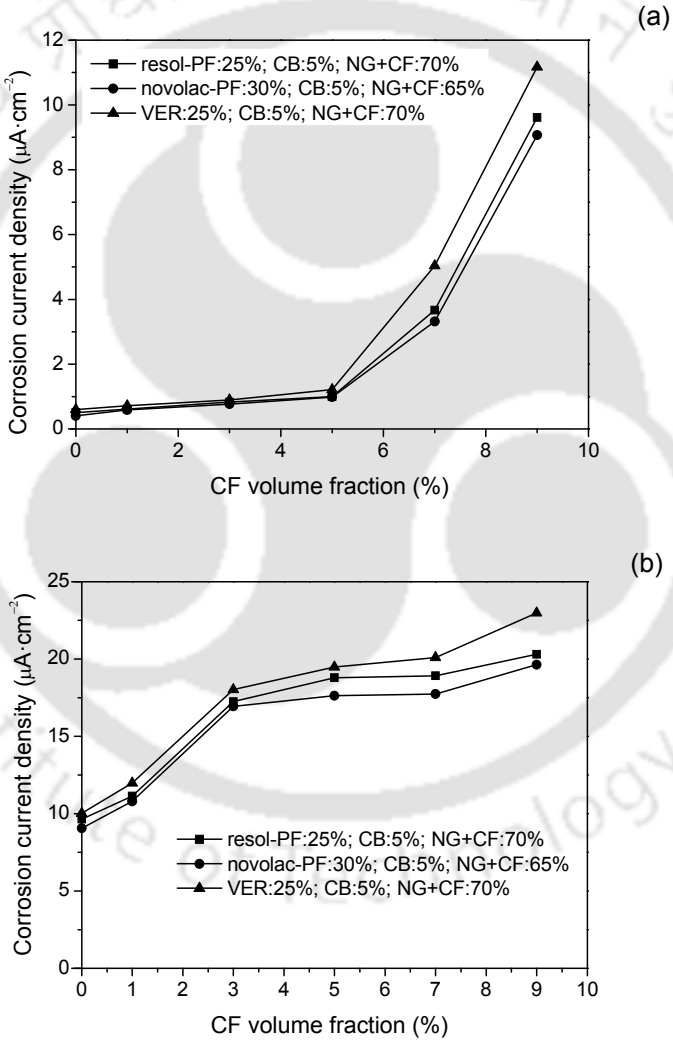

Figure 5.56: Effect of CF content on the corrosion current densities of composite bipolar plates for different resin systems at 80°C in 1M (a) H_2SO_4 and (b) NaOH solution; scan rate 1mV·s^{-1}

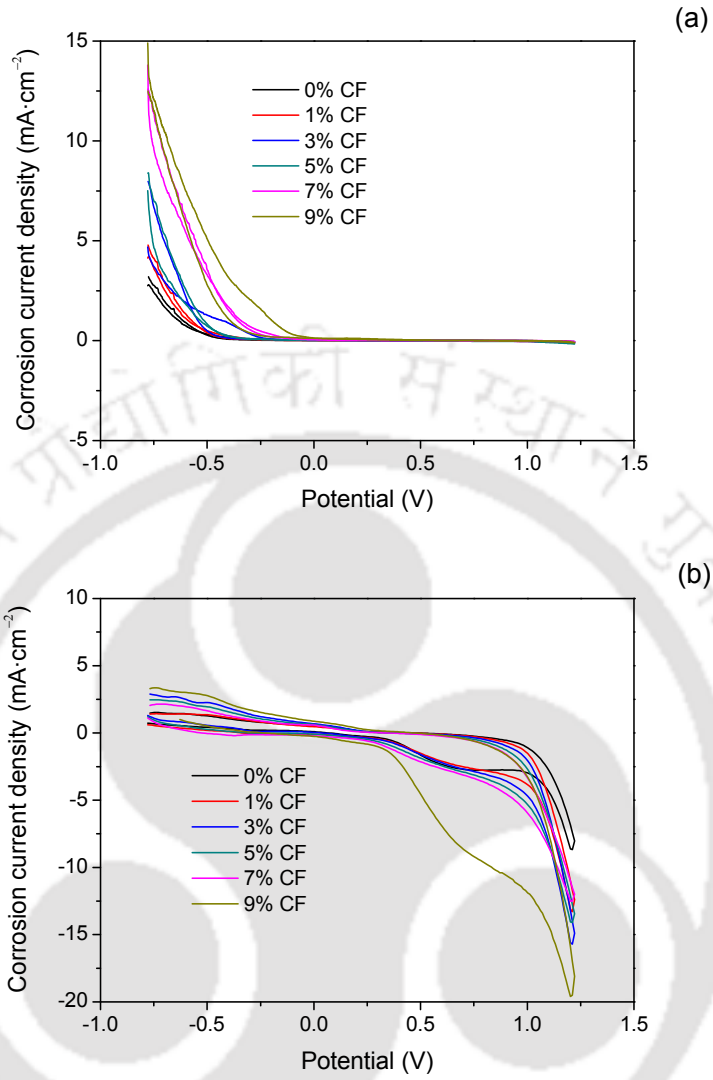

Figure 5.57: Cyclic voltammetry analyses of composite (novolac-PF:30%; CB:5%; NG+CF:65%), with different CF content for (a) 1.0M H_2SO_4 and (b) 1.0M NaOH solution with a scan rate of 1 mV·s^{-1}

5.6.7.2 *Cyclic voltammetry*

The cyclic voltammetry was performed to study the electrochemical stability of the novolac based composite bipolar plates at different CF content (fig. 5.57) at 80°C in acidic and alkaline environments. It can be seen from the cyclic voltammograms that the bipolar plates were quite stable in the acidic environment. Figure 5.57(b) shows the cyclic

voltammetry in alkaline environment and a plateau can be seen in the region from 0.32−1.02 V, which may be due to the passive layer formation during corrosion process. However, the passive layer breaks down after 1.02 V and the corrosion current density increases rapidly. It can also be seen that the voltammetric potential was shifted to more negative potential for NaOH than H_2SO_4 medium. Similar trends of cyclic voltammograms have also been reported for electrochemical electrodes made of glassy carbon and carbon fiber by Kelly et al. (1999), and Shuxuan et al. (2009), respectively. There may be possibility of the resin leaching from the sample on prolonged use of the bipolar plate and may contaminate the polymer electrolyte membrane [Barbir, 2005]. However, no such study was reported in the open literature and it was not observed in the current study [Kakati et al. 2010].

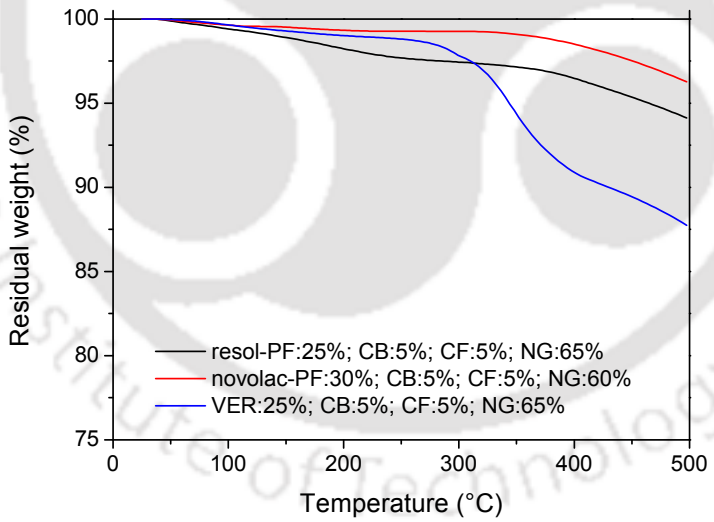

Figure 5.58: Thermal stability of the NG/CB/CF/resin composite bipolar plates at their optimum compositions

5.6.8 *Thermal stability of the NG/CB/CF/resin composite bipolar plates*

The thermal stability of the NG/CB/CF/resin composite bipolar plates was studied, in the temperature range 25–500°C, as per the procedure described in section 3.3.1.2. The

thermal stabilities of the NG/CB/CF/resin composite bipolar plates, at their optimum compositions, are shown in fig. 5.58. The residual weights of the resol-PF, novolac-PF, and VER based composite bipolar plates at 300°C, with 5% CF and CB, were 97.44, 99.27, and 97.85% respectively. Therefore, the developed bipolar plates will be thermally stable in the PEMFC or AFC fuel cell operating temperature.

5.6.9 *Morphological study of the NG/CB/CF/resin composite bipolar plates*

The micrographs of the NG/CB/CF/resin composite bipolar plates are shown in fig. 5.59. Figure 5.59(a) shows the micrograph of the resol-PF based composite bipolar plate. It is seen in the micrograph that the fibers are sandwiched between several NG particles and thus help in improving the mechanical strength of the composite bipolar plates. Similar, pattern was also observed in the case of novolac-PF and VER based composite bipolar plates as shown in fig. 5.59(b) and 5.59(c). Moreover, the CB particles were found to be spread in the interstices between NG-NG, NG-CF, and CF-CF. This effect ensures the contact between the NG and CF thus helps in increasing the mechanical strength as well as conductivity of the composite. The conductivity mechanism in the NG/CB/CF/resin composite bipolar plates has already been described in the section 5.6.5. The micrographs also confirm that the proposed mechanism is valid in the composites.

The effects of CF content on the properties of the NG/CB/CF/resin composite bipolar plates have been discussed on the section 5.6. The optimum CF content for the resol-PF, novolac-PF, and VER based composites were found to be 5% at the expense of NG. The detailed properties of the NG/CB/CF/resin composite bipolar plates at their optimum compositions are summarized in table 5.3 and compared with the target values.

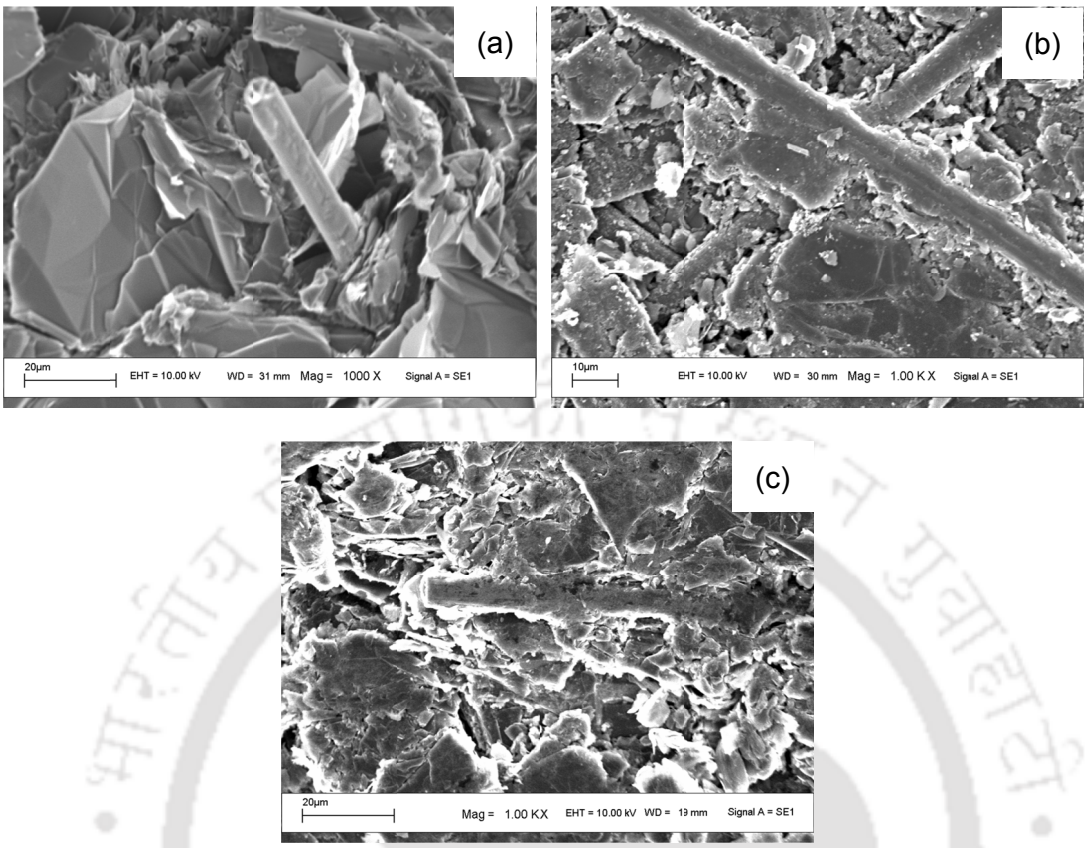

Figure 5.59: SEM images of representative NG/CB/resin composite bipolar plates for (a) resol-PF:25%; CB:5%; CF:5%; NG:65%, (b) novolac-PF:30%; CB:5%; CF:5%; NG:60%, and (c) VER:25%; CB:5%; CF:5%; NG:65%

5.7 Effect of graphene content on the properties of the composite bipolar plate

It can be observed from the table 5.3 that the through-plane electrical conductivities of the composites are edged below 100 $S{\cdot}cm^{-1}$. It may be note that the US-DOE has not mentioned whether the target electrical conductivity is for in-plane or through-plane but considering the same value for both the cases, there is a need to improve the through-plane electrical conductivities of the composite bipolar plates. Moreover, the increased conductivity will always be desired if other properties do not deviate much.

Table 5.3: Properties of NG/CB/CF/resin composite bipolar plates at the optimum compositions for different resin systems

Properties	**Target values**	**resol-PF:25%; CB:5%; CF:5%; NG:65%**		**novolac-PF:30%; CB:5%; CF:5%; NG:60%**		**VER:25%; CB:5%; CF:5%; NG:65%**	
Density ($g \cdot cm^{-3}$)	< 2.0	1.810		1.845		1.825	
H_2 permeability $\times 10^{-10}$ ($cm^3 \cdot cm^{-2} \cdot s^{-1}$)	10^4 (at 80°C and 3 bar)	5.67#	9.51*	6.22#	11.11*	7.42#	15.59*
Electrical conductivity ($S \cdot cm^{-1}$)	100	415.05 (∥)	99.70 (⊥)	285.54 (∥)	91.79 (⊥)	355.05 (∥)	95.95 (⊥)
Thermal conductivity ($W \cdot m^{-1} \cdot K^{-1}$)	10	145.3		128.26		132.4	
Flexural strength (MPa)	50	54.23		55.28		53.50	
Deflection at mid- span (%)	3–5	5.47		5.20		5.37	
Shore hardness	40	50		46		49	
Corrosion current density ($\mu A \cdot cm^{-2}$)	< 1	0.511	0.997†	0.262	0.986†	0.685	1.215†

∥ → in-plane ⊥ → through-plane

\# → H2 permeability at 25°C under 2 bar pressure

* → H_2 permeability at 50°C under 2 bar pressure

† → in rigorous simulated PEMFC environment

resol-PF → resol type phenol formaldehyde

novolac-PF → novolac type phenol formaldehyde

VER → vinyl ester resin

NG → natural graphite

CB → carbon black

CF → carbon fiber

Therefore, graphene was thought to be a good candidate to reinforce into the optimum composition of the bipolar plate at the expense of NG. Thus the graphene was developed thermochemically and characterized thoroughly as described in the sections 5.2.1–5.3.7. The optimum compositions of each resin system were considered as the base composition and 1% of the NG was replaced with the developed graphene. Please note that only a preliminary study was conducted in order to find the effect of graphene on the composite bipolar plate. The graphene reinforced composite bipolar plates were developed and characterized for density, hydrogen permeability, electrical conductivity, thermal conductivity, flexural strength, deflection at mid-span, and corrosion current density. The SEM micrographs of a graphene reinforced composite bipolar plate are shown in fig.5.60. However, it is very difficult to trace the graphene sheets in the micrographs of composite bipolar plates because of the transparent nature of the graphene as shown in fig. 5.14.

Figure 5.60(a) shows representative SEM images of a developed composite bipolar plate (novolac-PF:30%; CB:5%; CF:5%; GN:1%; NG:59%). It is observed that the NG, CB, and CF are well bonded within the composite. However, the graphene is not clearly visible in the micrograph. Therefore, a micrograph in higher magnification is shown in fig. 5.60(b). It is found in the micrograph that the graphene sheets were sandwiched between the NG particles and as a result, the in-plane as well as the through-plane electrical conductivity of the composite was increased. Table 5.4 shows the properties with 1% graphene for different composites. The in-plane electrical conductivities of the NG/CB/CF/resin bipolar plates were 415.05, 285.54, and 355.05 $S \cdot cm^{-1}$ for resol-PF, novolac-PF, and VER based composites, respectively.

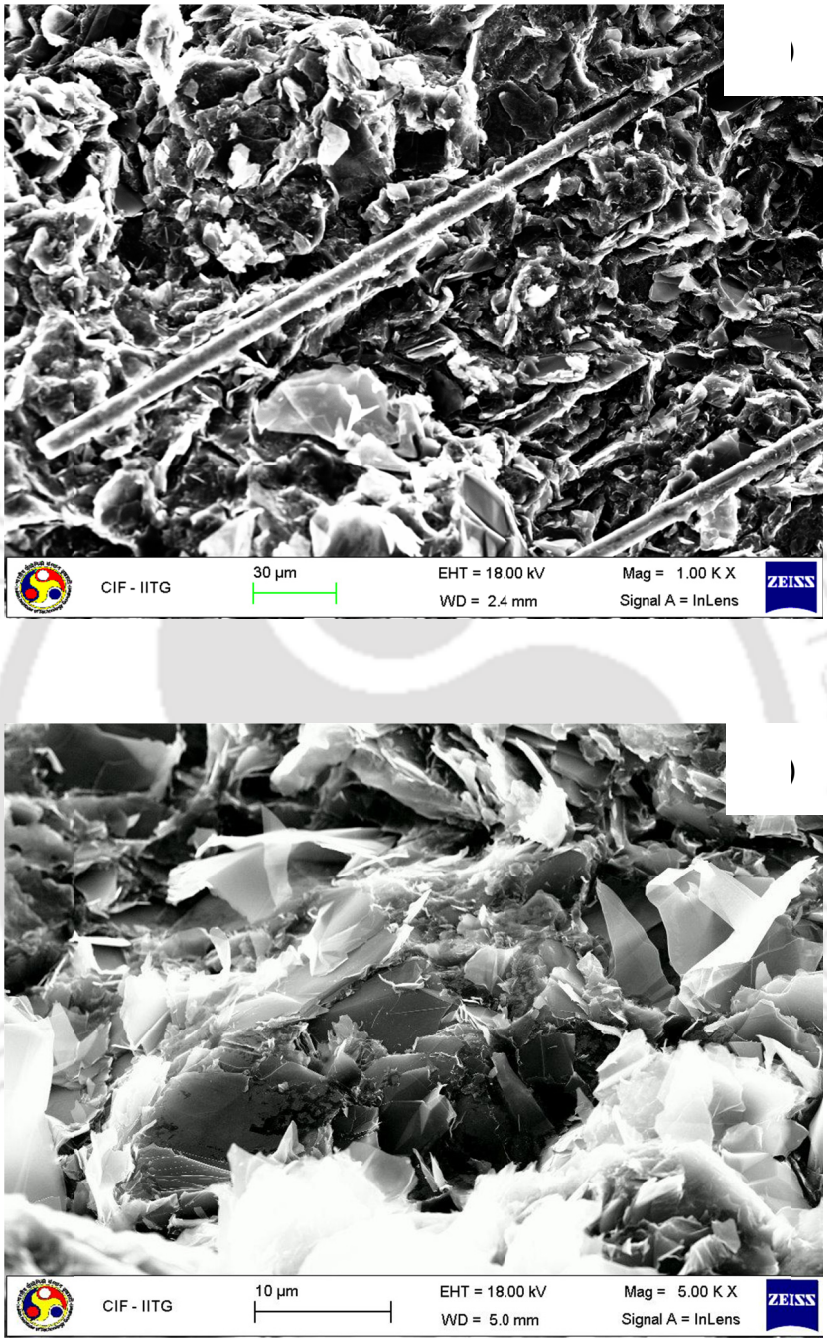

Figure 5.60: FESEM micrograph novolac-PF:30%; CB:5%; CF:5%; GN:1%; NG:59%

Table 5.4: Properties of graphene reinforced carbon-polymer composite bipolar plates for different resin systems

Properties	**Target values**	**resol-PF:25%; CB:5%; CF:5%; GN:1%; NG:64%**		**novolac-PF:30%; CB:5%; CF:5%; GN:1%; NG:59%**		**VER:25%; CB:5%; CF:5%; GN:1%; NG:64%**	
Density ($g \cdot cm^{-3}$)	< 2.0	1.804		1.837		1.819	
H_2 permeability $\times 10^{-10}$ ($cm^3 \cdot cm^{-2} \cdot s^{-1}$)	10^4 (at 80°C and 3bar)	3.45#	7.15*	5.97#	11.11*	3.91#	7.15*
Electrical conductivity ($S \cdot cm^{-1}$)	100	435.31 (∥)	130.17 (⊥)	311.33 (∥)	123.5 (⊥)	376.03 (∥)	129.79 (⊥)
Thermal conductivity ($W \cdot m^{-1} \cdot K^{-1}$)	10	145.9		129.77		134.4	
Flexural strength (MPa)	50	57.28		60.09		59.35	
Deflection at mid- span (%)	3–5	5.85		5.9		6.10	
Shore hardness	40	66		62		67	
Corrosion current density ($\mu A \cdot cm^{-2}$)	< 1	0.526	0.998†	0.265	0.989†	0.687	1.217†

∥ → in-plane ⊥ → through-plane

→ H2 permeability at 25°C under 2 bar pressure

* → H_2 permeability at 50°C under 2 bar pressure

† → in rigorous simulated PEMFC environment

resol-PF → resol type phenol formaldehyde

novolac-PF → novolac type phenol formaldehyde

VER → vinyl ester resin

NG → natural graphite

CB → carbon black

CF → carbon fiber

GN → graphene

There was a marginal improvement in the mechanical strengths and deflections at mid-span of the graphene reinforced composite bipolar plates. Similarly, the graphene has little impact on the hydrogen permeabilities of the composite bipolar plates. It can be seen from the table that the target values for all the properties have been achieved. However, the corrosion current density of the VER based graphene reinforced composite in rigorous simulated PEMFC environment were a few decimal above the target values. It is to be noted that the corrosion environment has not been defined in the US-DOE benchmark. Therefore, a rigorous environment was considered on a safer side. The performance of the bipolar plates in the real PEMFC was carried out as per the procedure described in the section 3.4.3. The performance of the fuel cell is discussed in the subsequent sections.

5.8 Fuel cell performance analysis

A PEMFC setup was developed as discussed in the section 3.4.1 and the developed bipolar plates were used to study the performance of the fuel cell. The MEA for fuel cell testing was developed as per the procedure mentioned in the section 3.4.2. Figure 5.61 shows the micrograph of cross sectional view of the MEA. The catalyst coated microporous layers are clearly visible in the micrograph. The microporous layers were evenly spread over the membrane. It is observed from the micrograph that the components of the microporous layers have punched the membrane. If it were the case then the resistance of the MEA would have dropped down. However, the resistance of the membrane and the MEA were checked individually and found approximately same. It confirmed that there is no short-circuiting of the MEA and thus no punching on the membrane. The apparent image of punctured membrane was visible in the membrane as the microporous layer was rolled, by the knife edge, during sample preparation for SEM analysis.

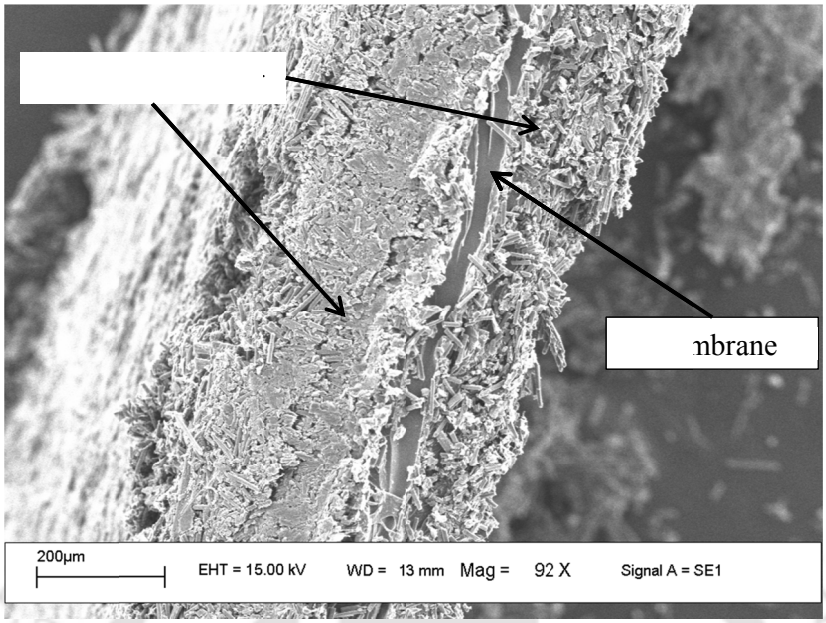

Figure 5.61: SEM image of MEA showing the microporous layer and membrane

The developed MEA was used to study the performance of the PEMFC. It is worthy to mention that a fresh MEA, with same composition, was used to study the performance of the PEMFC for each pair of bipolar plates. It was done in order to avoid the aging effect of the MEA on the performance of the fuel cell.

The performance of the fuel cell was carried out initially at different temperature. Figure 5.62 shows the performance of PEMFC operated at 25, 30, 40, and 50°C using optimum composition of resol-PF/NG composite bipolar plate. Figure 5.62 show that the fuel cell shows better performance at elevated temperature. In the current setup, the best performance was achieved at 50°C operating temperature. It is expected that the fuel cell performance would be increased by increasing the temperature up to at least 80^{o}C. However, due to the limitation in the experimental set up we could not analyze the performance of the fuel cell above 50^{o}C. Therefore, rest of the experiments are reported here were carried out at 50°C.

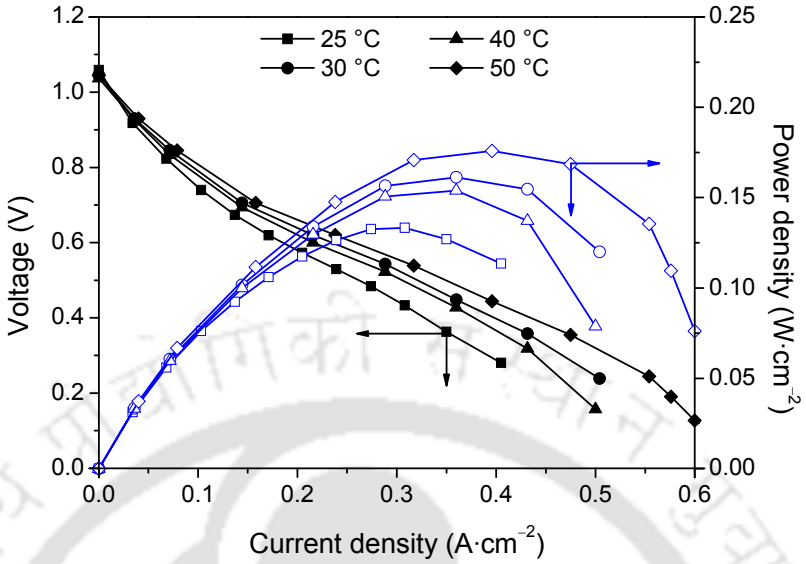

Figure 5.62: Effect of temperature on the *i–V* performance of the fuel cell using (NG:75%; resol-PF:25%) composite bipolar plate

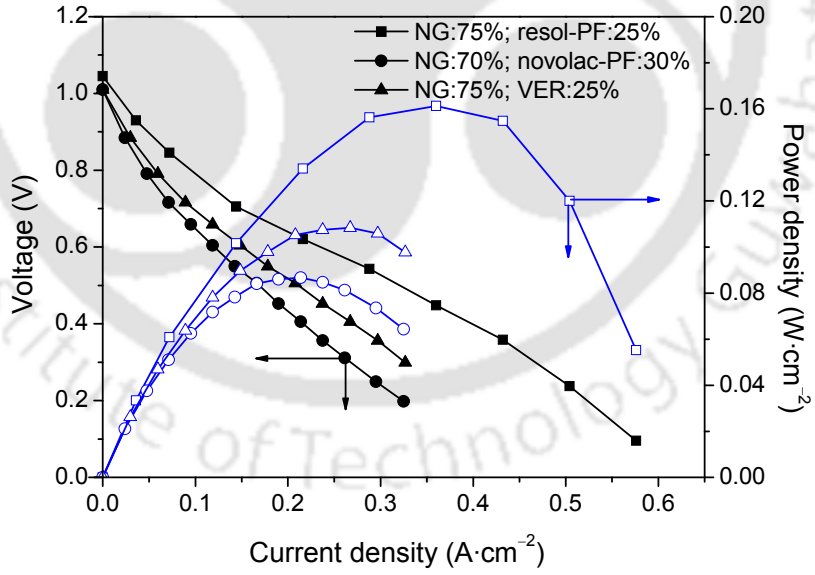

Figure 5.63: Performance of fuel cell with NG/resin composite bipolar plates at their optimum compositions

Figure 5.63 shows the performance of the fuel cell using NG/resin composite bipolar plates, at their optimum compositions with different reinforcements. It can be seen from the figure that the fuel cell with NG:75%; resol-PF:25% composite bipolar plate shows best performance among the three resin systems. This may be attributed due to the higher electrical conductivity and hydrogen permeability of the resol-PF based composite bipolar plate. However, the power out of the unit cell was quite low. The maximum power density of the unit cell was 161.28 $mW \cdot cm^{-2}$ at 448 $mA \cdot cm^{-2}$ or 360 mV.

The unit cell performance evaluation was also carried out using the bipolar plates with the optimum composition of the NG/CB/resin systems. The *i–V* performances of the unit cell using those bipolar plates are shown in fig. 5.64. It was observed that the performance of the unit cell, for NG/CB/resin composite bipolar plates, was better than the performance of the cell using NG/resin composite bipolar plates. The peak power density of the fuel cell, for NG:70%; CB:5%; resol-PF:25% composite bipolar plates, was 386 $mW \cdot cm^{-2}$ with a current density of 707.86 $mA \cdot cm^{-2}$. Therefore, reinforcement with 5%CB, at the expense of NG, improves the peak power density by 2.3 times. This improvement is attributed due to the improvement of overall properties of the composite bipolar plate, upon reinforcement with CB. For 5% CB content, the in-plane electrical conductivity of the resol-PF based composite was increased from 364 to 425 $S \cdot cm^{-1}$. Similarly, the through-plane electrical conductivity of the composite was enhanced by 12.41 $S \cdot cm^{-1}$. Moreover, CB impregnation also decreased the hydrogen permeability of the composite bipolar plate. It was expected that the decrease in the hydrogen permeability reduce the concentration loss. The fuel cell also showed better performance in the ohmic region of the *i–V* characteristics.

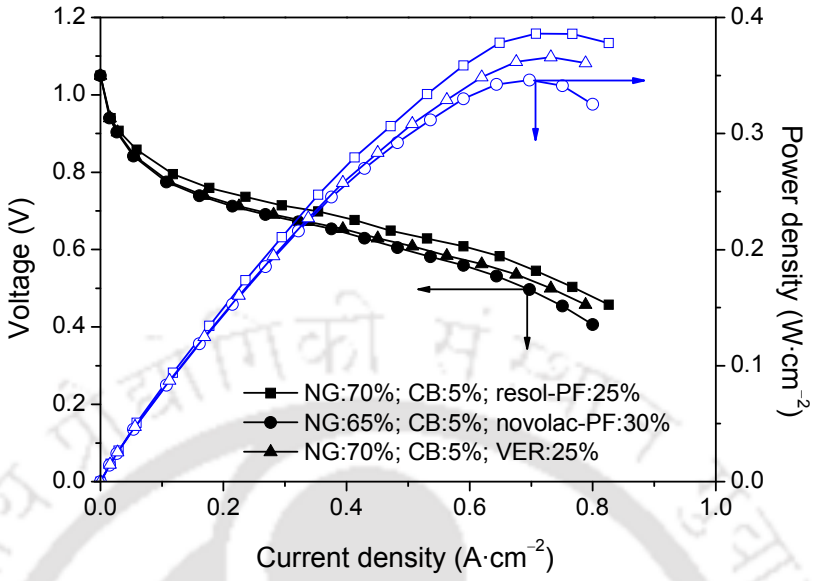

Figure 5.64: Performance of fuel cell with NG/CB/resin composite bipolar plates at their optimum compositions; operating temperature 50°C

The performance of the fuel cell using developed bipolar plates with optimum compositions of the NG/CB/CF/resin composites are shown in fig. 5.65. The figure shows that there was a marginal improvement in the performance of the fuel cell for NG/CB/CF/resin composite bipolar plates, in comparison to the NG/CB/resin composites. The peak maximum power densities of the unit cell, with NG/CB/CF/resin composite bipolar plates, were around 397, 368, and 380 mW·cm^{-1} for resol-PF, novolac-PF, and VER based composites, respectively. The increase in the power density may be attributed due to the improvement in the through-plane electrical conductivity of the composite bipolar plates. The peak power densities of the fuel cell, with the optimum compositions of the composite bipolar plates, are summarized in the table 5.5.

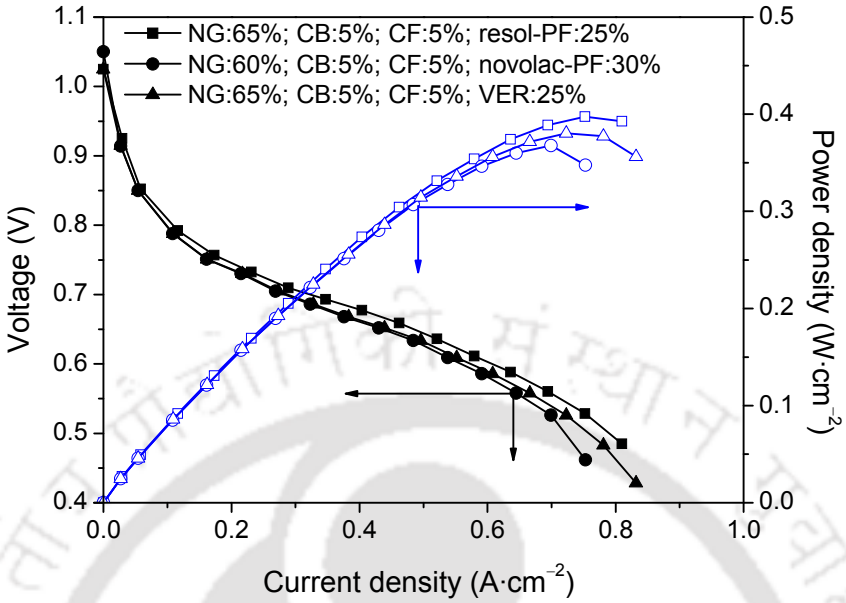

Figure 5.65: Performance of fuel cell with NG/CB/CF/resin composite bipolar plates at their optimum compositions; operating temperature 50°C

The *i–V* performance analysis of the fuel cell was further studied using the graphene reinforced composite bipolar plates. The *i–V* and *i–P* characteristics of the unit cells with graphene reinforced composite bipolar plates are shown in fig.5.66. The figure shows that the peak power density of the fuel cell was maximum with the graphene reinforced resol-PF resin composite (NG:64%; CB:5%; CF:5%; GN:1%; resol-PF:25%) bipolar plates. As seen in the table 5.5, there were around 10% improvements in the power densities of the fuel cell with the developed graphene reinforced composite bipolar plates. The *i–V* and *i–P* characteristics enhanced marginally due to the improvement in the in-plane as well through-plane electrical conductivities of the graphene composites. Moreover, there was a marginal improvement in the hydrogen permeabilities of the graphene reinforced composite bipolar plates over the NG/CB/CF/resin composites. The reduced hydrogen permeabilities bipolar plates may have positive effect on the performance of the fuel cell.

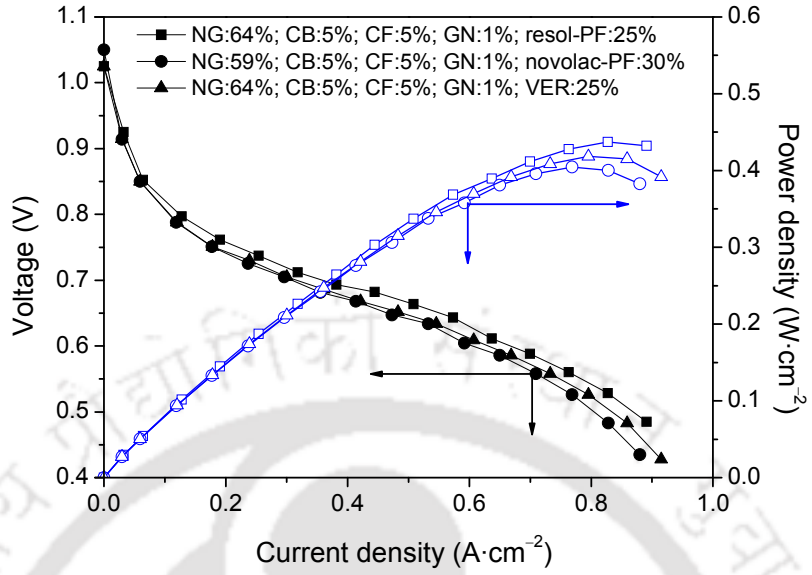

Figure 5.66: Performance of a single PEMFC with graphene (GN) reinforced NG/CB/CF/resin composite bipolar plates at their optimum compositions; operating temperature 50°C

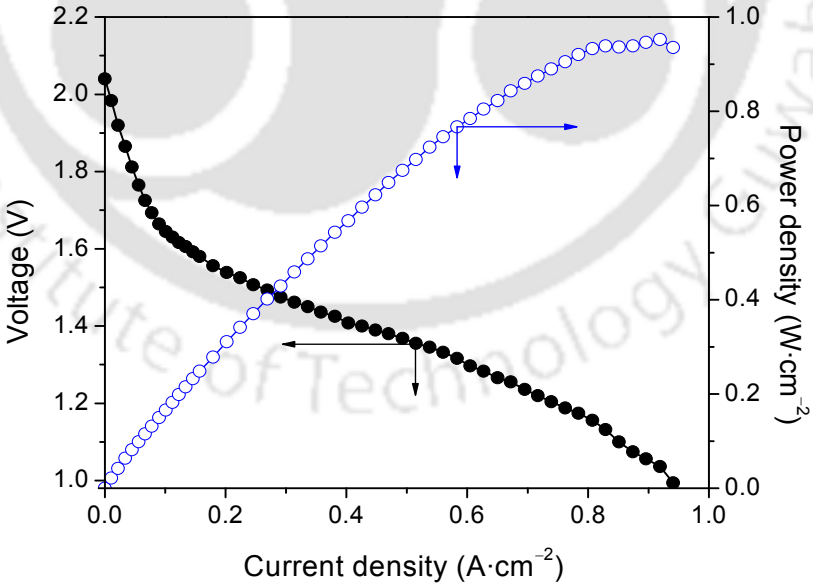

Figure 5.67: Performance of fuel cell stack (2 cells) with developed bipolar plates (NG:64%; CB:5%; CF:5%; GN:1%; resol-PF:25%); operating temperature 50°C

The bipolar plates were also developed, with flow channels on both the sides, to study its performance in fuel cell stack. A fuel cell stack with two cells were designed and developed to study the $i-V$ performance. The $i-V$ performance of the fuel cell stack with representative bipolar plates is shown in fig. 5.67. The bipolar plates showed slightly better performance in fuel cell stack than in the case of single cell application. Therefore, the developed bipolar plates are also suitable for stack development.

Table 5.5: Peak performance of PEMFC using optimum compositions of the developed bipolar plates

Bipolar plate's composition	**Current density ($mA \cdot cm^{-2}$)**	**Voltage (V)**	**Peak power density ($mW \cdot cm^{-2}$)**
resol-PF:25%; NG:75%	360	0.448	161
resol-PF:25%; CB:5%; NG:70%	708	0.546	386
resol-PF:25%; CB:5%; CF:5%; NG:65%	752	0.529	397
resol-PF:25%; CB:5%; CF:5%; GN:1%; NG:64%	827	0.529	437
novolac-PF:30%; NG:70%	214	0.406	087
novolac-PF:30%; CB:5%; NG:65%	644	0.532	342
novolac-PF:30%; CB:5%; CF:5%; NG:60%	699	0.526	368
novolac-PF:30%; CB:5%; CF:5%; GN:1%; NG:59%	769	0.526	404
VER:25%; NG:75%	268	0.406	108
VER:25%; CB:5%; NG:70%	732	0.499	366
VER:25%; CB:5%; CF:5%; NG:65%	723	0.526	380
VER:25%; CB:5%; CF:5%; GN:1%; NG:64%	795	0.526	418

Chapter 6

Results of Electrical Conductivity Modeling

Results of Electrical Conductivity Modeling

The electrical conductivity of resol-PF/NG composite bipolar plate was predicted using modified Ondracek model (eq.4.5) [Kakati et al., 2009]. It was found that the Ondracek model was not suitable to predict the electrical conductivity of the composite bipolar plate for multiple filler systems. Moreover, the model could predict the electrical conductivity of a particular section of the composite, where the micrographs were taken. Digital image processing of a large number of micrographs could result in better prediction of the actual electrical conductivity. Therefore, modified GEM equation was applied to predict the electrical conductivity of the composite bipolar plate with various compositions.

6.1 Electrical conductivity of two-component systems

The electrical conductivities of the composite bipolar plates for different compositions were modeled using modified GEM equation (eq. 4.8).

The electrical conductivity of the resin/NG composite bipolar plates can be defined with the help of the following equation [Kakati et al., 2011].

$$\frac{\phi_P\left(\sigma_P^{1/t}-\sigma_m^{1/t}\right)}{\sigma_P^{1/t}+A\sigma_m^{1/t}}+\frac{\phi_{NG}\left(\sigma_{NG}^{1/t}-\sigma_m^{1/t}\right)}{\sigma_{NG}^{1/t}+A\sigma_m^{1/t}}=0 \qquad 6.1$$

where, the subscripts P and NG represent for resin and NG, respectively. The electrical conductivities of the graphite particle are 1.02×10^5 and 2.22×10^4 $S\cdot cm^{-1}$ for in-plane and through-plane, respectively [Powell and Childs, 1972]. As the composite is anisotropic, there is a need to define t individually for the in-plane and through-plane electrical conductivities of the composite. The predicted data (ϕ_{NG},σ_m) were correlated with the experimental ones in order to find the correct value of the exponent t. The constants in eq.4.7, were calculated by the iterative process and shown in the table A1 in Annexure.

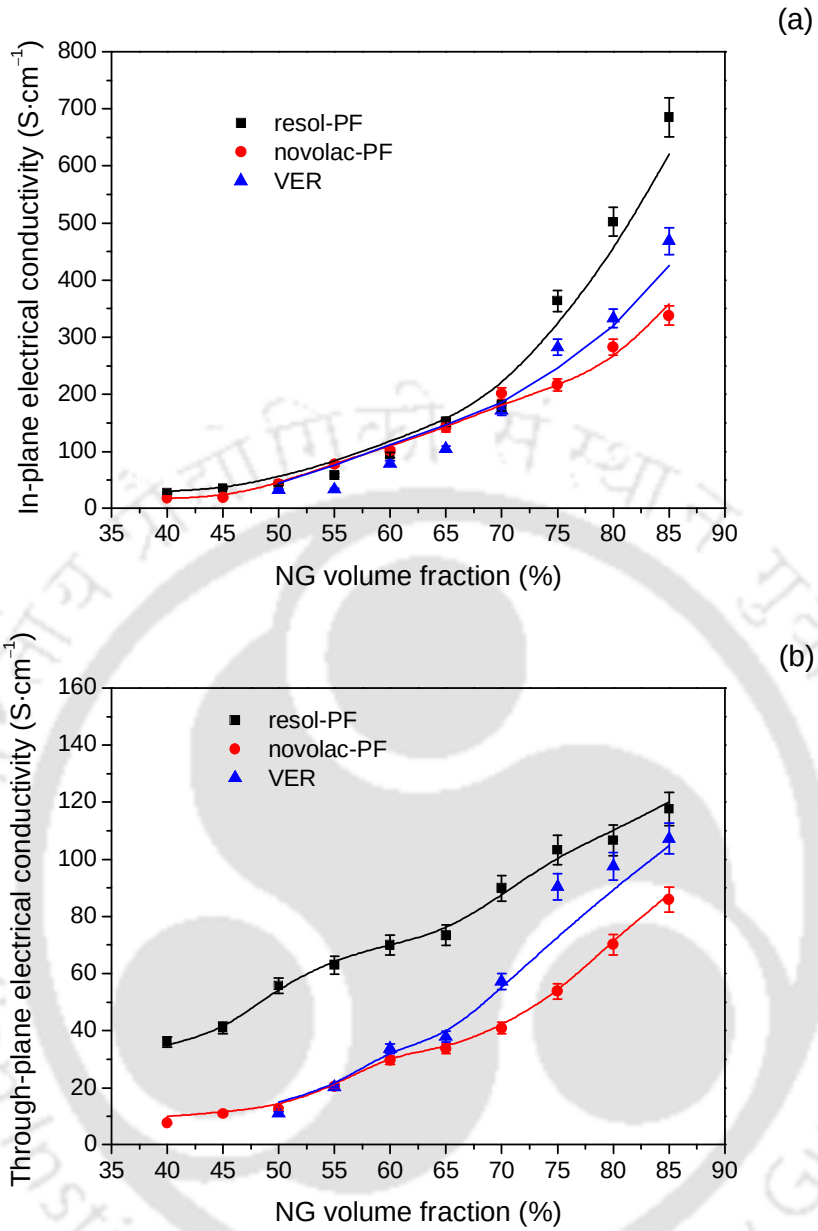

Figure 6.1: The (a) in-plane and (b) through-plane electrical conductivities of resin/NG composite bipolar plates and its predicted values (symbol: experimental values, line: predicted values)

Figure 6.1 shows the electrical conductivity of the composite bipolar plate for different volume fraction of NG. The increase in NG content increases the electrical conductivity of the composite. The composite becomes conductive due to the tunnelling of electrons from one NG particle to the adjacent NG particle through a resistance barrier caused by

the insulating resin matrix. The probability of an electron migrating from one NG particle to another NG through the insulating resin matrix is inversely proportional to the thickness of the insulating resin layer. The insulating barrier between two adjacent NG particles goes on decreasing with the increase in NG content.

From the fig. 6.1(a), it can be seen that the in-plane electrical conductivity of the composite is higher than the through-plane electrical conductivity. The anisotropic electrical conductivity of the NG particles itself is the main reason behind it. The graphite particles are fairly isolated from each other and randomly distributed within the resin matrix in low graphite content. Therefore, the electrical conductivity of the composite was more isotropic in low graphite content. However, the graphite flakes tend to align parallel to the pressure direction as one goes on increasing the graphite content. It can be observed that the in-plane electrical conductivities of the bipolar plate, with more than 60% NG content, fulfils the target (>100 $S.cm^{-1}$) for composite bipolar plate (table 1.2). But the through-plane electrical conductivity of the bipolar plates still requires improvement. Therefore, CB was used, at the expense of NG, to enhance the in-plane as well as through-plane electrical conductivities of the composite. It can be seen in fig. 6.1(b), that the through-plane electrical conductivities of the resin/NG composite bipolar plates were also well predicted by the eq.6.1.

6.2 Electrical conductivity of three-component system

The electrical conductivity of the composite with NG, PF and CB can be predicted with the adapted GEM equation as shown in eq.4.8. The generalized equation reduces to the following form for three-component system [Kakati et al., 2011].

$$\frac{\phi_P\left(\sigma_P^{1/t}-\sigma_m^{1/t}\right)}{\sigma_P^{1/t}+A\sigma_m^{1/t}}+\frac{\phi_{NG}\left(\sigma_{NG}^{1/t}-\sigma_m^{1/t}\right)}{\sigma_{NG}^{1/t}+A\sigma_m^{1/t}}+\frac{\phi_{CB}\left(\sigma_{CB}^{1/t}-\sigma_m^{1/t}\right)}{\sigma_{CB}^{1/t}+A\sigma_m^{1/t}}=0 \qquad 6.2$$

where, the subscript CB represents the carbon black.

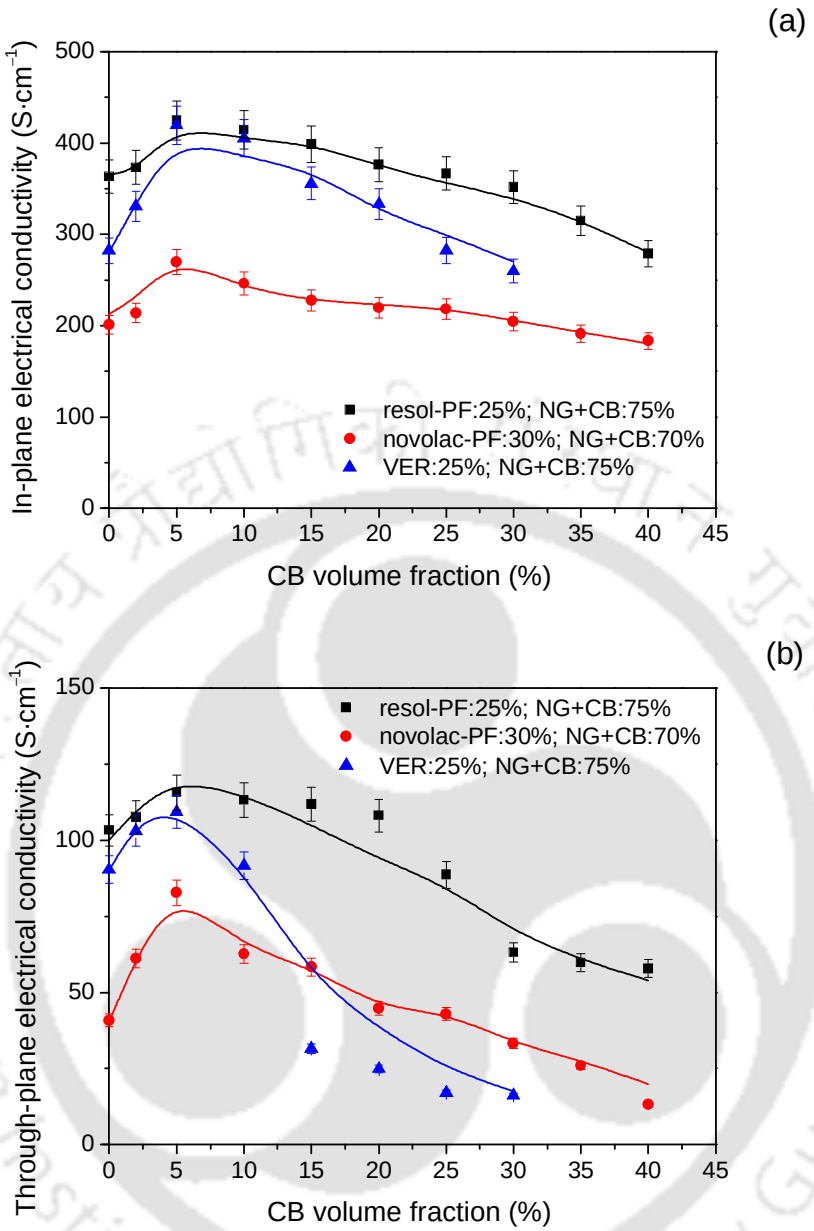

Figure 6.2: The (a) in-plane and (b) through-plane electrical conductivities of resin/NG/CB composite bipolar plates and its predicted values (symbol: experimental values, line: predicted values)

Figure 6.2 shows that the experimental values are well predicted for the electrical conductivities of the composite bipolar plate with PF:30%; (NG+CB):70%. The empirical values of the constants are given in the table A1 in Annexure. The inclusion of CB, at the expense of NG, improves both the in-plane and through-plane electrical conductivity of

the composite bipolar plate. However, the effect of reinforcement with CB was more effective for through-plane electrical conductivity of the composite. This particular effect can be explained with the help of synergistic effect of NG–CB in phenolic resin matrix [Clingerman et al., 2002]. It can also be described with the help of simple resistive network where different individual resistances are summing up and execute the final resistance of the composite. Thus, the resultant resistance of the composite should increase with the inclusion of CB at the expense of NG. However, in the present case the tiny CB particles are accommodated in the space between two proximal NG particles. Therefore, carbon black works like an electrical bridge and reduces the total resistance of the composite. Therefore, where resin and the filler (CB) are in between the two conducting NG flakes, it can also be considered that the resistance offered by the PF and the CB are in parallel connection and hence the total resistance of the composite will be reduced.

6.3 Electrical conductivity of four-component system

The composite was further reinforced to enhance the electrical as well as mechanical properties of the composite. It was already mentioned that the CF showed highly anisotropic behaviour under the influence of electric field. It has higher electrical conductivity along the length of the fibre in comparison to the radial direction. Therefore, the orientation of fibres changes the electrical conductivity of the composite. Figure 6.3 shows that the electrical conductivity of the composite improves slightly in the low CF loading and it reaches maximum for 5% CF content. But in higher CF loading, from 5 to 9%, the electrical conductivity of the composite was decreased due to the agglomeration of the fibres. The electrical conductivity mechanism in the NG/CB/CF/resin systems may also be understood with the help of the tunnelling effect and resistive network as explained earlier.

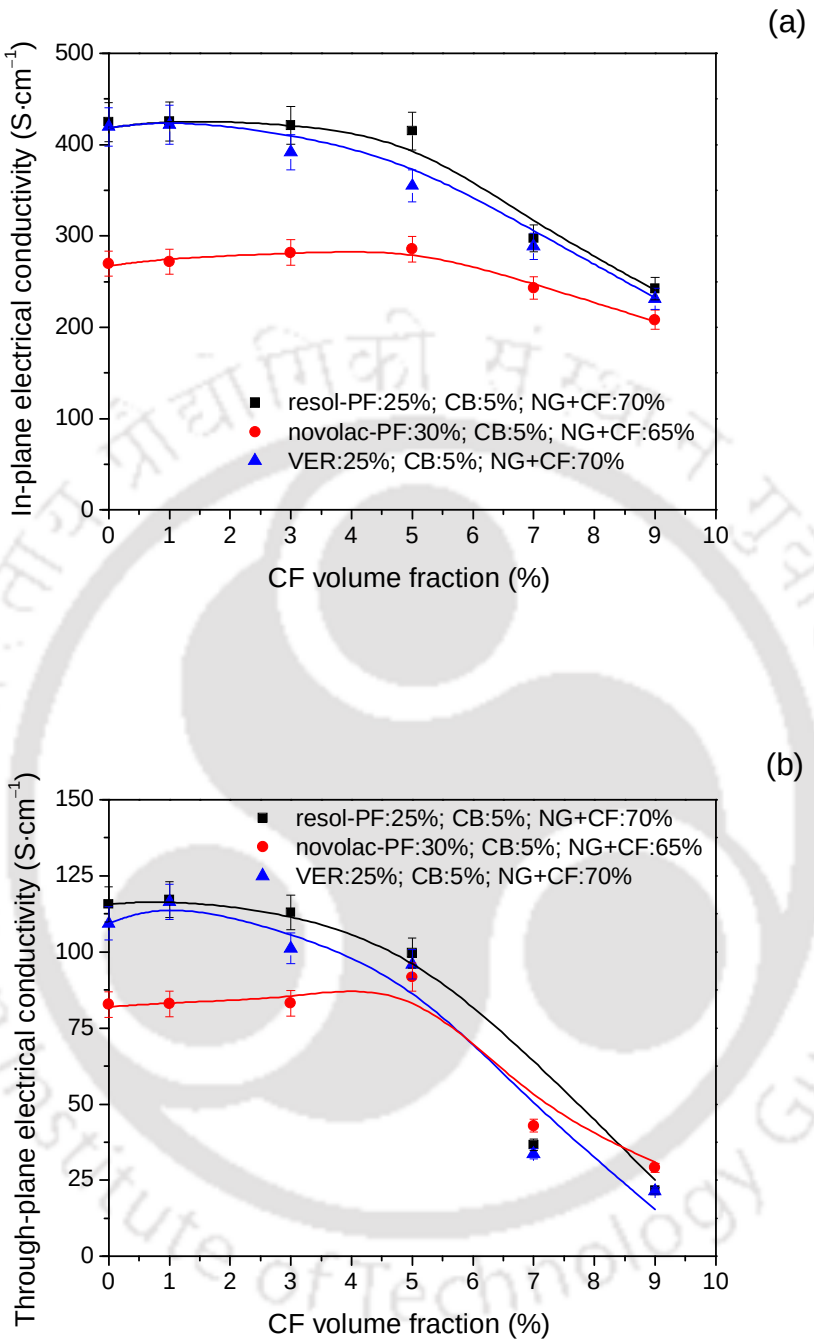

Figure 6.3: The (a) in-plane and (b) through-plane electrical conductivities of resin/NG/CB/CF composite bipolar plates and its predicted values (symbol: experimental values, line: predicted values)

The GEM equation for the electrical conductivity of the composite bipolar plate with NG, CF, CB and PF is given by the following equation [Kakati et al., 2011].

$$\frac{\phi_P\left(\sigma_P^{1/t}-\sigma_m^{1/t}\right)}{\sigma_P^{1/t}+A\sigma_m^{1/t}}+\frac{\phi_{NG}\left(\sigma_{NG}^{1/t}-\sigma_m^{1/t}\right)}{\sigma_{NG}^{1/t}+A\sigma_m^{1/t}}+\frac{\phi_{CB}\left(\sigma_{CB}^{1/t}-\sigma_m^{1/t}\right)}{\sigma_{CB}^{1/t}+A\sigma_m^{1/t}}+\frac{\phi_{CF}\left(\sigma_{CF}^{1/t}-\sigma_m^{1/t}\right)}{\sigma_{CF}^{1/t}+A\sigma_m^{1/t}}=0 \qquad 6.3$$

where, subscript CF represents carbon fibre. The empirical values of the constants were found and listed in Annexure. It can be seen in fig.6.3 that the predicted electrical conductivity is in well agreement with the experimental values.

The adapted GEM equation could well predict the electrical conductivities of the composites for multiple component systems. However, the modelling for electrical conductivity of graphene reinforced composite was not carried out due to the lack of sufficient experimental data.

Chapter 7

Conclusions and Future Scope

Conclusions and Future Scope

7.1 Conclusions

The carbon-polymer composite bipolar plates for PEMFC were developed by compression molding technique. The composite bipolar plates were developed using three different resin matrix, viz. resol-PF, novolac-PF, and VER. The reinforcements used in the development of the composite bipolar plates, for each resin systems, were NG, CB, CF, and graphene. The TGA and DSC analyses of the resins were carried out to find the curing temperature of each resin. It was found that the curing of the PF and VER were complete within 220 and 180°C, respectively. Therefore, the molding temperatures of the composite for PF and VER based composites were considered as 220 and 180°C, respectively. Moreover, the optimum molding temperatures were confirmed by developing and characterizing the resin/NG composite bipolar plates. Therefore, the composite bipolar plates were later developed at these optimum molding temperatures only.

The reinforcements (NG, CB, and CF) were thoroughly characterized by SEM, XRD, TGA, and particle size analyzer. The XRD analysis showed that the unit cells of NG particles exhibitshexagonal crystals with a C-axis length of 6.712Å. The detailed analysis of the XRD pattern showed that the lengths of the other two axes were approximately 2.456Å. However, the CB and CF were found to exhibit amorphous nature in XRD analysis. The particle size analysis of the NG showed that around 60 vol.% of the NG particles were having diameter 30–80µm. Similarly, it was found from the analysis that 56.13 vol.% of the CB particles were having diameter below 100nm. The particle size was also confirmed from the SEM analysis. The SEM analysis also showed that the diameter of the CFs was within the range of 6–7µm.

The graphene, being one of the highest electrically conductive materials, has been synthesized using thermochemical exfoliation of NG and was incorporated into the composite bipolar plate. The SEM, EDX, XRD, and AFM analyses showed that monolayer graphene was produced by thermochemical exfoliation. The absence of graphite 002 peak in the diffractogram confirmed that the developed graphene was monolayer in nature. Moreover, the measured thickness of the developed graphene was around 1 Å, which confirmed that monolayer graphene was developed. The TGA analysis showed that the thermal stability of the graphene was more or less similar to the NG.

After thorough characterization of the resins and reinforcements, the resin/NG composite bipolar plates were developed to find out the optimum resin content. The developed bipolar plates were thoroughly characterized and the optimum resin contents for resol-PF, novolac-PF and VER resins were 25, 30, and 25%, respectively. The thermal conductivity, density, hydrogen permeability, and corrosion current density of the optimum resin/NG composite bipolar plates were within the required target properties of the composite bipolar plates for PEMFC applications. However, the through-plane electrical conductivities, flexural strength, and deflection at mid-span of the composites were lagging behind the target values. Similarly, shore hardness of the resol-PF and novolac-PF based composite were also below the target properties at the optimum resin content. Therefore, a nominal volume fraction of the NG was replaced with CB to improve the overall properties of the composite bipolar plates. It was found that the density as well as the hydrogen permeability of the composite was decreased at the optimum CB content. However, CB loading above 5% increased the hydrogen permeability and corrosion current density of the composite bipolar plates. Similarly, the electrical conductivities, thermal conductivity, and mechanical strength of the composite

also showed negative effects for CB content above 5%. Therefore, 5% was considered as the optimum CB content for further studies. The density, in-plane electrical conductivity, thermal conductivity, hydrogen permeability, and flexural strength of the resin/NG/CB composite bipolar plates at their optimum compositions were within the target values. The corrosion current densities of these composite bipolar plates, in rigorous simulated PEMFC environment, were within the target value. However, the deflections at mid-span of the NG/CB/resin composite bipolar plates, at 5% CB content, were below the required values. Moreover, the through-plane electrical conductivity of the novolac-PF based composite was also lagging behind the target electrical conductivity of the composite bipolar plate. Therefore, CF was used at the expense of NG, to improve the mechanical properties of the composite bipolar plates. It was found that the flexural strength and deflections at mid-span of the composites increased with increase in CF content. However, the electrical conductivity of the composite decreased rapidly after 5% CF content. Similarly, the hydrogen permeability and corrosion current density of the composite bipolar plates also increased rapidly above 5% CF content. Therefore, the optimum compositions for the three resin systems were considered as resol-PF:25%, CB:5%, CF:5%, NG:65%; novolac-PF:30%, CB:5%, CF:5%, NG:60%; and VER:25%, CB:5%, CF:5%, NG:65%. The detailed properties of these composites were given in table 5.3. It was found that the target values for all the properties were achieved by the above composites. However, the through-plane electrical conductivity of the composite bipolar plates edge behind the target electrical conductivity. Moreover, the VER based composite bipolar plates, at 5% CF content, showed slightly higher corrosion current density in rigorous simulated PEMFC environment.

The optimum compositions of the resin/NG/CB/CF composite were further reinforced with 1% graphene, at the expense of NG, to improve the through-plane electrical conductivity of the bipolar plates. The properties of the resin/NG/CB/CF/graphene composite bipolar plates are shown in table 5.4. It was found that the in-plane as well as the through-plane electrical conductivities of the composite bipolar plates were increased substantially. The electrical conductivity of the multiple component systems could be explained by the simple resistive network as explained in the fig.5.53. There was a marginal improvement in the mechanical strengths and deflections at mid-span of the graphene reinforced composite bipolar plates. Similarly, the graphene had little impact on the hydrogen permeabilities of the composite bipolar plates. It can be seen that the target values for all the properties have been achieved. The contact resistance of the optimum compositions of the composite bipolar plate was measured as per the method described by Avasarala and Halder(2009). The highest contact resistance of the bipolar plates was recorded as 3.75 $m\Omega \cdot cm^{-2}$, at 3MPa pressure, for novolac-PF:30%; NG:70% composite. However, it was below the earlier reported values of contact resistance for composite bipolar plates [Kuo and Chen, 2006; Li et al., 2008, Avasarala and Halder, 2009]. The corrosion current density of the VER based graphene reinforced composite in rigorous simulated PEMFC environment were a few decimal above the target values. It is to be noted that the corrosion environment has not been defined in the US-DOE benchmark. Therefore, a rigorous environment was considered.

The electrical conductivities of the composite bipolar plate were predicted with the help of the GEM equation. It was found that the electrical conductivities of the composite bipolar plates were well predicted by the adapted GEM equation.

A PEMFC system was developed to study the performance of the developed bipolar plates in real fuel cell. The performance of the fuel cell was increased with the increase in operating temperature. The peak performance of the PEMFC with the optimum compositions of the developed bipolar plates for different resin systems are listed in table 5.5. It was found that the power density of the fuel cell was increased gradually with successive reinforcements of CB, CF, and graphene to the resin/NG composite. The peak power density of the fuel cell, with resol-PF:25%, CB:5%, CF:5%, NG:65% composite bipolar plate was 437mW·cm^{-2}, at current density 827mA·cm^{-2}. Similarly, the peak power density of the fuel cell, with the final optimum compositions of novolac-PF and VER based composite bipolar plates, were 404 and 418mW·cm^{-2}, respectively. The current density of the fuel cell at these peak power densities were 769 and 795 mA·cm^{-2}, respectively.

It was found that the developed bipolar plate achieved all the target properties and listed in the table 5.4. Thus the study fulfills the objective of the research work. However, in order to further make the bipolar plate more effective, some future scope for the research is shown in the section 7.2.

7.2 Future scope

- The through-plane electrical conductivity of the resin/NG/CB/CF composite bipolar plates was dramatically improved by the use of graphene, at the expense of NG. Therefore, graphene has tremendous potential in the development of highly conductive composite bipolar plate. A study on the properties of composite bipolar plate with varying graphene concentration may be useful to find the optimum composition.

- The bipolar plates were developed by compression molding technique in the current studies. However, the composite bipolar plates can also be developed by injection molding technique for commercial production.
- The performance of the developed bipolar plates was tested in a unit cell of PEMFC and thus there is a need to study the bipolar plates in a fuel cell stack.
- In the present study, the developed bipolar plates were having parallel flow channels. The performance of the fuel cell may be analyzed using bipolar plates with different flow patterns.

References

References

1. Abens, S., Proton exchange membrane fuel cell development with lightweight component materials, Technical Report, DAAH01-94-C-R184, 1995, Energy Research Corporation, Danbury, Connecticut.
2. Adrianowycz, O.L., Marcinkoski, J., Tyler, R., Benjamin, T.G., Next generation bipolar plates for automotive PEM fuel cells. Annual progress report, DOE Hydrogen Program, US Department of Energy, Washington, DC; 2009. 1108–1112.
3. Alford, T.L., Feldman, L.C. Mayer, J.W., Fundamentals of Nanoscale Film Analysis, Noyes Publications, Springer, New York, USA, 2007.
4. Andujar, J.M., Segura, F., Fuel cells: History and updating. A walk along two centuries, Renewable and Sustainable Energy Reviews, 13 (9), 2009, 2309–2322.
5. Antunes, R.A., Oliveira, M.C.L., Ett, G., Ett, V., Corrosion of metal bipolar plates for PEM fuel cells: A review, International Journal of Hydrogen Energy, 35 (8), 2010, 3632–3647.
6. Appleby, A.J., Fuel cell technology and innovation, Journal of Power Sources, 37 (1-2), 1992, 223–239.
7. Appleby, A.J., Fuel cell technology: Status and future prospects, Energy, 21 (7-8), 1996, 521–653.
8. Appleby, A.J., Fuel cells and hydrogen fuel, International Journal of Hydrogen Energy, 19 (2), 1994, 175–180.
9. Avasarala, B., Haldar, P., Effect of surface roughness of composite bipolar plates on the contact resistance of proton exchange membrane fuel cell, Journal of Power Sources, 188, 2009, 225–229.
10. Avinash, M.B., Subrahmanyam, K.S., Sundarayya, Y., Govindaraju, T., Covalent modification and exfoliation of graphene oxide using ferrocene, Nanoscale 2, 2010, 1762–1766.
11. Bacon, F.T., Fuel cells, past, present and future, Electrochimica Acta, 14 (7), 1969, 569–585.
12. Bacon, F.T., The development and practical application of fuel cells, International Journal of Hydrogen Energy, 10 (7–8), 1985, 423–430.
13. Balberg, I., A comprehensive picture of the electrical phenomena in carbon black–polymer composites, Carbon, 40 (2), 2002, 139–143.

14. Barak, M., Fuel cells-present position and outstanding problems, Advanced Energy Conversion, 6 (1), 1966, 29–32.
15. Barbir, F., PEM Fuel Cells: Theory and Practice, Burlington, MA: Elsevier Academic Press; 2005.
16. Barton, R.L., Keith J.M., King J.A., Electrical conductivity model evaluation of carbon fiber filled liquid crystal polymer composites, Journal of Applied Polymer Science, 106, 2007, 2456–2462.
17. Barton, R.L., Keith, J.M., King, J.A., Development and modeling of electrically conductive carbon filled liquid crystal polymer composites for fuel cell bipolar plate applications, Journal of New Materials for Electrochemical Systems, 10, 2007, 225–229.
18. Barton, R.L., Keith, J.M., King, J.A., Electrical conductivity modeling of carbon filled polypropylene based resins for fuel cell bipolar plate applications, Journal of New Materials for Electrochemical Systems, 11, 2008, 181–186.
19. Baur, E., Preis, H., Fuel-cells with rigid conductors, Zeitschrift fuer Elektrochemie und Angewandte Physikalische Chemie, 43, 1937, 727–732.
20. Baur, E., Preis, H., Fuel-cells with rigid conductors, Zeitschrift fuer Elektrochemie und Angewandte Physikalische Chemie, 44, 1938, 695–698.
21. Berger, C., Song, Z., Li, T., Li, X., Ogbazghi, A.Y., Feng, R., Dai, Z., Marchenkov, A.N., Conrad, E.H., First, P.N., de Heer, W.A., Ultrathin Epitaxial Graphite: 2D Electron Gas Properties and a Route toward Graphene-based Nanoelectronics, The Journal of Physical Chemistry B, 108 (52), 2004, 19912–19916.
22. Bhattacharya, S., Tandon, R., Sachdev, V., Electrical conduction of graphite filled high density polyethylene composites; experiment and theory, Journal of Materials Science, 44 (9), 2009, 2430–2433.
23. Bhlapibul, S., Pruksathorn, K., Preparation of graphite composite bipolar plate for PEMFC, Korean Journal of Chemical Engineering, 25 (5), 2008, 1226–1231.
24. (a) Blunk, R., Elhamid, M.H.A., Lisi, D., Mikhail, Y., Polymeric composite bipolar plates for vehicle applications, Journal of Power Sources, 156(2), 2006, 151–157.
(b) Blunk, R., Zhong, F., Owens, J., Automotive composite fuel cell bipolar plates: Hydrogen permeation concerns, Journal of Power Sources, 159 (1), 2006, 533–542.
25. Boehm, H.P., Setton, R., Stumpp, E., Nomenclature and terminology of graphite intercalation compounds, Pure and Applied Chemistry, 66 (9), 1994, 1893–1901.

26. Brodie, B.C., On the atomic weight of graphite, Philosophical Transactions of the Royal Society of London, 149, 1859, 249–259.
27. Bundy, F.P., Bassett, W.A., Weather, M.S., Hemley, R.J., Mao, H.K., Goncharov, A.F., The pressure-temperature phase and transformation diagram for carbon; updated through 1994, Carbon, 34 (2), 1996, 141–153.
28. Busick, D.N., Wilkinson, M.S., Low-cost composite materials for polymer electrolyte fuel cells bipolar plates, Technical Report, LA-UR-98-4129, 1998, Los Alamos National Lab., New Mexico, USA.
29. Carmo, M., Linardi, M., Poco, J.G.R., H_2O_2 treated carbon black as electrocatalyst support for polymer electrolyte membrane fuel cell applications, International Journal of Hydrogen Energy, 33, 2008, 6289–6297.
30. Carmona, F., Ravier, J., Electrical properties and mesostructure of carbon black-filled polymers, Carbon, 40, 2002, 151–156.
31. Casit, F.A., Talbot, R.C., Polyester and vinyl ester resins, In: Peters, S.T., Editor, Handbook of Composites, Chapman & Hall, 2nd Edition, 1998, 34–47.
32. Chalk, S.G., Miller, J.F., Wagner, F.W., Challenges for fuel cells in transport applications, Journal of Power Sources, 86 (1–2), 2000, 40–51.
33. Chanda, M., Roy, S.K., Plastic Technology Handbook, 4th Edition, CRC press, Florida, USA, 2006, 4.88–4.92.
34. Chandra, S., Sahu, S., Pramanik, P., A novel synthesis of graphene by dichromate oxidation, Materials Science and Engineering B, 167, 2010, 133–136.
35. Chang, H., Kim, J.R., Cho, J.H., Kim, H.K., Choi, K.H., Materials and processes for small fuel cells, Solid State Ionics, 148 (3–4), 2002, 601–606.
36. Chang, H., Koschany, P., Lim, C., Kim, J., Materials and processes for light weight and high power density PEM fuel cells, Journal of New Materials for Electrochemical Systems, 3 (1), 2000, 55–60.
37. Chen, C.-K., Kuo, J.-K., Nylon 6-CB polymeric conductive plastic bipolar plates for PEM fuel cells, Journal of Applied Polymer Science, 101, 2006, 3415–3421.
38. Chen, E., History, In: Hoogers, G., Editor, Fuel Cell Technology Handbook, CRC Press, Florida, 1, 2003, 2.1–2.40.
39. Chen, L.J., He, Z.R., Yang, S.H., The Development of a Heterogeneous Composite Bipolar Plate of a Proton Exchange Membrane Fuel Cell, Journal of Fuel Cell Science and Technology, 2 (1), 2005, 14–20.

40. Chen, S., Bourell, D.L., Wood, K.L., Fabrication of PEM fuel cell bipolar plate by indirect SLS, The 15th Solid Freeform Fabrication Symposium Proceedings, August 2004, 244–256.
41. Chen, W., Yan, L., Preparation of graphene by a low-temperature thermal reduction at atmosphere pressure, Nanoscale, 2, 2010, 559–563.
42. Chervinko, J., Fan, Q., Onischak, M., Marianowski, L.G., Method for bipolar plate manufacturing, U.S. Patent 20030104257A1, 2003.
43. Cho, E.A., Jeon, U.-S., Ha, H.Y., Hong, S.-A., Oh, I.-H., Characteristics of composite bipolar plates for polymer electrolyte membrane fuel cells, Journal of Power Sources, 125 (2), 2004, 178–182.
44. Choi, H.S., Han, D.H., Hong, W.H., Lee, J.J., (Titanium, chromium) nitride coatings for bipolar plate of polymer electrolyte membrane fuel cell, Journal of Power Sources, 189, 2009, 966–971.
45. Chow, S., Adhesive developments in forest products, Wood Science and Technology, 17, 1983, 1–11.
46. Chung, D.D.L., Electrical applications of carbon materials, Journal of Materials Science, 39 (8), 2004, 2645–2661.
47. Clingerman, M.L., Weber, E.H., King, J.A., Schulz, K.H., Synergistic effects of carbon fillers in electrically conductive nylon 6,6 and polycarbonate based resins, Polymer Composites, 23 (5), 2002, 911–924.
48. Colling, P.M., Norton, R.V., Martin, J.E., Selection and evaluation of carbon-resin composites for bipolar plates for hydrogen fuel cells, Technical Report, AD A070185, 1978, Ashland Chemical Co., Columbus, Ohio, USA.
49. Cunningham, B.D., Baird, D.G., Development of bipolar plates for fuel cells from graphite filled wet-lay material and a compatible thermoplastic laminate skin layer, Journal of Power Sources, 168 (2), 2007, 418–425.
50. Cunningham, B.D., Baird, D.G., The development of economical bipolar plates for fuel cells, Journal of Materials Chemistry, 16 (45), 2006, 4385–4388.
51. Cunningham, B.D., Huang, J., Baird, D.G., Development of bipolar plates for fuel cells from graphite filled wet-lay material and a thermoplastic laminate skin layer, Journal of Power Sources, 165 (2), 2007, 764–773.

52. Davies, D.P., Adcock, P.L., Turpin, M., Rowen, S.J., Bipolar plate materials for solid polymer fuel cells, Journal of Applied Electrochemistry, 30 (1), 2000, 101–105.
53. Davis, J.H., Composite bipolar plate separator structures for polymer electrolyte, U.S. Patent 0001743, 2002.
54. Del Rio, C., Ojeda, M.C., Acosta, J.L., Carbon black effect on the microstructure of incompatible polymer blends, European Polymer Journal, 36 (8), 2000, 1687–1695.
55. Del Rio, C., Ojeda, M.C., Acosta, J.L., Escudero, M.J., Hontanon, E., Daza, L., New polymer bipolar plates for polymer electrolyte membrane fuel cells: Synthesis and characterization, Journal of Applied Polymer Science, 83, 2002, 2817–2822.
56. Demirbas, A., Fuel cells, In: Biohydrogen for Future Engine Fuel Demands, Springer, London, England, 2009, 221–239.
57. Dhakate, S.R., Mathur, R.B., Kakati, B.K., Dhami, T.L., Properties of graphite-composite bipolar plate prepared by compression molding technique for PEM fuel cell, International Journal of Hydrogen Energy, 32 (17), 2007, 4537-4543.
58. Dhakate, S.R., Mathur, R.B., Sharma, S., Borah, M., Dhami, T.L., Expanded graphite-based electrically conductive compositesas bipolar plate for PEM fuel cell, International Journal of Hydrogen Energy, 33, 2008, 7146–7152.
59. Dhakate, S.R., Mathur, R.B., Sharma, S., Borah, M., Dhami, T.L., Development and characterization of expanded graphite-based nanocomposite as bipolar plate for polymer electrolyte membrane fuel cells (PEMFCs), Energy & Fuels, 22 (5), 3329–3334.
60. Dhakate, S.R., Mathur, R.B., Sharma, S., Borah, M., Dhami, T.L., Influence of Expanded Graphite Particle Size on the Properties of Composite Bipolar Plates for Fuel Cell Application, Energy & Fuels, 23 (2), 2009, 934–941.
61. Dhakate, S.R., Mathur, R.B., Sharma, S., Borah, M., Dhami, T.L., Development and characterization of expanded graphite-based nanocomposite as bipolar plate for polymer electrolyte membrane fuel cells (PEMFCs), Energy & Fuels, 22 (5), 3329–3334.
62. Dhathathreyan, K.S., Rajalakshmi, N., Polymer electrolyte membrane fuel cell, In: S. Basu, Editor, Recent Trends in Fuel Cell Science and Technology, Springer, New Delhi, India, 2007, 40–115.

63. Du, C., Ming, P., Hou, M., Fu, J., Shen, Q., Liang, D., Fu, Y., Luo, X., Shao, Z., Yi, B., Preparation and properties of thin epoxy/compressed expanded graphite composite bipolar plates for proton exchange membrane fuel cells, Journal of Power Sources, 195 (3), 2010, 794–800.
64. Du, L., Jana, S.C., Highly conductive epoxy/graphite composites for bipolar plates in proton exchange membrane fuel cells, Journal of Power Sources 72, 2007, 734–741.
65. Du, L., Jana, S.C., Hygrothermal effects on properties of highly conductive epoxy/graphite composites for applications as bipolar plates, Journal of Power Sources, 182, 2008, 223–229.
66. Du, Q., Zheng, M., Zhang, L., Wang, Y., Chen, J., Xue, L., Dai, W., Ji, G., Cao, Preparation of functionalized graphene sheets by a low-temperature thermal exfoliation approach and their electrochemical supercapacitive behaviors, Electrochimica Acta, 55, 2010, 3897–3903.
67. Du, X.S., Xiao, M., Meng, Y.Z., Hay, A.S., Synthesis and properties of poly(4,4'-oxybis(benzene)disulfide)/graphite nanocomposites via in situ ring-opening polymerization of macrocyclic oligomers, Polymer, 45 (19), 2004, 6713–6718.
68. Duo, I., Fujishima, A., Comninellis, C., Electron transfer kinetics on composite diamond (sp^3)–graphite (sp^2) electrodes, Electrochemistry Communications, 5, 2003, 695–700.
69. Dweiri, R., Sahari, J., Electrical properties of carbon-based polypropylene composites for bipolar plates in polymer electrolyte membrane fuel cell (PEMFC), Journal of Power Sources, 171 (2), 2007, 424–432.
70. Dweiri, R., Sahari, J., Microstructural image analysis and structure–electrical conductivity relationship of single- and multiple-filler conductive composites, Composite Science and Technology, 68, 2008, 1679–1687.
71. Era, V.A., Mattila, A., Thermal analysis of thermosetting resins, Journal of Thermal Analysis, 10, 1976, 461–469.
72. Falko, V.I., Geim, A.K., Graphene: Emerging matter in two dimensions, The European Physical Journal - Special Topics, 148 (1), 2010, 1–4.
73. Frysz, C.A., Shui, X., Chung, D.D.L., Carbon filaments and carbon black as a conductive additive to the manganese dioxide cathode of a lithium electrolytic cell, Journal of Power Sources, 58 (1), 1996, 41–54.

74. Fu, Y., Hou, M., Lin, G., Hou, J., Shao, Z., Yi, B., Coated 316L stainless steel with Cr_xN film as bipolar plate for PEMFC prepared by pulsed bias arc ion plating, Journal of Power Sources, 176 (1), 2008, 282–286.
75. Fu, Y., Hou, M., Xu, H., Hou, Z., Ming, P., Shao, Z., Yi, B., Ag–polytetrafluoroethylene composite coating on stainless steel as bipolar plate of proton exchange membrane fuel cell, Journal of Power Sources, 182, 2008, 580–584.
76. Gaur, B., Rai, J.S.P., Curing and decomposition behaviour of vinyl ester resins, Polymer 33 (19), 1992, 4210–4214
77. Geim, A.K., MacDonald, A.H., Graphene: Exploring carbon flatland, Physics Today, 60, 2007, 35–41.
78. Geim, A.K., Novoselov, K.S., The rise of graphene, Nature, 6, 2007, 183–191.
79. Geng, Y., Wang, S.J., Kim, J.K., Preparation of graphite nanoplatelets and graphene sheets, Journal of Colloid and Interface Science 336, 2009, 592–598.
80. Ghouse, M., Abaoud, H., Al-Boeiz, A., Al-Zaharani, S., Fabrication and characterisation of the graphite bi-polar plates used in a 0.25 kW PAFC stack, International Journal of Hydrogen Energy, 23 (8), 1998, 721–730.
81. Ghouse, M., Abaoud, H., Al-Boeiz, A., Operational experience of a 1 kW PAFC stack, Applied Energy, 65 (1–4), 2000, 303–314.
82. Granata Jr, S.J., Woodle, B.M., Fuel cell plates with skewed process channels for uniform distribution of stack compression load, U.S. Patent 4853301, 1989.
83. Grove, W.R., On the gas voltaic battery–Experiments made with a view of ascertaining the rationale of its action and its application to eudiometry. Philosophical Magazine, 24 (159), 1844, 268–278.
84. Grove, W.R., On the gas voltaic battery–Experiments made with a view of ascertaining the rationale of its action and its application to eudiometry. Philosophical Magazine, 24 (160), 1844, 346–354.
85. Grove, W.R., On the gas voltaic battery–Experiments made with a view of ascertaining the rationale of its action and its application to eudiometry. Philosophical Magazine, 24 (161), 1844, 422–432.
86. Grove, W.R., On Voltaic Series and the Combination of Gases by Platinum, Philosophical Magazine and Journal of Science, 14 (86), 1839, 127–130.
87. Grubb, W.T., Fuel cell, General Electric, U.S. Patent 2913511, 1959.

88. Grubb, W.T., Niedrach, L.W., Batteries with Solid Ion-Exchange Membrane Electrolytes, Journal of the Electrochemical Society, 107 (2), 1960, 131–135.
89. Gruenspecht, H., International Energy Outlook 2010-Highlights, US Energy Information Administration, accepted on 01-06-2010.
90. Guo, Z., Liang, X., Pereira, T., Scaffaro, R., Hahn, H.T., CuO nanoparticle filled vinyl-ester resin nanocomposites: Fabrication, characterization and property analysis, Composites Science and Technology, 67 (10), 2007, 2036–2044.
91. Gurland, J., An estimate of contact and continuity of dispersions in opaque samples, Transactions of the Metallurgical Society, 236, 1966, 642–646.
92. Heinzel, A., Mahlendorf, F., Niemzig, O., Kreuz, C., Injection moulded low cost bipolar plates for PEM fuel cells, Journal of Power Sources, 131 (1–2), 2004, 35–40.
93. Heiser, J.A., King, J.A., Konell, J.P., Sutter, L.L., Electrical conductivity of carbon filled nylon 6,6. Advances in Polymer Technology, 23, 2004, 135–146.
94. Heo, S.I., Yun, J.C., Oh, K.S., Han, K.S., Development of preform moulding technique using expanded graphite for proton exchange membrane fuel cell bipolar plates, Journal of Power Sources, 171 (2), 2006, 396–403.
95. Heras, N. De, las, Roberts, E. P. L., Langton, R., Hodgson, D.R., A review of metal separator plate materials suitable for automotive PEM fuel cells, Energy and Environmental Science, 2, 2009, 206–214.
96. Hermann, A., Chaudhuri, T., Spagnol, P., Bipolar plates for PEM fuel cells A review, International Journal of Hydrogen Energy, 30 (12), 2005, 1297–1302.
97. Hoeckelman, LA., Environmental protection and sealing. In: Miracle DB, Donaldson SL, (Eds.). ASM Handbook: Composites, vol. 21, ASM International, USA, 2001, 659–665.
98. Hogarth, M.P., Ralph, T.R., Catalysis for Low Temperature Fuel Cells, Platinum Metals Review, 46 (4), 2002, 146–164.
99. Hoggins, J.T., Watts, G.F., Process for molding corrosion resistant fuel cell collecting plates, U.S. Patent 4359438, 1982.
100. (a) Hsiao, M.C., Liao, S.H., Yen, M.Y., Su, A., Wu, I.T., Hsiao, M.H., Lee, S.J., Teng, C.C. Ma, C.C.M., Effect of graphite sizes and carbon nanotubes content on flowability of bulk-molding compound and formability of the composite bipolar plate for fuel cell, Journal of Power Sources, 195 (17), 2010, 5645–5650.

(b) Hsiao, M.C., Liao, S.H., Yen, M.Y., Ma, C.C.M., Lee, S.J., Chen, Y.H., Hung, C.H., Lin, Y.F., Xie, X.F., Electrical and thermal conductivities of novel metal mesh hybrid polymer composite bipolar plates for proton exchange membrane fuel cells, Journal of Power Sources, 195 (2), 15, 2010, 509–515.

101. http://www.schunk-group.com/sixcms/media.php/1722/e_FU%204369.pdf [accessed 02.02.2010]
102. http://www1.eere.energy.gov/hydrogenandfuelcells/mypp/pdfs/fuel_cells.pdf [accessed 02.02.2010]
103. Huang, J., Baird, D.G., McGrath, J.E., Development of fuel cell bipolar plates from graphite filled wet-lay thermoplastic composite materials, Journal of Power Sources, 150 (4), 2005, 110–119.
104. Hui, C., Hong-bo, L., Li, Y., Jian-xin, L., Li, Y., Study on the preparation and properties of novolac epoxy-graphite composite bipolar plate for PEMFC, International Journal of Hydrogen Energy, 35 (7), 2010, 3105–3109.
105. Hummer, W., Offman, R., Preparation of graphite oxide, Journal of the American Chemical Society, 80, 1958, 1339.
106. Hwang, I.U., Yu, H.N., Kim, S.S., Lee, D.G., Suh, J.D., Lee, S.H., Ahn, B.K., Kim, S.H., Lim, T.W., Bipolar plate made of carbon fiber epoxy composite for polymer electrolyte membrane fuel cells, Journal of Power Sources, 184, 2008, 90–94.
107. Ibeh, C.C., Phenol-formaldehyde resins, In: Goodman, S.H., Editor, Handbook of Thermoset Plastics, Noyes publications, Westwood, New Jersey, USA, 1998; 2nd ed., 23–71.
108. Iqbal, Z., Pratt, J., Matrunich, J., Guiheen, J.V., Dai, H., Rehg, T., Narasinham, D., Nanocomposite for fuel cell bipolar plate, U.S. Patent 6572997, 2003.
109. Jayakumar, K., Pandiyan, S., Rajalakshmi, N., Dhathathreyan, K.S., Cost-benefit analysis of commercial bipolar plates for PEMFC's, Journal of Power Sources, 161 (1), 2006, 454–459.
110. Jones, DA., Principles and Prevention of Corrosion. 2nd ed. USA: Prentice Hall; 1996.
111. Kahlbaum, G.W.A., Darbishire, F.V., The Letters of Faraday and Schoenbein, Basle and London, 1899, 1836–1862.

112. Kakati, B.K., Guptha, K.R., Verma, A., Fabrication of composite bipolar plate for proton exchange membrane fuel cell, Journal of Environmental Research and Development, 4, 2009, 202−211.
113. Kakati, B.K., Guptha, K.R., Verma, A., Numerical optimization of channel and rib width of proton exchange membrane fuel cell bipolar plate, International Journal of Chemical Sciences, 5, 2007, 1590–1602.
114. Kakati, B.K., Sathiyamoorthy, D., Verma, A., Electrochemical and mechanical behaviour of carbon composite bipolar plate for fuel cell, International Journal of Hydrogen Energy, 35, 2010, 4185–4194.
115. Kakati, B.K., Yamsani, V.K., Dhathathreyan, K.S., Sathiyamoorthy, D., Verma, A., Carbon 47, 2009, 2413–2418.
116. Kamarudin, S.K., Daud, W.R.W., Md.Som, A., Takriff, M.S., Mohammad, A.W., Technical design and economic evaluation of a PEM fuel cell system, Journal of Power Sources, 157 (2), 2006, 641–649.
117. Kang, S.J., Kim, D.O., Lee, J.H., Lee, P.C., Lee, M.H., Lee, Y., Lee, J.Y., Choi, H.R., Lee, J.H., Oh, Y.S., Nam, J.D., Solvent-assisted graphite loading for highly conductive phenolic resin bipolar plates for proton exchange membrane fuel cells, Journal of Power Sources, 195, 2010, 3794–3801.
118. Keith, J.M., Barton, R.L., King, J.A., Electrical Conductivity Modelling of Carbon-Filled Liquid Crystal Polymer Composites, Journal of Applied Polymer Science, 102, 2006, 3293–3300.
119. Keith, J.M., King, J.A., Miller, M.G., Tomson, A.M., Thermal conductivity of carbon fiber/liquid crystal polymer composites, Journal of Applied Polymer Science, 102 (6), 2006, 5456–5462.
120. Kelly, R.S., Weiss, D.J., Chong, S.H., Kuwana, T., Charge-selective electrochemistry at high-surface-area carbon fibers, Analytical Chemistry 71, 1999, 413–418.
121. Kenny, J.M., Pisaniello, G., Farina, F., Puzziello, S., Calorimetric analysis of the polymerization reaction of phenolic resin, Thermochimica Acta, 269–270, 1995, 201–211.
122. Kim, J.W., Kima, N.H. Kuilla, T., Kim, T.J., Rhee, K.Y., Lee, J.H., Synergy effects of hybrid carbon system on properties of composite bipolar plates for fuel cells, Journal of Power Sources, 195, 2010, 5474–5480.

123. King, J.A., Morrison, F.A., Keith, J.M., Miller, M.G., Smith, R.C., Cruz, M., Neuhalfen, A.M., Barton, R.L., Electrical conductivity and rheology of carbon-filled liquid crystal polymer composites, Journal of Applied Polymer Science, 101 (4), 2006, 2680–2688
124. King, J.A., Tucker, K.W., Meyers, J.D., Weber, E.H., Clingerman, M.L., Ambrosius, K.R., Factorial design approach applied to electrically and thermally conductive nylon 6,6, Polymer Composite, 22, 2001, 142–154.
125. Kinoshita, K., In: Carbon: electrochemical and physicochemical properties, Willey, New York, 1988, 86–166.
126. Kinumoto, T., Nagano, K., Tsumura, T., Toyoda, M., Thermal and electrochemical durability of carbonaceous composites used as a bipolar plate of proton exchange membrane fuel cell, Journal of Power Sources, 195 (19), 2010, 6473–6477.
127. Koizumi, K., Charles, T., De Keyser, H., Phenolic molding compounds, In: Phenolic Resins: A Century of Progress, Springer-Verlag, Berlin Heidelberg, Germany, 2010, 383-437.
128. Kuan, H.C., Ma, C.C.M., Chen, K.H., Chen, S.M., Preparation, electrical, mechanical and thermal properties of composite bipolar plate for a fuel cell, Journal of Power Sources, 134 (1), 2004, 7–17.
129. Kuo, J.K., Chen, C.K., A novel Nylon-6-S316L fiber compound material for injection molded PEM fuel cell bipolar plates, Journal of Power Sources, 162 (1), 2006, 207–214.
130. Kurachenkov, V.I., Igonin, L.A., Curing mechanism for phenol-formaldehyde resins, Journal of Polymer Science Part A-1: Polymer Chemistry, 9 (8), 1971, 2283–2289.
131. Landauer, R., Electrical conductivity in inhomogeneous media, AIP Conference Proceedings, 40, 1978, 2–43.
132. Landis, L., Tucker, J.L., Making better fuel cells: through-plane resistivity measurement of graphite-filled bipolar plates, White paper, kei2400wp2, 2002, Keithley Instruments, Inc., Cleveland, Ohio, USA.
133. Larminie, J., Dicks, A., Fuel Cell Systems Explained, Wiley, New York, 2000.
134. Lawrance, R.J., Low cost bipolar current collector-separator for electrochemical cells, U.S. Patent 4214969, 1980.

135. Lee, H.S., Kim, H.J., Kim, S.G., Ahn, S.H., Evaluation of graphite composite bipolar plate for PEM (proton exchange membrane) fuel cell: Electrical, mechanical, and molding properties, Journal of Materials Processing Technology, 187-188, 2007, 425–428.
136. Lee, J.H., Jang, Y.K., Hong, C.H., Kim, N.M., Li, P., Lee, H.K., Effect of carbon fillers on properties of polymer composite bipolar plates of fuel cells, Journal of Power Sources, 193, 2009, 523–529.
137. Lee, Y.B., Lee, C.H., Lim, D.S., The electrical and corrosion properties of carbon nanotube coated 304 stainless steel/polymer composite as PEM fuel cell bipolar plates, International Journal of Hydrogen Energy, 34 (24), 2009, 9781–9787.
138. Lenghaus, K., Qiao, G.G., Solomon, D.H., Model studies of the curing of resole phenol-formaldehyde resins Part 1. The behaviour of ortho quinone methide in a curing resin, Polymer, 41, 2000, 1973–1979.
139. Lenghaus, K., Qiao, G.G., Solomon, D.H., The effect of formaldehyde to phenol ratio on the curing and carbonisation behaviour of resole resins, Polymer, 42 (8), 8, 2001, 3355–3362.
140. Lens, P., Proton exchange membrane fuel cells: description and applications, In: Biofuels for fuel cells: renewable energy from biomass fermentation, IWA Publishing, London, 2005, 271–286.
141. Li, D., Wang, Y., Xu, L., Lu, J., Wu, Q., Surface modification of a natural graphite/phenol formaldehyde composite plate with expanded graphite, Journal of Power Sources, 183 (2), 2008, 571-575.
142. Li, X., Sabir, I., Review of bipolar plates in PEM fuel cells: Flow-field designs, International Journal of Hydrogen Energy, 30 (4), 2005, 359–371.
143. Li, X., Thermodynamic performance of fuel cells and comparison with heat engines, In: Zhao, T.S., Kreuer, K.D., Nguyen, T.V., Editor(s), Advances in Fuel Cells, Elsevier Science, Oxford, 1, 2007, 1–46.
144. (a) Liao, S.H., Hung, C.H., Ma, C.C.M., Yen, C.Y., Lin, Y.F., Weng, C.C., Preparation and properties of carbon nanotube-reinforced vinyl ester/nanocomposite bipolar plates for polymer electrolyte membrane fuel cells, Journal of Power Sources, 176 (1), 2008, 175–182.

(b) Liao, S.H., Yen, C.Y., Weng, C.C., Lin, Y.F., Ma, C.C.M., Yang, C.C.H., Tsai, M.C., Yen, M.Y., Hsiao, M.C., Lee, S.J., Xie, X.F., Hsiao, Y.H., Preparation and properties of carbon nanotube/polypropylene nanocomposite bipolar plates for polymer electrolyte membrane fuel cells, Journal of Power Sources, 185 (2), 2008, 1225–1232.

145. (a) Liao, S.H., Weng, C.C., Yen, C.Y., Hsiao, M.C., Ma, C.C.M., Tsai, M.C., Su, A., Yen, M.Y., Lin, Y.F., Liu, P.L., Preparation and properties of carbon nanotube/polypropylene nanocomposite bipolar plates for polymer electrolyte membrane fuel cells, Journal of Power Sources, 195 (1), 2010, 263–270.

(b) Liao, S.H., Hsiao, M.C., Yen, M.Y., Ma, C.C.M., Lee, S.J., Su, A., Tsai, M.C., Yen, M.Y., Liu, P.L., Novel functionalized carbon nanotubes as cross-links reinforced vinyl ester/nanocomposite bipolar plates for polymer electrolyte membrane fuel cells, Journal of Power Sources, 195 (23), 2010, 7808–7817.

(c) Liao, S.H., Yen, C.Y., Hung, C., Weng, C.C., Tsai, M.C., Lin, Y.F., Ma, C.C.M., Pan, C., Su, A., One-step functionalization of carbon nanotubes by free-radical modification for the preparation of nanocomposite bipolar plates in polymer electrolyte membrane fuel cells, Journal of Materials Chemistry, 18, 2008, 3993–4002.

146. Lin, C., Chung, D.D.L., Effect of carbon black structure on the effectiveness of carbon black thermal interface pastes, Carbon 45, 2007, 2922–2931.

147. Liu, N., Luo, F., Wu, H., Liu, Y., Zhang, C. and Chen, J., One-Step Ionic-Liquid-Assisted Electrochemical Synthesis of Ionic-Liquid-Functionalized Graphene Sheets Directly from Graphite, Advanced Functional Materials, 18 (10), 2008, 1518–1525.

148. Liu, Z., Guo, Q., Shi, J., Zhai, G., Liu, L., Graphite blocks with high thermal conductivity derived from natural graphite flake, Carbon, 46 (3), 2008, 414–421.

149. Loutfy, R.O., Hecht, M., Low cost molded plastic fuel cell separator plate with conductive elements, U.S. Patent 6511766, 2003.

150. Lu, W., Chung, D.D.L., A comparative study of carbons for use as an electrically conducting additive in the manganese dioxide cathode of an electrochemical cell, Carbon, 40, 2002, 447–449.

151. Lux, F., Models proposed to explain the electrical conductivity of mixtures made of conductive and insulating materials, Journal of Material Science, 28, 1993, 285–301.
152. Ma, C., Zhang, L., Mukherjee, S., Ofer, D., Nair, B., An investigation of proton conduction in select PEM's and reaction layer interfaces-designed for elevated temperature operation, Journal of Membrane Science, 219 (1-2), 2003, 123–136.
153. Ma, L., Warthesen, S., Shores, D.A., Evaluation of materials for bipolar plates in PEMFCs, Journal of New Materials for Electrochemical Systems, 3, 2000, 221–228.
154. Maciel, G.E., Chuang, I.S., Gollob, L., Solid-state ^{13}C NMR study of resol-type phenol-formaldehyde resins, Macromolecules, 17 (5), 1984, 1081–1087.
155. Maheshwari, P.H., Mathur, R.B., Dhami, T.L., Fabrication of high strength and a low weight composite bipolar plate for fuel cell applications, Journal of Power Sources, 173 (1), 2007, 394–403.
156. Malliaris, A., Turner, D.T., Influence of particle size on the electrical resistivity of compacted mixtures of polymeric and metallic powders, Journal of Applied Physics, 42, 1971, 614–618.
157. Mamunya, Y.P., Davydenko, V.V., Pissis, P., Lebedev, E.V., Electrical and thermal conductivity of polymers filled with metal powders, European Polymer Journal, 38, 2002, 1887–1897.
158. Marianowski, L.G., 160°C proton exchange membrane (PEM) fuel cell system development, Technical Report, DE-FC26-99FT40656, 2001, Gas Technology Institute, USA.
159. Martinot, E., Sawin, J., Renewables Global status report: 2009 Update. REN21, Renewable Energy Policy Network and Worldwatch Institute, 2009.
160. Mathur, R.B., Dhakate, S.R., Gupta, D.K., Dhami, T.L., Aggarwal, R.K., Effect of different carbon fillers on the properties of graphite composite bipolar plate, Journal of Materials Processing Technology, 203 (1–3), 2008, 184–192.
161. McEnaney, B., Structure and bonding in carbon materials, In: Burchell, T.D., Editor, Carbon Materials for Advanced Technologies, Elsevier Science Ltd., Oxford, UK, 1999, 1–33.
162. McLachlan, D.S., Equations for the conductivity of macroscopic mixtures. Journal of Physics C: Solid State Physics, 19, 1986, 1339–1354.

163. (a) McLachlan, D.S., An equation for the conductivity of binary mixtures with anisotropic grain structures. Journal of Physics C: Solid State Physics, 20, 1987, 865–877.

(b) McLachlan, D.S., Equation for the conductivity of heterogeneous binary media, Journal of Applied Physics, 26, 1987, 901–902.

164. McLachlan, D.S., Burger, J.P., An analysis of the electrical conductivity of the two phase PdH_x system, Solid State Communication, 65, 1988, 159-161.

165. McLachlan, D.S., Morphology dependence of the resistivity and meissner curves in two-phase superconductors, Solid State Communication, 69, 1989, 925–929.

166. McLachlan, D.S., A quantitative analysis of the volume fraction dependence of the resistivity of cermets using a general effective media equation, Journal of Applied Physics, 68, 1990, 195–199.

167. Mehta, V., Cooper, J.S., Review and analysis of PEM fuel cell design and manufacturing, Journal of Power Sources, 114 (1), 2003, 32–53.

168. Meyer, J.C., Geim, A.K., Katsnelson, M.I., Novoselov, K.S., Obergfell, D., Roth S., Girit, C., Zettl, A., On the roughness of single- and bi-layer graphene membranes, Solid State Communication 143 (1–2), 2007, 101–109.

169. Middelman, E., Kout, W., Vogelaar, B., Lenssen, J., de Waal, E., Bipolar plates for PEM fuel cells, Journal of Power Sources, 118 (1-2), 2003, 44–46.

170. Mighri, F., Huneault, M.A., Champagne, M.F., Electrically conductive thermoplastic blends for injection and compression molding of bipolar plates in the fuel cell application, Polymer Engineering & Science, 44 (9), 2004, 1755–1765.

171. Miller, M.G., Keith, J.M., King, J.A., Edwards, B.J., Klinkenberg, N., Schiraldi, D.A., Measuring thermal conductivities of anisotropic synthetic graphite–liquid crystal polymer composites, Polymer Composites, 27 (4), 2006, 388–394.

172. Mulder, G., Ridder, F.D., Coenen, P., Weyen, D., Martens, A., Evaluation of an on-site cell voltage monitor for fuel cell systems, International Journal of Hydrogen Energy 33, 2008, 5728–5737.

173. Muller, A., Kauranen, P., von Ganski, A., Hell, B., Injection moulding of graphite composite bipolar plates, Journal of Power Sources, 154 (2), 2006, 467–471.

174. Nikam, V.V., Reddy, R.G., Corrosion studies of a copper-beryllium alloy in a simulated polymer electrolyte membrane fuel cell environment, Journal of Power Sources, 152, 2005, 146–155.

175. Novoselov, K.S., Geim, A.K., Morozov, S.V., Jiang, D., Zhang, Y., Dubonos, S.V., Grigorieva, I.V., Firsov, A.A., Electric Field Effect in Atomically Thin Carbon Films, Science, 306 (5696), 2004, 666–669.
176. Oh, M.H., Yoon, Y.S., Park, S.G., The electrical and physical properties of alternative material bipolar plate for PEM fuel cell system, Electrochimica Acta, 50 (2–3), 2004, 777–780.
177. Ondracek, G., Kravchenko, I.S., Composites: General considerations, relationship between microstructure and effective properties, application of composites in developing materials with specified properties, Powder Metallurgy and Metal Ceramics, 32, 1993, 350–354.
178. Park, S.Y., Floresca, H.C., Suh, Y.J., Kim, M.J., Electron microscopy analyses of natural and highly oriented pyrolytic graphites and the mechanically exfoliated graphenes produced from them, Carbon 48, 2010, 797–804.
179. Penner, S.S., Appleby, A.J., Baker, B.S., Bates, J.L., Buss, L.B., Dollard, W.J., Fartis, P.J., Gillis, E.A., Gunsher, J.A., Khandkar, A., Krumpelt, M., O'Sullivan, J.B., Runte, G., Savinell, R.F., Selman, J.R., Shores, D.A., Tarman, P., Commercialization of fuel cells, Energy, 20 (5), 1995, 331–470.
180. Pierson, H.O., Handbook of Carbon, Graphite, Diamond and Fullerenes, Noyes Publications, Park Ridge, NJ, USA, 1993, 43–69.
181. Powell, R.L., Childs, G.E., Thermal Conductivity, In: Gary, D.E., Editor, American Institute of Physics Handbook, McGraw−Hill, New York, 1972, Ch. 4.
182. Pozio, A., Zaza, F., Masci, A., Silva, R.F., Bipolar plate materials for PEMFCs: A conductivity and stability study, Journal of Power Sources, 179, 2008, 631–639.
183. Prater, K.B., Polymer electrolyte fuel cells: a review of recent developments, Journal of Power Sources, 51 (1-2), 1994, 129–144.
184. Probst, N., Grivei, E., Structure and electrical properties of carbon black. Carbon, 40, 2002, 201–205.
185. Qureishi, S.P., Phenolic Resins, in: Miracle, D.B., Donaldson, S.L. (Eds.). ASM Handbook: Composites, vol. 21, ASM International, USA, 2001, 120–125.
186. Radhakrishnan, S., Ramanujam, B.T.S., Adhikari, A., Sivaram, S., High-temperature, polymer-graphite hybrid composites for bipolar plates: Effect of processing conditions on electrical properties, Journal of Power Sources, 163 (2), 2007, 702–707.

187. Ramanathan, T., Abdala, A.A., Stankovich, S., Dikin, D.A., Herrera-Alonso, M., Piner, R.D., Adamson, D.H., Schniepp, H.C., Chen, X., Ruoff, R.S., Nguyen, S.T., Aksay, I.A., Prudhomme, R.K., Brinson, L.C., Functionalized graphene sheets for polymer nanocomposites, Nature Nanotechnology 3, 2008, 327–331.

188. Rao, B.S., Madec, P.J., Marechal, E., Synthesis of vinyl ester resins, Polymer Bulletin, 16 (2), 1986, 1436–2449.

189. Rinn, G., Bornbaum, S., Graphite bipolar plates for PEM fuel cells, Ceramic Forum International, 82, 2005, E33–E36.

190. Roberge, P.R., Handbook of Corrosion Engineering. McGraw-Hill Professional, USA, 2000, 485–577.

191. Rosu, L., Cascaval, C.N., Rosu, D., Curing of vinyl ester resins- Rheological behaviour, Journal of Optoelectronics and Advanced Materials, 8 (2), 2006, 690–693.

192. Ruge, M., Buchi, F.N., PE Fuel Cells: Evaluation of Concepts for a Bipolar Plate Design and Construction, In: Brooman, E.W., Doyle, C.M., Cominellis, C., Winnick, J., Editor(s), Proceedings of the Symposium on "Energy and Electrochemical Processes for a Cleaner Environment", 200th Meeting of the Electrochemical Society, San Francisco, Sept. 3–7, 2001, 165–173.

193. Sammes, N.M., Boersma, R., Small-scale fuel cells for residential applications, Journal of Power Sources, 86 (1-2), 2000, 98–110.

194. Sanchez-Gonzalez, J., Macias-Garcia, A., Alexandre-Franco, M.F., Gomez-Serrano, V., Electrical conductivity of carbon blacks under compression, Carbon, 43 (4), 2005, 741–747.

195. Schniepp, H.C., Li, J.L., McAllister, M.J., Sai, H., Herrera-Alonso, M., Adamson, D.H., Prud'homme, R.K., Car, R., Saville, D.A., Aksay, I.A., Functionalized Single Graphene Sheets Derived from Splitting Graphite Oxide, The Journal of Physical Chemistry B, 110 (17), 2006, 8535–8539.

196. Scholta, J., Rohland, B., Trapp, V., Focken, U., Investigations on novel low-cost graphite composite bipolar plates, Journal of Power Sources, 84 (2), 1999, 231–234.

197. Scott, T.F., Cook, W.D., Forsythe, J.S., Kinetics and network structure of thermally cured vinyl ester resins, European Polymer Journal, 38 (4), 2002, 705–716.

198. Seo, M.K., Park, S.J., Effect of Graphite Nanofibers on Poly(methyl methacrylate) Nanocomposites for Bipolar Plates, Bulletin of Korean Chemical Society, 30 (3), 2009, 671–674.
199. Sessions, J., Field measurement of cable tensions for skyline logging systems, Technical Report, SD254.071273, 1976, Forest Research Laboratory, Oregon, USA.
200. Shuxuan, L., Chenguang, Y., Huankun, Z., Liu, Y., Hanwen, S., Determination of resorcinol on glassy carbon electrode modified by carbon nanotube and its application in wastewater analysis, Chemical Journal on Internet, 11, 2009, 3.
201. Siroma, Z., Fujiwara, N., Iroi, T., Yamazaki, S., Senoh, H., Yasuda, K., Taminoto, K., Electrochemical corrosion of carbon materials in an aqueous acid solution, Electrochemistry 75, 2007, 258–260.
202. Soldano, C., Mahmood, A., Dujardin, E., Production, properties and potential of graphene, Carbon, 48, 2010, 2127–2150.
203. Spurrier, F.R., Apparatus for supplying electrolyte to fuel cell stacks, U.S. Patent 4572876, 1986.
204. Spurrier, F.R., Pierce, B.L., Wright, M.K., Fuel cell plates with improved arrangement of process channels for enhanced pressure drop across the plates, U.S. Patent 4631239, 1986.
205. Srinivasan, C., Graphene-Mother of all graphitic materials, Current Science, 92 (10), 2007, 1338–1339.
206. Srivastava, N.K., Mehra, R.M., Study of the electrical properties of polystyrene–foliated graphite composite, Material Science-Poland, 27, 2009, 109–122.
207. Stankovich, S., Dikin, D.A., Piner, R.D., Kohlhaas, K.A., Kleinhammes, A., Jia, Y., Wu, Y., Nguyen, S.T., Ruoff, R.S., Synthesis of graphene-based nanosheets via chemical reduction of exfoliated graphite oxide, Carbon, 45 (7), 2007,1558–1565.
208. Steele, B.C.H., Heinzel, A., Materials for fuel-cell technologies, Nature, 414, 2001, 345–352.
209. Stone, C., Morrison, A. E., From curiosity to 'power to change the world®', Solid State Ionics, 152-153, 2002, 1–13.
210. Stoye, D., Phenolic resins, In: Stoye, D., Freitag, W., Editor(s), Resins for coatings: chemistry, properties, and applications, Hanser/Gardener, Cincinnati, USA, 1966, 123–159.

211. Surampudi, S., Narayanan, S.R., Vamos, E., Frank, H., Halpert, G., LaConti, A., Kosek, J., Surya Prakash, G.K., Olah, G.A., Advances in direct oxidation methanol fuel cells, Journal of Power Sources, 47 (3), 1994, 377–385.
212. Takahashi, K., Kameda, T., Shibatani, H., Graphitic or carbonaceous moldings and processes for producing the same, U.S. Patent 4929404, 1990.
213. Tchmutin, I.A., Ponomarenko, A.T., Krinichnaya, E.P., Kozub, G.I., Efimov, O.N., Electrical properties of composites based on conjugated polymers and conductive fillers. Carbon, 41, 2003, 1391-1395.
214. Thongruang, W., Spontak, R.J., Balik, C.M., Correlated electrical conductivity and mechanical property analysis of high-density polyethylene filled with graphite and carbon fiber, Polymer, 43 (8), 2002, 2279–2286.
215. Tomantschger, K., McClusky, F., Oporto, L., Reid, A., Kordesch, K., Development of low cost alkaline fuel cells, Journal of Power Sources, 18 (4), 1986, 317–335.
216. Trick, K.A., Saliba, T.E., Mechanisms of the pyrolysis of phenolic resin in a carbon/phenolic composite, Carbon, 33 (11), 1995, 1509–1515.
217. Uchida, M., Aoyama, Y., Tanabe, M., Yanagihara, N., Eda, N., Ohta, A., Influences of both carbon supports and heat-treatment of supported catalyst on electrochemical oxidation of methanol, Journal of the Electrochemical Society, 142, 1995, 2572–2576.
218. Valles, C., Drummond, C., Saadaoui, H., Furtado, C.A., He, M., Roubeau, O., Ortolani, L., Monthioux, M., Pnicaud, A., Solutions of Negatively Charged Graphene Sheets and Ribbons, Journal of the American Chemical Society, 130 (47), 2008, 15802–15804.
219. Wang, H., Brady, M.P., Teeter, G., Turner, J.A., Thermally nitrided stainless steels for polymer electrolyte membrane fuel cell bipolar plates: Part 1: Model Ni–50Cr and austenitic 349™ alloys, Journal of Power Sources, 138, 2004, 86–93.
220. Wang, M., Leithch, M., Xu, C., Synthesis of phenol-formaldehyde resol resins using organosolv pine lignins, European Polymer Journal, 45, 2009, 3380–3388.
221. Wang, M., Woo, K.D., Kim, D.K., Lou, T., Huang, Z., Study on impregnation of polytetrafluoroethylene in graphite for use as fuel cell collector, International Journal of Hydrogen Energy, 30 (9), 2005, 1027–1030.

222. Wang, S., Chen, Z.H., Ma, W.J., Ma, Q.S., Influence of heat treatment on physical-chemical properties of PAN-based carbon fiber, Ceramics International, 32, 2006, 291–295.
223. Wang, X.L., Zhang, H.M., Zhang, J.L., Xu, H.F., Tian, Z.Q., Chen, J., Zhong, H.X., Liang, Y.M., Yi, B.L., Micro-porous layer with composite carbon black for PEM fuel cells, Electrochimica Acta, 51 (23), 2006, 4909–4915.
224. Wang, Y., Anderson, C., Formation of thin transparent conductive composite films from aqueous colloidal dispersions, Macromolecules, 32 (19), 1999, 6172–6179.
225. Washington, K.B., Wilkinson, D.P., Voss, H.H., Laminated Fluid Flow Field Assembly for Electro-chemical Fuel Cells, U.S. Patent 5300370, 1994.
226. Wilson, M.S., Busick, D.N., Composite bipolar plate for electrochemical cells, U.S. Patent 6248467, 2001.
227. Wind, J., Spah, R., Kaiser, W., Bohm, G., Metallic bipolar plates for PEM fuel cells, Journal of Power Sources, 105 (2), 2002, 256–260.
228. Wolf, H., Porada, M.W., Electrically conductive LCP–carbon composite with low carbon content for bipolar plate application in polymer electrolyte membrane fuel cell. Journal of Power Sources, 153, 2006, 41–46.
229. Wu, B., Fu, Y., Xu, J., Lin, G., Hou, M., Chromium nitride films on stainless steel as bipolar plate for proton exchange membrane fuel cell, Journal of Power Sources, 194 (2), 2009, 976–980.
230. Wu, M., Shaw, L.L., A novel concept of carbon-filled polymer blends for applications in PEM fuel cell bipolar plates, International Journal of Hydrogen Energy, 30 (4), 2005, 373–380.
231. Wu, M., Shaw, L.L., Electrical and mechanical behaviors of carbon nanotube-filled polymer blends, Journal of Applied Polymer Science, 99 (2), 2006, 477–488.
232. Xia, L., Li, A., Wang, W., Yin, Q., Lin, H., Zhao, Y., Effects of resin content and preparing conditions on the properties of polyphenylene sulfide resin/graphite composite for bipolar plate, Journal of Power Sources, 178, 2008, 363–367.
233. Xiao, M., Lu, Y., Wang, S.J., Zhao, Y.F., Meng, Y.Z., Poly (arylene disulfide)/graphite nanosheets composites as bipolar plates for polymer electrolyte membrane fuel cells, Journal of Power Sources, 160 (1), 2006, 165–174.

234. Yan, X., Hou, M., Zhang, H., Jing, F., Ming, P., Yi, B., Performance of PEMFC stack using expanded graphite bipolar plates, Journal of Power Sources, 160 (1), 2006, 252–257.

235. Yang, C., Srinivasan, S., Arico, A.S., Creti, P., Baglio, V., Antonucci, V., Composite Nafion/zirconium phosphate membranes for direct methanol fuel cell operation at high temperature, Electrochemical and Solid-State Letters, 4 (4), 2001, A31–A34.

236. Yang, G., Liu, H., Bai, L., Jiang, M., Zhu, T., Preparation and characterization of novel poly(vinyl ester resin) monoliths, Microporous and Mesoporous Materials, 112 (1-3), 2008, 351–356.

237. Yasuda, H., Units of gas permeability constants, Journal of Applied Polymer Science, 19, 2529–2536.

238. Yen, C.-Y., Liao, S.-H., Lin, Y.-F., Hung, C.-H., Lin, Y.-Y., Ma, C.-C.M., Preparation and properties of high performance nanocomposite bipolar plate for fuel cell, Journal of Power Sources, 162 (1), 2006, 309–315.

239. Yin, Q., Li, A.J., Wang, W.Q., Xia, L.G, Wang, Y.M., Study on the electrical and mechanical properties of phenol fomaldehyde resin/graphite composite for bipolar plate, Journal of Power Sources, 165 (2), 2007, 717–721.

240. Yin, Q., Sun, K.N., Li, A.J., Shao, L., Liu, S.M., Sun, C., Study on carbon nanotube reinforced phenol formaldehyde resin/graphite composite for bipolar plate. Journal of Power Sources, 175, 2008, 861–865.

241. Yokoyama, M., Yamaura, S., Kimura, H., Inoue, A., Production of metallic glassy bipolar plates for PEM fuel cells by hot pressing in the supercooled liquid state, International Journal of Hydrogen Energy, 33 (20), 2008, 5678–5685.

242. Zaidi, S.M.J., Research Trends in Polymer Electrolyte Membranes, In: Zaidi, S.M.J., Matsuura, T., Editor(s), Polymer Membranes for Fuel Cells, Springer, 2009, 7–19.

243. Zhang, H.B., Zheng, W.G., Yan, Q., Yang, Y., Wang, J.W., Lu, Z.H., Ji, G.Y., Yu, Z.Z., Electrically conductive polyethylene terephthalate/graphene nanocomposites prepared by melt compounding, Polymer, 51, 2010, 1191–1196.

244. Zhang, X., Looney, M.G., Solomon, D.H., Whittaker, A.K., The chemistry of novolac resins: 3. ^{13}C and ^{15}N n.m.r. studies of curing with hexamethylenetetramine, Polymer, 38 (23), 1997, 5835–5848.

245. Zhang, X., Shen, L., Xia, X., Wang, H., Du, Q., Study on the interface of phenolic resin/expanded graphite composites prepared via in situ polymerization, Material Chemistry and Physics, 111, 2008, 368–374.

246. Zhang, X., Solomon, D.H., Phase Structures of Hexamine Cross-Linked Novolac Blends- 1: Blends with Poly(methyl methacrylate), Macromolecules, 27 (18), 1994, 4919-4926.

247. "The Nobel Prize in Physics 2010 - Scientific Background", Nobelprize.org, 29 Oct 2010, http://nobelprize.org/nobel_prizes/physics/laureates/2010/sci.html

Annexures

Annexure A1: Optimization of Molding Temperature

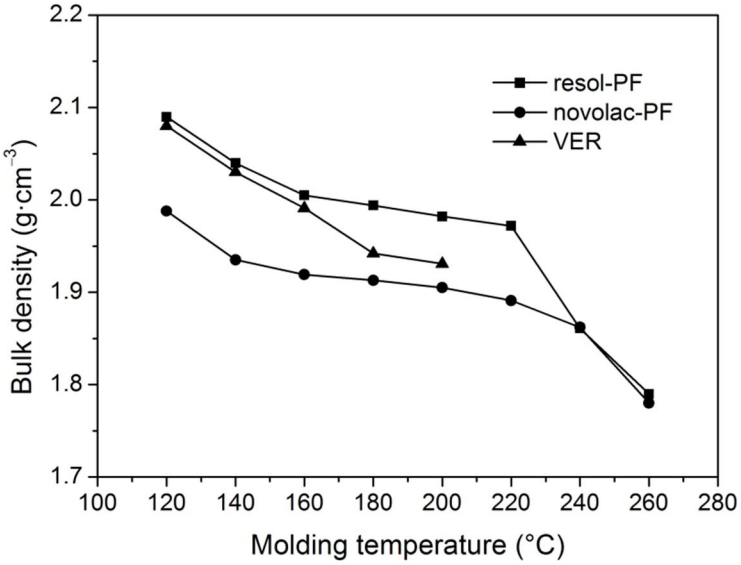

Figure A1.1: Effect of molding temperature on density of resin/NG composite bipolar plates

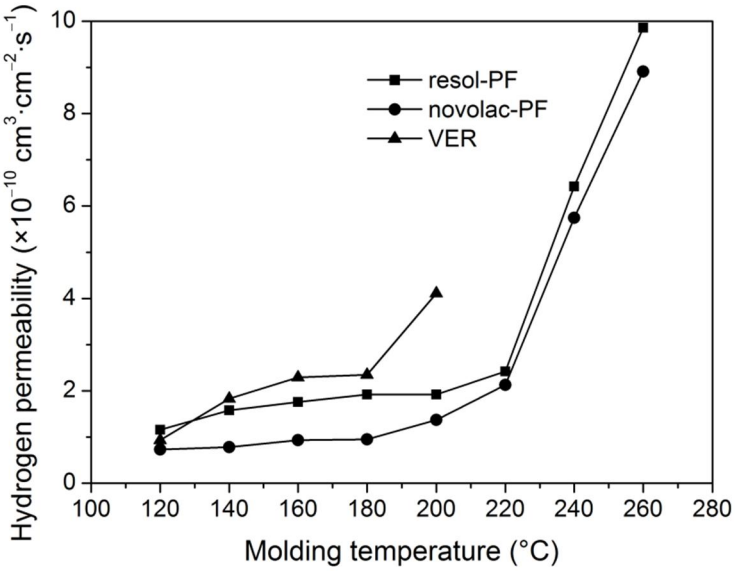

Figure A1.2: Effect of molding temperature on the hydrogen permeability of resin/NG composite bipolar plates at room temperature

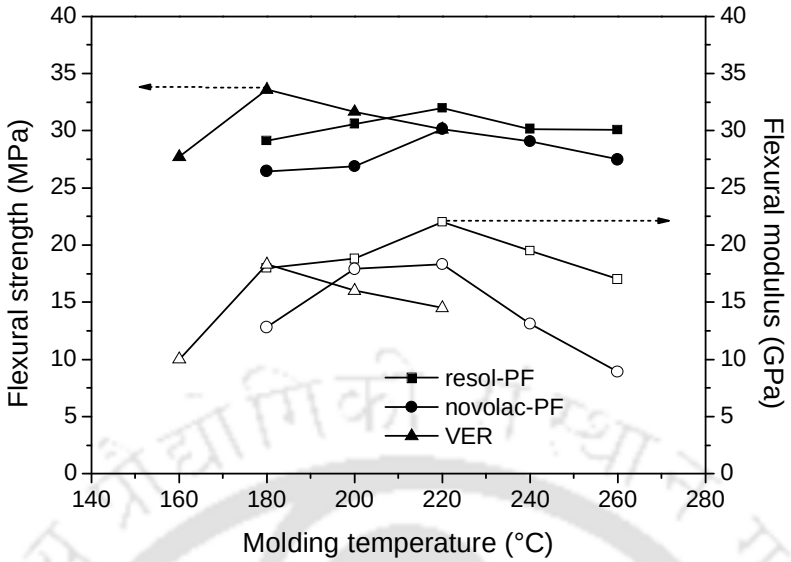

Figure A1.3: Effect of molding temperature on the flexural strength and flexural modulus of resin/NG composite bipolar plates

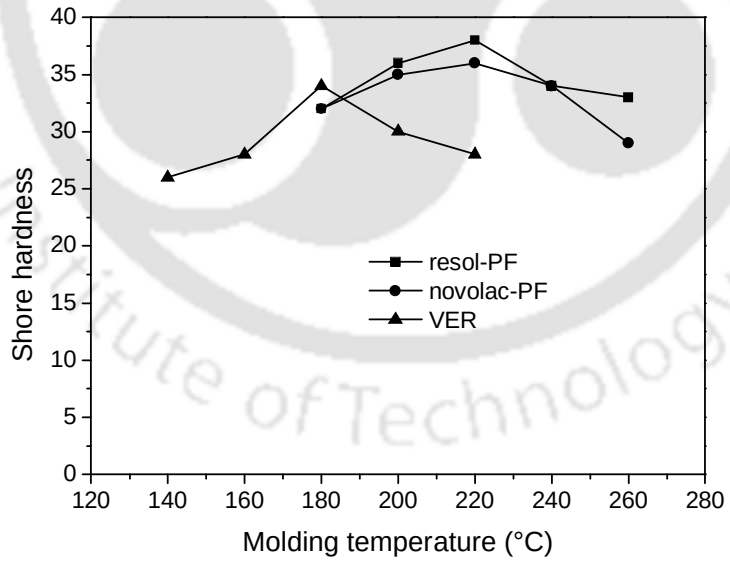

Figure A1.4: Effect of molding temperature on shore hardness of resin/NG composite bipolar plates

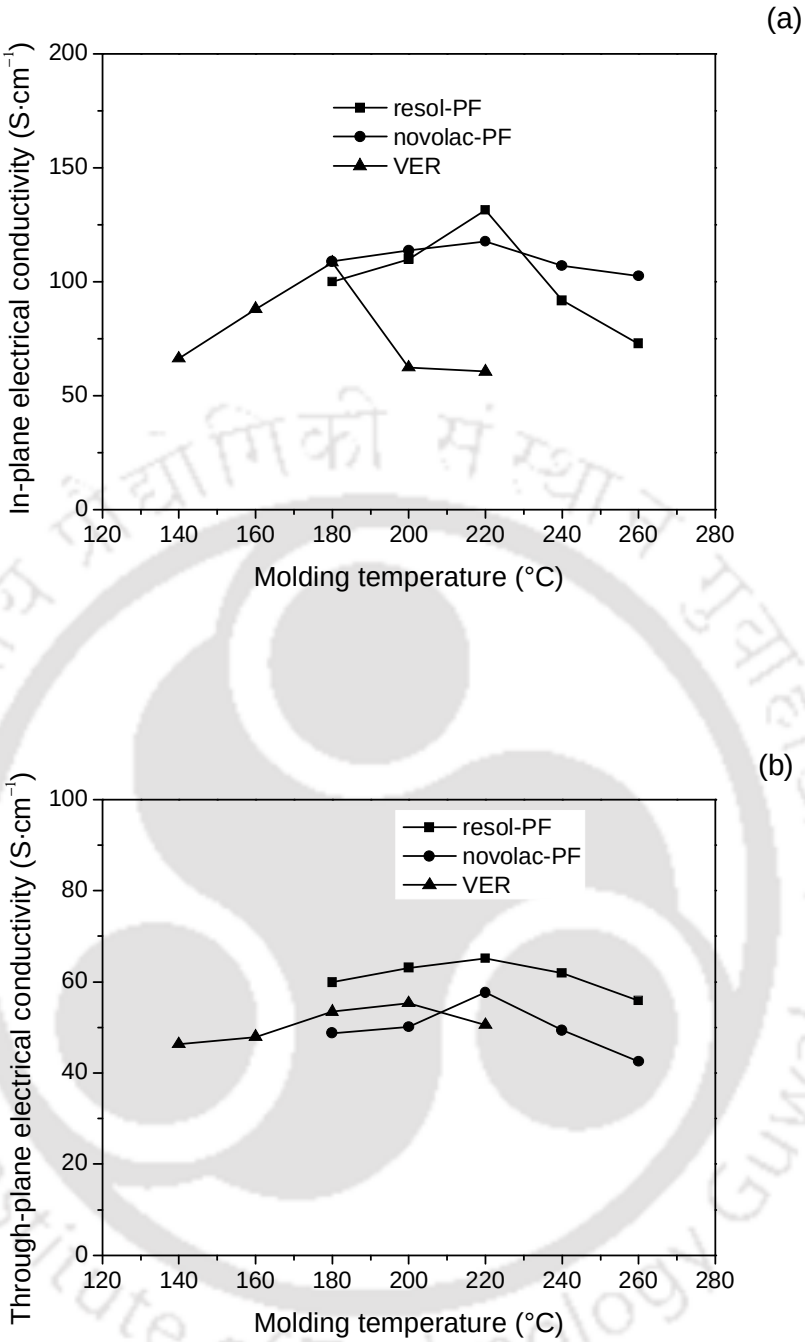

Figure A1.5: Effect of molding temperature on (a) in-plane and (b) through-plane electrical conductivities of the resin/NG composite bipolar plates

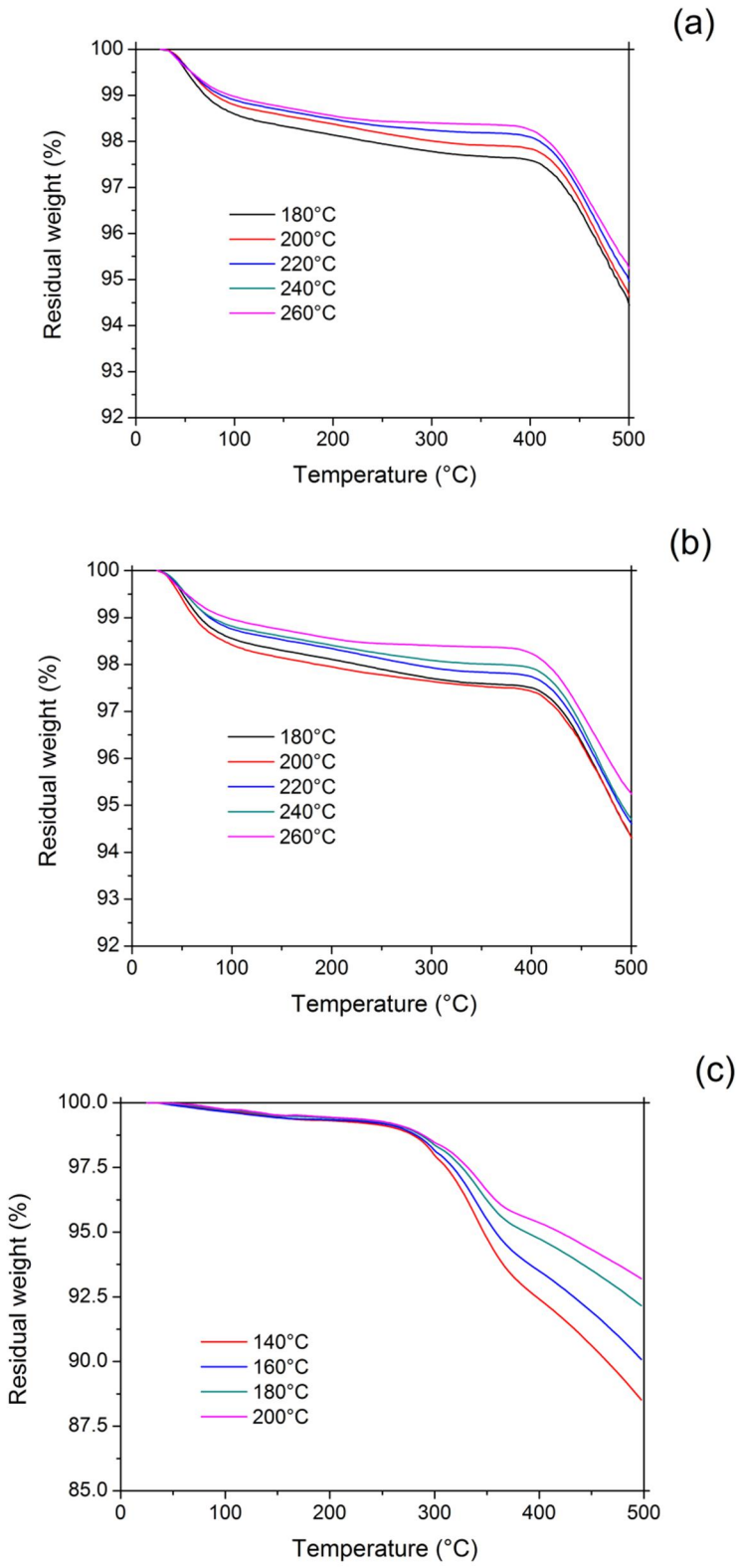

Figure A1.6: TGA thermograms showing the effect of molding temperature on the thermal stability of (a) novolac-PF, (b) resol-PF, and (c) VER based composite bipolar plates

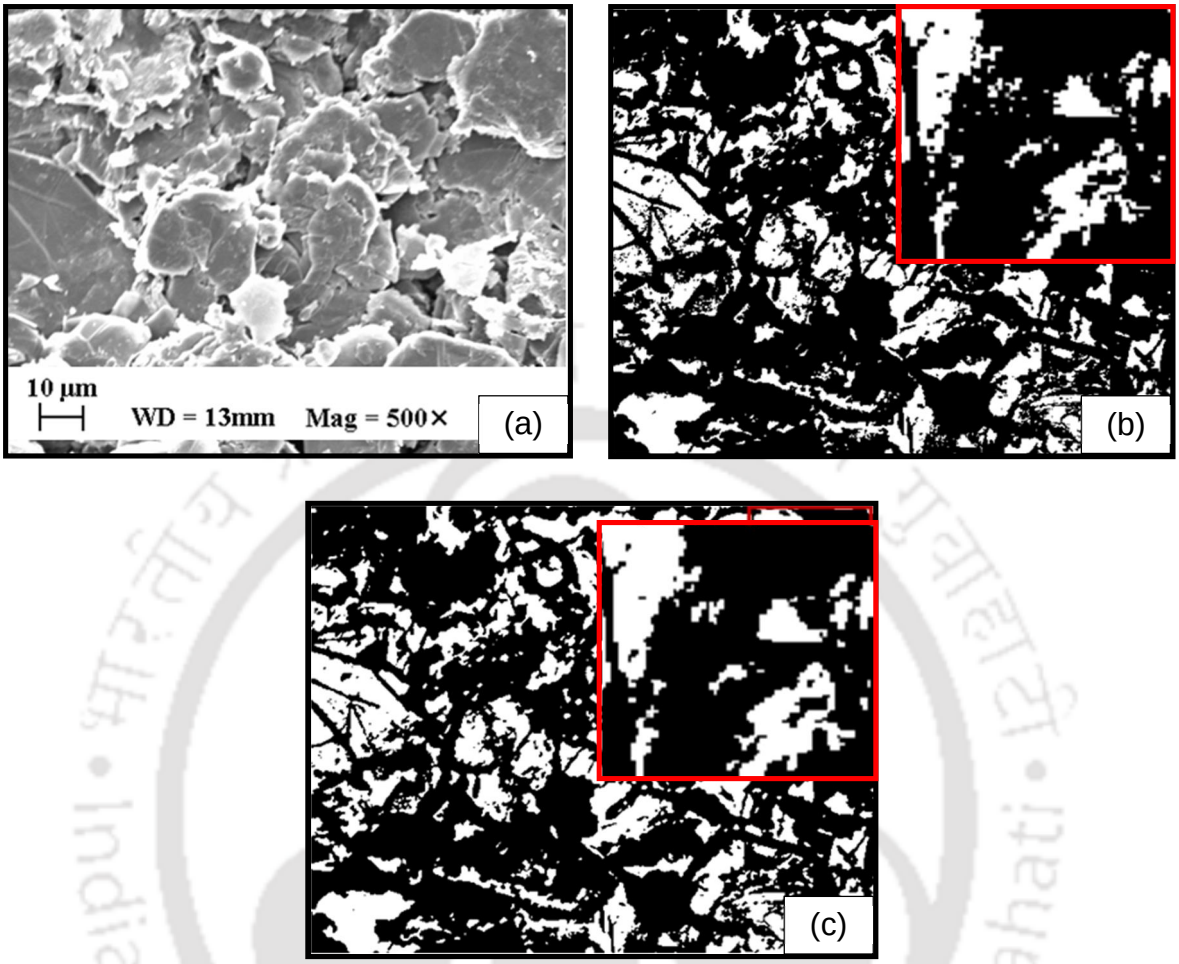

Figure A2.1: (a) SEM micrograph of the composite bipolar plate (with #300mesh size NG), (b) binary image of the same micrograph and (c) filtered binary image where the point like particles in the binary image are removed; magnified view of a particular portion is shown in the inset to show the effect of filtering

Figure A2.1 shows the representative SEM and digitally processed images of 75% graphite and 25% resol-PF composite bipolar plate. Figure A2.1(a), a portion of the SEM image, shows that the flaky graphite particles are well distributed and oriented in the plane of the composite. Figure A2.1(b) shows the binary image of the SEM for further study. In the fig. A2.1(b), resin and graphite particles are represented by white and black

color, respectively. The point like particles, of diameter equal to 0.2 µm or less, were filtered out from fig. A2.1(b) and are shown in fig. A2.1(c). The difference between original and filtered binary image is distinctly visible in the inset of the respective picture. Figure A2.1(c) was used for determining the shape and orientation factors of the graphite particles in the composite. It is to be noted that the shape factor obtained will not be only for a particle but will also represent the continuous cluster of the graphite particles as discussed earlier. High electrical conductivity is an essential characteristic of the composite bipolar plate, which can be achieved by the continuous path of the electrical conductor in the direction of external current collector of the fuel cell. Moreover, for any graphite particle, the shape factor may vary depending upon its inclination with the plane. Thus, low shape factor is a desired property compared to high shape factor of the same size particles due to the projection of the graphite particle. Therefore, low shape factor will serve the purpose as the graphite particles are highly conductive in the plane.

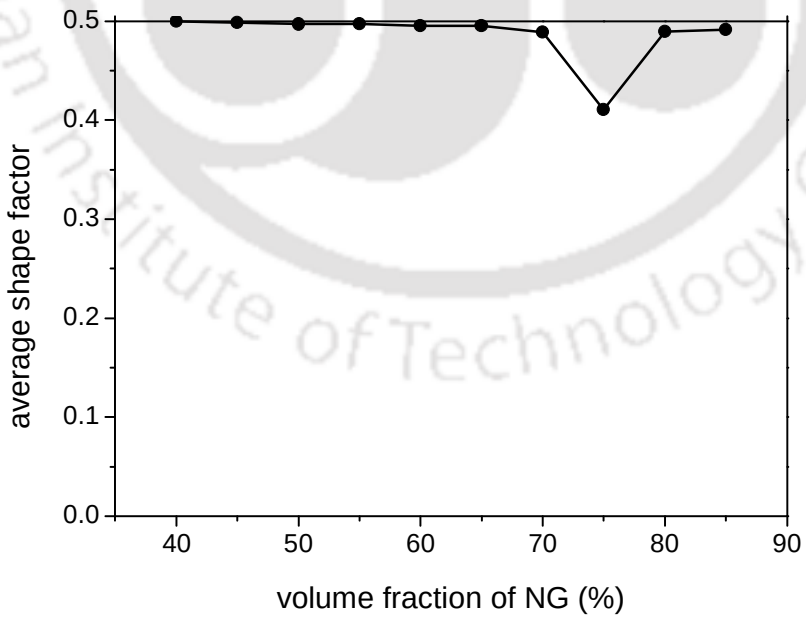

Figure A2.2: Effect of NG content on average shape factor of the filler

Figure A2.2 shows the effect of graphite volume fraction on the average shape factor. The average shape factor decreases slowly with the increase in the graphite content. This decrease was due to the replacement of the excessive resin by graphite particles. At 75% graphite content the average shape factor sharply decreased to 0.41 from its previous value of 0.49. When the graphite content was further increased the shape factor again increased because of the creation of pores that was resulted due to insufficient quantity of the resin in the matrix. Thus, 75% is the optimum graphite content at which the graphite particles do not have any excessive resin and the graphite particles are well connected with each other and well bonded with the resin.

The above explanation is verified with the help of porosity analysis (fig.A2.3) of the composite. Moreover, the other mechanical properties of the composite also reduced on further increase in the graphite content (above 75%) in the composite bipolar plate.

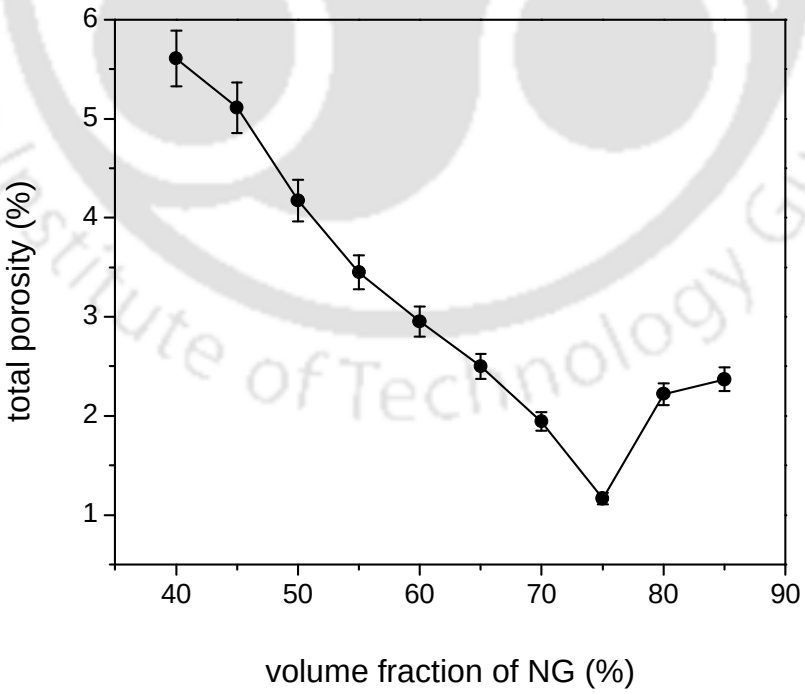

Figure A2.3: Effect of NG content on the total porosity of the composite

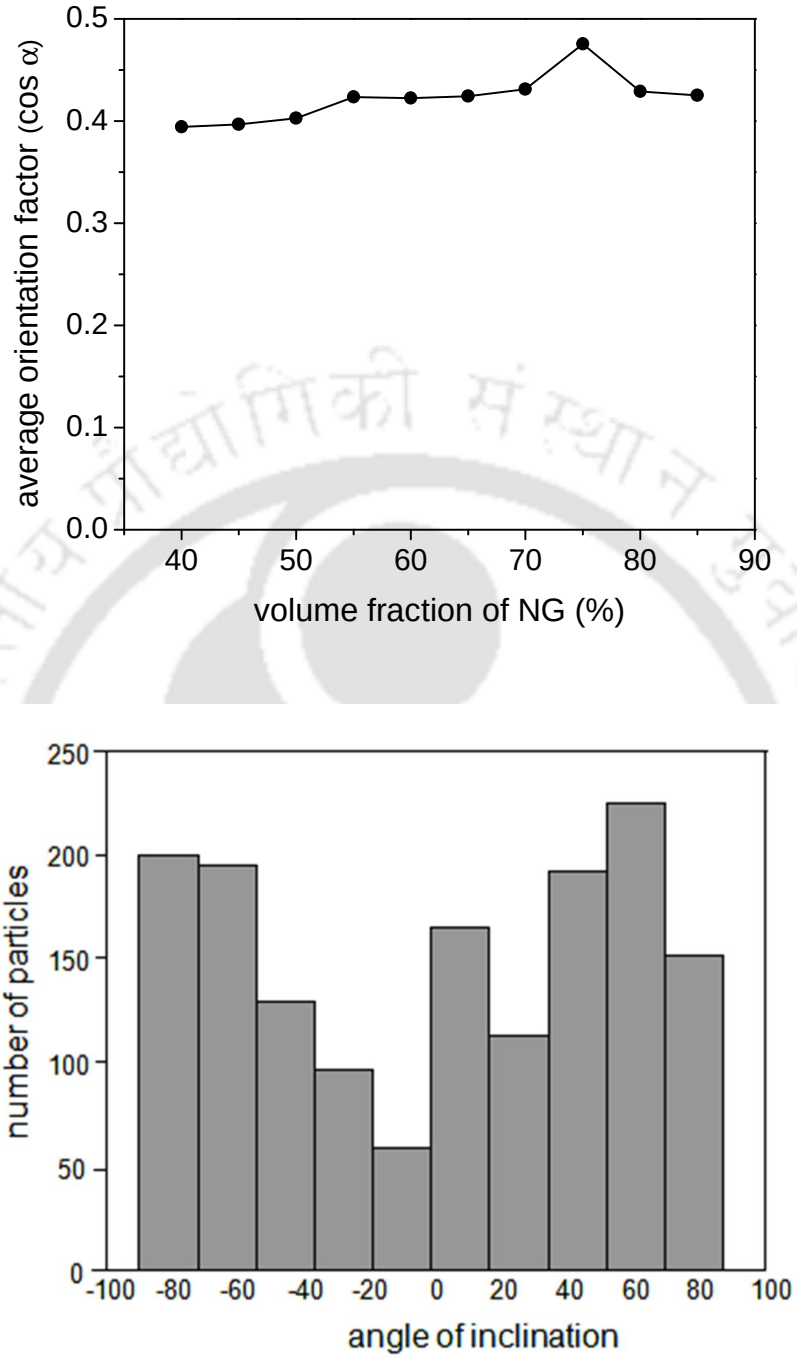

Figure A2.4: (a) Effect of filler content on the average orientation factor of the composite, and (b) histogram of graphite particles with different orientation factors (75% graphite content)

The orientation of the graphite particles in the composite is an important parameter as graphite has anisotropic electrical properties. It has high electrical conductivity along the

basal plane in comparison to the perpendicular direction to the basal plane. The average orientation factor versus volume fraction of the composite is shown in fig. A2.4(a). From the fig. A2.4(a), it can be seen that the average orientation factor is maximum for 75% graphite content in the composite. At 75% filler volume fraction the average orientation factor of the fillers is 0.4755, which means that the average angle of inclination is ±61.60°. This shows that the graphite particles are homogeneously distributed in the composite at that particular orientation factor [Dweiri et al., 2008]. A representative histogram is shown in the fig. A2.4(b) for 75% graphite content in the composite. The histogram shows the pattern of the angle of inclination with the number of particles in the composite.

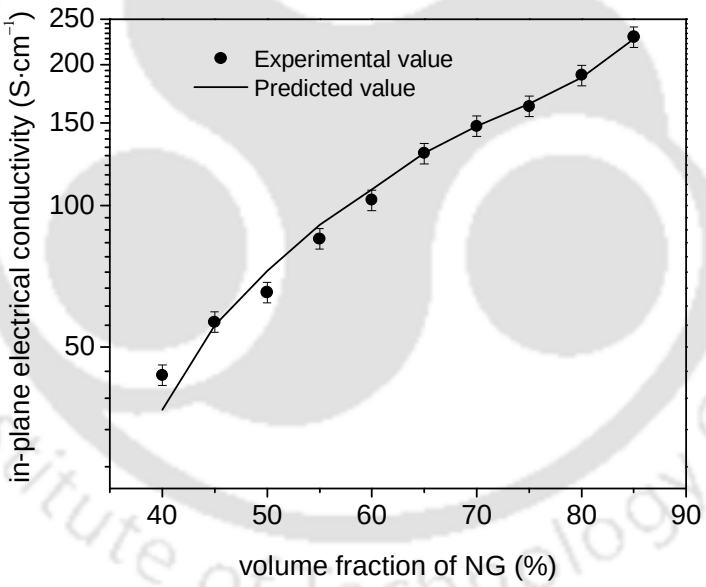

Figure A2.5: Effect of the graphite content (#300 mesh size) on electrical conductivity of the bipolar plate and its predicted values by Ondracek model

Figure A2.5 shows that the experimental and predicted electrical conductivity of the resol-PF/NG composite for different NG content. From the fig. A2.5, it can be seen that

the conductivity of the composite increases with the increase in NG content and follows inverse "S" pattern. In the lower region of the pattern (40% to 55%) the electrical conductivity increases with a slightly higher rate due to the decrease in insulating resin in the smearing region of the graphite particles. In the middle region (55% to 75%) of the pattern, the rate decreases. It may be because the available resin was just sufficient to fill the interstices of the graphite particles. However, in the top section (75% to 85%) of the pattern the electrical conductivity rate further increases with slightly higher rate due to the compacted graphite particles, where the resin content was not enough to provide any insulating barrier.

The experimental data are well predicted by the model as shown by the line in the figure. The parameter δ for resol-PF/ NG system was found to be 1.7346. The higher value of the electrical conductivity of the composite is desirable. However, the selection of the graphite composition is guided by the shape and orientation factors as discussed earlier. As per the recent benchmark given by Department of Energy, USA the recommended value of electrical conductivity for bipolar plate is >100 $S \cdot cm^{-1}$ [Jayakumar et al., 2006; Cunningham et al., 2007; Kakati et al., 2007]. Thus, the composite at 75% graphite is a suitable bipolar plate for the fuel cell application as it shows the electrical conductivity of 165 $S \cdot cm^{-1}$. Through plane electrical conductivity of the composite bipolar plates was also measured and for 75% graphite content it was found to be 103.3 $S \cdot cm^{-1}$.

Table A2.1: List of constants for GEM equation

Composition	a		b	
	in-plane	through-plane	in-plane	through-plane
Resol-PF/NG	0.0378	1.1960	0.0882	0.9500
Resol-PF/NG/CB	24.1709	38.2158	−2.4805	−2.5778
Resol-PF/NG/CB/CF	19.9230	18.9786	0.3495	5.7369
Novolac-PF/NG	0.0378	1.1960	0.0882	0.0295
Novolac -PF/NG/CB	3.6210	0.0140	9.5620	−0.0060
Novolac -PF/NG/CB/CF	0.1095	0.0725	0.0010	−0.1312
VER-PF/NG	0.0378	1.1960	0.0882	0.0295
VER -PF/NG/CB	25.1637	34.0154	−2.4478	−0.2143
VER-PF/NG/CB/CF	20.1992	18.9786	0.3405	5.7369

Research Output

Research output

Papers published in peer reviewed international journals

1. **Kakati, B.K., Sathiyamoorthy, D., Verma, A., "Semi-empirical modeling of electrical conductivity for composite bipolar plate with multiple reinforcements", *International Journal of Hydrogen Energy*, In Press, DOI: 10.1016/j.ijhydene.2011.02.136.**

2. **Kakati, B.K., Sathiyamoorthy, D., Verma, A., "Electrochemical and mechanical behavior of carbon composite bipolar plate for fuel cell", *International Journal of Hydrogen Energy* 2010, 35 (9), 4185–4194.**

3. **Kakati, B.K., Yamsani, V.K., Dhathathreyan, K.S., Sathiyamoorthy, D., Verma, A., "Electrical conductivity of composite bipolar plate for fuel cell application", *Carbon* 2009, 47 (10), 2413–2418.**

4. **Kakati, B.K., Guptha, K.R., Verma, A., "Fabrication of composite bipolar plate for Proton Exchange Membrane Fuel Cell", *Journal of Environmental Research and Development* 2009, 4 (1), 202–211.**

5. **Kakati, B.K., Guptha, K.R., Verma, A., "Numerical optimization of channel and rib width of proton exchange membrane fuel cell bipolar plate", *International Journal of Chemical Sciences* 2007, 5 (4), 1590–1602.**

Published in Conference Proceedings:

6. **Kakati, B.K., Ghosh, A., Verma, A., "Graphene reinforced composite bipolar plate for polymer electrolyte membrane fuel cell", in Proceedings of ASME 2011 *5th International Conference on Energy Sustainability & 9th Fuel Cell Science, Engineering and Technology Conference 2011*, 7–10 August, 2011, Washington DC, USA.**

7. **Kakati, B.K., Verma, A., "Development of composite bipolar plate for PEM Fuel Cell", in *Second International Conference on Materials for the Future*, 23–25 February, 2011, Kerala, India.**

8. **Kakati, B.K., Dhruw, R., Verma, A., "Performance of polymer electrolyte membrane fuel cell using vinyl ester resin based composite bipolar plate", in *Chemcon 2010*, 27–29 December, 2010, Chennai, India.**

9. **Kakati, B.K., Yamsani, V.K., Sathiyamoorthy, D., Verma, A., "Semi-empirical modeling of electrical conductivity for composite bipolar plate with multiple reinforcements", in *International Symposium & Exhibition on Fuel Cell Technologies: FUCETECH 2009*, 11–13 November, 2009, Mumbai, India.**

10. **Kakati, B.K., Kumar, P., Dhruw, R., Verma, A., "A structure oriented model for the electrical conductivity of composite bipolar plate", in *CHEMFERENCE 09*, 22–23 August, 2009, Indian Institute of Technology Madras, Chennai, India.**

11. **Kakati, B.K., Guptha, K.R., Verma, A., "Fabrication of composite bipolar plate for Proton Exchange Membrane Fuel Cell", in *International Congress on Environmental Research*, 18–20 November, 2008, Goa, India.**

12. **Kakati, B.K., Guptha, K.R., Verma, A., "Numerical optimization of channel and rib width of polymer electrolyte membrane fuel fell bipolar plate", in National Conference on Frontiers in Chemical Engineering, 12–14 December, 2007, IIT Guwahati, Assam, India.**

About the author

The author joined Department of Chemical Engineering, Indian Institute of Technology Guwahati, Guwahati, Assam, India, in December 2006 as a full time Ph.D. scholar. Before joining IIT Guwahati, the author completed M.Sc. in Physics followed by M.Tech. in Energy Technology from Tezpur University, Tezpur, Assam, India. He won the prestigious gold medal in M.Tech. in Energy technology. Moreover, the author was also recognized by Marquis Who's Who in the year 2010–2011, for the valuable contribution in the field of science and technology. The author holds the post of the chief editor of XOBDO.ORG – A multi-lingual online dictionary for north-eastern languages.

The author published 10 research papers in several peer reviewed high impact factor international journals. He has also presented several scientific and technical research papers in national and international seminars and symposiums. At present, he is also the reviewer of several international journals.